

Orchestrating Mass Deployment of Electric Vehicles in Distribution Grids A Systematic Framework for Advancing EV Smart Charging

Yu, Y.

10.4233/uuid:c88d2913-c496-48cd-96b3-8c34014350d8

Publication date

Document Version Final published version

Citation (APA)

Yu, Y. (2024). Orchestrating Mass Deployment of Electric Vehicles in Distribution Grids: A Systematic Framework for Advancing EV Smart Charging. [Dissertation (TU Delft), Delft University of Technology]. https://doi.org/10.4233/uuid:c88d2913-c496-48cd-96b3-8c34014350d8

Important note

To cite this publication, please use the final published version (if applicable). Please check the document version above.

Copyright

Other than for strictly personal use, it is not permitted to download, forward or distribute the text or part of it, without the consent of the author(s) and/or copyright holder(s), unless the work is under an open content license such as Creative Commons.

Please contact us and provide details if you believe this document breaches copyrights. We will remove access to the work immediately and investigate your claim.



INVITATION

You are cordially invited to the public defence of my PhD thesis titled:

Orchestrating
Mass Deployment of
Electric Vehicles in
Distribution Grids

A Systematic Framework for Advancing EV Smart Charging

on October 24th, 2024 Thursday, at 10:00 a.m. in the Aula of TU Delft Mekelweg 5 Delft

The defence is preceded by an introductory presentation at 9:30 and followed by a reception.

Yu Yunhe y.yu-4@tudelft.nl

Paranymphs Wang Zi Aditya Shekhar





ORCHESTRATING MASS DEPLOYMENT OF ELECTRIC VEHICLES IN DISTRIBUTION GRIDS

A Systematic Framework for Advancing EV Smart Charging

> Yunhe Yu 俞云鹤

ORCHESTRATING MASS DEPLOYMENT OF ELECTRIC VEHICLES IN DISTRIBUTION GRIDS

A Systematic Framework for Advancing EV Smart Charging

Dissertation

for the purpose of obtaining the degree of doctor at Delft University of Technology by the authority of the Rector Magnificus, prof. dr. ir. T.H.J.J. van der Hagen, chair of the Board for Doctorates to be defended publicly on Thursday, 24th October 2024 at 10:00 o'clock

by

Yunhe Yu 俞云鹤

Master of Science in Sustainable Energy Technology, Delft University of Technology, The Netherlands. Born in Nanjing, China This dissertation has been approved by the promotors.

Composition of the doctoral committee:

Rector Magnificus, chairperson

Prof. dr. ir. P. Bauer,
Delft University of Technology, *promotor*Dr. ir. G. R. Chandra Mouli,
Delft University of Technology, *copromotor*

Independent members:

Prof. dr. rer. pol. M. Wietschel, Fraunhofer ISI

Prof. dr. ir. R. N. A. Bekkers,
Prof. dr. M. M. de Weerdt,
Prof. dr. ir. Z. Lukszo,
Dr. ir. J. L. Rueda Torres,

Eindhoven University of Technology
Delft University of Technology
Delft University of Technology

Though not part of the committee, Dr. ir. A. Shekhar of Delft University of Technology has contributed greatly to the preparation of this dissertation.







A great portion of this dissertation is part of project Orchestrating Smart Charging in Mass Deployment (OSCD). OSCD was supported by ERA-NET Cofund Electric Mobility Europe (EMEurope) under Grant EME-35.

Printed by: Gildeprint

Cover by: Mark Wolf and Yu Yunhe with the help of OpenAI Dell-E

Copyright © 2024 by Y. Yu

ISBN 978-94-6384-651-6

An electronic copy of this dissertation is available at https://repository.tudelft.nl/.

The struggle itself toward the heights is enough to fill a man's heart.

One must imagine Sisyphus happy.

- Albert Camus, < The Myth of Sisyphus>

向高峰的拼搏本身足以充盈人心;我们必须设想西西弗是幸福的。 — 阿尔贝·加缪,《西西弗神话》

Though not every fragment of existence is touched by significance, we humans ceaselessly chase meaning in the unnoticed and unseen.

Whether Sisyphus was happy remains a glimpse I can no longer discern.

I dedicate this book to the most significant glimmers in my life: my dearest mom and dad, my beloved Mark, and my cutest paw friend, Tuoba.

> 纵然世间万物未必尽含深意, 吾众生人心无休,恒于纤毫寸芒处追寻真谛。 西西弗是否幸福早已化作我不复辨析的惝恍残象。

谨以此书献给我生命中至深至远的微光: 我最亲爱的妈妈爸爸,心爱的波尼,以及我最可爱的爪友,拖把。

Contents

Su	Summary xi				
Sa	menv	atting		xiii	
中	文总统	法		xv	
1	Intr	oductio	on	1	
	1.1	In the	pursuit of sustainability, a systematic solution is needed	1	
	1.2		rch scope and objectives	2	
	1.3	Thesis	outline and key research offerings	4	
2	EV-0	Grid in	tegration – A backdrop sketch	7	
	2.1	What	unregulated EV charging brings to the current grids	7	
	2.2	Basic	practices of EV smart charging	8	
		2.2.1	SC design dimensions	8	
		2.2.2	The key players and the communication protocols	10	
	2.3	EV sm	hart charging algorithm invention — A step by step journey \dots	11	
		2.3.1	Seeking balance in intricacy	11	
		2.3.2	From conceptualisation to actual implementation	13	
3	Pros	spects a	and pitfalls of the mass EV deployment in distribution grids	15	
	3.1	Introd	uction	15	
		3.1.1	Literature review	16	
		3.1.2	Contributions	18	
		3.1.3	Structure of the chapter	18	
	3.2	Metho	odology: Data-Driven Approach for Realistic Grid Impact Evaluation	18	
		3.2.1	Grid Specific Data	19	
		3.2.2	Load and Photo-Voltaic (PV) profiles	21	
		3.2.3	EV penetration representation	22	
		3.2.4	Historical measurement-based EV fleet and demand profile gener-		
			ation	25	
		3.2.5	Methodology and simulation data	26	
	3.3	Simula	ation Results and impact factor discussion	26	
		3.3.1	Results of different grid types and countries	30	
		3.3.2	Impact factor discussion	31	
	3.4	Comp	arison of Different Grid Behaviour with Key Indicators	34	
		3.4.1	The magnitude of grid congestion	34	
		3.4.2	Duration and scale of the grid congestion	36	
		3.4.3	Key takeaway	38	
	3.5	Concl	usion and recommendation	38	

Ber	ıchmarl	k study of heuristic EV charging tactics			
4.1	Introd	uction			
	4.1.1	Background on Advanced Smart EV Charging Algorithms			
	4.1.2	Simple and Practical Charging Scheduling Approach			
	4.1.3	Contributions and the chapter Structure			
4.2	EV Ch	narging Scheduling Methods			
	4.2.1	Price Signal Method			
	4.2.2	Voltage Droop Method			
	4.2.3	Average Rate Method			
4.3	Simula	ation Methodology and System Information			
4.4		arative Simulation Results for Grid Performance with Different Char-			
	ging Schemes				
	4.4.1	Grid Congestion Alleviation and Charging Session Feature Correlations			
	4.4.9				
	4.4.2	Loading Value Distribution Exploration			
	4.4.3	Overloading Assessment on Individual element			
4 5	4.4.4	Key Takeaways			
4.5		cheme Analysis			
4.6		ing Process Evaluation			
	4.6.1	Charging Completion			
	4.6.2	Charging Cost			
4.7	Concli	usions			
	Centralised EV charge management schemes aiming grid congestion as-				
	gement				
5.1		uction			
	5.1.1	Literature review			
5.2		odology			
	5.2.1	Phase 1: Grid congestion detection			
	5.2.2	Phase 2: Congestion diagnosis and target EVSE detection			
	5.2.3	Phase 3: EV charging scheme execution			
5.3	Model	ling of elements and scenarios			
	5.3.1	Grid features			
	5.3.2	PV and load profiles			
	5.3.3	EV data			
	5.3.4	Simulation setups and scenarios			
5.4	Simula	ations Results			
	5.4.1	Grid congestion mitigation			
	5.4.2	User satisfaction			
	5.4.3	Overcompensation of grid overloading			
5.5		usion and recommendations			
	_ 51151				
		al EV smart charging algorithm development with HIL exper-			
		aluation			
6.1	Introd	uction			

	6.2	Architecture of system model and algorithm	99				
		6.2.1 System architecture	99				
		6.2.2 Smart charging algorithm description	100				
		6.2.3 Algorithm execution and the Flexible receding horizon scheme	102				
	6.3	Hardware-Software configuration	103				
		6.3.1 HIL setup	103				
		6.3.2 Testbed/Algorithm interface	106				
	6.4	Assumptions and test scenarios	107				
		6.4.1 Grid model and input data	107				
		6.4.2 Simulation scenarios	109				
	6.5	Results and analysis	111				
		6.5.1 Base case	111				
		6.5.2 Impact of stochasticity	114				
		6.5.3 Efficacy of incorporating grid limitation	116				
		6.5.4 Comparison	117				
	6.6	Conclusions and recommendations	119				
7	Sma	Smart charging algorithm advancement addressing experiment results					
	and	visioning implementations	121				
	Introduction	121					
	7.2	Algorithm mathematical build explained	123				
		7.2.1 System structure	123				
		7.2.2 Smart charging algorithm	124				
	7.3	Algorithm implementational practice	129				
		7.3.1 Future EV inclusion	129				
		7.3.2 Passive stochasticity coping mechanism	130				
	7.4	Simulation setup, input data and assumptions	133				
	7.5	Results	135				
		7.5.1 Smart charging performance evaluation	135				
		7.5.2 Stochasticity management validation	144				
		7.5.3 Pursuing optimality					
	7.6		152				
8	Key	insights	155				
Bi	bliog	raphy	161				
			175				
Αι	ıthor	profile	177				

Summary

The rapid growth in EV market share aligns with the EU's push for transportation electrification, presenting challenges to power grids alongside the rise of distributed renewable energy. Successful execution of charging sessions relies on the seamless operation of key players and components in the complex EV charging ecosystem. Therefore, addressing the EV-grid integration challenges requires a comprehensive, implementational and holistic approach.

This thesis exhibits a systematic study on integrating Electric Vehicles (EVs) with Low Voltage (LV) distribution grids, divided into two main parts. The first part delves into an extensive analysis of the potential issues the grids may encounter, exploring the what, how, and to what extent these challenges arise. The second part focuses on offering empirical solutions to the observed challenges viewed from the Distribution System Operators (DSOs) standpoint and aggregators' perspectives, respectively.

Mass EV deployment in distribution grids — Uncontrolled charging and heuristic benchmarks

In the first part of this thesis, a comprehensive study is conducted on the mass deployment of EVs in distribution grids through grid load flow analysis. This is followed by a comparative investigation of representative heuristic EV charging strategies, assessing their effectiveness in alleviating grid congestion, reducing costs, and fulfilling charging requests.

The EV uncontrolled charging study investigates grid congestion and its influencing factors across twenty-one grids in three EU countries, covering three grid types. The analysis spans winter and summer and considers weekday/weekend variations with four EV penetration levels. The scrutiny of the magnitude, scale, and duration of grid congestion reveals several key insights. A coinciding overloading trend is generally exhibited among all grid components, with the grid's intrinsic characteristics being the primary factors contributing to congestion risks. It is also perceived that the voltage issues may surface well before line overloading becomes evident, and severe overloading predominantly occurs at main buses and in local pockets with high consumption loads. Overall, Most grids can accommodate up to 50% EV penetration without experiencing significant congestion.

Then, the trade-offs among three heuristic EV charging tactics — considering grid performance, charging demand fulfilment, and economic benefits — are perused across three different grid types and four increasing EV penetration levels during both summer and winter. The research outcome indicates that even though the heuristic EV charging methods evince acceptable outcomes, their imperfections, which stem from the narrow specialities and limited system information, can result in unbalanced or even biased results. This is notably apparent when grid congestion, charging cost and user satisfaction, including both charging fulfilment and fairness, are competing for the finite system resources. Therefore, the logic design and the selection of reference parameters for heuristic methods must be carefully evaluated to lay the groundwork for the development of smart charging

algorithms in the second part of this thesis.

Grid congestion management and EV smart charging algorithm development

The second major topic of this thesis is to provide feasible systematic solutions to the current and anticipated challenges confronted by grids while serving other key stakeholders' interests in the EV charging ecosystem. This effort is demonstrated through two critical approaches in this thesis. First, developing a Power Transfer Distribution Factors (PTDF) based grid congestion prevention/mitigation mechanism from the DSO perspective. Second, designing, advancing and validating a flexible and reliable hierarchical mixed integer programming (MIP) EV smart charging algorithm from the aggregator prospect.

The formulated PTDF-based LV grid congestion management algorithm is embedded with three centralised EV charging management schemes. These schemes alleviate the congestion by targeting the elements that are pivotal to overloading, pursuing impartiality among all users concerning charging management and maximising overall energy transfer to the EVs, respectively. This algorithm integrates the full grid information and solves the problem through linear programming (LP) and iterative calculations. The algorithm demonstrates its success in completely preventing or alleviating congestion with 50% and 100% EV penetration across two grids respectively. It achieves this with high efficacy through: prioritising efficiency, fairness among EV users, and charging priorities, in accordance with the design of each scheme. On the other hand, the core mechanism of the algorithm — suspending charging until the EV is fully charged or departs — leads to extended EV charging queuing size and duration, and results in an overcompensation phenomenon in overloading reduction, when coupled with the grid's voltage deviation. This advocates that grid congestion mitigation could be more efficiently pursued in tandem with distributed EV smart charging.

The smart charging algorithm development consists of the following key steps: ① A primary version of the hierarchical MIP algorithm, featuring a passive stochasticity processing function and adhering to the tech specifications of protocols such as IEC/ISO 15118 and IEC 61851-1, is proposed. ② The primary-version algorithm is verified and assessed in a Power Hardware-In-the-Loop (PHIL) testbed adapting real LV grid across 8 scenarios. These scenarios address practical challenges of inaccuracy in PV and Load Prediction, EV charging information mismatch and grid restriction incorporation. ③ Based on the experimental results, the algorithm's effectiveness is further enhanced in: levelling charging current command for a steadier charging process, upgrading grid balancing services and acquiring a higher level of proximity to optimality. Additionally, the stochasticity managing function is strengthened for ad hoc admittance of (future) erratic charging events and self-correction of charging parameters.

The algorithm's functionalities, effectiveness are proven to be viable and can converge to proxi-optimality. It is discovered that asset aggregation and optimisation improvement are remarkably beneficial in FCR service provision, while heuristic charging methods hold great potential to further advance the algorithm's outcome towards optimality.

Samenvatting

De snelle groei van het marktaandeel van elektrische voertuigen sluit aan bij de EUstimulans voor de elektrificatie van transport, wat nieuwe uitdagingen met zich meebrengt voor elektriciteitsnetten, met name door de toename van decentrale hernieuwbare energiebronnen. Het succesvol uitvoeren van laadsessies vereist een naadloze samenwerking tussen belangrijke actoren en componenten binnen het complexe ecosysteem van EV-laden. Het aanpakken van de uitdagingen rond de integratie van elektrische voertuigen en het elektriciteitsnet vereist daarom een uitgebreide, uitvoerbare en holistische benadering.

Deze scriptie presenteert een systematische studie naar de integratie van elektrische voertuigen (EV's) in laagspanningsnetten en is opgesplitst in twee hoofdonderdelen. Het eerste deel biedt een uitgebreide analyse van de mogelijke problemen waarmee deze netten geconfronteerd kunnen worden, waarbij de aard, oorzaak en omvang van deze uitdagingen worden onderzocht. Het tweede deel richt zich op het aanbieden van empirische oplossingen voor de geconstateerde uitdagingen, vanuit het perspectief van zowel netbeheerders (DSO's) als aggregatoren.

Grootschalige integratie van EV's in distributienetten: Ongecontroleerd laden en heuristische benchmarks

In het eerste deel van deze scriptie wordt een uitgebreide studie uitgevoerd naar de grootschalige inzet van EV's in distributienetten, gebaseerd op een analyse van de netbelasting. Dit wordt gevolgd door een vergelijkend onderzoek naar representatieve heuristische laadstrategieën voor EV's, waarbij hun effectiviteit wordt beoordeeld op het verlichten van netcongestie, het verlagen van kosten en het vervullen van laadverzoeken.

De studie naar ongecontroleerd laden van EV's onderzoekt netcongestie in eenentwintig netten in drie EU-landen, rekening houdend met seizoens- en weekvariaties en vier niveaus van EV-penetratie. De analyse toont aan dat overbelasting vaak samenvalt in alle netcomponenten, waarbij de intrinsieke kenmerken van het net de belangrijkste factoren zijn. Spanningsproblemen kunnen optreden voordat kabels overbelast raken, en ernstige overbelasting komt vooral voor bij hoofdverdelers en in gebieden met hoge belasting. De meeste netten kunnen tot 50% EV-marktaandeel aan zonder significante congestie.

Vervolgens wordt een vergelijking gemaakt tussen drie heuristische laadmethoden voor EV 's met betrekking tot netprestaties, het vervullen van de laadvraag en economische voordelen voor drie verschillende nettypes voor vier toenemende niveaus in het marktaandeel van EV's, gedurende zowel zomer als winter. Hoewel de methoden bevredigende resultaten opleveren, kunnen hun beperkte specialisaties in de algoritmes en onvolledige systeeminformatie leiden tot ongebalanceerde resultaten, vooral wanneer netcongestie, laadtarieven en gebruikerstevredenheid concurreren om schaarse middelen. Daarom moeten het logische ontwerp en de selectie van referentieparameters voor heuristische methoden zorgvuldig worden geëvalueerd om de basis te leggen voor de ontwikkeling van slimme laadalgoritmen in het tweede deel van deze scriptie.

Congestiebeheer en de ontwikkeling van slimme EV-laadalgoritmen

Het tweede hoofdonderwerp van deze scriptie richt is het bieden van haalbare systematische oplossingen voor de huidige en verwachte uitdagingen waarmee netten worden geconfronteerd, terwijl tegelijkertijd rekening wordt gehouden met de belangen van andere belangrijke stakeholders binnen het EV-laadecosysteem. Dit wordt gedaan middels twee benaderingen. Ten eerste, het ontwikkelen van een op *Power Transfer Distribution Factors* (PTDF) gebaseerd mechanisme voor voorkomen van netcongestie vanuit het perspectief van de netbeheerder. Ten tweede, het ontwerpen en verbeteren van een *hierarchical mixed integer programming*(MIP) slim EV laadalgoritme vanuit het oogpunt van de aggregator.

Het geformuleerde PTDF-gebaseerde algoritme voor congestiemanagement in laagspanningsnetten is voorzien van drie gecentraliseerde laadbeheerschema's voor elektrische voertuigen. Deze schema's verlichten de congestie door zich te richten op de elementen die cruciaal zijn voor overbelasting, door onpartijdigheid tussen alle gebruikers te waarborgen met betrekking tot laadbeheer en door het maximaliseren van de totale energieoverdracht naar de EV's, respectievelijk. Het algoritme maakt gebruik van alle netinformatie en lost het probleem op door middel van mixed integer lineair programming (MILP) iteratieve berekeningen. Het algoritme toont zijn succes aan door volledige preventie of verlichting van congestie te realiseren bij respectievelijk 50% en 100% EV-marktaandeel in twee verschillende netten. Dit wordt bereikt met hoge doeltreffendheid door prioriteit te geven aan efficiëntie, eerlijkheid tussen EV-gebruikers en laadprioriteiten, in overeenstemming met het ontwerp van elk schema. Aan de andere kant leidt het kernmechanisme van het algoritme – het opschorten van het laden tot de EV volledig is opgeladen of vertrekt – tot langere wachttijden en een overcompensatiegenomeen in een poging overbelasting te verminderen. Dit suggereert dat congestiemitigatie efficiënter kan worden bereikt met gedistribueerd slim laden van EV's.

Het slimme laadalgoritme wordt ontwikkeld in drie stappen: ① Een eerste versie van het hiërarchische MIP-algoritme, met een passieve functie voor het verwerken van stochastische processen, wordt voorgesteld. Dit algoritme voldoet aan de technische specificaties van protocollen zoals IEC/ISO 15118 en IEC 61851-1. ② Deze versie wordt getest in een *Power Hardware-In-the-Loop* (PHIL) omgeving. Dit gebeurt aan de hand van met 8 scenario's die praktische uitdagingen zoals PV-voorspellingsfouten, netbeperkingen en mismatch in EV-informatie aanpakken. ③ Op basis van de experimentele resultaten is de effectiviteit van het algoritme verder verbeterd op verschillende gebieden: het uitvlakken van het laadstroomcommando voor een stabieler laadproces, het verbeteren van netbalanceringsdiensten en het bereiken van een hogere mate van nabijheid tot optimaliteit. Daarnaast is de functie voor het beheren van stochastische variabiliteit versterkt, zodat het algoritme beter kan inspelen op onregelmatige laadmomenten in de toekomst en zelf de laad parameters kan aanpassen.

De functionaliteiten en effectiviteit van het algoritme zijn bewezen haalbaar en kunnen dicht bij optimaliteit komen. Het blijkt dat asset-aggregatie en optimalisatieverbeteringen opvallend gunstig zijn voor het leveren van FCR-diensten, terwijl heuristische laadmethoden veel potentie hebben om het resultaat van het algoritme verder richting optimaliteit te brengen.

中文总结

电动汽车的市场份额以和欧盟推动交通电气化相契合的步调迅速增长,这和分布式可再生能源的兴起一并给电网带来了挑战。在复杂的电动汽车充电生态系统中,关键参与者和组件之间的无缝运行,决定了充电过程能否顺利进行。因此,应对电动汽车的并网挑战,需要一个详尽的,可执行的,且整体性的解决方案。

这篇论文分两个主要部分对电动汽车(EV)与低压(LV)配电网的集成进行了系统性的研究。第一部分深入分析了电网可能面临的潜在问题,并探讨这些挑战的性质、成因及影响程度。第二部分则从配电系统运营商(DSO)和聚合商的角度,分别提出了应对这些挑战的实际解决方案。

配电网中大规模电动汽车的部署--无序充电与启发式基准

本论文的第一部分通过电网潮流分析,对电动汽车在配电网中的大规模部署进行了全面研究。随后,对几种具有代表性的启发式电动汽车充电策略进行了比较分析,评估它们在缓解电网拥堵、降低成本和满足充电需求方面的有效性。

针对电动汽车无序充电的研究调查了三个欧盟国家的二十一个电网的拥塞情况及其影响因素,三种电网类型涵盖其中。研究范围不仅包含冬季和夏季对比,考虑工作日和周末的变化,还统括了四种电动汽车的应用渗透率。本论文通过对电网拥塞的规模、程度和持续时间的深入探讨揭示了若干关键推论。研究表明,所有电网组件普遍表现出一致的过载趋势,而电网的固有特性是导致拥堵风险的主要原因。此外,电压问题往往在线路过载变得急迫之前就开始出现,而严重过载通常发生在主母线和高负荷消耗的局部区域。总体而言,大多数电网可以在不出现明显拥堵的情况下,容纳高达50%的电动汽车渗透率。

接下来,论文对三种启发式电动汽车充电策略进行了权衡分析—并重点考察电网性能、充电需求的满足以及经济效益—这些分析覆盖了三种不同的电网类型和四个逐步提升的电动汽车渗透水平,并探索了冬夏的季节影响。研究结果表明,尽管采用启发式电动汽车充电策略的结果尚可,但其狭窄的适用面和有限的系统信息可能会导致结果偏颇甚至产生较大偏差。当电网拥塞、充电成本和用户满意度(包括充电满足率和公平性)等指标在有限的系统资源中相互竞争时,策略的局限性尤为明显。因此,启发式充电方法的逻辑设计和参考参数的选择必须谨慎评估,以为智能充电算法的开发奠定坚实的基础—这将在论文的第二部分详细阐述。

电网拥塞管理与电动汽车智能充电算法的开发

本论文的第二大主题是为电网当前及预期面临的挑战提供可行的系统解决方案,并同时兼顾电动汽车充电生态系统中其他关键利益相关者的需求。这一努力通过论文中的两个核心方法得以体现。首先,从配电系统运营商(DSO)的角度开发了基于功率传输分布因子(PTDF)的电网拥塞预防和缓解机制。其次,从聚合商的角度设计了一种灵活且可靠的分层混合整数规划(MIP)电动汽车智能充电算法,并对其进行了改进升级和验证。

本论文提出的基于 PTDF 的低压电网拥塞管理算法结合了三种集中式电动汽车充电管理程式。各程式分别通过:针对关键过载元件、确保所有用户的充电公平性以及最大化电动汽车能量传输,来缓解电网拥堵。该算法融合了电网的完整信息,并

通过线性规划(LP)和迭代计算解决问题。该算法分别在两个有50%和100%电动汽车渗透率的电网中成功地验证了其预防和缓解拥堵的功能。根据三个程式的设计,该算法分别通过以下方式高效地实现了这一目标:优先专注拥塞解决效率,确保电动汽车用户之间的公平性,以及合理分配充电优先级。然而,该算法的核心机制——暂停充电直至电动汽车充满或离开—导致了电动汽车充电排队规模的扩大和等待时间的延长,并在电网电压偏差的影响下,在减缓电网过载时出现了过度补偿现象。这表明,电网拥塞的缓解可以通过与分布式电动汽车智能充电结合更有效地实现。

智能充电算法开发包括以下关键步骤:①首先提出一个初始版本的分层 MIP 算法,该算法具有被动随机性处理功能,并遵循 IEC/ISO 15118和 IEC 61851-1等协议的技术规范。②对初始版本算法在搭载有真实低压电网的电力硬件在环(PHIL)测试平台上进行验证和评估。该测试涉及8种不用应用场景,这些场景对应了光伏和用户端负载预测不准确、电动汽车充电信息不匹配以及叠加电网限额等的实际应用制约。③基于实验结果,我们对初始版本算法进行了全盘升级,这包括平整充电电流以实现更稳定的充电过程,改良电网辅助服务,并进一步逼近最优解。此外,算法的随机性管理功能也得到了加强,以便更好地处理未来的充电突发事件,充电过程中的参数自我校准功能也添加其中。

该算法在功能性和有效性方面得到了验证,并且能够逐步收敛至近似最优解。研究表明,资产聚合与优化改进在提供频率控制储备(FCR)服务方面极具优势,而启发式算法也在助力进一步逼近优化算法最优解方面潜力巨大。

Introduction

1.1. In the pursuit of sustainability, a systematic solution is needed

As sustainability has become one of the hottest topics around the world, the European Union has set an ambitious target of "Striving to be the first climate-neutral continent" with the European Green Deal [1]. Transportation serves as a cornerstone of the energy transition, with the European Green Deal aiming to reduce care emissions by 55% by 2030. Achieving a 90% emission reduction from the overall transportation sector is plausible with tenacious aspiration. Establishing a reliable emission-neutral refuelling network across Europe is indispensable to succeed in this ambition. The initial milestone towards the primary goal — to construct three million public charging stations by 2030 — is to have one million public charging stations available by 2025 [2]. Transitioning a larger proportion of current energy sources into Renewable Energy (RE) resources is another vital composition of the European Green Deal, which inevitably requests more power grid connections, especially since solar and wind power plants are going to be more abundant. Therefore, a reliable and durable pan-European power network is the foundation for realising the Green Deal.

With the rapid pace of the electrifying industry, businesses and households, it is expected that the electricity demand will grow 60% at the latest 2030 [3]. On top of that, a substantial portion of sporadic RE is installed in decentralised locations, which adds uncertainty to the grid and challenges the grid's stability. At the distribution grid level, the congestion takes place on an intermittent basis. For example, the public service info provided by the Dutch Distribution System Operator (DSO) association shows that there were at least eleven congestion incidents that happened in October 2023 [4]. As about 40% of the running distribution grids are older than 40 years and because the grid upgrade permit waiting time varies between 4-10 years due to cost constraints as well as material and personnel shortages, congestion is expected to increase in the future [3]. The compounded factors above present DSOs with a critical challenge: coordinating between generation and consumption amidst increasing demand, all within a tight timeline for grid revamp.

Anticipating the imbalance between grid capacity availability and new connection requests will only escalate in the coming years, non-firm contracts are suggested as a provisional solution as the full capacity will only be available under certain conditions. Although the grid's physical limits may be reached during peak hours, there are still ample capacities during off-peak hours, and this available capacity is offered to users through non-firm connections without the need to add extra physical connections. An adequate non-firm connection method can ease the urgency for grid reinforcement and conceivably

become a long-term solution [5]. In the realm of Electrical Vehicle (EV) and distribution grid integration, scheduled charging and/or smart uni/bi-directional charging can offer magnified flexibility, and help exploit the available capacity to its fullest instead of adding extra burden to the grid. Considering the potential benefits to the grids and the economic advantages, enabling smart charging and bidirectional charging while encouraging the installation of new chargers are specially promoted by the European Commission [6]. Conclusively, a systematic EV and distribution grid integration solution is urgently needed to bolster up the grid upgrade, and ultimately, this solution becomes part of the grid modernisation.

Research gap and solutions offered by this thesis

The development of an effective and feasible solution is based on a profound understanding of the problem and its origin, a comprehensive investigation of the performance-altering criteria, followed by a complete recognition of the implementational requirements. Though numerous studies in the EV and grid integration field comprise topics like grid congestion analysis and management, charging algorithm design, and experimental validation, a systematic solution is yet to be provided. Duly, this thesis presents a systematic EV and Low Voltage (LV) distribution grid integration research, starting with a thorough study of EV mass deployment in the distribution grid, then extending to grid congestion management exploration, and concludes with the design, validation and advancement of a flexible and prudent EV smart charging algorithm.

1.2. Research scope and objectives

The objective of this thesis is:

Design a multi-functional, flexible and reliable systematic solution enabling EV mass deployment in distribution grids.

To achieve this objective, the following sub-objectives together with their constituent research actions, are the vital intermediate steps. Each objective is reflected in at least one thesis chapter, which is highlighted at the end of each objective.

- O1 Quantify the grid congestion caused by vast EV connections, analyse the factors that induce and/or alter the congestion, and investigate the level of the congestion in magnitude, scale, duration, as well as temporal and geographical perspectives. Ch. 3
 - 1. Identify the major elements that cause and influence the severity of grid congestion.
 - 2. Assess which of the observed congestion issues are of particular concern and the reasons behind these concerns.
 - 3. Estimate the level of EV penetration that the grids can sustain in their current state.
 - 4. Pinpoint the key differences between grid types concerning the above subjects.

With the understanding of the above-investigated grid congestion issues, it is intriguing to check the effectiveness and restraint of the existing practical heuristic EV charging regulating methods (e.g. in pilot projects), and benchmark their performance to serve as the inspiration and reference for advanced smart charging algorithm development.

- O2 Inspect representative heuristic EV charging scheduling tactics, and appraise their abilities in serving the development of the advanced smart charging algorithm. Ch. 4
 - 1. Rioanlise the selection on the target heuristic EV charging methods.

- 2. Assess to what extent can these heuristics reconcile the grid congestion.
- 3. Explore traits other than grid congestion that shall be inspected.
- 4. Identify the characteristics of the chosen charging practices that favour the EV smart charging design.

Then the next objective is to develop a distribution grid level tool which can identify the EV charging induced grid issues and compose a counter technique from the DSO perspective.

O3 - Contrive an EV charging management mechanism that aims to minimise or even forestall grid congestion from the DSO point of view. Ch. 5

- 1. Establish methods for identifying the location, components, and degree of grid congestion.
- 2. Compute the minimal proportion of active grid loading that must be managed to restore the grid to its rated operating range.
- 3. Devise strategies for managing EV charging to efficiently mitigate the grid congestion.
- 4. Coincide the charging request fulfilment with fairness in charging management amidst all EVs.

The actualisation of mass EV smart charging requires the Charging Station Management System, which is often operated by aggregators, and the next key objective is to formulate the algorithm from the aggregator's point of view. Moreover, an imperial verification of such algorithm is a vital quality control step, thus the following two complementary objectives, O4 and O5, are determined. The invented algorithm can be verified by the experiments and the testing results can, in turn, signify the upgrade potentials in the algorithm.

O4 - Design a multi-functional and flexible smart charging algorithm from the aggregator's prospect, with an augment based on the experimental evaluation. Ch. 6, Ch. 7

- 1. Formulate the smart charging algorithm, define its objective(s) and constraints.
- 2. Deliberate on the suitable control structure and algorithm type for implementation.
- 3. Compose a way to facilitate the real-time capability of the algorithm.
- 4. Seek the balance between computational complexity and algorithmic performance.
- 5. Design a mechanism to address and manage the system uncertainties.
- 6. Outline the implementational requirements that must be accommodated for successful deployment.

The experiments can not only validate and assess the algorithm performance, but most importantly, can also disclose which feature can be improved

- 7. Identify the functions of the algorithm that can be improved and determine how to achieve them.
- O5 Validate and assess the proposed smart charging algorithm through simulation and Hardware-In-the-Loop (HIL) experiments. Ch. 6
 - 1. Construct the HIL setup and incorporate the implementational components (Hardware).
 - 2. Integrate the grid model and algorithm into the HIL setup, ensuring its real-time attribute (Software).
 - 3. Conduct both simulation and empirical assessments, evaluating the algorithm's performance.

- 4. Establish criteria for evaluating the algorithm and determine the appropriate methods of comparison.
- 5. Appraise the performance of the proposed algorithm across different scenarios and distinguish areas for enhancement.
- 6. Scrutinise the pros and cons of the proposed algorithm compared to benchmark methods.

Based on the insight obtained from the HIL experimental exploration, what elements of the algorithm could be upgraded is condensed.

7. Recognise the feasible upgrades to the algorithm and actualise them.

1.3. Thesis outline and key research offerings

Ch. 2 The background information

In Chapter 2, the general background information concerning the smart charging algorithm development is presented from "What, Why and How" three dimensions.

Ch. 3 The impact of uncontrolled EV charging on distribution grids is studied in Chapter 3.

An extensive analysis of congestion was conducted on 21 actual grids of three types (Urban, Sub-urban and Rural) from three European countries (Austria, Germany and the Netherlands) covering the grid performance impact factors including grid type, EV penetration level, seasonal changes in load, PV and EV demand, weekday-weekend alteration in EV demand, location of charging sessions (home, semi-public and public) as well as EV charger accessibility. Grid performance is evaluated based on the magnitude, duration and scale of the impact for node voltage drop, transformer and line loading as a function of increased EV penetration. The interrelation between the impact and the grid feature is also inspected.

Ch. 4 In Chapter 4, the investigation of heuristic EV charging tactics is presented.

Three simple heuristic charging methods are compared vertically with each other and with uncontrolled charging from the perspectives of grid congestion prevention, charging cost minimisation and EV charging completion through simulations on six real LV distribution grids jointly with four EV penetration levels in two representative seasons. By studying the fundamental impact of every single factor, including different charging price schemes, of the chosen three charging methods, the benchmark criteria are then provided for the reference of future smart charging evaluation. The practical requirements of exercising charging protocol IEC61851 is also deliberated.

Ch. 5 Chapter 5 introduces centralised EV charging management schemes aiming at grid congestion mitigation.

A high-efficacy, centralised grid congestion recognition and mitigation algorithm with the Direct Load Control (DLC) mechanism involving Power Transfer Distribution Factors (PTDF) is developed. The congestion management algorithm is combined with three proposed EV Charging Management Schemes (CMSs) where congestion alleviation efficiency, EV user fairness and EV charging priority are selected as the primary targets, respectively. The over-compensation of the grid congestion mitigation phenomenon is also discussed. The algorithm's efficacy is analysed from both DSO and user perspectives, including branch overloading, voltage dip and EV charging demand satisfaction.

The computed grid supply allocation could serve as an input – grid capacity constraint for local energy system optimisation.

Ch. 6 The composition of the EV smart charging algorithm from the aggregator's stand-point and the follow-up Hardware-In-the-Loop (HIL) experiments validation are explained in Chapter 6.

A hierarchical Mixed-Integer Programming (MIP) EV smart charging algorithm is designed for LV distribution grid applications, in which a flexible receding horizon scheme is equipped as a passive mechanism to handle stochasticity within the algorithm. The implementational constraints arising from EVSE-EV communication protocols are integrated into the proposed algorithm. A comprehensive assessment utilising a Real-Time Digital Twin (RTDT)-based HIL setup encompassing eight scenarios is performed. The scenarios explore the algorithm's performance considering input information stochasticity, user behaviour uncertainty and the integration of grid limitations. Finally, detailed guidance for upgrading the proposed algorithm, drawn from the results obtained through HIL simulations, is offered.

Ch. 7 The formulation and assessment of the enhanced smart charging algorithm which is built on the foundation — the primary version introduced in Chapter 6 — is explicated in Chapter 7.

The algorithm advancement emphasises two aspects: effectuality and operability. The improvement in effectuality incorporates charging current setpoint levelling, upscale grid balancing service provision and optimality pursuing. The operability enhancement focuses on the ability to process unforeseen changes in charging sessions, synchronise EV states, and dynamically rectify charging control following the charging relevant parameters. The algorithm functional appraisal features the stochasticity management function validation, quantification of the charging cost savings, offering grid balancing service and assessing the degree of propinquity towards optimality. The results substantiate the accurate functioning of the upgraded smart charging algorithm. Additionally, a heuristic-inspired approach in gaining proximity to optimality is established.

Ch. 8 Finally, the conclusion obtained and the recommendations observed from this thesis are offered in Chapter 8.

The flow chart of the thesis structure is illustrated in Fig. 1.1.

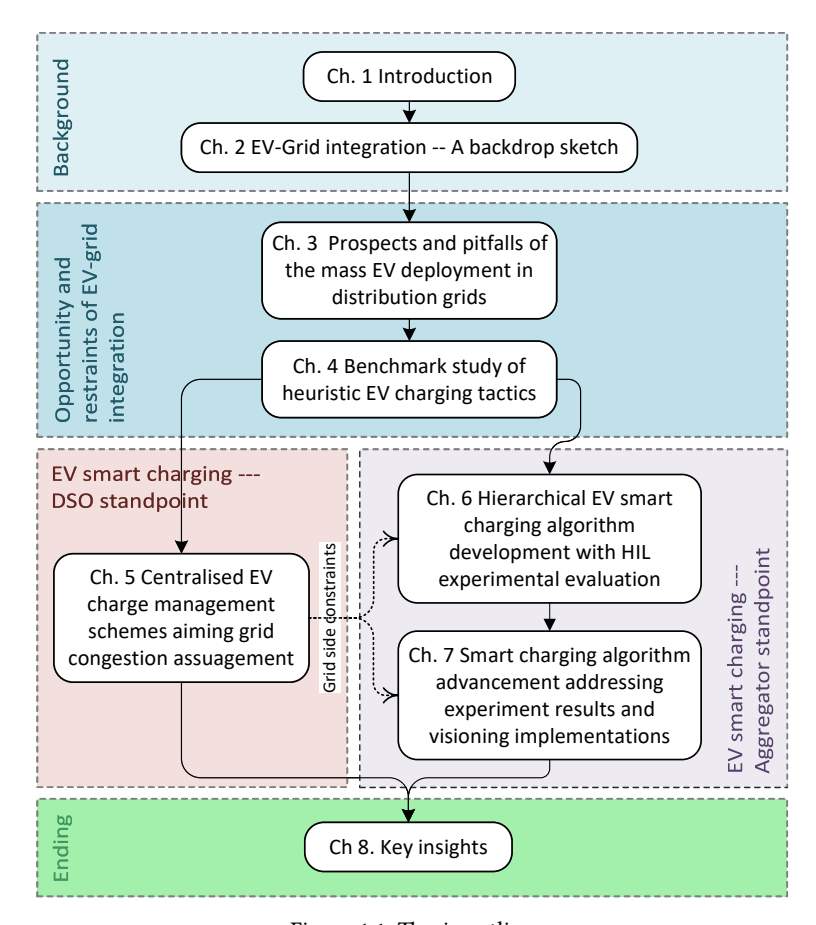


Figure 1.1: Thesis outline

EV-Grid integration – A backdrop sketch

2.1. What unregulated EV charging brings to the current grids

Mass deployment of Electric Vehicles (EVs) can have a detrimental effect on the Low Voltage (LV) distribution networks due to the increased peak demand and unpredictable charging behaviours. The increased number of EVs increases the total demand for power and energy, which can lead to an overload of system assets like transformers and lines [7, 8]. With the growing quantity of EV owners, the increased peak load can be much higher than the percentage of increased EV share. This is because the new charging demand of EVs will most likely stack on top of the existing peak demand. The transformer is thereby under high risk of increased loading, resulting in a decreased lifetime, eventual overloading and ultimately the destruction of the transformer [9, 10]. Furthermore, higher EV penetration levels can aggravate system power losses and voltage deviation, especially at the far end of the lines [11, 12]. It has been found that even with a low level of EV penetration, the furthest nodes already experienced measurable voltage deviations [13].

Assessment of the impact of uncontrolled EV charging on grids has been widely conducted in numerous studies. These studies explored assorted grid types and sizes from standard testing feeders [14, 15] to real Medium Voltage (MV) [16, 17] and LV [18, 19] grids. The topics discussed in these works include the temporal pattern of grid congestion occurrence, the degree of peak demand escalation, the cumulative impact on grids with incremental EV penetration, the highest bearable EV penetration level, and the progression of grid overloading issues and the strained components. It is found that usually between 3:00 and 9:00 a.m. is a congestion-free time window where barely any excessive power loading is sourced from EV charging [14, 20]. A range of 10-40% grid peak load growth can be expected from 20-45% EV penetration levels [14, 15]. The EV penetration level that can be accommodated without causing significant grid problems varies from 20-50% [16, 19, 21, 22] and this range is comparably observed in MV as well as LV grids. Regarding the grid components that are more susceptible to grid overloading, the transformer and line capacities are worth concern [17, 21] in MV grids, while in LV grids the voltage drop is a noticeable issue besides the branch overloading [23, 24].

Although the presence of grid congestion depends on many determinants such as: grid inherent features, problematic components, tolerable EV penetration levels, base load level, distributed energy resources (DRE) installation, and EV driving and charging habits. The electricity grid in its current state would not be able to host the full scale transportation

electrification that is expected without intervention. Apart from hardware reinforcement, grid overloading can be reduced with the use of decentralised generation such as Photovoltaic (PV) [25]. However, power mismatch arising due to the uncertain nature of these resources can lead to local pockets of network congestion that can be avoided if PV to EV charging is integrated [26]. Given the existing physical limitations of the grid, upgrading the infrastructure or implementing smart charging solutions are viable options. Although EV smart charging cannot completely circumvent the need for substantial investments in grid infrastructure upgrades, it still emerges as a cost-effective choice for the time being.[27] The utilisation of EV smart charging is a fast applicable approach for grid congestion prevention, in contrast to the more time-consuming process of upgrading the grid [28, 29].

2.2. Basic practices of EV smart charging

2.2.1. SC design dimensions

The design of a smart charging algorithm considers at least three fundamental dimensions, The optimisation objectives, the selection of suitable algorithms and the control scheme. The characteristic composition of each dimension is subject to the target user, the involved stakeholders, the system architecture and the information availability. **Popular objectives**

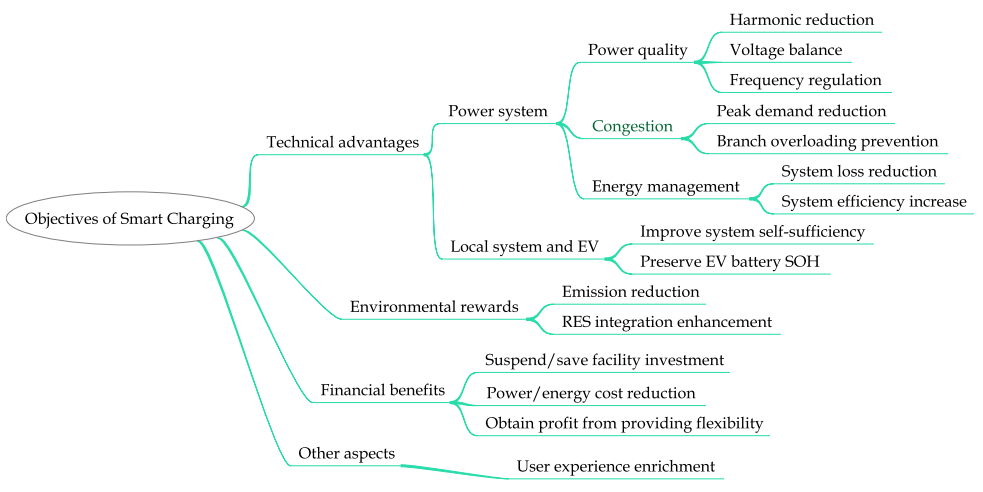


Figure 2.1: Summary of major objectives of smart charging

The set objective(s) of EV smart charging algorithms can be categorised into four groups, namely technical, environmental, financial and other aspects. It is established that the vast integration of EVs into the grid will possibly be accompanied by considerable pressure added to the grid. The primary goal of many algorithms is then to ensure a smooth operation of the EV-connected system. Another compelling drive of the algorithm is its potential financial profits for the user, like saving electricity costs or even yielding extra income by trading on the relevant market, such as providing auxiliary services to the grid. The implementation of a smart charging algorithm can also benefit the environment by decreasing

emissions from combustion cars and supporting further installation of RES [30–33]. A summary of potential smart charging objectives is plotted in Fig. 2.1.

Algorithm types

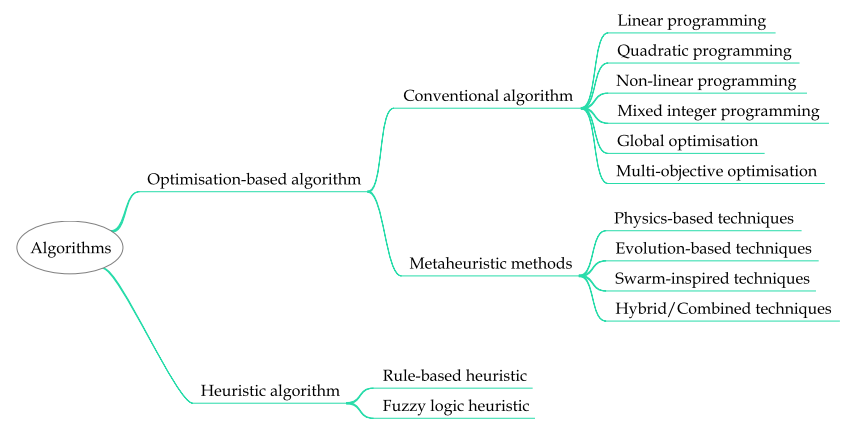


Figure 2.2: Summary of common optimisation algorithms

The route to achieve the set objective is through the design and execution of algorithms. The algorithms that are applied in energy systems can usually be divided into two groups: one is heuristic, and the other one is optimisation-based.

The heuristic algorithm operates on a straightforward and efficient principle, in that EV charging scheduling and energy system regulation can be obtained in short time and with low cost. Albeit optimality cannot be promised in the acquired outcome, good results can always be expected in its designated implementation scenarios [34]. Solving an optimisation problem is fundamentally searching for the best possible solution out of all feasible candidates. If the user aims to find the precise solution through calculus-based search or enumerative search methods, then the conventional optimisation algorithm is the suitable approach. On the other hand, if the optimisation problem is considerable in size and may contain multiple local optimals, then the nature-inspired guided random search technique — meta-heuristic — should be chosen. Ultimately, the determination of algorithm type is rooted in the characteristics of the to-be-solved optimisation problem [35–37]. The summary of common algorithm types that are used in energy systems is exhibited in Fig. 2.2

Algorithm control structures

There are three common control structures that are used in actualising smart charging algorithms, they are: centralised, decentralised and hierarchical control. Centralised control, also called direct control, is solely carried out by the central EV aggregator in its region. Centralised control requests smooth and rapid communication to obtain each EV's information, and it also needs a stable computational capacity to optimise all EVs' charging processes at once. The decentralised control is also known as indirect, distributed or local control scheme. This control structure is oriented by individual local units such as households and EV owners. The employment of this control scheme implies that the local unit holds a degree of intelligence, like a home energy management system or a self-embedded EV charge scheduling function. The hierarchical or hybrid control structure is the hybrid version of both centralised and decentralised control. This scheme shares a centralised

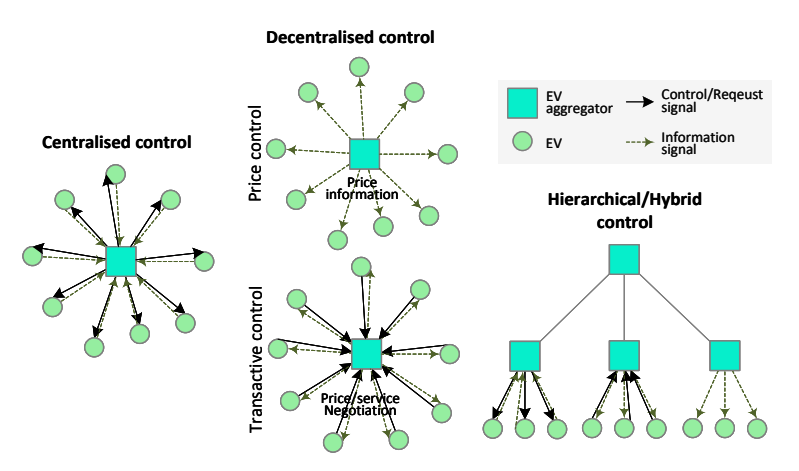


Figure 2.3: Example of common Control structure

control mechanism, but not on a system-wide scale. Instead, this scheme partitions the system into smaller groups and assigns sub-aggregators in between [38–41]. The three control schemes and their common examples can be found in Fig. 2.3.

2.2.2. The key players and the communication protocols

In the field of integrating EVs into the distribution grid, if only consider the operational aspects without worrying about roaming and financial settlement, there are four key players that are essential. They are the (Distribution) System Operators (SO), the EVSE, the EV, and the middle level entity(ies) between SO and EVSE. Multiple layers and players could co-exist between the SO and the EVSE such as different levels of aggregators. For simplification, one general middleman — Charge Point Operator (CPO) and/or aggregator (Aggr.) — is used. CPO operates and maintains the chargers while the Aggr. aggregates and manages the charging process of large amount of EVs, and the CPO can take the role of an Aggr. Currently, there are five smart charging relevant communication protocols that bridge the information exchange between key players. The illustrative summary is shown in Fig. 2.4.

Figure 2.4: The smart charging applicational key players and protocols

Protocol Open Smart Charging Protocol (OSCP) is used to communicate the available capacity of energy/power for consumption or production from the *Capacity Provider*, for example power system operator, to the *Flexibility Provider*, which is the entity that manages the *Flexibility resource* — a controllable prosumer device like stand-alone batteries. The OSCP can be applied to an expanded range of devices in energy systems although it was initially designed for EV smart charging [42].

The Open Automated Demand Response (OpenADR) Communications Specification, as its name suggests, is drafted with the purpose of automating the Demand Response (DR)

actions. This specification is a communication model that enables two-way communication between the energy service provider, the aggregator and the end user. OpenADR translates and communicates the demand response signal like DR event requests or price information from the *Virtual Top Node (VTN)*, such as energy service provider or aggregator, to the *Virtual End Node (VEN)*, like aggregator or end user. The end-use recipient of the DR signal takes actions according to the DR signal through its automated DR program, and OpenADR communicates this response back to its VTN [43].

The Open Charge Point Protocol 2.0 (OCPP) is equipped to support the communication needed for EV smart charging between the Charging Station Management System (CSMS), for example, the back-office of the Charge Point Operator (CPO) which serves as an aggregator, and the Electric Vehicle Supply Equipment (EVSE). The smart charging related information like identification information, charging session timing, metering data, charging profile and so on, is exchanged through OCPP. Similar to OSCP, OCPP also expands its applicable use cases beyond EV smart charging. A new module called Device Model allows the activity-monitoring of devices other than EVSE like transformer, and stand-alone battery in the system [44].

When it comes to communication between the EVSE and the EV, protocol IEC 61851-1 and ISO 15118 are the most commonly applied ones. IEC 61851-1 comprises the electrical safety matters and the operation conditions of the EVSE, and the EVSE-EV communication which serves both AC and DC charging involving charging Mode 1-4. Physical signals that indicate the vehicle states, charging process initialisation, and maximum allowed charging current are transmitted through the control pilot [45]. ISO 15118 compliance with basic signalling specified by IEC 61851-1 and extends to High Level Communication (HLC) which facilitates attributes like identification, load levelling, value-added services as well as payment. These advanced features hence capacitate bi-directional power transfer, plug-and-play, and wireless charging proficiencies through ISO 15118 [46–48].

2.3. EV smart charging algorithm invention — A step by step journey

2.3.1. Seeking balance in intricacy

The sizable EV-integrated distribution grid is a complex system consisting of diverse key players whose interests intertwine or even compete with each other, like market platform, system operator, aggregator, e-mobility service provider, charge point operator and user. Like any other complex system, the primitive challenge for EV smart charging algorithm design is the availability of system information and the consonance among controversial interests/inclinations/predilections of enclosed parties.

Follow the holistic angle

Incomplete information or oversight of relevant aspects of the system could lead to non-optimal or even biased results. For example, study [49] highlights that the charging method that heavily relies on price signalling can lead to a second peak in demand on the service transformer, whose severity and time of occurrence are sensitive to the number of users, the considered price signal as well as its correlation with the base load. Similarly, [50] suggests that even though the charging cost are reduced by 11-16 % with the price-signal-relied optimisation method, an increase in energy loss of 4.3 % relative to uncontrolled

charging is observed. Accessible grid information is essential in helping ease the grid impact induced by EV charging, while the charger and EV driving information are vital to the charging experience. The decentralised charging method combining node voltage data and the EV SOC information introduced by [51] proves that both under-voltage and transformer overloading probability drops significantly as compared with uncontrolled charging while saving 11.5 %in charging cost. The outcomes of EV charging scheduling methods involving voltage-droop mechanisms tend to be sensitive to the charge point location in the grid, especially their branch distance from the substation. That is because downstream nodes opposite to the substation have a relatively greater voltage drop due to the higher impedance of the distribution branch [52]. Awareness of load demand distribution, grid components' specification as well as their geographic information is helpful in compensating for the potential discrimination[53] EV user habit information such as car arrival time, parking duration and charging preferences like priority, price etc., can not only benefit the performance of the charging algorithm, but also improve the user experience. The enhanced EV user experience includes reduced charging cost and comes with a fulfilled charging request [54], preserved battery lifespan [55, 56], less queuing time [57], and equitable power division when the grid is at risk of overloading [58].

There is no doubt that the availability of data is the precondition for many functionalities in EV charging algorithms, and it is built upon the accuracy and rapidity of the data transfer among included parties. The EV charging management system proposed in paper [59] suggests a bidding process within a transactive energy market in which the EV fleet information is requested beforehand, as well as the EV users' preference towards the clearing price. On top of that, the EV users who choose to participate in this trading are expected to provide their power limit and price-power response curve every time interval. Similarly, study [60] incorporated several aspects other than EV scheduling in its optimisation problem including systematic supply-demand balancing, PV power generation, energy storage as well as V2G performance. To facilitate all these capabilities, the predictive data of the system in the time scale of day-ahead, hourly till real-time is required. Therefore, high-quality and stable communication serves as the backbone of the complex system.

Trade-off between objectives

As introduced in Chapter 2.2, Most of the controlled charging of EVs share one or more of the four prevailing primary targets[61–64]: (i) grid impact mitigation, (ii) profit maximisation, (iii) enhance service to EV users, and (iv) improved renewable energy resource utilisation.

To achieve multiple targets with one single smart charging scheme, multi-objective or multi-level optimisations are often used, which in turn increase the requirement for the amount, accuracy and speed of the communication. A good example is that the EV smart charging method proposed in research [56] not only incorporates battery lifetime protection and PV power generation into the stochastic dynamic programming but also integrates grid capacity as well as energy storage optimisation in its objective function. However, the primary targets can become competitive towards each other under certain operational conditions. For instance, iresearch suggests in [62] that prioritising peak shaving can half the maximum demand, albeit at the cost of 5-10 % increase in average energy costs. Further, while the method proposed in [63] successfully satisfies load congestion

and voltage drop constraints relative to 70% exceeded constraints in uncontrolled scenario's, it is noted that location-specific customer demands may lead to a fairness challenge, warranting further investigation. An interesting approach in [64] attempts to include fairness in imposing grid limitations by setting priority criteria for coordinated EV charging depending on available parking time and energy demand of the connected cars. Study [51] compares two decentralised charging algorithms of which one takes the user's priority into consideration and the other one doesn't. The results show that with the user priority-infused method, an average of 15% charging cost reduction is obtained at a cost of up to 26% increased transformer overloading probability and a rise of supply failure rate.

These leading algorithms highlight the importance of multi-objective optimisation in addressing the underlying trade-offs using accurate information and fast communication between different agents.

Complexity in system design

Realising advanced functionalities in a complex system is challenging. Complex hierarchical control structures are often employed to incorporate multiple functions in advanced EV charging algorithms. Paper [65] proposes a two-level hierarchical charging coordination algorithm where the upper-level controller is in charge of grid power dispatch and the station-level controller manages the local charging scheduling. The algorithm in [66] has three levels of actions and each of which shares different functionalities. The first level participates in the day-ahead (DA) or real-time (RT) market and obtains the quantity of cleared energy, the second level aims to optimally dispatch the energy budget obtained from level one to the EVs in the system and finally, the objective of the third level is to respond to the up and down regulation requests. Apart from compound structures associated with multi-objective optimisation, smart charging algorithms also deal with uncertain load demand forecasting, renewable energy generation and arrival/departure time of the EVs, usually by employing a multi-timescale optimisation scheme. In [67], building operational cost reduction of approximately 6 % was achieved using a two-stage algorithm for DA scheduling and RT operation as compared to the baseline case where only prediction of PV output was considered. Similarly, an algorithm developed in [60] optimises the system in four stages along the time scale from prediction to DA, hourly-ahead and finally to RT to show that even though EV energy consumption is the same, the overall cost with an hour-ahead schedule is 1.55 times higher than RT control mainly due to uncertainty in PV generation.

All the above-mentioned challenges would become exponentially harder in the realenvironment applications, in which practical constraints are taking place. Thenceforth, the imperial validation is the next exercise in line.

2.3.2. From conceptualisation to actual implementation

The feasibility and functionality of practical EV charging scheduling methods have been successfully validated using several pilot projects [68–71]. It is pivotal to broaden this initiative for the practical verification, enhancement and eventual demployment of smart charging algorithms. Other than the variety of configurations applied such as diverse EV charging behaviours, different grid topologies and scales, varying local loads and renewable energy generations, as well as fluctuating electricity prices, the main challenge in implementing smart charging in real applications lies in coordinating the entire system.

From a technical point of view, the supporting system that facilitates EV charging covers the physical components like the grid connection, the EVSE, EV and their accessories; the information and communication systems including both the developed smart charging algorithm and the control system embedded in EVSE and EV, along with communication protocols linking these discrete components together [72, 73].

A working intact EV smart charging system requests the proper function of each component, and indispensably, the compatibility and coordination among individual components[74], protocol interoperability [75] and communication reliability and synchronicity [76]. Whether the SC algorithm works as expected is determined by how harmonious the rest of the information and communication part of the system functions. A rightful communication protocol is a must for a successful interface between components and the realisation of specific functions [77]. Therefore, conducting a system integrity examination is essential to ensure a smooth implementation of the EV smart charging algorithm. Due to the complex nature of the system, conducting exhaustive validations of the system integrity and evaluating its performance in real systems is formidable. Exploiting the Power Hardware-In-the-Loop (PHIL) setup as an experiment platform has become a popular intermediate solution, thanks to its flexibility in providing quasi-real testing environments as well as modular testing components [78].

Nevertheless, even if the system operates as expected, inevitable errors may still present during EV charging due to intrinsic characteristics of the system components. For example, the communication latency from the CPO to the EV is expected and the duration could be up to 60 s [79]. Given that the EVSE only sets the maximum charging current and the EV determines the actual charging current, the disparity between the setpoint and the real charging current can be up to 53% [80]. It is therefore essential to consider the aforementioned complexities in smart charging algorithm design. By doing so, the algorithm can be better equipped to handle complex implementation obstacles, ultimately achieving a flexible and reliable charging experience for users.

Prospects and pitfalls of the mass EV deployment in distribution grids

In this chapter, the impact of Electric Vehicle (EV) uncontrolled charging with four levels of EV penetration in overall 21 real low voltage distribution grids in two seasons is analysed. The employed real grid data is provided by distribution system operators from three European countries: Austria, Germany and the Netherlands. At least six grids in each country were considered and they are categorised into three types, namely rural grids, suburban grids and urban grids. The EV charging data used in this study is based on real measurements or surveys. The seasonal and the weekday-weekend factors are also considered in the EV charging impact research. Three key congestion indicators, the transformer loading, line loading and node voltage as well as several other evaluation indexes are studied. The results reveal that the majority of the simulated grids had no or minor moments of mild overloading while a few rest grids have critical issues. Among all the grids, suburban grids are the most vulnerable to massive EV integration. Out of the evaluated grids, those who are located in Germany have the highest redundancy for high EV penetration accommodation. Overall, the impact of uncontrolled EV charging depends on the combination of EV charging demand as well as the grid's inherent features.

3.1. Introduction

It is well established that the market penetration of Electrical Vehicles (EVs) is rapidly growing and consequentially, the technological impact of this mass deployment has attracted considerable research attention [14, 20, 81–83]. The grid impact is particularly relevant because the conventional uncontrolled charging strategy, in which the EVs start to draw the rated power at the instant of connection, can result in numerous simultaneous charging events [84]. The widely implemented level 2 AC charging has a rated power that can be high as 22 kW (3 phase 32A) [45]. Such charging requirements due to an anticipated increase in EV penetration levels can stress the facilitating distribution grid infrastructure, such that it can cause transformer overloading and lifetime reduction [14, 20, 82, 85, 86], line overloading [20, 82, 87], voltage drop below acceptable limits at the far-end of the feeder [14, 20, 82, 86], higher distribution losses [14, 20, 82], power mismatch between

^oThis chapter is based on paper: Y. Yu, D. Reihs, S. Wagh, A. Shekhar, D. Stahleder, G. R. C. Mouli, F. Lehfuss, and P. Bauer, Data-driven study of low voltage distribution grid behaviour with increasing electric vehicle penetration. *IEEE Access*, vol. 10, pp. 6053–6070, 2022

supply and demand, phase imbalance [20, 86], as well as harmonic distortion [88]. It is suggested in [83] that future work investigating the grid impact with increased EV penetration can be scaled up when real-world transportation and power data becomes available. The specific aim of this chapter is to contribute towards this goal and provide realistic insight based on the acquired on-field data sets.

3.1.1. Literature review

The influence of data-driven uncertainties in driver behaviour and energy demand of the EVs toward the grid impact of uncontrolled charging is considered in [14-16, 20]. For example, [14] uses data of the daily miles driven and the arrival times to show that the load demand for a 34-node IEEE test feeder has no noticeable change from 3:00 a.m to 11:00 a.m even with 45 % EV penetration level, resulting in approximately 11 % (in summer) and 15 % (in winter) increased peak from the average loading ratio. In [20] the IEEE RTS load profile data was clustered into representative curves to show there is no loading variation for IEEE 123-node test feeder substation in 3:00 a.m to 9:00 a.m window even considering 100 % EV penetration, but the probability of overloading the 50 kVA transformer increased to 35 % with the peak demand increasing linearly by 2-3 % for every 10 % increase in EV penetration. Study [16] tested four charging methods with several scenarios including the uncontrolled method with a 33-buses sample grid and assess the impact on the distribution system. It is found that EV penetration levels of 28.1-46.5% can be accommodated in the system without violating the grid constraints. An 11 kV 38-node typical UK sample distribution system was used in [15] to test three representative uncontrolled EV charging scenarios and one "smart" charging scenario. The results indicate a 35.8% peak load growth with 20% EV penetration in the worst uncontrolled charging case. However, these papers consider standard test grids in the study and therefore, extending the insight with real distribution grid data can be useful.

Research [89] studies the charging impact of 0 to 500 EVs in a modified IEEE 13-bus system as well as a 25-bus real Taiwan distribution system. One thousand iterative Monte Carlo simulations were conducted to study the stochastic effect of both the feeder load and EV charging while using measured data at two large charging stations. It appears in the results that for the real grid there is no voltage drop violation even with the worst scenario, but for the IEEE standard grid the congestion problems are already present with 200 EVs and the under-voltage problem develops earlier than the line congestion. Two distribution systems located at a residential-urban area and an industrial-residential area with 35, 51, 62% EV penetration levels were modelled in [90]. This study examines the impact of two charging patterns (valley and peak hours) and found that a maximum of 19% total actual network cost is required to increase the capacity and accommodate all charging requests. Paper [21] investigates three real distribution grids (urban, rural and commercial) with 20, 40, 60, 80 % EV penetration levels. The result shows that transformer overloading can already be observed for 20% EV penetration in the urban grid, but in the rural grid, the EV penetration can increase to 40%. None of the grids has under-voltage problems, and line loading is not discussed in the paper. Study [17] investigates EV integration into a cluster of real distribution grids with 39-feeders in the USA. The examined network contains a mix of area types, where half of the feeders supply residential areas and the rest are distributed among industrial, commercial and agricultural areas. The EV charging data is modelled based on real vehicle itineraries and only one EV penetration level (one EV per household) is analysed. The study concludes that 58% of the feeders reach their power capacity limit and 47% of the grids have shown line overloading problem, yet none of the grid's experiences voltage drop to lower than 0.9 p.u.. What is the maximum number of EVs that can be integrated into the grid is explored in [91]; the mobility of EVs are also considered. Two Swedish distribution networks where one residential network with 3 feeders and 26 substations and one commercial network with 4 feeders and 9 substations are employed. When the system runs in normal conditions, only in one case which all EVs only charge at home in the residential area can the grid accommodate less than 100% EV penetration. However, if any feeder is disconnected due to maintenance, the grid can experience overloading even without any EV charging. Besides, none of the grids has any under-voltage problem in the simulations. Study [18] considers an even larger area in the Netherlands where the simulated network contains 55 distribution systems that consist of a total of 12,000 substations. It is assumed in this study that EVs only charge at home with two fixed power levels, and the charging profile is generated based on a big dataset of Dutch driving patterns. An increase EV penetration trend along with time up to 75% in the year 2040 was assumed and 49% of the transformers experience overloading issues at the worst scenario. All the works mentioned above focus on the big scale in which the grid performance of MV distribution systems is evaluated as a whole, a closer insight into each LV distribution grid would be beneficial.

While [23] investigates a real LV distribution grid in Norway to suggest an overload and under-voltage tolerance up to 20% and 50% EV penetration level respectively, the paper highlights the limitation that the charging profile is derived from a single household load profile and thereby neglecting the uncertainties in arrival and departure time as well as energy demand that can occur with mass deployment of EVs. The results suggest a 20% EV penetration tolerance boundary with no grid limitation violation.

In paper [24], historical driving data was used to generate home EV charging profiles and four EV penetration levels from 25% to 100% were tested on a real Danish LV distribution grid model. The paper explores grid loading and phase unbalance caused by EV charging. It is found in this study that the loading induced by EV charging at home is not high as expected due to a relatively low simultaneous factor (45%). It's also concluded that a 30-50% EV penetration is the maximum acceptable uncontrolled charging integration rate, depending on the characteristics of the grid. Researchers of [19, 22] ran a plentiful of Monte Carlo simulations to investigate the EV charging impact of 0-100% penetration levels on two real British LV distribution grids whose grid types are not specified. The EV data implemented for simulation is originally from a one-year-long site trial. The main discovery regarding uncontrolled EV charging impact is: the transformer overloading is the main issue in network 1 while voltage drop is the main challenge of network 2. The upper limit of EV accommodation without grid congestion problem is 40% for network1 (thermal limit) and 20% for network 2 (voltage limit). Another study inspects both real transmission and distribution grids performance with 0-100% EV penetration with real EV charging data [92]. In the paper, three LV distribution grids were investigated, rural, suburban and urban. It is found that with 100% EV penetration, there is voltage drop violation and possible transformer overloading. However, the results might still vary a lot and strongly depend on the local EV, households and grid features. Besides, it is predicted that by 2030, 10% of the distribution grids will suffer from transformer overloading issues

and 5% of the distribution grids will have under-voltage problems. In total, 28% of grids would require upgrades.

Therefore, it is extremely compelling to investigate what might be the influence factors of the outcome and if there is any internal trend we can summarise when studying the grid performance with massive EV integration.

3.1.2. Contributions

The focus of this chapter is to use measured probabilistic data pertaining to energy demand, arrival and departure time of EVs to investigate the impact of uncontrolled charging for several actual grids in Europe. The findings are useful and add to the body of knowledge in the following aspects:

- We show that Suburban grids have relatively higher congestion issues compared to rural and urban grids.
- We also investigate how the type of grid in different countries affects the grid impact
 of uncontrolled EV charging. Austrian distribution grids are most vulnerable to grid
 congestion, followed by the Netherlands, while German grids are most robust seeing
 no overloads even with the highest modelled EV penetration.
- The grid performance impact factors including seasonal changes in load, PV and EV demand, weekday-weekend changes in EV demand, location of charging sessions (home, semi-public and public) as well as EV charger accessibility are investigated and discussed. All the above factors have not been dealt with together in previous works
- Grid performance is evaluated based on magnitude, duration and scale of the impact for node voltage drop, transformer and line loading as a function of increased EV penetration. The interrelation between the impact and the grid feature is also inspected.

The numerical results for these key observations are comparatively quantified using grid simulations and presented in the subsequent sections.

3.1.3. Structure of the chapter

The simulation setup and the data-driven approach is in-detailed explained in Section 3.2. The simulation results of three countries and three grid types are analysed in Section 3.3. The study of grid performance impact factors including winter-summer, weekday-weekends, plus EV charger accessibility is also placed in Section 3.3. The detailed interpretation over several grid performance key indicators is given in Section 3.4. Finally, Section 3.5 reports on the studies conclusions and recommendations for future work.

3.2. Methodology: Data-Driven Approach for Realistic Grid Impact Evaluation

In this section, three layers of data-driven considerations of simulation input data are described, followed by the depiction of the simulation methodology as well as the output data.

- 1. Actual Grids segregated by (a) geography (b) function. (Section 3.2.1)
- 2. Historical power profiles in the corresponding grid. (Section 3.2.2)

3. Measured EV charger data and survey-based car driving data pertaining to charging energy demand, arrival and departure time based on different charger types. (Section 3.2.3, 3.2.4)

In each subsection, how the raw data was acquired and pre-processed are explained respectively.

3.2.1. Grid Specific Data

Actual representative grids from three countries, namely, the Netherlands (NL), Germany (DE) and Austria (AT) are obtained from the Distribution System Operators (DSO). Further, three different functional grid types; rural (RR), suburban (SUB) and urban (UB); are considered. For each of these 9 categories, at least two test grid data per type per country is acquired, as summarised in Chapter Appx. 3.5.

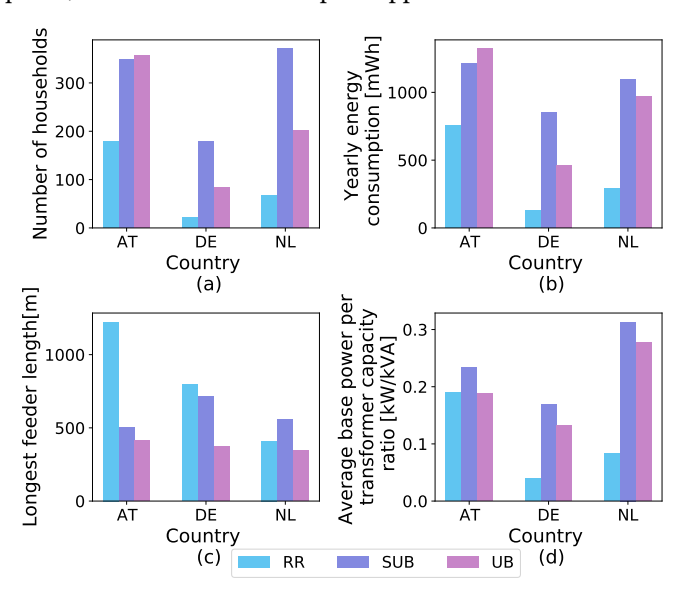


Figure 3.1: Comparison of basic grid features based on the 9 categories defined for the country and functional type (a) total number of households (b) yearly energy consumption (c) length of the longest feeder (d) the ratio of average baseload power with the total transformer capacity

Fig. 3.1 compares the average values of the listed basic features based on 3x3 defined categories. The compared basic features are: total number of households ($N_{\rm hh}$); yearly energy consumption ($E_{\rm yr}$); length of the longest feeder, which is the length of the feeder from the transformer to the farthest end of the grid ($L_{\rm f,max}$), and the ratio ($\tau_{\rm b,avg}^{\rm norm} = P_{\rm avg}^{\rm trafo}/C_{\rm tot}^{\rm trafo}$) of average base load power ($P_{\rm avg}^{\rm trafo}$) with the total transformer capacity ($C_{\rm tot}^{\rm trafo}$). $\tau_{\rm b,avg}^{\rm norm}$ value is related to minimum reserve capacity and it can be used to identify which grids are relatively more vulnerable to overloading. In Fig. 3.2, all grids are clustered into two groups based on their number of households and yearly energy consumption. Cluster 2 grids have both high $N_{\rm hh}$ and $E_{\rm yr}$ values and Cluster 1 grids have relatively low $N_{\rm hh}$ and $E_{\rm yr}$ values. Most of the SUB grids and AT grids fall in Cluster 2 while the majority of RR grids, as well

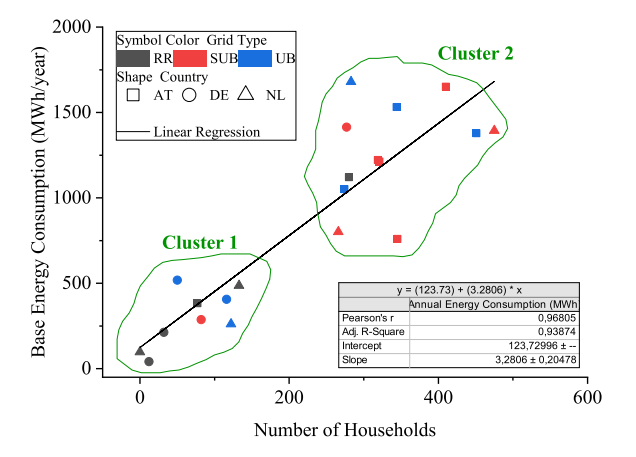


Figure 3.2: Clusters for base energy consumption as a function of the number of households for different category combinations of grid types and countries.

as DE grids, are in Cluster 1. The line features of each grid type in every country are also plotted and compared, which can be found in Fig. 3.3. Each dot in this box plot represents a line (cable) in the grids. Fig. 3.3 (a) shows the line rated current and it is clear that DE grids have a greater number of high-capacity lines compared to other countries. Similarly, the length of every line in each country is plotted in Fig. 3.3 (b). It can be observed that AT grids have relatively long lines and NL grids have shorter lines implemented.

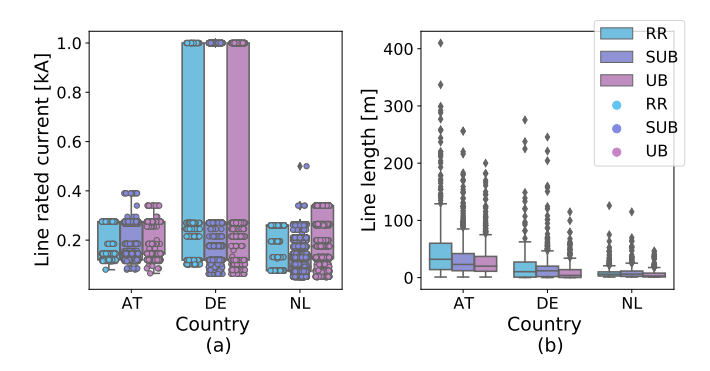


Figure 3.3: Grid line feature comparison between countries and grid types. (a) Line rated capacity in ampere (b) Line length in meter

Fig. 3.1-3.3 show that in general SUB grids have the highest $N_{\rm hh}$, $E_{\rm yr}$ and $\tau_{\rm b,avg}^{\rm norm}$ relative to other functional categories for the given country. An out-liner to this trend are the $N_{\rm hh}$ and $E_{\rm yr}$ values of AT-UB grids, which are both slightly higher than the AT-SUB grids. Since EV penetration is assumed proportional to the $N_{\rm hh}$ in this chapter, it can be inferred that an increase in serviced EVs for the given penetration level will be maximum for the SUB functional category. RR grids have the lowest $N_{\rm hh}$, $E_{\rm yr}$ and $\tau_{\rm b,avg}^{\rm norm}$ across functional

categories for any given country. Therefore, it is least prone to increase in EV penetration. However, RR grids have relatively high $L_{\rm f,max}$ (NL grid is an out-liner). Therefore it is important to determine the minimum node voltage levels in these grids.

It can be inferred that for all functional category types, DE grids have maximum country-specific reserve capacity as indicated by lowest $N_{\rm hh}$, $E_{\rm yr}$ and $\tau_{\rm b,avg}^{\rm norm}$. Furthermore, the number of serviced EVs per grid is lowest in DE for a given penetration level. In general, AT grids have the highest $N_{\rm hh}$, $E_{\rm yr}$ and $\tau_{\rm b,avg}^{\rm norm}$ across functional categories, indicating lowest reserve capacity and a high number of serviced EVs for the given penetration. NL-SUB grids have the highest $N_{\rm hh}$ and therefore suggesting the highest increment in number of serviced EVs for the given penetration. At the same time, relatively high $\tau_{\rm b,avg}^{\rm norm}$ indicates a low reserve capacity in NL-SUB grids, making them vulnerable to transformer overloads. Furthermore, a significantly higher $L_{\rm f,max}$ value for AT-RR grids suggests a wider spread of service area in these grids, thereby suggesting issues related to low node voltages are more likely in the former.

3.2.2. Load and Photo-Voltaic (PV) profiles

In this study, the load and PV profiles were generated based on historical measurements or standardised profiles and the information of the unit, i.e. the each load's yearly energy consumption and the PV installation capacity.

The load energy consumption information of all three countries was provided together with the grid models by DSOs. The standardised load profile for Austria is available through AT Power Clearing & Settlement group [93], the standardised load profile for DE grids was obtained through the German Association of Energy and Water Industries, BDEW [94] and the standardised load profile for NL can be acquired from the Dutch Energy Data Exchange Association [95]. The standardised profiles are available for different load categories in each of the original data sources. For this study, three different categories are employed to model the baseload profiles. In Fig. 3.4, the load profiles of a load with 1000 kWh/yr energy consumption are presented for all three countries. For AT and DE grids, the three used profile types are household, business and agriculture. The load categorisation is slightly different for NL grids in that they are distinguished by connection capacities, namely E1, E2 and E3 type groups. E1 types are small size connections that can be considered as households. E2 types are medium size connections with a different peak time compared to E1 types, and this type group is usually seen in small businesses like shops and companies. The E3 type group are other big capacity connections, for example, manufactures, farms. Fig. 3.4 not only compares the seasonal difference between different profiles but also shows the variations during weekdays and weekends. Almost all summer profiles are slightly smaller than the winter profiles except the business profile in AT. We can also see from this figure that business profiles in AT, DE and E2, E3 profiles in NL drop during the weekend. Therefore, the summer baseload is lower than the winter baseload for a certain grid. For a grid with more small business loads, a decreased weekend baseload could be expected.

For AT grids, the information of the installed PV is available in the grid models provided by Austrian DSO. The standardised PV profile was derived from weather data using the Python package PVwatts from NREL [96]. The raw standardised PV profile is in an hourly resolution, but an interpolation method was applied and the fluctuation of the per-minute

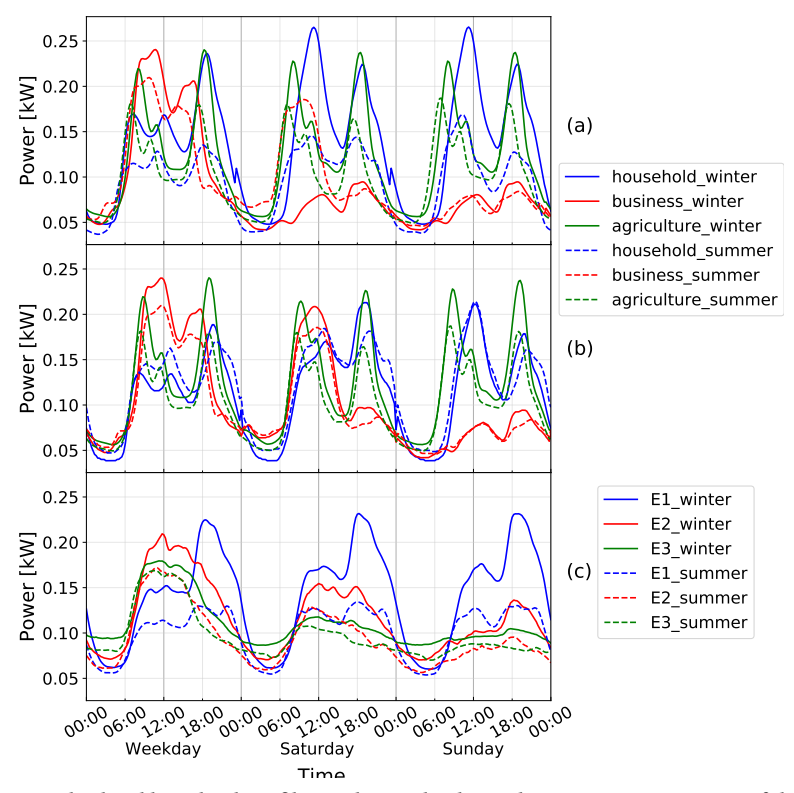


Figure 3.4: Standardised base load profiles with 1000 kWh yearly energy consumption of three countries, (a) AT, (b) DE, (c) NL

PV power is introduced in the profile during the simulation. Similarly, the PV information including the location and capacity of installed PV systems is included in the DE grid models. The PV standard profile was generated by Meteonorm software, where ambient temperature and wind speed were considered and an optimal azimuth and tilt angle was assumed [26]. The PV installation information was not available via Dutch DSOs, thus an assumption was made based on the PV installation [97, 98] and the Dutch households [99] statistics. The PV installation assumption for NL grids is 25% PV penetration in RR grids, 15% PV penetration in SUB grid, and 5% PV penetration in UB grid where each installation has a 2.5 kW rated power. The PV penetration is calculated based on the number of loads in the grid. The standardised PV profile of NL is generated based on previous work [100]. The standard PV profile of all three countries with a 1 kW capacity installation in one summer week and one winter week is shown in Fig. 3.5.

3.2.3. EV penetration representation

In this study, the EV penetration levels 0%, 20%, 50% and 80% were simulated, where the EV penetration is defined as the percentage of total cars in a certain grid. The EV penetration level in simulations is handled in the form of the total number of charging sessions. The number of EVs in a certain grid is calculated as the product of the total number of households ($N_{\rm hh}$), the car ownership distribution (car per household, $\alpha_{\rm car,hh}$)

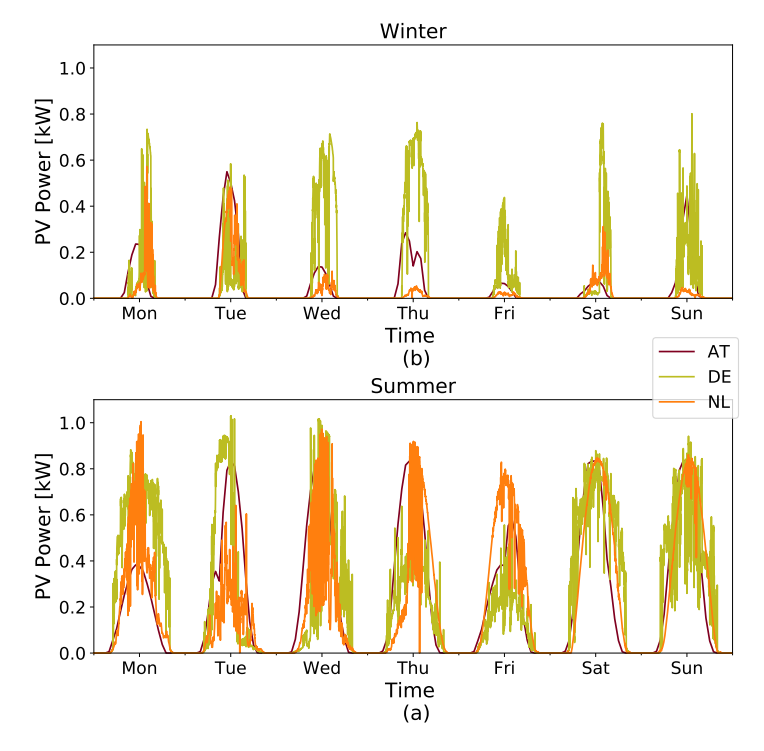


Figure 3.5: Standardised PV generation profiles with a 1kW peak rate of three countries (a) One sample winter week (b) One sample summer week

and the EV penetration level (γ_{EV}), as shown in Eq. (3.1).

$$N_{\rm EV} = N_{\rm hh} \times \alpha_{\rm car, hh} \times \gamma_{\rm EV}$$
 (3.1)

For all three countries, the number of households in the grid was provided by the DSOs. In AT models, car ownership is calculated based on the data of population, household size and the car per-capita registration data [101]. For NL, the car ownership data is assumed based on [102] and for DE the car ownership assumption data is provided by the German DSO. The summary of EV ownership distribution is shown in Table 3.1.

Table 3.1: EV ownership distribution

Car ownership distribution			Grid type			
$(\alpha_{\rm car,hh})$			RR	SUB	UB	
	AT		1.5	1.35	0.75	
Country	DE		1.6			
	NL		1.25	0.9	0.5	

To simulate the impact of excessive charging demand caused by massive connected EVs, the total number of EVs in a certain grid needs to be converted to the corresponding EV charging sessions. The total EV charging sessions in a grid is calculated by its total number

of EVs ($N_{\rm EV}$) times the charging frequency ($\beta_{\rm sess,EV}$), which is the average charging sessions per EV during a certain time period, as presented in Eq. (3.2).

$$N_{\text{sess}} = N_{\text{EV}} \times \beta_{\text{sess EV}} \tag{3.2}$$

In addition, the charging sessions are categorised into three types namely home, semi-public and public, based on their features like location of charging, time of arrival and duration of parking, as described in a previous study [103]. The charging sessions are then translated into different types of chargers to integrate into the grid simulation. Similar to local load and PV generation modelling, several data resources were used for EV charging demand modelling as well. Half of the EV demand data is based on the real measurement from EV chargers, so they are easy to be processed and ready to use. However, the other half of the raw EV demand data is based on real car driving statistics. This means extra steps are requested to convert these mobility data into EV charging demand. How these data were processed and implemented is explained in detail in the next section.

Approach 1 Approach 2 Raw data feature Car mobility based Charger measurement based Charge frequency ($\beta_{\text{sess,EV}}$) 0.9 per day 4 per week Grid type RR SUB UB RR SUB UB Home 90% 98% 74% 70% 50% 25% Charging session Semi-public 25% 5% 1% 15% 15% 12.5% distribution Public 5% 1% 15% 25% 12.5% 11%

Table 3.2: EV charging session distribution

Due to the nature of the raw EV charging demand data, there were two approaches implemented to model the increasing EV penetrations in the grid. For car mobility based data, approach 1 is applied. In this approach, the chargers are placed at every household, workplace and shop node and the total number of chargers is fixed for all EV penetrations. The higher the EV penetration level is, the more charging sessions will occur, hence more chargers will be used. The average EV charging frequency of this approach is an outcome of the EV trip modelling, and the value is 0.9 times per day. With charger measurement based data, approach 2 is employed. Unlike approach 1, the number of chargers increases along with the EV penetrations in approach 2, but the location of the chargers in lower EV penetrations will not change for higher EV penetrations. This means the higher EV penetration scenarios are modelled by only adding new chargers on top of lower EV penetration scenarios. The average EV charging frequency of this approach is assumed to be 4 sessions per week per EV [104]. For both approaches, the charging sessions in lower EV penetration scenarios are preserved and the new charging sessions are added for higher EV penetration levels in a different format. This makes sure the only difference between different EV penetrations is the added new charging sessions for a certain grid. The summary of EV charging session distributions of both approaches is shown in Table 3.2. How the charging profile of each charging session was modelled is introduced in the next section.

3.2.4. Historical measurement-based EV fleet and demand profile generation

The EV charging profile data consists of two parts, the EV fleet composition and the featured data of every charging session. Six to ten top-selling EVs in each country were selected to compose the EV fleet based on their market data in 2018 separately [101, 105, 106]. As introduced in the previous section, the two raw EV data resources lead to two approaches of charging session modelling as well. Approach one needs extra steps to convert EV trip data into charging session data including EV arrival/departure time, EV arrival SOC and charging energy requests. While approach 2 models EV charging sessions directly from charger point of view based on the real charger measurements. Approach one was applied to all the AT grids and half of the DE grids while approach two was applied to the rest of the grids.

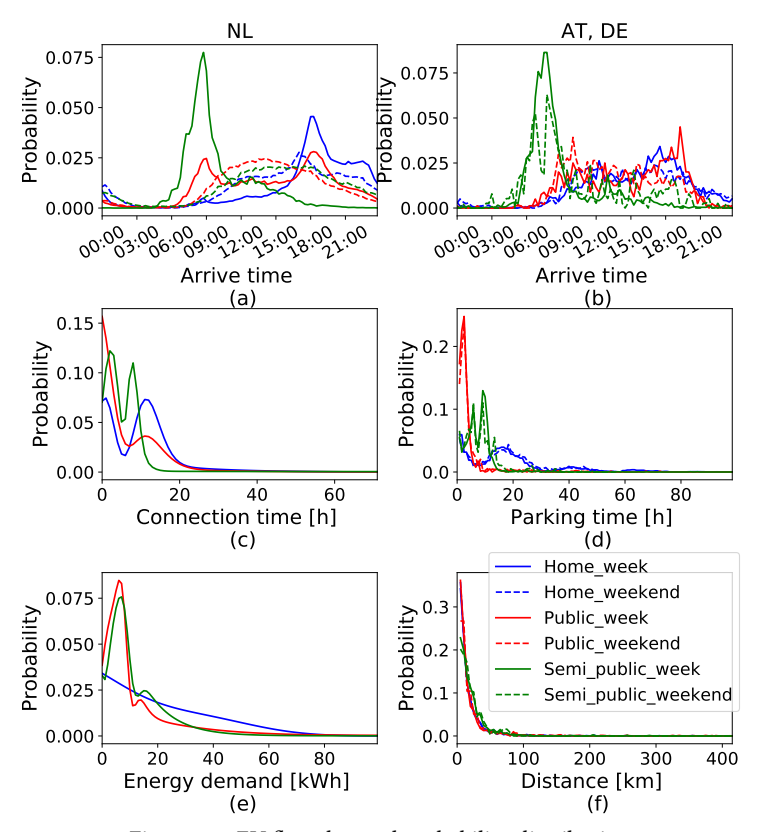


Figure 3.6: EV fleet demand probability distributions

For approach 1, the mobility survey "Österreich Unterwegs 2013/2014" [107] conducted by the Austrian ministry of transportation serves as a good base for the probabilistic modelling of typical driving behaviour observed in rural, suburban and urban areas in Austria. This survey contains information on 196,604 trips which offers the time, frequency and distance distribution of the trips throughout the week. A Monte Carlo Approach as de-

scribed in [108] was applied to generate specific trip data for each of the simulated electric vehicles by using the aforementioned EV fleet and trip data. In the end, these trip data were translated into time, location, duration and charging energy information at the chargers.

Approach 2 simulates the charging sessions from the charger perspective and the employed data is based on a study conducted by ElaadNL[104, 109]. In this study, more than 1.5 million charging sessions were recorded and analysed, and the probability distribution of featured information of charging sessions including EV arrival time, parking duration and charged energy were provided. A Monte Carlo Approach was implemented to generate the charging session data based on the EV fleet as well as the charging session featured data. For both methods, several boundaries were set to ensure there are no anomalies in the generated data.

The probability distributions of EV charging session's arrival time, parking time and the energy demand/driven distance are presented in Fig. 3.6. All data is distinguished between weekdays and weekends except the EV parking and energy demand data in the Netherlands. The plot of NL EV arrival time distributions indicates that every type of charging session presents at least one of the morning/evening arrival peaks during the week, while the weekends' arrival times are mainly accumulated in the latter half of the day. Apart from that, there is only minor weekday-weekends differences appeared in other distribution curves. Besides, the CC-CV charging stages of the battery were also considered in the charging profile modelling.

3.2.5. Methodology and simulation data

The simulations of this study were carried out with Python interfaced DIgSILENT Power-Factory load flow simulations. A Python script was written to read input and modify the parameters in Power-Factory, then to initiate the load flow calculation at every time step. After every step of load flow analysis, the results were read and stored by this script as well. The input data for simulations are the aforementioned profiles. The raw output data of the load flow contains the loading/power/losses information of all the branches (including the transformer, the cables as well as the other link elements like fuses, impedance), and the voltage information of every node at every time step. All the EV chargers are modelled as constant power loads since it is our intention to see the consequence of all EVs being charged with their rated power without the influence of voltage drop at the end of the feeders. In this study, the overloading limit of transformer and lines are set to be 100% of their ratings and the under-voltage threshold is set as 0.9 p.u. [110]. The raw data was then processed and analysed referring to these limits.

It should be noted that even though the input information used for simulation is based on real data, it cannot cover all the possible situations in real life. The local load, PV generations and EV charging patterns are uncertain naturally. This study picked one possible combination and executed deterministic simulations to give an insight into the distribution grid performance under the influence of uncontrolled EV charging. Based on the there-layer data-driven considerations, the derived results of our work are close to reality, and therefore the presented insight is useful.

3.3. Simulation Results and impact factor discussion

In this section, the simulation results are presented and compared. The possible impact factors of the results are analysed and discussed as well.

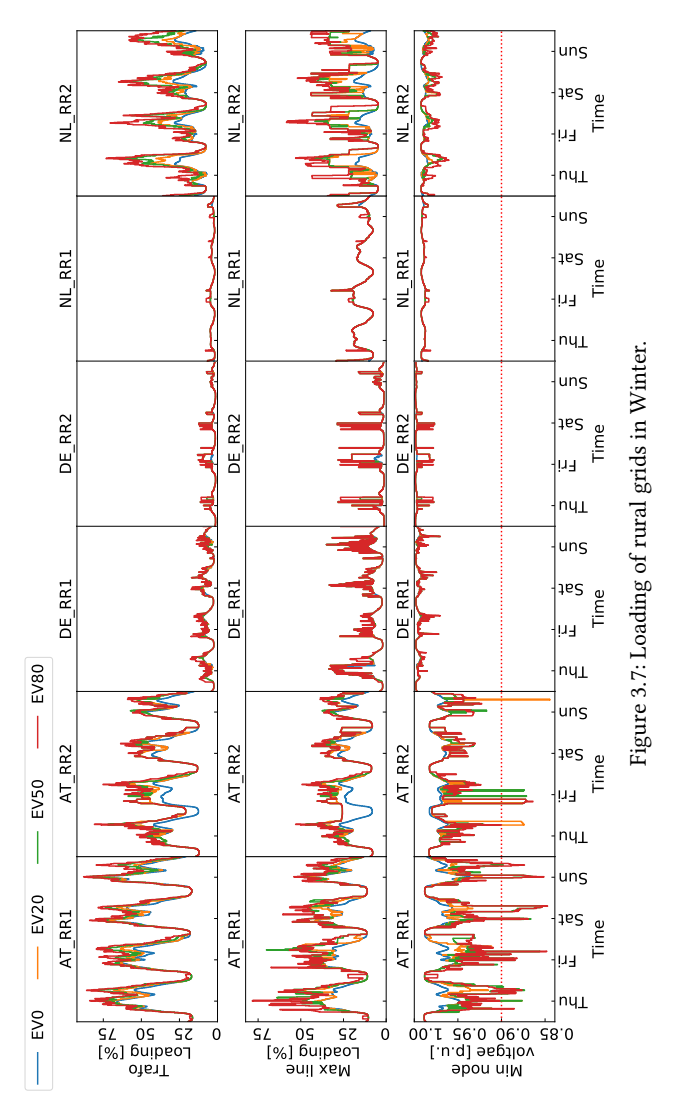
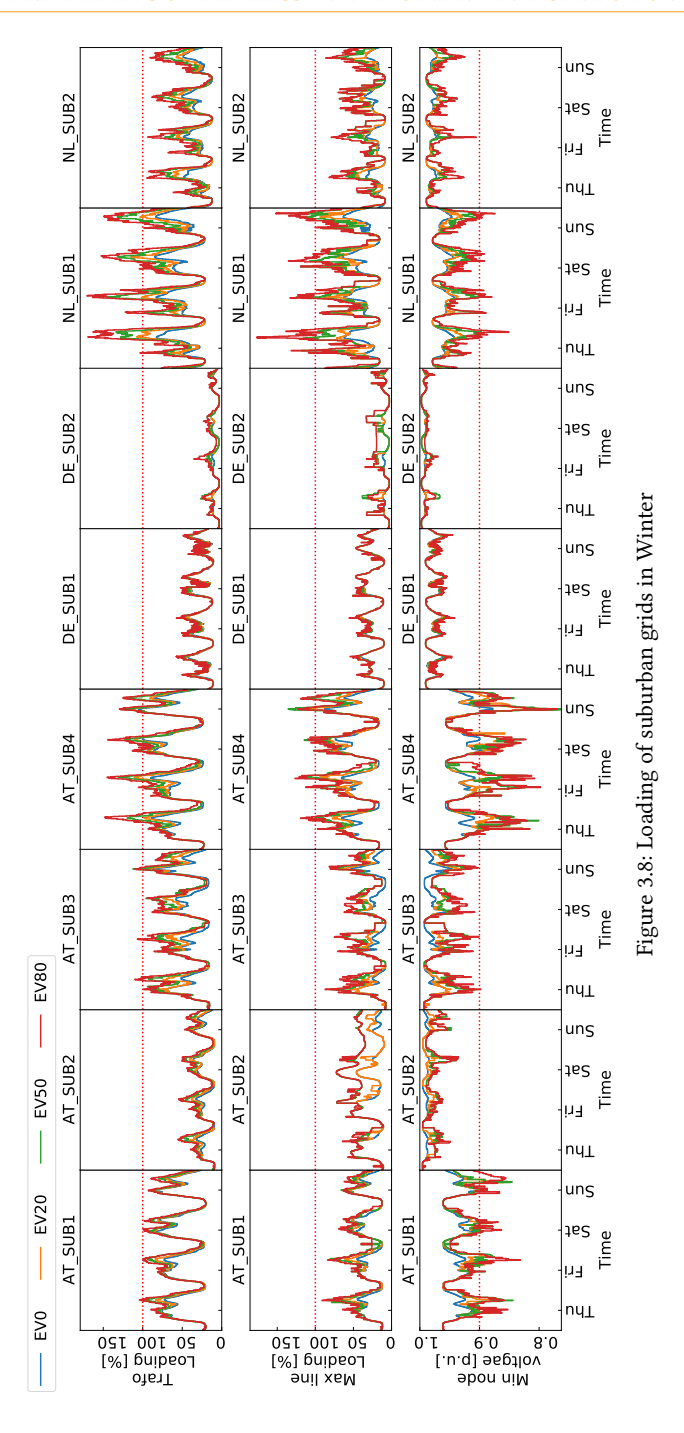
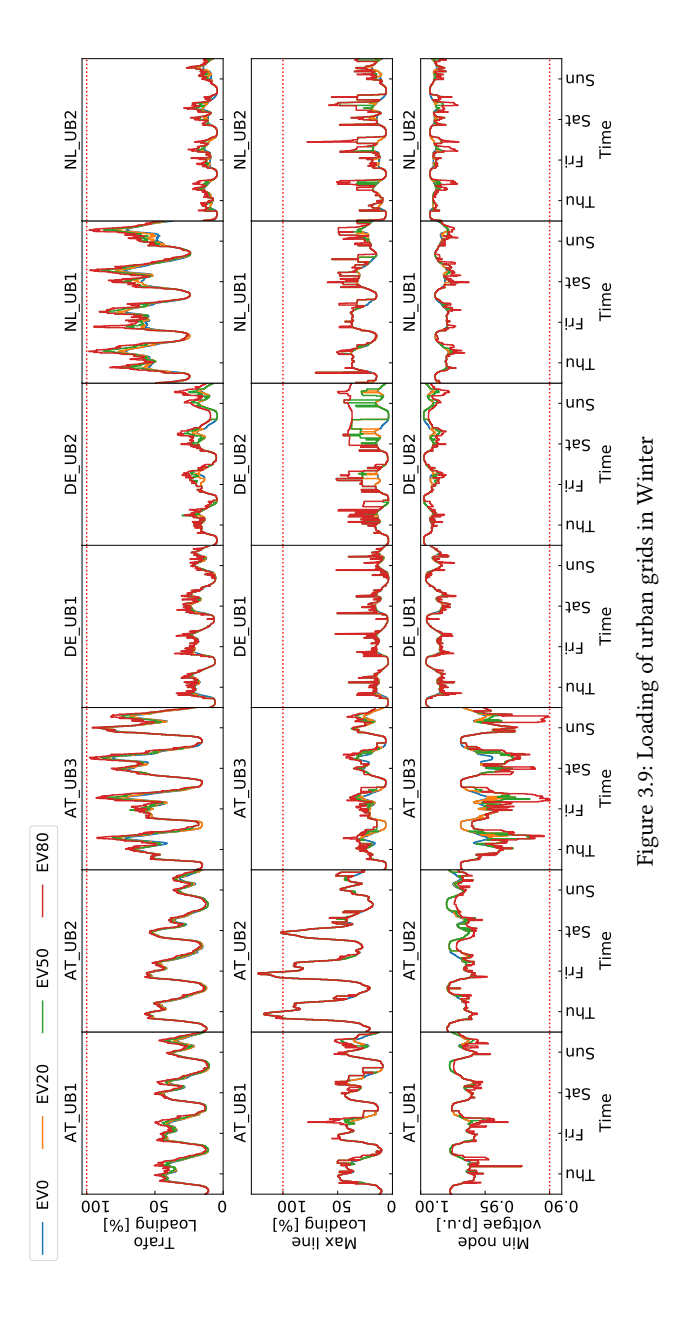


Fig. 3.7-3.9 show the results of transformer loading (top row), maximum line loading (middle row) and minimal node voltage (bottom row) versus time for three grid types in winter. The summer results can be found in Chapter Appx. 3.5. The maximum line loading is the loading value of the most loaded line among the whole grid at each time step, and similarly, the minimal node voltage plot shows the voltage value of the lowest voltage node among the whole grid at every moment. For maximum line loading and minimal node voltage plots, the presented results are not from a specific line or node, but the worst recorded value among all the relevant elements of the grid as a whole.

From Fig. 3.7-3.9 we can see that transformer, line and node results show a similar trend in most cases. When the transformers experience high loading, the maximum line loading also has the tendency to increase while the minimal node voltage is more likely to have



deep dips. These high loading moments usually occur on top of existing peaks that even without any charging EVs. This outcome is intuitive that the most uncontrolled charging



moments occur during morning peaks when people charge their cars at work or evening peaks when the users charge their cars once they are home. There are few occasions when the line loading or the node voltage do not share the same trend, for example, voltage drop in AT-RR grids, line loading in NL-RR2 and line loading in AT-UB2 grid. These phenomena were caused by local line overloading and regional voltage drop in remote areas of the grid.

3.3.1. Results of different grid types and countries

From Fig. 3.7 it can be noticed that none of the RR grids' transformers nor the lines are getting close to the overloading threshold. However, severe under-voltage problems already appear at some moment in both AT-RR1 and AT-RR2 grids with only 20% EV penetration. This under-voltage problem is purely caused by extremely long feeder length to the far-end of the grid, which is 1134 m and 1312 m separately. Besides, the EV charging adds a high level of extra loading to the RR grids that the transformer or line loading is doubled at some point even though the overall loading is within the limit.

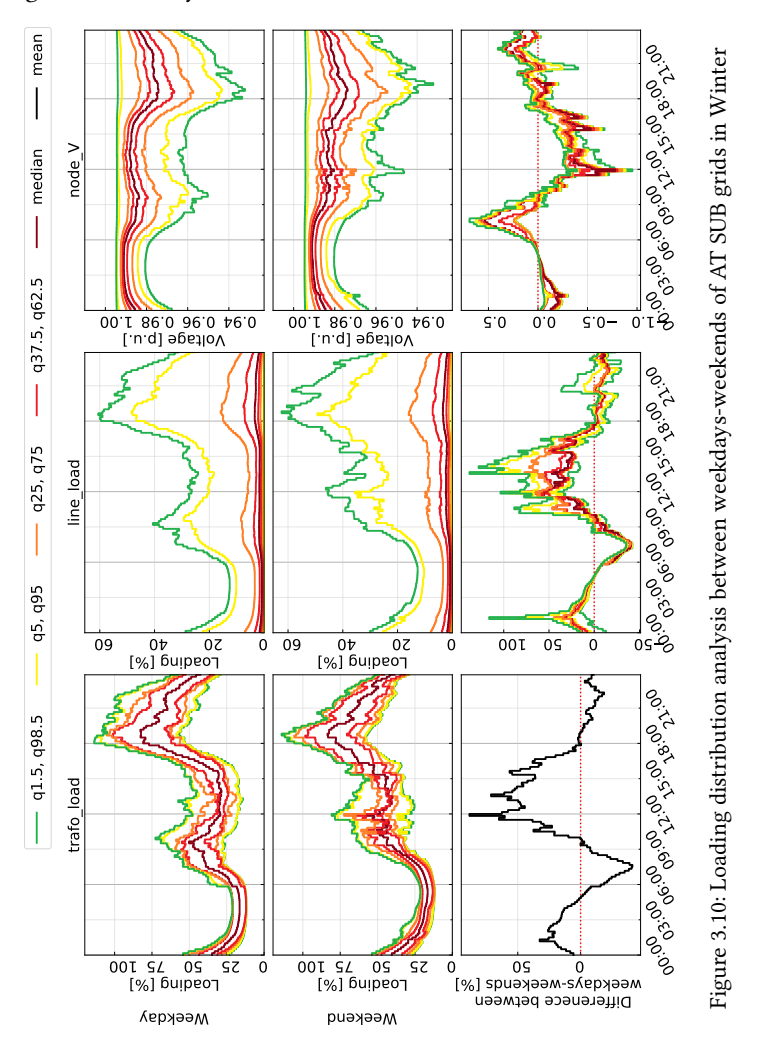
The plots of SUB grids in Fig. 3.8 present dissimilar results in comparison to the RR grids. Half of the SUB grids bear different forms, magnitudes and duration of overloading. There are several reasons behind this effect. On average, the SUB grids especially AT and NL SUB grids, have high household numbers as well as a high baseload demand. On top of that, the car ownership per household is also considerable for SUB grids, which induces a high absolute number of EVs in SUB grids. In the end, the exorbitant overall load demand passes beyond the grid limits, which suggest that the potential of SUB grids for a high EV penetration is very restricted.

In Fig. 3.9, the simulation results of UB grids are displayed. The plots show that except for AT-UB2, all the other grids are within the congestion boundaries with very few moments being on the verge of the limit. The line congestion that occurs in the AT-UB2 grid is not because of EV charging, but due to the high grid baseload and the limit of the partial grid facility. A few cables in the grid are already overloaded with only baseload consumption, which strongly suggests an upgrade for these cables. It can be also seen from this plot that the EV charging does not add extensively extra loading to the grid. The near breach moments are largely due to the high baseload. There are two possible reasons for this outcome. In our simulation settings, urban grids do not have many households, thus the absolute number of EVs are not as high. Secondly, urban grids tend to have a compact layout where the line lengths are shorter in comparison to other grid types, as introduced in Fig. 3.3. With a compact layout, the node voltages are less likely to drop dramatically. Both factors lead to relatively less problematic results in urban grids. In all simulations, none of the DE grids had any congestion problem while a considerable ratio of AT grids experienced transformer, line overloading and under-voltage problems. For NL grids, the overloading and voltage drop issues only develop in SUB grids. The simulation results confirm with the inference in Section 3.2.1.

One dominant reason of this outcome is the simulated DE grids have a relatively oversize-designed capacity compared to the other grids. This is signified by low $N_{\rm hh}$, $E_{\rm yr}$ and $\tau_{\rm b,avg}^{\rm norm}$ values of DE grids, whilst more lines with higher capacity are possessed by DE grids as displayed in Fig. 3.1 to 3.3. The same mechanism falls on AT grids. Features of AT grids including high $N_{\rm hh}$, $E_{\rm yr}$ values, long $E_{\rm f,max}$ and high ling length, suggesting they are more likely to encounter grid congestion issues in comparison with DE and NL grids. The simulation results show the corresponding tendency that a considerable ratio of AT grids experienced transformer (AT SUB1, SUB3, SUB4), line overloading (AT SUB4, UB2) and under-voltage problems (AT RR1, RR2, SUB1, SUB4, UB3).

3.3.2. Impact factor discussion

To investigate factors that influence the EV integrated grid performance is also an objective of this chapter. The impact of seasons, time of the week (weekday/weekends) as well as charger accessibility are discussed in this section.



Seasonal and time of the week results variations

The combination of PV generation, baseload and EV charging load affects the grid performance. Among these three inputs, baseload and EV charging load have weekday-weekend variations while PV generation and baseload deviate in different seasons.

The distribution analysis of all grid elements' loading values was performed and compared between the weekdays and the weekends. One analysis example is visualised in Fig. 3.10. The first two rows of this figure show the daily loading/voltage distribution of every element in this grid where the first row exhibits the weekday variations and the

second row represents the weekend fluctuations. The weekday-weekends loading percentage difference distribution is illustrated in the last row of the figure. The colour of the curves in this figure depicts various quantile values of this distribution. For example, q1.5-q98.5 lines mean 1.5% and 98.5% quantile, and these two lines signify the 97% confidence interval. The min-max values are not plotted in this graph since they are already included in the previous results section.

For all three categories of AT and NL grids, the percentage difference between weekend-weekday loading shows a similar sinusoidal trend for all grid elements: the weekend loading is higher than the weekday loading in two time periods (during post-midnight hours before 6:00 and during the mid-day between 9:00 and 18:00), and the weekend loading is lower than the weekdays' during the rest of the day. The exact time windows as well as the magnitude of the weekend-weekday loading difference varies between countries and grid categories. The weekend-weekday percentage difference of DE grids deviates during the day but it still shares the same early morning trend where the weekend loading is lower.

This weekday-weekend loading difference is an outcome of a temporal and scale shifted demand in the weekend, especially for AT and NL grids. The daily morning demand starts to increase significantly from 6:00 during the weekdays, but this situation is alleviated during the weekends. The rising of morning demand is delayed to a later moment of the day and a higher morning peak is observed in the meantime. As a result, a higher loading during the day in comparison to the weekdays has developed. Concurrently, the evening demand peak of the weekend appears slightly earlier than on the weekdays, but the duration of the high evening load lasts longer than on the weekdays. This explains the shrink of the evening peak as well as the increment of the post-midnight loading. The loading shift shows a different pattern in DE grids that the weekend loading subsides around 9:00 - 18:00 in comparison to the weekday loading. Apart from that, there are no other conspicuous disparities between weekdays and weekends that can be summarised.

This shifted demand is contributed by the baseload oscillation and the diverted EV arrival time. From the baseload comparison graph Fig. 3.4 we can see that the household baseload (household profile for AT/DE grids and E1 profile for NL grids) has a delayed rising trend yet an elevated morning peak in the weekend. On the other hand, the business profiles (E2 profile for NL grids) encounter a considerable decline in weekends to different degrees during various time windows for all three countries. The EV arrival time PDF plots in Fig. 3.6 (a) & (b) clearly signify the EV start charging time discrepancy between the weekdays and weekends. Since this study investigates an uncontrolled EV charging scheme, the EV arrival time equals the EV charging start time. The weekend EV arrival time in NL congregates with a mild ramp between 9:00 and 23:00 instead of clustering around morning and evening peaks at 9:00 and 18:00 respectively. Similarly, the weekend charging start time of AT and DE EVs happen less in both morning and evening peaks but more during the day between 9:00 and 18:00.

As introduced in Section 3.2.2, grids with more business/factory/agriculture types of loads have the tendency of experiencing less loading during the weekend. It is also suggested in Section 3.2.4 that there are lower EV charging peaks at weekends thanks to the spread-out arrival time distributions with a smoother ramp during the weekend. Even though some grids for instance AT-RR2, NL-SUB1, AT-SUB1 and DE-UB1 indeed have less severe loading during the weekend, the congestion level difference between weekdays and

weekends is inconsequential.

In this study, only a one-week length of simulation was conducted thus the observed weekday-weekends differences have their limitations. It is encouraged to explore more weeks throughout the whole year in future research.

For the difference between seasons, it is not surprising to see that all grids bear notably fewer congestion issues in Summer than in Winter. This change is caused by a lower load demand and a higher PV generation in summer along with a nonseasonal distinguished EV demand, which is indicated in Fig. 3.4-3.6. The employed EV input data in this chapter does not characterise seasonal deviations, but it is interesting to consider in future studies.

Impact of charger accessibility

There is one interesting effect that can be noticed in the simulation results, which is the branch loading and the voltage drop for 20% and 50% EV penetrations are worse than the 80% penetration case of some grids. For example, the last day of transformer loading in AT-SUB3, the second day of node voltage and line loading in DE-SUB2 and the node voltage of AT-RR2.

This phenomenon is specific to the way the simulation was set up and how the EV charging demand was modelled. EV charging demand modelling Approach 1 fixes the number of chargers in the grids and models the EVs charging sessions proportional to the EV penetration as explained in Section 3.2.3 and 3.2.4. This EV penetration increment modelling method introduces a situation when a new earlier charging session in a higher EV penetration scenario is added on top of an existing later charging session in the lower EV penetration scenario. If these two charging sessions happen to occur at the same location and within the same time window, a charging request overlap situation happens. Under this circumstance, the later session from the lower EV penetration scenario can no longer take place as planned when the earlier session from the higher EV penetration scenario occupies the charging slot. This leads to two outcomes, one is the later arrived EV waits in the queue for the already connected EV to finish. Alternatively, if there is a nearby available charging slot, the later arrived EV should move to a different slot. Hence, if the later charging session causes the overloading in lower penetration scenario could not happen due to an earlier session in higher EV penetration scenario, the worse overloading in lower EV penetration phenomenon occurs. This overlapping situation appeared several times in the simulation and it led to a slightly different EV charging profile even for the exact same charging session and eventually reflected in the grid loading results.

This queue mechanism induced by charging session overlap has a two-edged effect. It can passively reduce the potential congestion that new peaks will not be added infinitely to the existing peaks thanks to the physical limitation of available charging points. On the other hand, the queue effect can also increase the peak loading, if the delayed EV charging moves into another peak period or is connected to another slot located at the overloaded region. EV charging demand modelling Approach 1 mimics a situation where there is limited charger accessibility to the number of EVs. Differently, the EV demand modelling Approach 2 imitates another situation where there are enough charge points and they are always available for any EV to be charged whenever and wherever there is a request. This situation can lead to a circumstance where the charging demand happens during the peak time stack on each other without any limitation, resulting in an extremely high grid loading peak. One typical example is the transformer loading of day one in NL-SUB1 (Fig. 3.8).

This difference in the loading peaks is an outcome of how the EV demand is modelled, showing that whether there are enough chargers to the corresponding number of EVs can affect problems occurring at the node level for a very realistic setup.

3.4. Comparison of Different Grid Behaviour with Key Indicators

To better understand to what degree the grid congestion problems occur and what the influential factors are, several evaluation indexes are used to analyse the results.

3.4.1. The magnitude of grid congestion

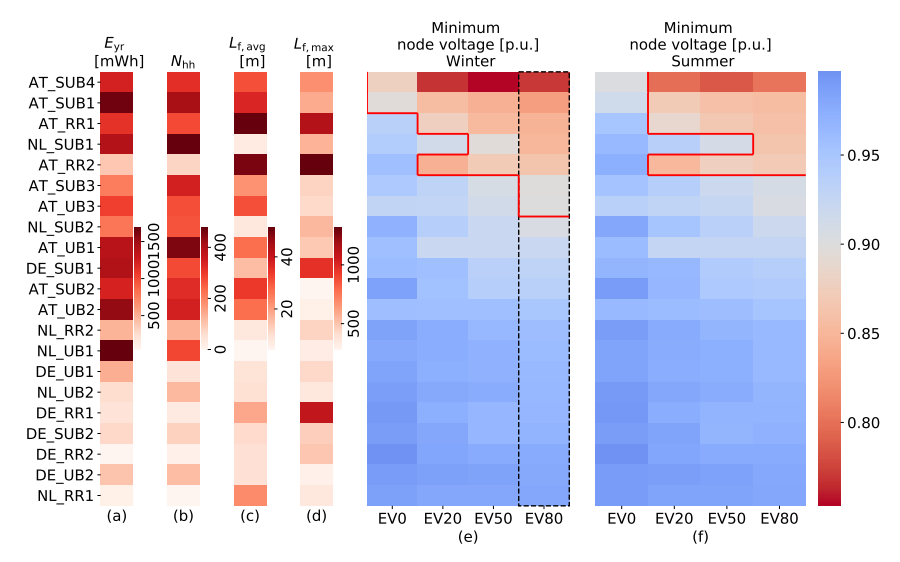
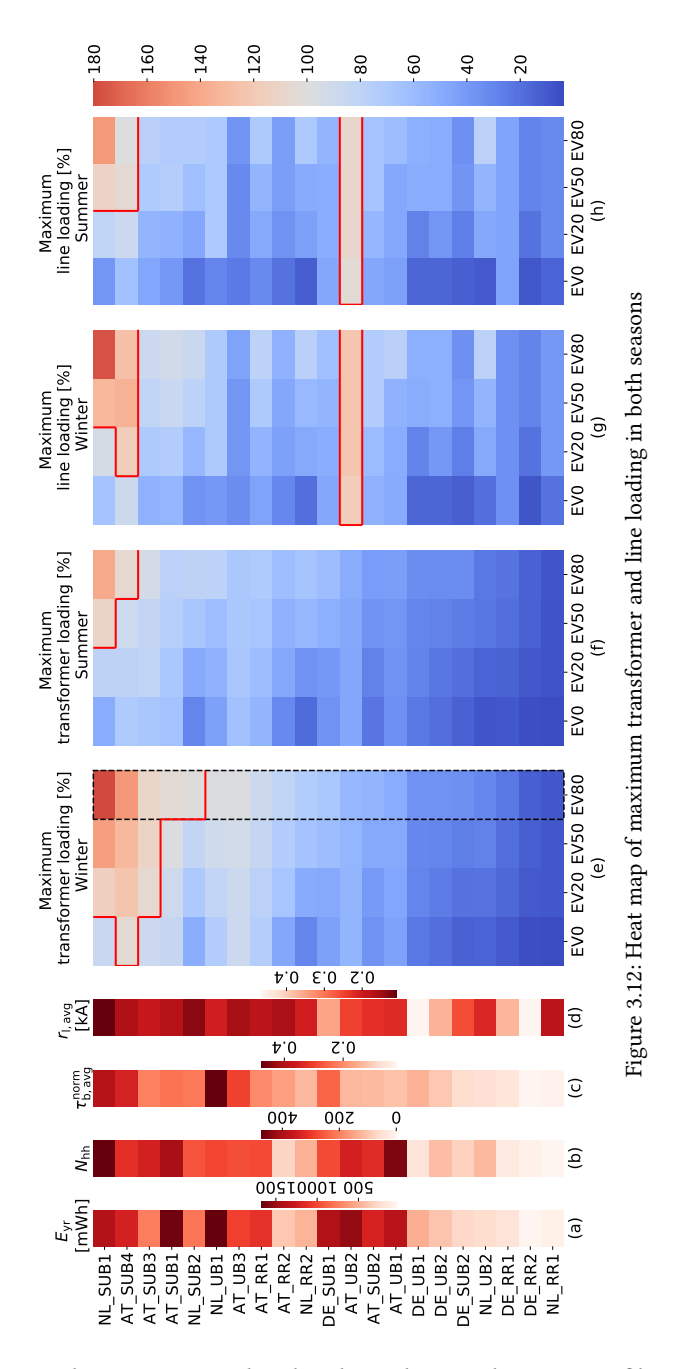


Figure 3.11: Heat map of minimal node voltage in both seasons

Fig. 3.12 and Fig. 3.11 show the amplitude of grid congestion with maximum loading values in descending order and minimum voltage values in an ascending order together with relevant grid features. The values in both figures are sorted based on the 80% EV penetration winter results, which are indicated by the black dash boxes. The common grid features for both plots are total yearly energy consumption (E_{yr}) and number of households (N_{hh}). Larger or higher density grids (higher E_{yr} and N_{hh}) have a tendency to experience more grid congestion issues. Apart from grid dimension, the ratio of average baseload power and the total transformer capacity ($\tau_{b,avg}^{norm}$) also relate to higher transformer and line loading. The average line ratings ($\eta_{,avg}$) instead do not show a strong connection with the line loading trend. However, for minimal node voltage, a clear association appears between the decreased minimal node voltage and the combination of average line length ($L_{l,avg}$) and the longest feeder length ($L_{l,max}$). The winter and summer results comparison has an expected effect that the grid congestion problem is milder in summer.

NL-SUB1 grid has the highest transformer and line peak loading and the highest loading growth caused by EV charging for two possible reasons. One is the grid feature, that NL-SUB1 has the highest $N_{\rm hh}$, the lowest $L_{\rm l.avg}$ and the second highest $\tau_{\rm b.avg}^{\rm norm}$ values among



all the grids. Another reason is related to how the EV charging profile is modelled, as previously mentioned in Section 3.3.2. The EV charging demand in NL grids was modelled with Approach 2 (charger approach), and the increased EV penetration is reflected as the increasing number of chargers. Any newly added EV in the grids has a guaranteed char-

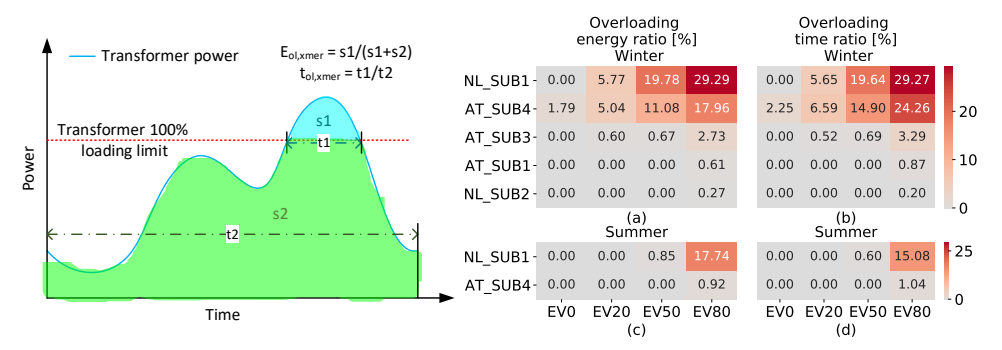
ging spot without having to wait in the queue during the busy time, unlike in the AT grids. This induces that all the EV charging requests will take place without delaying and leading to an extremely high loading peak.

The results where congestion problems present are circulated with red lines and it shows the ratio of problematic grids caused by EV uncontrolled charging is moderate, but the magnitude of overloading is significant for two SUB grids. Besides, there are more grids that have under-voltage problems than the number of grids with transformer and line overloading issues. Moreover, two out of seven under-voltage risk grids already suffer from under-voltage problems in winter even without EV charging and clearly, excessive EV demand does not help with the situation.

3.4.2. Duration and scale of the grid congestion

To study the duration and scale of the congestion issues, Fig. 3.13b and 3.14 are displayed. In Fig. 3.13b, the ratio of overloaded energy ($E_{\rm ol,xmer}$) and overloaded time ($t_{\rm ol,xmer}$) are presented and how they are calculated is explained in Fig. 3.13a. Two SUB grids experience up to 30% of transformer overloading duration as well as overloaded energy, which indicates these two grids request immediate attention, for example, charging scheduling or grid facility upgrades with even low EV penetration levels. Similarly, the scale of line congestion and node under voltage is presented in the format of percentage length of overloaded lines ($L_{\rm ol,line}$) and percentage number of under-voltage nodes ($N_{\rm uv,node}$) respectively.

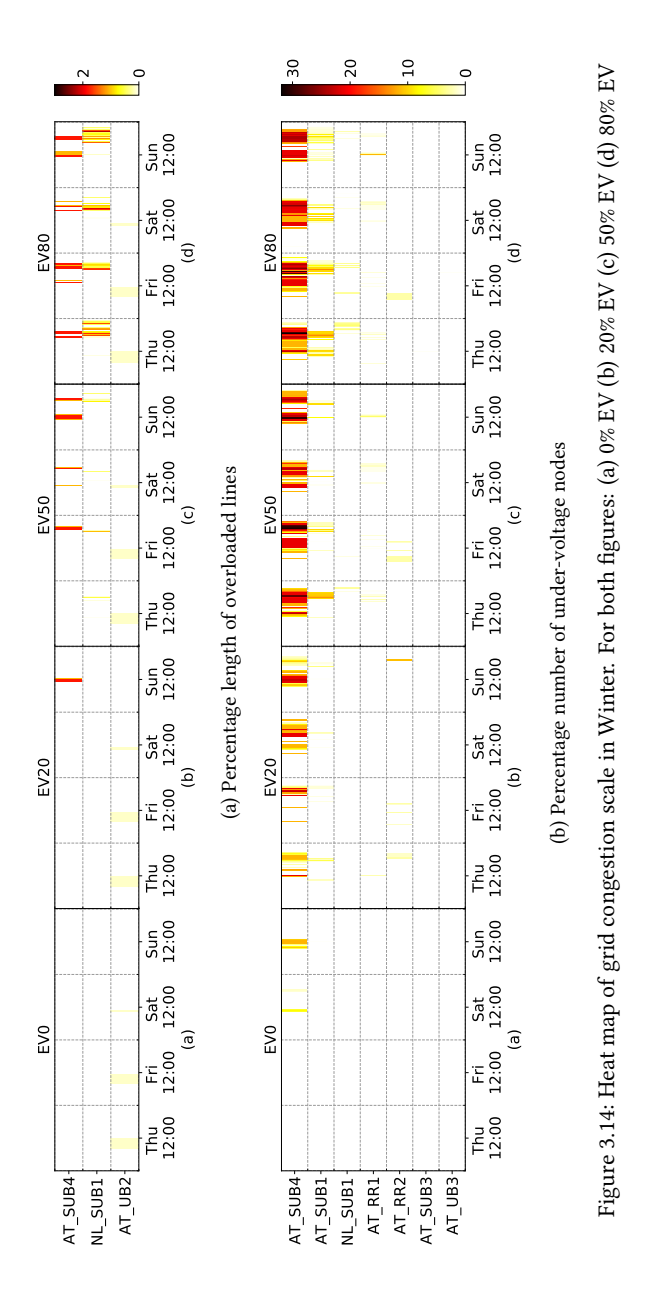
$$L_{\text{ol,line}} = \frac{\sum_{i=1}^{M_{\text{tot,l}}} l_{i,\text{ol}}}{\sum_{i=1}^{M_{\text{tot,l}}} l_{i}}, l_{i,\text{ol}} = \begin{cases} l_{i} & \text{if line i is overloaded} \\ 0 & \text{otherwise} \end{cases}$$
(3.3)



(a) Calculation explanation of overloaded energy(b) Heat map of grid congestion duration index: overloaded and time ratio

energy and time ratio

Figure 3.13: Duration and quantity of transformer overloading visualisation



$$N_{\rm uv,node} = \frac{\sum\limits_{i=1}^{N_{\rm tot,n}} n_{\rm i,uv}}{N_{\rm tot,n}}, n_{\rm i,uv} = \begin{cases} 1 & \text{if node i under-voltage} \\ 0 & \text{otherwise} \end{cases}$$
(3.4)

How $L_{\rm ol,line}$ and $N_{\rm uv,node}$ are calculated are described by Eq. (3.3) and Eq. (3.4) respect-

ively, where $M_{\rm tot,l}$ is the total number of lines, $N_{\rm tot,n}$ is the total number of nodes and $l_{\rm i}$ is the length of line i. The variation of $L_{\rm ol,line}$ and $N_{\rm uv,node}$ versus time is shown in Fig. 3.14 with an ascending order in y axis.

A maximum less than 3% $L_{\rm ol,line}$ value reveals the scale of line overloading is rather small that it only occurs at several featured lines. These lines are either central lines connected close to the transformer or local lines connected to high consumption loads. On the contrary, AT-SUB1 and AT-SUB4 have significantly high $N_{\rm uv,node}$ values. Especially for AT-SUB4, at least one-fifth of the grid is having under-voltage problems during almost half of the simulation time in 80% EV penetration scenario. This outcome pinpoints again that voltage drop is a fierce issue that needs to be solved in distribution grids. A small improvement on the facility, for example, a reconfiguration of the tap positions of the transformer, might already help with the situation.

3.4.3. Key takeaway

With the in-depth index comparison and analysis, it can be concluded that the majority of the grids do not face major congestion when penetrated with 50% EVs. Most of the problematic grids have a small scale and short duration of grid limit breaching. However, under-voltage is a problem worthy of attention, not only because more grids have higher magnitude, longer duration and bigger scale of voltage drop, but also because the voltage drop has a high vacillation rate on many occasions. Besides, a study [111] found that upgrade grid facilities, for example, the transformer capacity has very limited improvement on the voltage drop caused by a large amount of EV charging. That leaves less option for accommodating massive EV charging in LV grids, but on the other hand, it opens the opportunity to look into alternative methods, for example, smart charging scheduling, apart from the grid facility upgrades. It is an interesting aspect to research in future work.

3.5. Conclusion and recommendation

In this research work, the performance of 21 grids from three countries (Austria, Germany, Netherlands) with four EV penetration levels (0, 20, 50, 80%) in two seasons (Winter, Summer) are analysed and several interesting points are discussed. This chapter focuses on the grid performance comparison along with EV penetration levels, between countries, and of different grid types. The other impact factors including seasons, time of the week (weekdays or weekends) and charger accessibility are also studied. Several key indicators of the magnitude, duration and scale of the grid congestion aree examined. The overall performance of all grids is summarised in Table 3.3.

The grids from all three countries share a few similarities. First, the loading of transformer and lines, as well as minimal node voltage, share similar trends and the extra loading contributed by EV uncontrolled charging are predominantly added on top of the existing peaks. This phenomenon is rather apparent as most of charging events occur when the users come to work (morning peak) or get back home (evening peak). Secondly, the SUB grids in all three countries tend to endure more congestion issues in comparison to other grid types. This is because all SUB grids in the simulation have the highest household numbers as well as a relatively high car ownership ratio. This leads to a higher baseload consumption as well as an increased number of EVs which causes a higher total demand in comparison to RR and UB grids. Thirdly, partial loading of the grid shifts from early morning and evening towards the middle of the day on weekends. Even though some

	Transfe	ormer loading	Line loading		Node voltage			
	Mag.	Dur.	Mag.	Dur.	Scale	Mag.	Dur.	Scale
AT-RR					***	**	**	
AT-SUB	**	***	***	**	*	***	***	***
AT-UB			**	*	*	*	*	*
DE-RR								
DE-SUB								
DE-UB								
NL-RR								
NL-SUB	***	***	***	***	*	**	**	*
NL-UB								

Table 3.3: Summary of grid performance

Higher number of "*" means the problem is more severe. Mag.: Magnitude; Dur.: Duration

grids like AT-RR2 do encounter a slightly reduced loading during the weekends, the disparity of congestion level between weekdays and weekends is insignificant. Finally, all grids have fewer overloading issues in the summer compared to the winter because of a lower baseload consumption while receiving a higher PV generation.

The grid performance in each country also has its own characteristics. All simulated DE grids are designed with higher redundant capacities, therefore none of them had any issue in all the simulations. AT grids have the most incidence of congestion problems. Apart from SUB grids, AT-RR grids which have both transformer and lines operating well within the safe range still confront the risk of voltage drop below 0.9 p.u., with even 20% EV penetration, due to their excessively long longest feeder's length. NL-SUB1 grid has the highest transformer and line peak loading problem not only because of the grid features and the EV penetration level but also related to how the EV charging demand were modelled. The difference in simulation results due to two EV charging session modelling approaches regarding "EV penetration versus the available number of charging points in the grid" inspires future research ideas. Whether charging points should be installed or not and how many are in view of increasing EV penetrations is critical to investigate further.

Thirteen out of twenty-one simulated grids encounter no congestion in any form even with an 80% EV penetration level. Most of the congestion has a relatively short duration on a small scale, where smart charging scheduling is needed, and a good result can be expected. However, one NL-SUB grid and two AT-SUB grids showed massive transformer loading and voltage drop problems in both amplitude and scale manner, indicating a possible hard violation on the grid facility upper limit. Regarding the severe problematic grids, two possible solutions are desirable to investigate in future work. One is to develop a smart charging method to reschedule the crowded charging process and optimise the grid capacity usage. Another one is to identify the most susceptible point in the grid and upgrade the related facility.

Even though this uncontrolled EV charging impact study advocate a rather optimistic outcome regarding distribution grids integrated with high EV penetration levels, there are a few things shall be noted. All the baseloads implemented in the study are standardised load profiles, which are averaged and smoothed from real measurements. These standardised load profiles do not contain high-frequency power spikes and therefore do not

accurately reflect the real baseload fluctuations. Because of this, grids might face the risk of higher congestion in situ, especially since short moments of grid limits breach might occur more readily when the same level of EV penetration as in the simulations is accommodated. Besides, all the EV penetration calculations were based on the car ownership registration but not the actual car parking information. In reality, the location of car registration might be far removed from regular charging spots. Therefore, the EV commute and how the commute alters the EV distribution between different LV grids are worth investigating in the future.

Despite the simplification during the modelling and the data pre-processing, this chapter provides an insight into the uncontrolled EV influenced grid performance from different angles. The results of this study reflect what degree the EV uncontrolled charging overburdened the grids and what are the relevant impact factors, thus offering a valuable reference concerning future planning for DSOs.

3

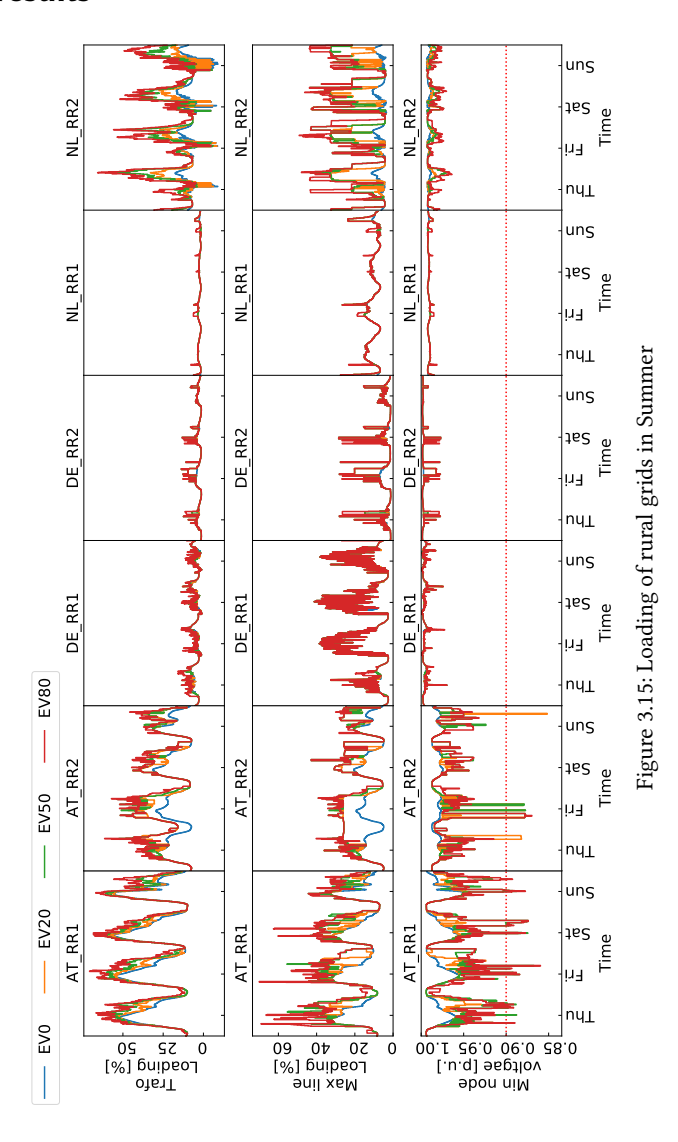
Chapter Appendix

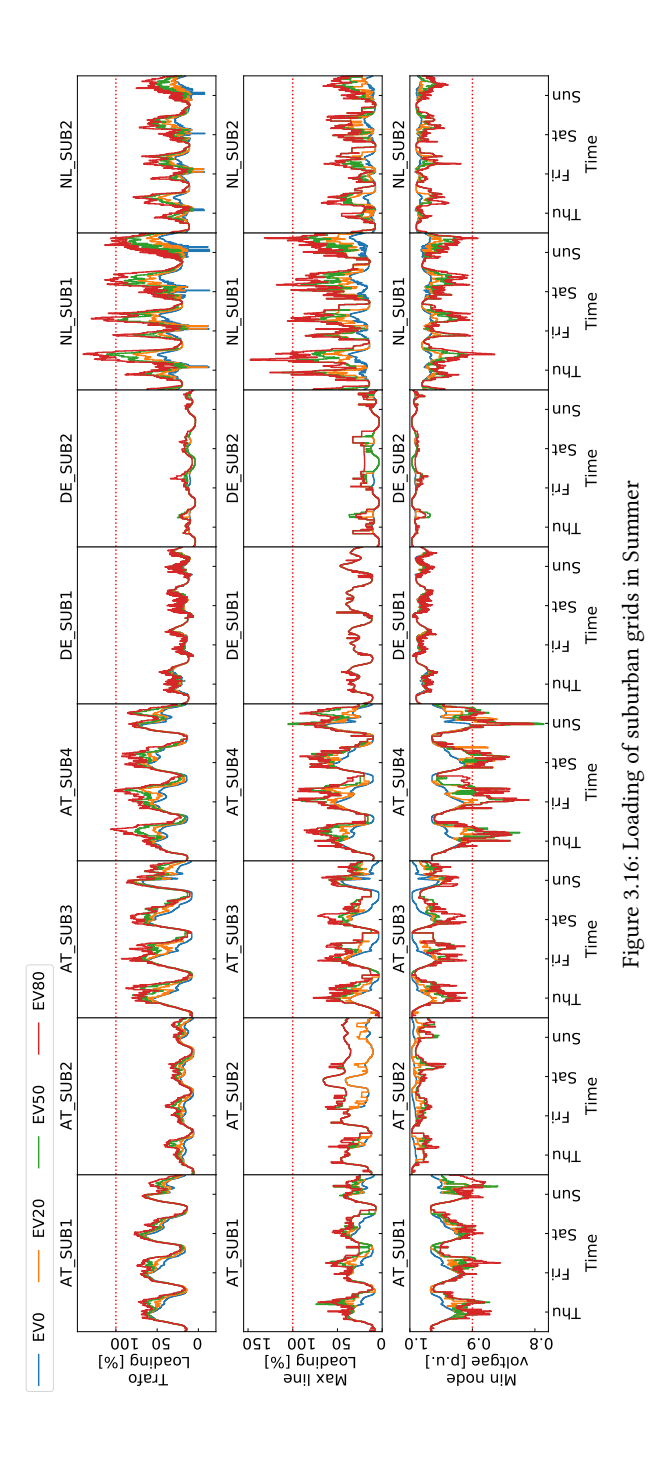
Grid characteristics

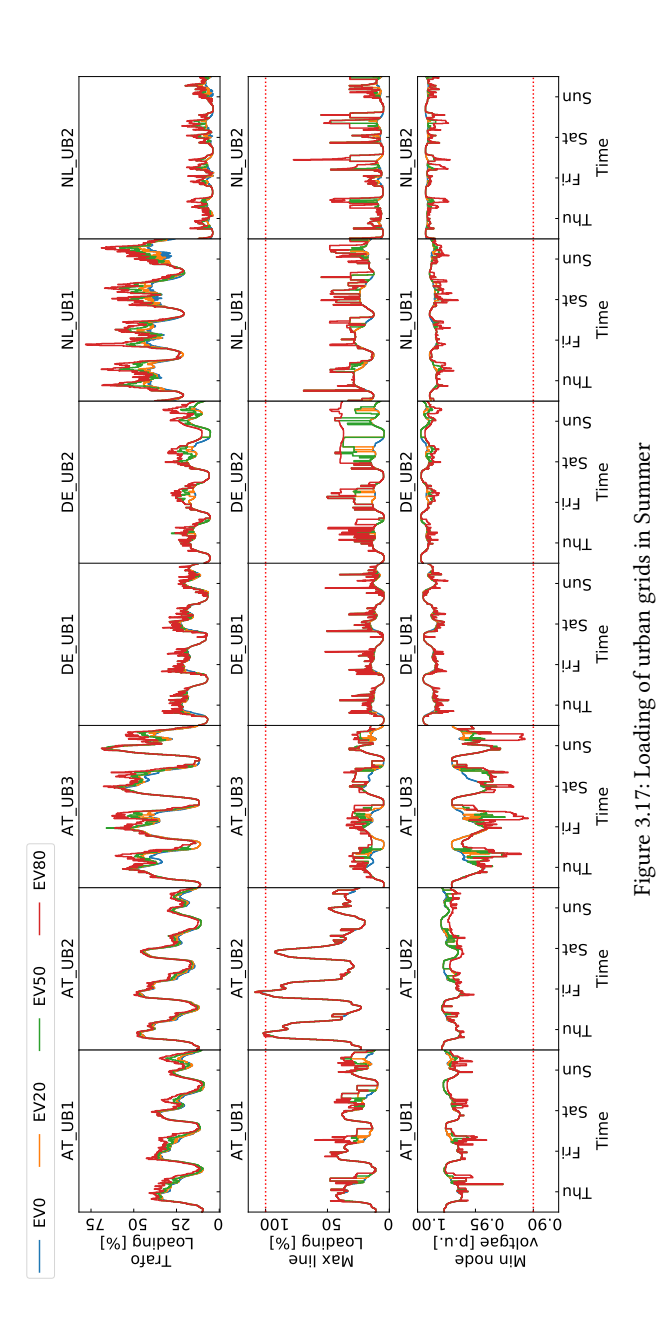
Table 3.4: Summary of all grids' characteristics

Grid	No. households	Yearly energy consumption [Mwh]	Avg. line length [m]	Longest feeder length [m]	No. transformer & capacity [kVA]
AT-RR1	280	1121.0	51.0	1134.0	1×630 kVA
AT-RR2	77	384.0	49.0	1312.0	1×250 kVA
AT-SUB1	410	1651.0	37.0	590.0	2×400 kVA
AT-SUB2	321	1213.0	34.0	280.0	1×400+1×630 kVA
AT-SUB3	345	760.0	22.0	457.0	1×400 kVA
AT-SUB4	319	1222.0	31.0	678.0	1×400 kVA
AT-UB1	451	1379.0	27.0	491.0	2×630 kVA
AT-UB2	344	1532.0	27.0	314.0	2×630 kVA
AT-UB3	274	1052.0	31.0	431.0	1×400 kVA
DE-RR1	32	213.5	18.9	1087.0	1×400 kVA
DE-RR2	12	42.0	10.0	499.987	1×250 kVA
DE-SUB1	277	1414.0	15.8	962.4	1×630 kVA
DE-SUB2	82	287.0	11.0	471.545	1×400 kVA
DE-UB1	50	518.0	9.5	436.672	1×400 kVA
DE-UB2	116	406	10	312.2	1×400 kVA
NL-RR1	3	98.0	22.8	367.8	1×400 kVA
NL-RR2	133	486.8	7.9	452.2	1×400 kVA
NL-SUB1	475	1394.1	7.3	566.0	1×400 kVA
NL-SUB2	266	800.8	8.1	546.6	1×400 kVA
NL-UB1	283	1680.2	4.4	332.5	1×400 kVA
NL-UB2	122	261.0	10.3	360.4	1×400 kVA

Summer results







44

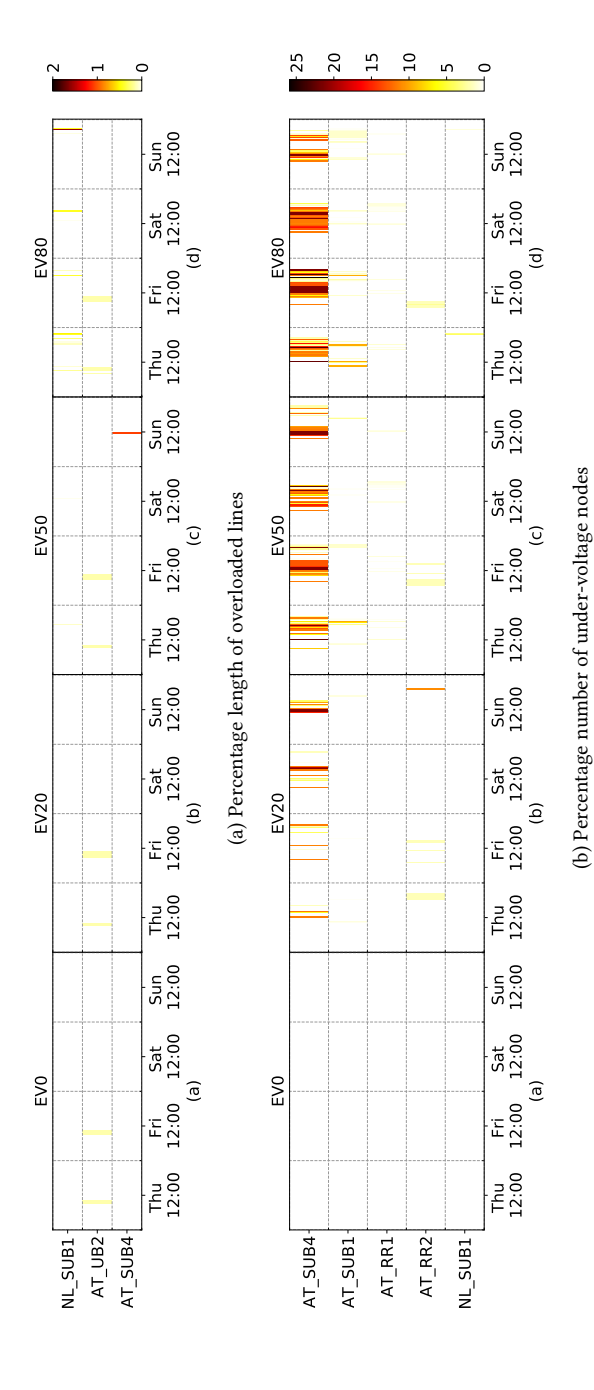


Figure 3.18: Heat map of grid congestion scale in Summer. For both figures: (a) 0% EV (b) 20% EV (c) 50% EV (d) 80% EV

Benchmark study of heuristic EV charging tactics

This chapter benchmarks the performance of three practical heuristic electric vehicle (EV) charging scheduling methods relative to uncontrolled charging (UNC) in low-voltage (LV) distribution grids. The charging methods compared are the voltage droop method (VDM), pricesignal-based method (PSM) and average rate method (ARM). Trade-offs associated with the grid performance, charging demand fulfilment and economic benefits are explored for three different grid types and four increasing levels of EV penetration for summer and winter. This study was carried out using grid simulations of six existing Dutch distribution grids, and the EV charging demand was generated based on 1.5 M EV charging sessions; therefore, the findings of this research are relevant for actual case studies. The results suggest that the PSM can be a preferred strategy for achieving a charging cost reduction of 6-11% when the grid performance is not a bottleneck for the given EV penetration. However, it can lead to an increased peak loading of the grid under certain operational conditions, resulting in a charging energy deficiency ratio of 4-8%. The VDM should be preferred if user information on the parking time and energy demand is not consistently available, and if the mitigation of grid congestion is critical. However, both unfinished charging events and charging costs increase with the VDM. The ARM provides the best balance in the trade-offs associated with the mitigation of grid congestion and price reduction, as well as charging completion. This research provides a perception of how to select the most appropriate practical charging strategy based on the given system requirements. The outcome of this study can also serve as a benchmark for advanced smart charging algorithm evaluation in the future.

4.1. Introduction

The electrification of transport has increased in the past years, leading to a fast increase in the electricity demand over the distribution grid. To study the integration of a massive amount of EVs into the distribution grids, the impact of uncontrolled EV charging on the grid utilities was explored in several benchmarking studies [23, 24, 26, 92, 103, 112]. Based on these benchmark studies, ample smart charging methods have been developed and studied in recent years [113, 114]. These algorithms in general are challenging to implement and have a trade-off between operating functionalities, input information and computational power. There are plentiful simpler and easier-to-implement EV charging methods

^oThis chapter is based on paper: Y. Yu, A. Shekhar, G. R. Chandra Mouli, and P. Bauer, Comparative impact of three practical electric vehicle charging scheduling schemes on low voltage distribution grids. *Energies*, vol. 15, no. 22, 2022.

that require much less communication and computation. Some of the methods are applicable for a broader spectrum of scenarios or offer a competitive, or even superior, performance [51, 115, 116]

It is our interest to explore what minimalism can bring to EV charging scheduling methods and to evaluate their effectiveness. In addition, it is also vital to assess the short-term EV charging methods before the innovative charging algorithms are ready to be launched with the support of relevant protocols and regulations [117].

In this chapter, three representative pragmatic rule-based EV charging scheduling methods are selected or proposed based on existing popular heuristic EV charging scheduling methods. The generic fundamental mechanism of the three methods is to control the EV charging power based on different criteria. A systematic analysis and comparison of their efficacy, including grid congestion mitigation, economic benefits and charging demand fulfilment, were carried out. In addition, this study provides an elementary reference point for the assessment of future-developed algorithms. It must be noted that different charging schemes can have diverse impacts on other factors, such as battery lifetime. However, the focus of our study is the above-mentioned three aspects, and therefore, the influence on the battery performance is beyond the scope of this research.

4.1.1. Background on Advanced Smart EV Charging Algorithms

Most of the controlled charging of electric vehicles (EVs) shares one or more of the four prevailing primary targets [61-64]: (i) grid impact mitigation, (ii) profit maximisation, (iii) enhancing the service to EV users and (iv) increasing the utilisation of renewable energy resources. To achieve multiple targets with one charging method, EV charging power is usually not the only parameter that must be tuned, especially in complex systems where other relevant parties are involved [56, 59-61]. On top of that, complex structures, such as hierarchical control schemes and multi-level optimisations, are composed [60, 65-67], which, in turn, increase the requirement for the amount, accuracy and speed of the communication [59, 61, 63]. For example, the EV charging management system proposed in paper [59] suggests a bidding process within a transactive market in which the EV fleet information, as well as the EV users' preference towards the clearing price, is requested beforehand. Similarly, study [60] investigates a systematic supply-demand balance, PV power generation and energy storage, as well as the V2G performance, within its EV charging optimisation problem using both hourly and day-ahead predictive data. The EV smart charging method proposed in research [56] not only incorporates battery lifetime protection and PV power generation into the stochastic dynamic programming but also integrates grid capacity, as well as energy storage optimisation, in its objective function.

The above-mentioned primary targets become competitive towards each other under some operational conditions. For example, it is suggested in [62] that prioritizing peak shaving can approximately half the maximum demand but leads to a 5–10% increase in average energy costs as a trade-off. Further, while the method proposed in [63] successfully satisfies the load congestion and voltage droop constraints relative to 70% of exceeded constraints in the uncontrolled method, it is suggested that location-specific customer demands may lead to a fairness challenge that needs further investigation. An interesting approach in [64] attempts to include fairness in imposing grid limitations by setting priority criteria for coordinated EV charging depending on the available parking time and energy demand of the connected cars. These leading algorithms highlight the importance

of multi-objective optimisation for minimizing a defined system cost function to address the underlying trade-offs using accurate information and fast communication between different agents.

Complex hierarchical control structures are often employed to incorporate multiple functions in advanced EV charging algorithms. Paper [65] proposes a two-level hierarchical charging coordination algorithm where the upper-level controller is in charge of the grid power dispatch and the station-level controller manages the local charging scheduling. The algorithm in [66] has three levels of actions, and each has different functionalities. The first level participates in the day-ahead (DA) or real-time (RT) market and obtains the quantity of cleared energy, the second level aims to optimally dispatch the energy budget obtained from level one to the EVs in the system and, finally, the objective of the third level is to respond to the up and down regulation requests.

Apart from trade-offs and compound structures associated with multi-objective optimisation, smart charging algorithms also deal with uncertain load demand forecasting, renewable energy generation and the arrival/departure time of the EVs, usually by employing a multi-timescale optimisation scheme. In [67], a building operational cost reduction of approximately 6% was achieved using a two-stage algorithm for DA scheduling and RT operation compared to the baseline case, where only a prediction of the PV output was considered. Similarly, an algorithm developed in [60] optimises the system in four stages along the time scale from the prediction to DA, hourly ahead and, finally, to RT, to show that even though the EV energy consumption is the same, the overall cost with an hour-ahead schedule is 1.55 times higher than RT control, mainly due to uncertainty in PV generation.

All of the above-mentioned challenges would become exponentially difficult in realenvironment applications, which consecutively makes simple charging methods compelling.

4.1.2. Simple and Practical Charging Scheduling Approach

Meanwhile, simple yet pragmatic heuristic EV charging algorithms have been suggested and tested in preceding works. Simple heuristic charging algorithms usually focus on regulating the EV charging procedure with three common approaches: reducing the charging cost, alleviating the grid impact and tuning the charging power from the user's point of view. This section gives an overview of simple heuristic charging methods.

Charging Cost Reduction Methods

The most popular reason for EV charge scheduling is cost reduction. The electricity price, such as the DA price or time of use (TOU) price, can reflect the grid loading level to some degree and is often selected as the price signal.

The objective of [118] is to minimise the EV charging cost based on the TOU price from a regulated market. This heuristic algorithm sorts the charging power from both temporal and magnitude perspectives and the expected outcome is that the charging requests of EV users are fulfilled with a lower cost in contrast to uncontrolled charging. In the end, 52.92% to 61.19% of the energy demand shifted from the highest to the lowest loaded time window (peak \rightarrow flat \rightarrow valley time), with a 39.67% to 51.52% cost reduction in contrast to uncontrolled charging. Similarly, a linear optimisation problem is formulated in [54] to minimise the EV charging cost from an aggregator's point of view. This method was

implemented in combination with three charging power adjustment programs with cost incentives, among which the users can pick in their own favour. The hourly price used in [54] was calculated based on the real-time cost of electricity generation, transmission and distribution. It was observed that, with a 50% EV penetration level, the charging peak power at midnight is reduced to around 50% relative to uncontrolled charging. In addition, the EV aggregator saves at least 5% in charging cost compared to the uncontrolled charging scenario and the savings increase further with increasing levels of EV penetration.

However, a deficiency of the price signal as the sole dependent charging control method is that it could cause a second load peak that can sometimes overtake the uncontrolled charging load peak; this negative side effect should not be overlooked. This is due to the simultaneous charging stimulated by the unified off-peak tariff in the system. Study [49] implemented a TOU price-based time-control EV charging method where different off-peak tariff starting moments in combination with various begin-to-charge schemes were investigated. It was found that this method could shift the EV charging demand into off-peak hours and mitigate the under-voltage violation in comparison to the uncontrolled charging method. Although the second peak in the load demand on the service transformer was observed starting between 11 p.m. to 12 a.m, this value did not exceed the peak observed for uncontrolled charging that occurred between 8 p.m-10 p.m. A similar trend in the minimal voltage was also encountered. It was concluded that the beginning moment of the off-peak tariff needs to be carefully demonstrated so that the balance between grid loading and charging completion can be obtained. The TOU price-based EV start charging time control method was also tested in [119] and it was noticed that a secondary peak appeared due to the simultaneous EV charging, but the peak was still around 20% less than the peak induced by uncontrolled charging. In addition to the time control charging method inducing the second peak issue, optimisation programming could also produce the same side effect. Study [50] proposed an EV charging optimisation method with the objective to minimise the charging price by referring to the DA spot market price. The results suggest that even though the charging cost is reduced by 11-16% with the proposed method, using only hourly price information is not sufficient. Simulations on actual grid data revealed the highest increment in system energy loss of 4.3% relative to uncontrolled charging in a residential area, whereas no significant difference in the commercial area was observed.

The employment of extra constraints might effectively balance out the second peak issue. For instance, study [120] presents a cost minimisation charging method based on a time-varying electricity price that reflects the net system demand, including the wind generation, as well as the EV demand. The results indicate that, as opposed to uncontrolled charging, the average peak loading of the grid reduces up to 8%, whereas the net present value of the grid investments increases by 25% in the low-wind-generation scenario. Incorporating the grid-related constraints directly into the model produces a more adequate effect. The charging profile of two TOU tariff-based delayed charging methods—concurrent or with Poisson distribution—was studied in [121], and it was found that both methods lead to a narrower peak time window with a higher peak value. However, with the grid condition limitation being considered in the form of a distribution system loading margin, the maximum EV penetration level was improved from the worst case of 8.5% to the best case of 142.6%. A loss-optimal charge strategy was used in helping to defer the infrastructure reinforcement of the distribution network in [50], and a 100% EV penetration

was achieved as opposed to 49% in the price-optimal case. The network peak load minimisation method proposed in [120] not only decreases the average peak grid loading by at least 5% compared to the cost minimisation method, but also helps to reduce the future grid component reinforcement requirement on MV distribution cables by 49.9% relative to the 29.5% of the cost minimisation method.

Grid Impact Mitigation Methods

Aside from the electricity price, the grid performance is often selected as the primary goal of the EV charging regulation method, considering the potential grid limitation violation caused by the massive EV charging demand as well as the competition between primary goals. In doing so, the grid characteristics are frequently integrated into the system model.

For example, the grid loss optimisation method developed in [50] adapts grid congestion indicators, such as the transformer and the line loading, as well as the voltage variations, into constraints. Alternatively, grid power limitation in a half-hour step was used in [64] to prevent overloading, but this method requires communication with the system operator for the grid power limit, as well as the load demand with prediction. Incorporating grid features into the optimisation is the most straightforward way to mitigate overloading issues. However, it also means that strong nonlinear features are introduced into the optimisation problem, which leads to complex non-linear (NL) programming solutions that increase the solving time. In addition, these methods often use centralised control schemes and request a high-level knowledge of the grid, which means a high requirement in communication and computational power [122, 123].

Decentralised control methods using locally available information such as node voltage as a reference is another common direct approach. The premise is that the node voltage measured at any given time is a function of grid loading in the associated branch and, therefore, the information on grid congestion can be extracted locally without communication. Study [49] formed a distributed optimisation problem, with its objective to minimise the local voltage deviation at every EV connection node. The results reveal that the peak load demand is largely shifted to the off-peak hours and the voltage droop issue is significantly improved with at least a 4.26% increased minimal voltage. Another popular method is the well-known voltage droop method, where the power drawn by the EV varies in proportion to the measured node voltage according to a heuristically set droop gain. A simple voltage droop charging method was studied in research [124]. The simulation results of a real urban residential LV grid revealed that the voltage droop charging method improves the minimal voltage by 14.7% and lowers the voltage unbalance factor by 32% as opposed to the uncontrolled charging. Nevertheless, the minimum voltage value of the grid is still under 0.9 p.u. with a maximum of 10.4% of the time duration in one week. This is probably related to a relatively low voltage droop response range being selected (0.85 to 0.9 p.u.). Study [125] proposed a phase-wise voltage-droop-based reactive power control algorithm. The phase-to-neutral voltage unbalance was alleviated by up to 56% and the minimum voltage was also improved by up to 6.3% with a negligible energy loss in contrast to the reference scenario.

Despite the persuasive grid overloading prevention ability, this strategy may lead to an unfair energy transfer to EVs connected at downstream nodes. This is because such locations are further away from the substation and have a relatively greater drop in voltage due to the higher impedance of the distribution branch [52].

To establish a fair utilisation of grid resources among vehicle owners while simultaneously alleviating the grid congestion, [53] adapted the threshold voltage at each node in accordance with its distance from the substation based on a learning algorithm using measured data. The peak power drawn increases by approximately 10-20% as the charging power of all houses reaches its equilibrium point compared to its initial status. However, this method requests the full information of the whole grid, including geographic information, as well as the grid local profile. A fair control scheme was proposed in paper [126] by using an exponential voltage droop curve, and the charging rate was altered based on the state of charge (SoC) of the EVs. This method successfully decreased the peak in the system load by 10-15%. Furthermore, the difference in time to fully charge between EVs connected at different nodes was scaled down to 60-70% with the SoC-involved adjustment in comparison with the SoC-free adjustment. This control method is only effective with a maximum of 50% EV penetration, and EVs at the far end will not be able to be fully charged if the EV penetration keeps growing. An EV SoC and local voltage-dependent fuzzy logic communication-free charging method was developed in [127]. Additionally, a zero membership function was assigned to the voltage range 0.95-1.025 p.u. to avoid the extensive voltage-reliant sensitivity of the charging rate. The performance comparison between the proposed method versus the traditional voltage droop method suggested a similar capability of grid overloading reduction, where the difference in the minimum voltage at the same far-end node was only 0.0023 p.u. Nevertheless, the proposed method has an outstanding strength in unfair charging realignment. The difference in the time until full charge between the upstream and downstream node-connected EV decreased by almost three hours relative to the traditional voltage droop charging method. Paper [51] introduced a rule-based decentralised charging method using historical node voltage data, as well as EV SoC information, to determine the charging rate. Both under-voltage and transformer overloading probability decreased significantly in comparison to uncontrolled charging. The results also imply that embedding extra information such as the EV arrival/departure time, urgency and charging energy demand into the algorithm would not certainly enhance the after-effect. Although an 11.5% charging cost saving was obtained, the transformer loading probability was up to 26% higher with a 0.42% higher failure to the supply rate.

As we can conclude from the above-reviewed papers, extra efforts, such as a sophisticated control scheme and additional information, are always requested to reconcile grid congestion and charging fairness.

EV User-Centric Charging Methods

Third-party information is not always a necessity in EV charging coordination. The EV charging impact alleviation in LV distribution grids can be attained by flattening or staggering the high EV charging powers from each other and from the base load demand. This can be achieved based solely on the charging-demand-related information, which makes this method EV-user-centric, as its primary constraint is the accomplishment of EV charging demand. Examples of popular EV-user-centric charging methods are: reduced power charging (also called average rate charging or individual peak shaving), delayed charging and random charging (with a random rate and/or at random times).

Charging by departure and individual peak shaving methods are investigated in [128].

In this study, the individual peak shaving presents a significant improvement in load peak reduction (up to 60%) while enhancing the PV self-consumption by 3.9% points. However, individual peak shaving is not as effective in grid impact mitigation during the night. Moreover, the charging by departure method could cause a slightly higher evening peak compared to the uncontrolled charging and has an insignificant increase in the PV self-consumption rate.

Four charging methods that fall into random charging or delayed charging categories were studied in [115]: random-in-window with fixed (RIW-FR) or varying rates (RIW-VR), pure-random charging and charging by departure. Among all methods, RIW-VR charging has the best efficacy in both charging peak reduction and load valley filling and RIW-FR is the runner-up, followed by the pure-random charging method. Nevertheless, similar to other research, the charging by departure method shifts the charging load to a later moment with the side effect of creating a second peak, even though this peak is lower than the one with uncontrolled charging.

User participation was included in [54], where three charging programs could be selected by users before the charging starts. The charging programs were allocated by different average charging speeds and matching charging prices. Depending on the program selection and the charging energy request, the charging time for each user varies. The simulation results of a distribution feeder in Ecuador prove that, with a user-selected average power charging method, the peak charging demand was reduced to around 38% of the uncontrolled charging peak power. If the minimal possible charging power is applied, the charging peak demand reduction can be up to half of the peak caused by uncontrolled charging [55]. It was also reported that the reduced charging power method with a charging rate depending on price could save an 11.8% cost per EV per day in Winter [129].

4.1.3. Contributions and the chapter Structure

To what extent the individual criterion is effective in EV charging scheduling and how it influences the system performance is essential and interesting. In this chapter, one method from each approach introduced in the previous section was selected and investigated. They are the price-signal-based method (PSM) for charging cost reduction, voltage droop method (VDM) for grid impact mitigation and the average rate method (ARM) for a user-centric charging approach. Each method only utilises single and specific information as a control reference, where PSM only uses the price signal, VDM solely employs the local voltage value and ARM just exploits user-provided charging session knowledge.

Since each charge scheduling method only considers one factor, the pros and cons of each method are magnified while the trade-offs between them are pronounced. Node voltages correlate well with the loading patterns of the local grid; thus, VDM discriminates against the chargers located downstream of the central substation. On the other hand, PSM can eliminate this location-specific charging behaviour, but communication for price signals is necessary. Furthermore, both VDM and PSM aim to postpone the EV charging demand based on heuristically chosen slopes independent of the user information; hence, these methods are vulnerable to the possibility of incomplete charging events. The ARM takes into account only the EV user input data, which contain the parking time and energy demand information to guarantee that the EV charging requirements are met. However, the charging method is unaware of the grid operating conditions and its performance becomes user dependent.

It is important to benchmark the advanced smart EV charging algorithms using simplified methods targeting either a single objective or ones that are structurally less complex in their implementation to ensure scalability. By studying the fundamental impact of every single factor with our chosen three charging methods, the benchmark criteria are then provided for the reference of future smart charging evaluation. The contributions of our work are listed as follows:

- Three heuristic charging methods were compared vertically with each other and with uncontrolled charging from several perspectives: grid congestion prevention, charging cost minimisation and EV charging completion.
- The comparison was accomplished by means of grid simulations. The simulations on six real LV distribution grids jointly with four EV penetration levels (0, 20, 50, 80%) were investigated in two representative seasons (winter, summer).
- The practical limitation of charging protocol IEC61851 was deliberated, where the charging current has a minimum value of 6 A with discrete incremental steps.
- An in-depth analysis with respect to different charging price schemes is carried out

In Section 4.2, the mathematical principles for the considered charge scheduling methods (PSM, ARM and VDM) are described in detail. The system description of six grid types in the Netherlands, simulation methodology, key assumptions and measured statistical data pertaining to the energy demand, arrival and departure time of EVs is discussed in Section 4.3. Simulation results related to the grid performance in terms of transformer and line loading and the node voltage droop with the considered charging schemes are compared with UNC in Section 4.4. In Section 4.5, the impact of the PSM scheme is explored in more detail. The trade-offs associated with charging demand fulfilment and charging costs are quantified in Section 4.6 and, finally, the key conclusions are highlighted in Section 4.7.

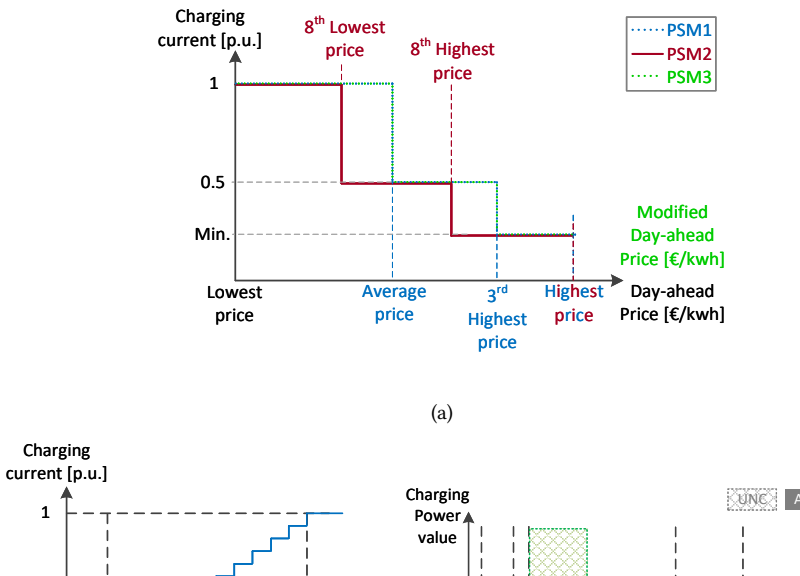
4.2. EV Charging Scheduling Methods

In this chapter, the per-unit format of charging power/current is presented since the rated charging power/current differs for every EV and charger brand. The base EV charging power/current ($p_j^{\text{base}}/i_j^{\text{base}}$) per unit calculation of each EV and charger combination is introduced in Eq. (4.1), wherein $p_j^{\text{max}}/i_j^{\text{max}}$ represent the maximum charging power/current of EV j, and $p_j^{\text{EVr}}/i_j^{\text{EVr}}$ is the maximum charging power/current of the charger at which EV j is connected to it. Therefore, the base EV charging power/current means the maximum allowable charging power/current for a particular EV–charger pair.

$$p_{j}^{\text{base}} = Min. \left\{ p_{j}^{\text{max}}, p_{j}^{\text{EVr}} \right\} \text{ , } i_{j}^{\text{base}} = Min. \left\{ i_{j}^{\text{max}}, i_{j}^{\text{EVr}} \right\} \tag{4.1}$$

One of the most commonly applied AC charger with EV communication protocols in Europe is IEC61851. The charger gives an upper limit of charging current via a pulse-width modulation (PWM) signal through the control pilot (CP) of the connector. According to this protocol, the lowest non-zero charging current set-point is 6 A [45]. Even though the EV is the master in the negotiation, it was assumed in this chapter that the EV charging current always follows the set-point given by the chargers [130]. The constant-voltage (CV) battery charging stage was not considered in the control scheme in this chapter. Therefore, 6 A was set as the minimum charging current in this study. In addition, the charging current/power of the EVs and the set-point given by the charger are not continuous [45].

A discrete charging scheme was then applied and the resolution of the charging current set-point was set to be 1 A. Three charging methods are explained in the following context, and their control scheme illustrations are presented in Fig. 4.1



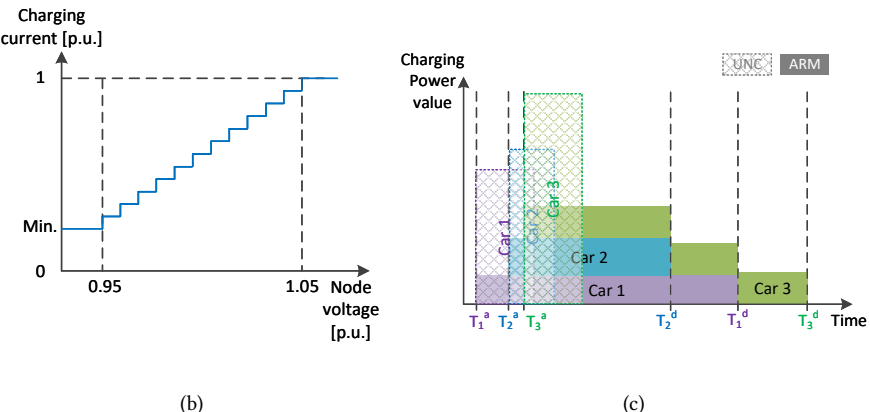


Figure 4.1: Illustration of three charging methods' control mechanism: (a) PSM, (b) VDM, (c) ARM.

4.2.1. Price Signal Method

The idea of the PSM is inspired by the commonly applied TOU-tariff-based time control charging method introduced in Section 4.1 and a field implemented in the pilot project "Flexpower" in Amsterdam, The Netherlands [68]. The TOU method controls the on and off charging status based on the peak-valley price time window and the Flexpower project increases or decreases the charging current limit based on the time of day. The PSM combines two approaches, and the idea is to limit the EV charging current solely based on the electricity price. This price signal could be a predicted intra-day market (IDM) price, a day-ahead market (DAM) price, a predicted market price that reflects the grid congestion or a different type of market price that is available prior to the activation moment of the charging scheduler. In the European market, the DAM price for the next whole day is released one day ahead at 12:00 noon, and the price is fixed for every hour [131]. The

APX Dutch DAM price is then selected as the price signal for PSM due to its advantages of having an early accessibility and a long duration that lasts for 24 h [132]. Without the necessity of collecting local information such as local voltage or the user departure time and charging energy demand, the maximum allowable per unit charging rate of all of the connected EVs is tuned by referring to the DAM price signals.

$$i_{t,j}^{PSM} = \begin{cases} 1 \times i_j^{base}, & \text{if } c_{t,j} \in C_{low} \\ 0.5 \times i_j^{base}, & \text{if } c_{t,j} \in C_{medium} \\ Min. (6A), & \text{if } c_{t,j} \in C_{high} \end{cases}$$

$$(4.2)$$

In this study, we propose a three-price-segment scheme where the price of the next day is divided into three high (C_{high}) , medium (C_{medium}) and low (C_{low}) segments and each segment corresponds to one charging current level. An hourly DAM price signal means that the charging power adjustment is also in a step of one hour. The hourly PSM charging current $(i_{t,j}^{PSM})$ for EV j is limited based on the hourly DAM price $(c_{t,j})$, which is demonstrated in Eq. (4.2).

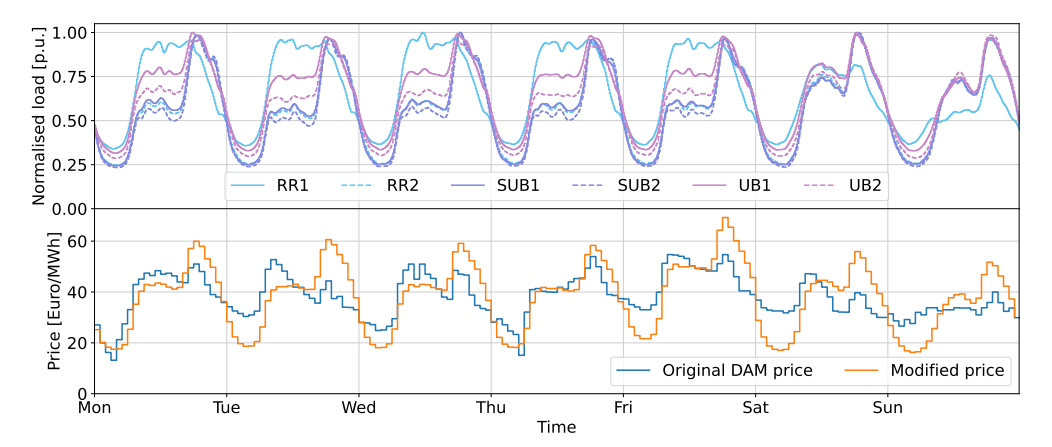


Figure 4.2: Normalised baseloads of six grids compare with two price signals.

Energy prices such as DAM or IDM prices only reflect the supply-demand relation from an energy production-consumption balance perspective but not from a power transmission and distribution perspective. Hence, a separate congestion market is required to factor in the grid loading conditions or to adjust the energy prices in such a way that it can reflect grid congestion as well. To compare how close the DAM price reflects the grid congestion, the normalised grid total baseloads of all six grids and the DAM price of the same time period are plotted in Fig. 4.2. From this plot, it can be observed that even though the DAM price shows a day-and-night price fluctuation and there are two peak hours during the day, the load variation is not well replicated by the price signal. Unfortunately, there is no mature congestion market available in the Netherlands [133] that contains the grid loading information. Hence, a modified DAM price signal is proposed based on the Dutch DAM price. The new price signal is modified by referring to the average base power consumption trend of all six grids, and it shares the same daily mean values as the original DAM price. The curve of the modified price signal can be seen in Fig. 4.2.

Moreover, how the price segment division impacts the effectiveness of PSM is also appealing to study. Two price segment division methods were thus explored. One method is to divide the daily 24 h price into three parts: the top three prices as C_{high} , all prices below the daily average price as C_{low} and the rest of the prices in between, which are categorised as C_{medium} . This method inhibits the time window, during which, the EV charge has a minimal current in order to reduce the limitation on the charging demand as much as possible. The second segment division method is to simply divide the 24 h into three equal parts that are each 8 h long. This division method means that the EVs can be charged with full current for only 8 h of a day, and, in another 8 h, the EV can only be charged with its lowest possible current.

To cover two price signals and two price segment division methods, three PSM schemes are proposed and studied in this chapter. The scheme detail is summarised in Table 4.1 and the schematic of three PSM control schemes is shown in Fig. 4.1 (a).

Method	PSM1	PSM2	PSM3
Price signal	DAM price	DAM price	Modified DAM price
Price segment division		Equally divided into 8 h	$egin{array}{c} C_{high} \colon \text{Top 3} \\ C_{low} \colon \text{Below daily average} \\ C_{medium} \colon \text{The rest} \end{array}$

Table 4.1: PSM methods explanation.

4.2.2. Voltage Droop Method

The VDM tested in this chapter is simply the traditional voltage droop method [52]. A voltage droop response range of 0.95–1.05 p.u., within which, the charging current increases proportionally, was selected to confine the voltage fluctuation within the allowable range as much as possible [110]. When the voltage surpasses the droop response range, the charging current was set to its min/max value. The regulation rules are listed in Eq. (4.3).

$$i_{t,j}^{VDM} \begin{cases} = 1 \times i_{j}^{base}, \text{ if } v_{t,j} \ge 1.05 \text{ p.u.} \\ \propto v_{t,j}, \text{ if } v_{t,j} \in (0.95, 1.05) \\ = Min.(6\text{A}), \text{ if } v_{t,j} \le 0.95 \text{ p.u.} \end{cases}$$

$$(4.3)$$

The VDM was set to only take actions at every fixed time step to prevent the massive oscillations of the current. The trigger timing of the VDM can be adjusted and is synchronised with the simulation time steps. The charging current alteration versus node voltage is plotted in Fig. 4.1 (b).

4.2.3. Average Rate Method

The ARM is relatively simple yet fairly effective for grid congestion prevention, and it was selected from existing work [55]. The ARM reduces the charging impact on the grid while acknowledging the user's requirement and will ensure the full charge of the EV if the user indeed departs as indicated. The ARM spreads out the charging process along the whole EV parking duration, which is only possible if each of the EV users' arrival time T_j^a departure time T_j^d and required energy demand d_j are known. The diagram of the ARM is shown in Fig. 4.1 (c).

$$p_{j}^{ARM} = Min. \{ Max. \{ p_{j}^{ar}, p_{j}^{min} \}, p_{j}^{base} \}, \text{ where } p_{j}^{ar} = \frac{d_{j}}{(T_{j}^{d} - T_{j}^{a})}$$
 (4.4)

Eq. (4.4) depicts how the charging power of EV j (p_j^{ARM}) is determined. The p_j^{ar} was calculated and compared with the base power of the EV and charger combination (p_j^{base}) as well as the minimal charging power p_j^{min} , which was determined by the minimum charging current of 6 A. Afterwards, the ARM charging power was rounded so that the charging current is an integer.

The effectiveness of the ARM is directly related to the duration of the EV parking time within a certain range: the longer the EV parks, the more likely the charging power is to get lower. However, the charging power cannot be infinitely small due to the p_j^{\min} constraint. This constraint leads to the EV parking duration and energy demand being no longer important after a certain threshold. All EVs will be charged with the minimal power p_j^{\min} in that situation. On the contrary, a very short parking time could deteriorate the efficacy of the ARM when the value of p_j^{ar} is close to p_j^{base} . Additionally, the performance of the ARM is also sensitive to the arrival time; for example, if an EV arrives 1–2 h before the peak hour and leaves after the peak hour. Compared to the UNC, with which, the charging process would have been finished before the peak hour, the ARM prolongs the charging process starting from the valley moment and unnecessarily extends the whole charging process to the peak hours. This might lead to an elevated peak loading in the grid.

4.3. Simulation Methodology and System Information

Grid	No. HH	Yearly Energy Consum. [MWh]	PV Installation [kWp]	Avg. Line Length [m]	Longest Feeder Length [m]	No. Transformer and Capacity [kVA]
RR1	3	98.0	2.5	22.8	367.8	1 × 400 kVA
RR2	133	486.8	87.5	7.9	452.2	1 × 400 kVA
SUB1	475	1394.1	180	7.3	566.0	1 × 400 kVA
SUB2	266	800.8	100	8.1	546.6	1 × 400 kVA
UB1	283	1680.2	37.5	4.4	332.5	1 × 400 kVA
UB2	122	261.0	17.5	10.3	360.4	1 × 400 kVA

Table 4.2: Summary of grids' characteristics.

The comparison of three different EV charging scheduling methods was accomplished by PowerFactory simulations and Python data analysis. The simulations of six grids with four EV penetration levels in one winter week and one summer week were conducted with 10 min resolution. Three charging methods were compared with each other, as well as compared to the UNC method from grid performance and charging cost perspectives, as well as charging completion perspective. UNC method was designated in this chapter as immediate EV charging with its rated power as soon as the EV is plugged into the charger.

The six tested grids were real Dutch LV distribution grids provided by the Dutch Distribution system operator (DSO). The tested grids were categorised into three types based on their geographical and functional features, namely rural (RR) grids, suburban (SUB) grids and urban (UB) grids, with two grids per type being considered. The detailed grid features can be found in Table 4.2.

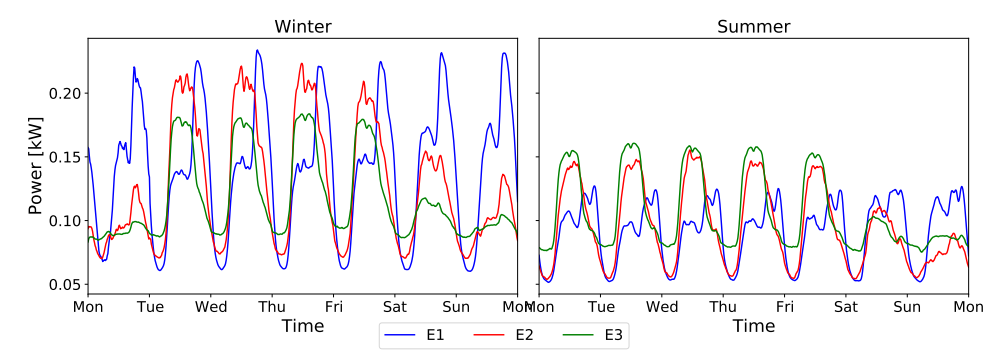


Figure 4.3: Sample load profile for a 1000 kWh yearly energy consumption in both seasons.

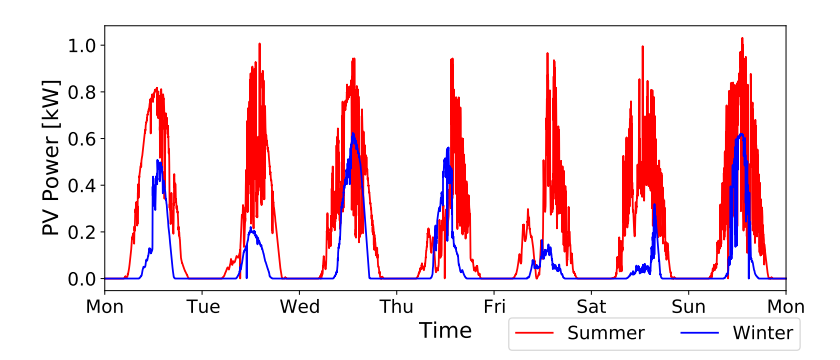
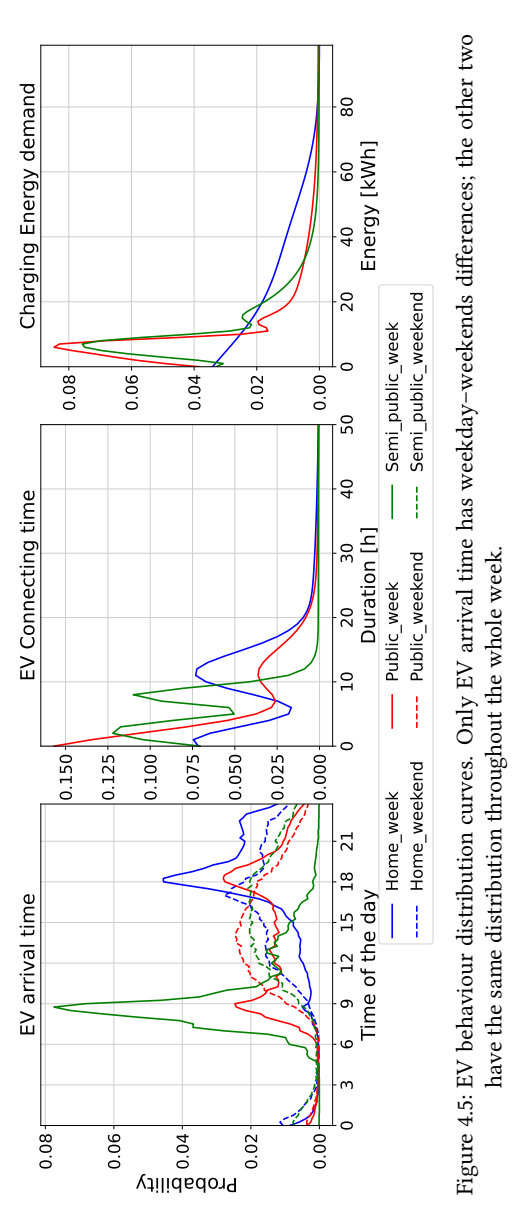


Figure 4.4: Sample PV profile for a 1 kW installation in (a) winter, (b) summer.

The grid baseload profile was modelled based on the load features that were contained in the grid models and the Dutch standardised load profiles [95]. The standard profiles for a 1000 kWh yearly energy consumption load is presented in Fig. 4.3. The profile name in the figure depicts the electrical load type in various scales and patterns. The PV profile modelling was based on a previous study [100]. The one-minute resolution sample profile of a 1 kWp PV installation is shown in Fig. 4.4. It was assumed in this study that RR grids have 25% PV penetration, SUB grids contain a 15% PV penetration and, in UB grid, there is only 5% PV penetration. It was also assumed that, for each installation, the PV peak power is 2.5 kW [97, 98].

In this study, the EV data consisted of two parts: one part is the EV fleet composition and the other part is the EV users' charging habits, including EV arrival time, EV parking time, energy requests and the EV charging frequency.



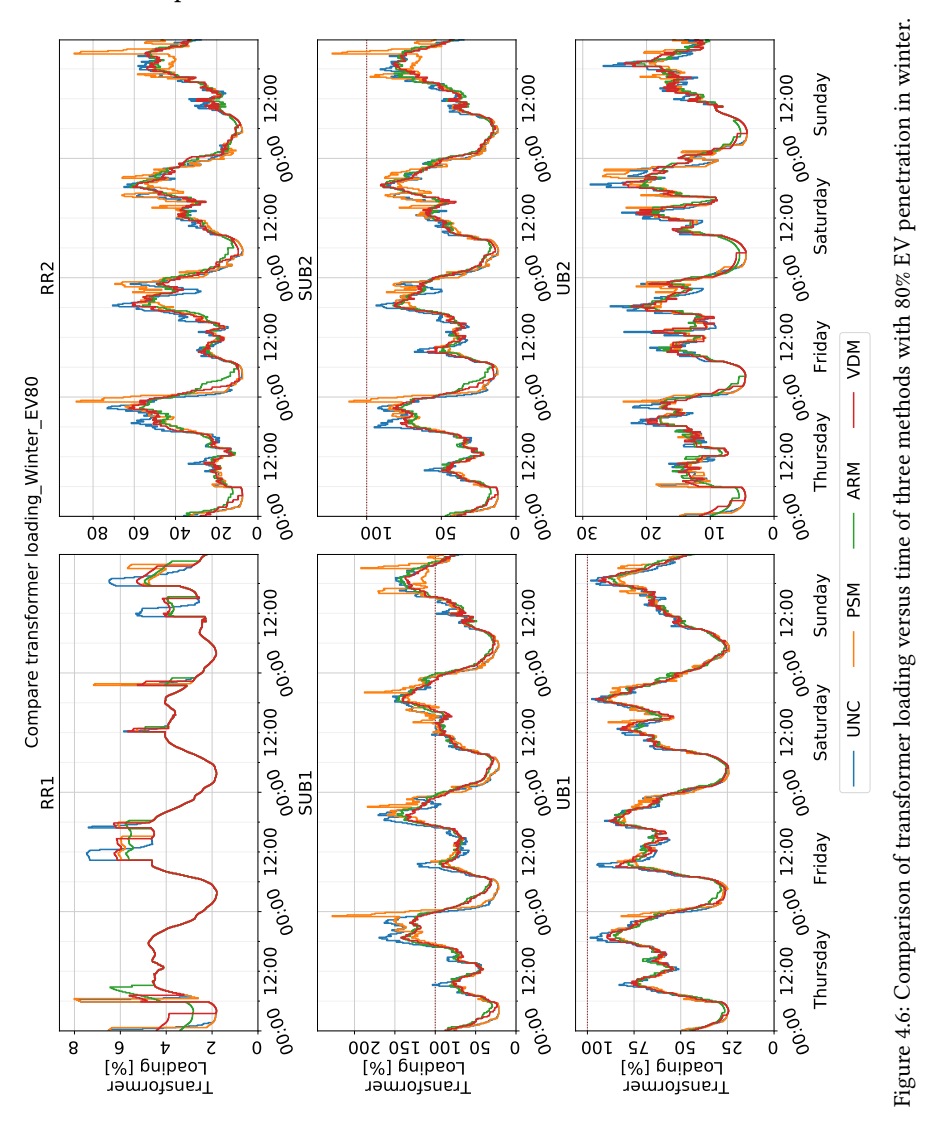
The EV fleet selection was based on the Dutch market data [105]. Top 10 EV models whose battery capacities vary from 35.8 to 90 kWh were modelled in the simulation. The EV charging behaviour data are based on a study that contains 1.5 M real EV charging sessions from charger measurements [104, 109]. The charging sessions can be classified into three typical groups subject to their temporal-spatial features, such as charging location, time of arrival and parking duration. These three groups were identified as home, semi-public and public charging session types, as explained in [103]. The share of charging session groups per grid type is as follows: 70% of the total charging sessions in RR grids are home typ,e and this value is 50% for SUB grid and 25% for UB grids. The rest of the charging sessions were equally divided into semi-public and public types [105]. The probability distribution curves of EV arrival time, EV connection time and charging energy requests of three charging session types are shown in Fig. 4.5.

Finally, the modelling of EV charging profile was accomplished by combining the EV fleet data and the EV charging behaviour. The EV chargers were modelled as LV loads in the grid, and they were all assumed to be three-phase AC chargers with a 32 A max per phase connection. The increase in EV penetration was modelled as the growth in EV charging sessions, and, subsequently, the rising charger numbers. The EV charging sessions, the location and

the capacity of the chargers in the lower EV penetration level were retained. This modelling method also ensures that the only difference between a higher and a lower EV penetration level in a particular grid is the additional EV charging sessions. In addition, all of the charging sessions, including arrival–departure time, arrival SoC and energy demand, were exactly the same for the four charging methods. A detailed description of the grid models and how the simulation data were generated can be found in our previous work [134].

4.4. Comparative Simulation Results for Grid Performance with Different Charging Schemes

In this section, the impact of ARM, VDM and PSM1 on the grid performance in terms of grid congestion alleviation, loading value distribution and overloading on each element is assessed and compared with UNC.



4.4.1. Grid Congestion Alleviation and Charging Session Feature Correlations

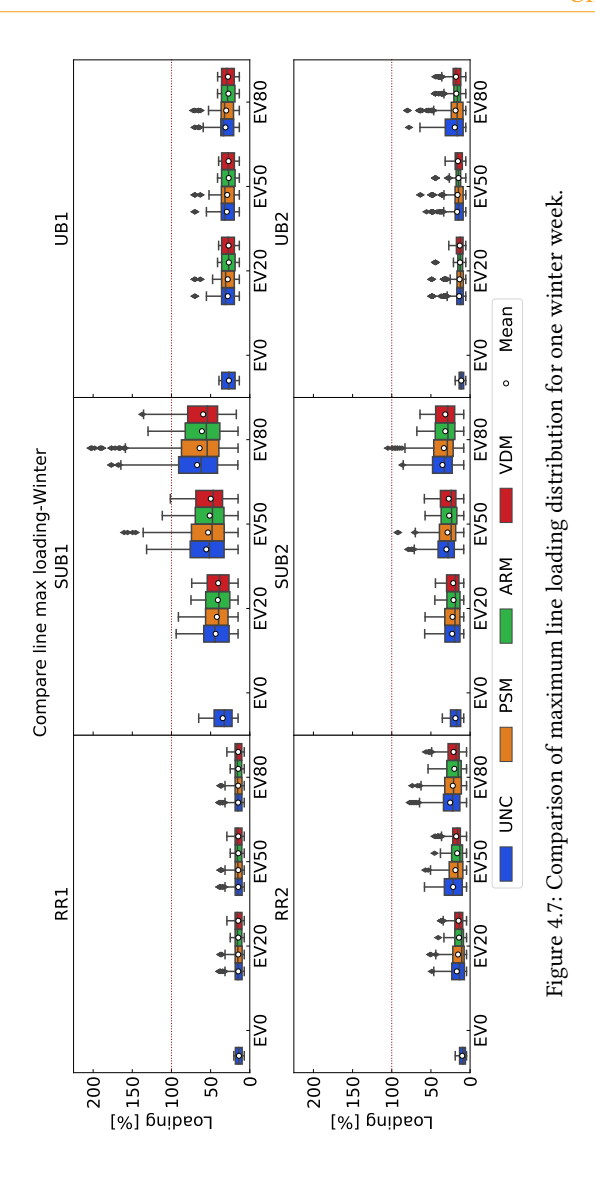
In Fig. 4.6, the transformer loading of four charging methods in an EV 80% scenario in winter is presented, with time as the x-axis. It can be observed that the peak transformer

loading is reduced with the ARM and VDM relative to UNC, whereas it is higher with PSM1. This tendency is particularly relevant for both SUB grids as well as UB2 and RR2 with a high EV penetration, posing a risk of higher overloads if the PSM is used. For example, in the SUB1 grid with EV80 scenario, the topmost transformer loading value of the PSM is 28.7% higher than the UNC and 59.71% higher than the VDM highest transformer loading value.

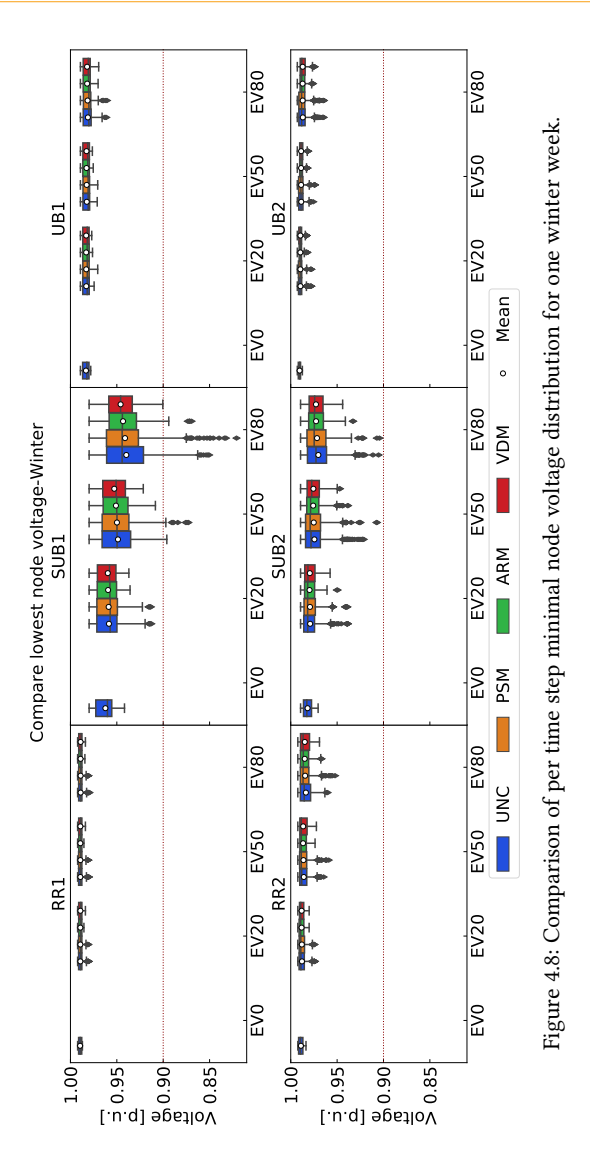
However, while the PSM mitigates the morning peaks and partial evening peaks that are spotted in UNC, shifted new spikes arise later in the evening between 19:00 and 24:00. This is because the PSM curtails the EV charging power and restricts the energy being delivered during the high-energy-price period. When the energy price drops so that the power restriction is lifted, the stockpiled charging demand of yet-connected EVs is released simultaneously, resulting in an abrupt power spike. It can be inferred that this shifted excessive peak demand phenomenon is exacerbated when the most frequent EV arrival time coincides with the peak of the baseload. This is especially the case when a long parking time is expected in the arrived EVs, which is typical for home charging sessions, as shown in the arrival distribution curve exhibited in Fig. 4.5. On the other hand, semipublic and public charging sessions have relatively short parking times and the EVs arrive less frequently in the evening, which coincides with the base-load peak moment. It is also less likely to have a public or semi-public charging session with a duration that extends beyond the evening peak hours and, therefore, most charging events are expected to be completed before the peak hour restriction imposed by the PSM is lifted. Consequently, the shifted peak phenomenon induced by the PSM is significant for SUB grids, in which, home chargers are dominant, and is not observable in UB grids where a higher proportion of public and semi-public charging sessions occur. Based on these inferences, it is suggested that grids with a higher proportion of home chargers are more sensitive to the worsening of the peak load due to PSM charging. At the same time, the expected benefit in terms of cost minimisation and charging demand fulfilment can be lower where short parking times and uniform arrival times dominate, as is the case with public and semi-public chargers; this shall be explored in subsequent sections. Additionally, the profile in Fig. 4.6 shows a peak loading shifting phenomenon between weekdays and weekends, but no essential charging method performance change is observed.

4.4.2. Loading Value Distribution Exploration

The numerical distribution analysis on loading values was performed in our study and the maximum line loading among all lines at every moment in one winter week is shown in Fig. 4.7. The bottom and top edge of the box indicate the 25–75% quantile of the data distribution and the top and the bottom of the I-shape line mark the 1.5–98.5% quantile of the data distribution. The short dashed line in the middle of the colour box signifies the median of all of the data points and the white dot points out the average value of this data group. From this plot, one can recognise that the PSM still exacerbates the line overloading issue, yet it does lower the 25–75% quantile range relative to the UNC results. It is further observed that a slight reduction in the average value of maximum line loading is achieved with the PSM, ARM and VDM-based charging relative to the UNC method, except for three cases in the PSM (RR1 with EV20 and 50, UB1 with EV20) and two cases in the VDM (RR1 with EV20 and 50). The highest reduction in the mean value of the maximum line loading of 7.74% is reached by the VDM in the SUB1 grid with the EV80 scenario. This result



hints that all three charging methods are useful in reducing line loading in the majority of cases. Regarding transformer loading, the margin of the mean and median loading value among all cases is less than 3.5%. In addition, the 25–75% quantile range of the PSM is enlarged in comparison to UNC whereas both the ARM and VDM have a narrower 25–75% quantile range. This implies that the ARM and VDM are effective in not only lowering the peak loading but also in smoothing the loading curve, which makes the data points more concentrated around their median values. This can be clearly pinpointed in Fig. 4.6 as well. The distribution analysis of the minimum node voltage delivers a consistent conclusion, as can be observed in Fig. 4.8. Additionally, the VDM charging scheme performs the best in limiting the greatest voltage drop in the grid, even compared to the ARM.

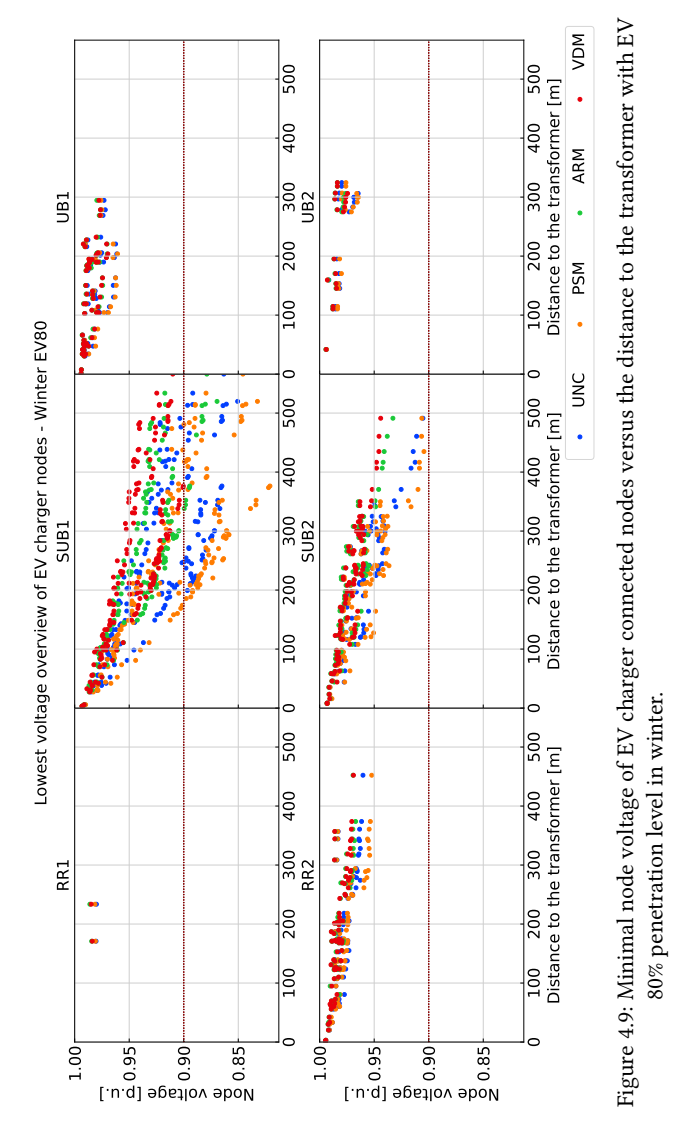


4.4.3. Overloading Assessment on Individual element

A spatial examination of line loading and node voltage distribution along the course of the branch reveals how four charging methods diverge the congestion level of each line and each node.

A scatter plot of the minimum voltage of each EV-connected node versus their distance toward the transformer is presented in Fig. 4.9. The minimal node voltage decreases proportionally to their distance to the transformer. The VDM successfully brings the lowest node voltage back from 0.8506 p.u. with UNC to above 0.9 p.u.. Moreover, the percentage of nodes that ever encountered under-voltage with the VDM reaches 0% instead of 23.53% for UNC. The ARM also has a considerable under-voltage avoidance ability, where, in the

SUB1 grid, the minimum voltage is improved to 0.8695 p.u., whereas the percentage of nodes that have under-voltage problems drops to 5.27% Even though the PSM aggravates the voltage droop problem,



The PSM aggravates the maximum loading of a large number of lines, especially the lines that are closer to the transformer in SUB and UB grids. Many of these lines are part of the main branches; this implies that a simultaneous load growth happens in their downstream sub-branches. The raised loadings that are developed in the sub-branches are passed on to the upper stream main feeders and thus cause this excessive and aggregated main feeder overloading. One example can be seen in Fig. 4.10, in which, the grid loading heatmap of the SUB1 grid with the PSM1 charging method with EV 80% penetration in winter is

exhibited. This heatmap is captured at the highest line loading moment, and the yellow circle denotes the location of the transformer.



Figure 4.10: Grid loading heatmap of SUB1 grid with PSM with EV 80% penetration in winter, highest line loading moment.

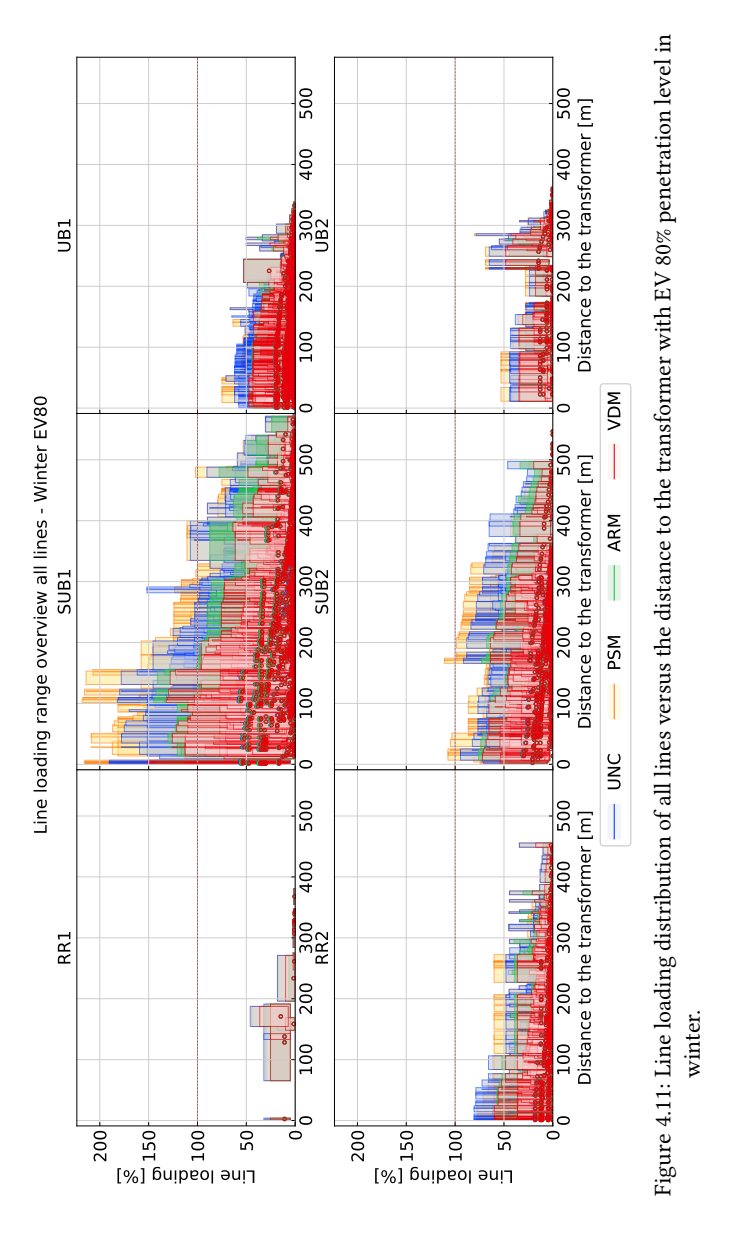
In addition, for every charging method in a particular grid, the maximum line loading has a tendency to decline when its distance to the transformer increases. This trend is clearly shown in the loading distribution plot (Fig. 4.11) of all lines during the whole simulation period. The ARM has the smallest slope of line loading versus distance to the transformer in comparison with other charging methods. That is due to the ARM being the only method that curtails the charging power at every possible moment, and the charging power is constant once the procedure starts. As for the VDM, it curtails the maximum loading of every line the most among all charging methods.

After all, the ARM successfully restrains the charging current of every charging session at every moment within a very low range. A total of 92.61% of the charging current is lower than 10 A for the ARM, whereas this value is 46.49% for UNC, 60.33% for PSM1 and 82.79% for VDM.

4.4.4. Key Takeaways

The VDM functions the best in mitigating the grid loading in all grids from three aspects, and the ARM is the runner-up. Although a previous study [65] obtained a non-ideal grid congestion relief effect using a droop response range lower than 0.9 p.u, our results suggest that the VDM is a parameter-sensitive method. If the voltage boundary is set properly, the grid congestion mitigation could be improved considerably. At the same time, the VDM achieves the given performance solely based on local node voltage measurement, which can be preferable when user information regarding the parking time and energy demand is not available consistently, which is an essential requirement for the ARM.

Despite the fact that the PSM exacerbates the grid peak loading magnitude in SUB and RR grids, it still contributes to shortening the overloading duration even in the most overloaded SUB1 grid with an 80% EV penetration. The grid, 69.74% of the time, does not have



any kind of grid limitation violation, and the PSM improves it to 70.54% of the time. This value is 72.22% for the ARM and 73.81% for the VDM. The PSM causes worse overloading spikes in grids with a large portion of home charging sessions, but it works well to alleviate the loading in UB grids by shifting the charging demand peak to a later less congested moment. Therefore, the proposed PSM is still a good choice for grids with lower EV penetration levels and with a lower portion of home charging sessions, particularly considering the benefits related to charging costs, as shall be later explored.

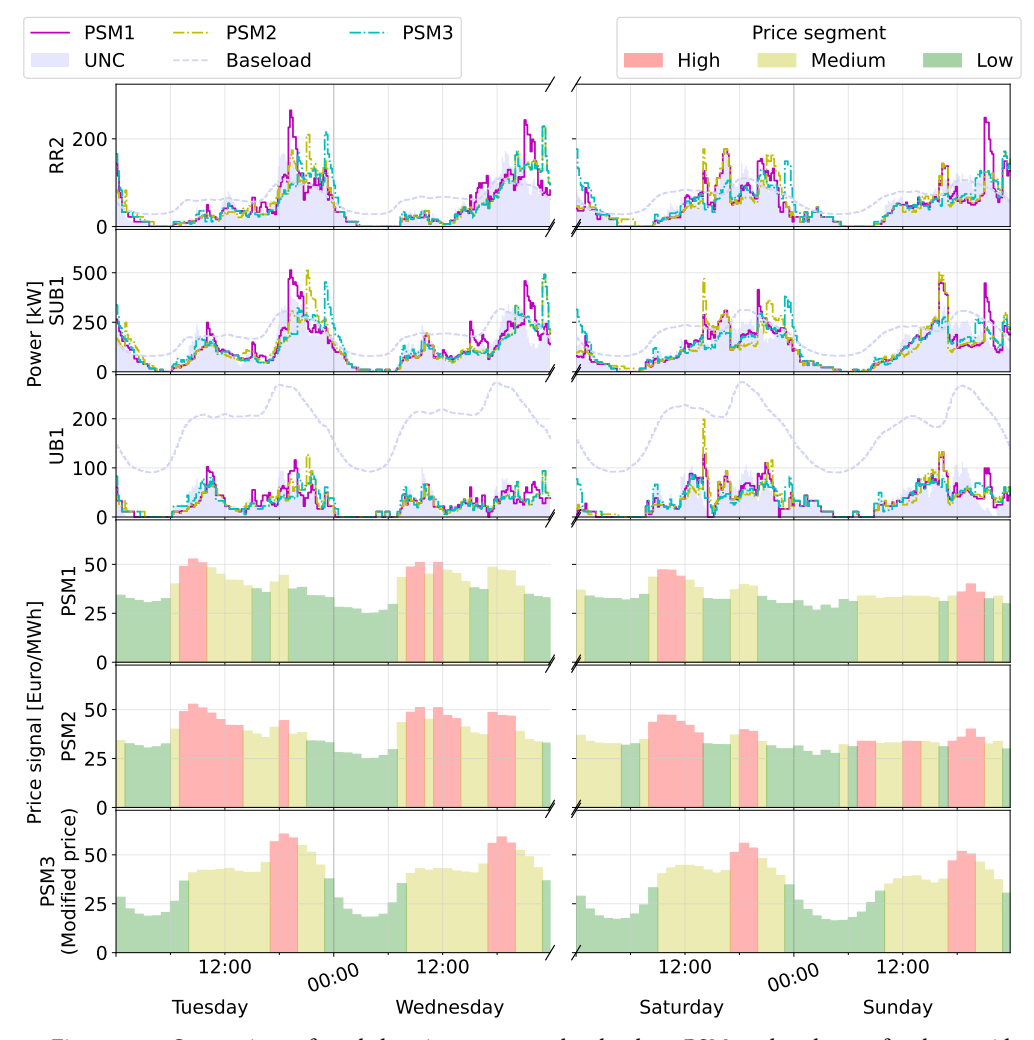


Figure 4.12: Comparison of total charging power under the three PSM study schemes for three grids (top three plots), with the corresponding price signals (bottom three plots).

4.5. PSM Scheme Analysis

To further explore the grid performance deterioration due to the shifted higher peak caused by the PSM, the total EV charging power per grid with three PSM schemes of the EV 80% scenario are compared in this section. The purpose is to see the grid impact when different heuristic restrictions are imposed by using different price signals and various price segment division methods. The sum of all EV charging power with three PSM schemes in three grids (one each type) for four days in winter (two weekdays and two weekends) with an EV 80% penetration level is shown in Fig. 4.12. The sum EV charging power of UNC, as well as the total baseload power, are also presented for reference. The daily price segment schematics of three PSM schemes are displayed in the same plot.

From this graph, it can be spotted that the evening peaks of the EV charging power are postponed and substantially boosted by all PSM schemes in comparison with UNC. This transition happens when the price segment switches from medium to low, causing the charging current limit to shift from 50% to no limit. PSM2 delays the evening peaks further and it decreases the peak amplitude compared to PSM1. This is because PSM2 has a longer duration of low and medium price segments than PSM1, and the EVs have less time to charge with a higher power during the day. On Saturday afternoon at 14:00, PSM2 causes an extremely high power spike in comparison to PSM1 and PSM3. The reason behind this can be found in the PSM2 price segment plot. On Saturday at 14:00, the price jumped from the high segment to the low segment, which means that the charging current limit leaps directly from the minimum level to the maximum level. All of the connected EVs that were charging with minimum current were all tuned to their maximum charging current simultaneously, leading to this high peak value. Comparatively, PSM3 has the best relative performance regarding delaying the power peak as close to the valley moment as possible and lowering the peak power values with the help of the baseload trend adapted price signal. For the overnight charging EVs, the switch to the maximum charging current moment can be further delayed to between 2 abd 6 a.m. the next day when the baseload hits its lowest point.

The natural limitation of the PSM is that, for every round of the price division segment update, it only looks at the 24 h time window from 00:00 to 00:00 the next day, though most home charging sessions with EVs arriving at night would stay overnight. Nonetheless, the renewed price segment starts at 00:00, making the overnight charging control lack continuity. There are two approaches that could potentially resolve this problem. One is to diminish the length of the low price segment and, additionally, to force the medium–maximum charging current transition moment to occur only between 2 and 6 a.m. Another approach is to renew the price segment with a higher frequency and shorten the total control length from 24 h to, for example, 12 h. Because the DAM price of the next day releases at 12:00, the price of the next day can be involved in the new price segment division after 12:00. A potential beneficial point at which to renew the price segment is 18:00, when the evening peak starts. Once the price segment division plan and update frequency are improved as recommended, we believe that the PSM can also be quite effective in lowering the grid loading.

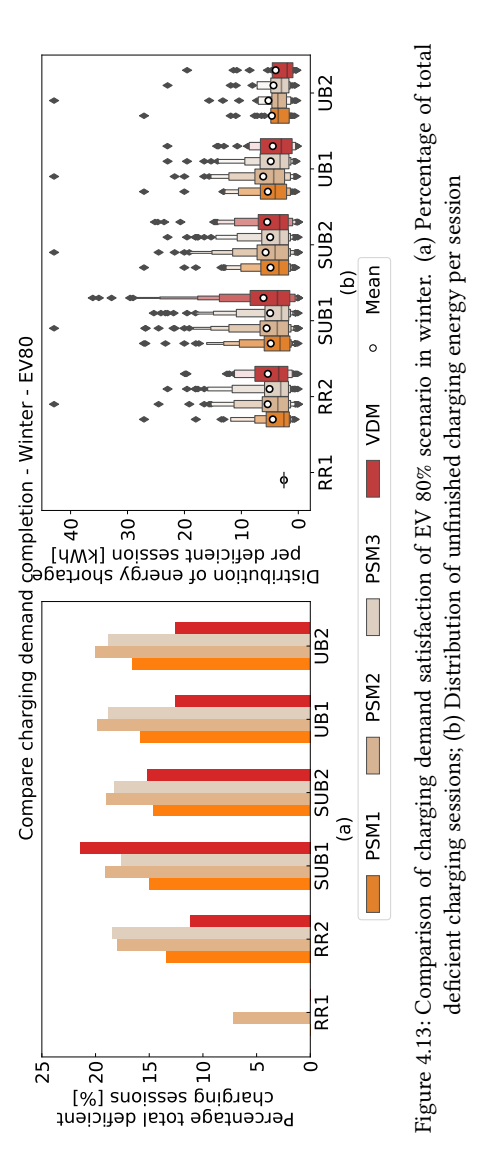
4.6. Charging Process Evaluation

In this section, how the charging process is influenced by three methods is evaluated from charging cost and charging satisfaction perspectives.

4.6.1. Charging Completion

It is assumed that, with UNC, the charging process is terminated when the EV battery is full or when the charged energy reaches the user's expectation. For the exact same charging session, the energy charged with UNC is set as a target for comparison. Due to the nature of the ARM, all of the charging requests input by users in advance are fulfilled, but this is not the case for the PSM and VDM. This is primarily due to the fact that these techniques do not factor in the information related to the energy demand or the parking time of the EV. The comparison of the charging demand completion of EV 80% in one winter week is displayed in Fig. 4.13. In this figure, (a) shows the percentage events of total events

whose charged energy is less than the UNC method, whereas (b) shows, among all of these deficient charging events, the distribution of per-session incomplete charging energy.



From Fig. 4.13, it can be noticed that the charging completion of the VDM is similar to or better than the PSM, except for SUB grids. This is correlated with the grid congestion levels. The VDM directly responds to the grid condition and, in the simulations of this research, the node voltage value is strongly synchronised with the overall grid congestion. For SUB grids, there are more occasions with a longer duration of grid overloading in comparison with the other two types of grids as shown in Section 4.4. The VDM limits the charging current, especially when the voltage is low, whereas SUB1 grids have the highest duration and scale of voltage drops, leading to a strict charging current limitation. As a result, the energy demand of 20.04% of sessions in SUB1 grids is not fulfilled because of the limitation in comparison with the PSM (on average 17.07%) and ARM (0%).

For all grids, all PSM schemes have a similar and stable influence regarding charging completion in both percentages of the deficient session and deficient energy per session. It is easy to interpret that all EVs in all grids use the same centralised control rule and that no other variables are involved in this charging tuning procedure, unlike the VDM, which uses varying local voltages. However, among the three PSM charging schemes, PSM2 has the highest charging demand incomplete rate. As explained in Section 4.5, the control scheme of PSM2 extends the duration of maximum

and medium price segments, which correspond to the minimum and 50% of the full charging current. This means that more EVs have to charge with a lower power for a longer time, which might be even longer than the EV parking time, eventually causing this highest unfinished charging ratio.

4.6.2. Charging Cost

How three charging methods influence the charging cost in comparison with UNC is studied in this section. Both absolute and relative costs were analysed considering the charging demand completion rate as diverse between methods, even with the exact same charging session. The total charging cost (C_{total}^{ch}) and the total charging energy (E_{total}^{ch}) from all six grids, as well as the ratio of total savings (γ_{total}^{save}) and the total energy-deficient ratio (ϵ_{total}^{def}) of all charging methods with respect to UNC with 80% EV in winter are summarised in Table 4.3.

Season	Compare Items	UNC	PSM1	PSM2	PSM3	ARM	VDM
	$C_{total}^{ch} [\in]$	1900.79	1766.25	1701.88	1737.29	1834.32	1902.00s
Winter	Ysave [%]	-	7.08	10.46	8.60	3.50	-0.06
winter	Etotal [kWh]	45,664.63	43,671.41	42,576.50	43,137.44	45,763.09	43,711.11
	ϵ_{total}^{def} [%]	-	4.36	6.76	5.53	0	4.28
	$C_{total}^{ch} [\in]$	2789.20	2599.73	2510.90	2617.83	2721.22	2844.47
Summer	Y save [%]	-	6.79	9.98	6.14	2.44	-1.98
	E_{total}^{ch} [kWh]	45,664.63	43,666.40	42,368.90	43,205.43	45,763.09	44,119.27
	ϵ_{total}^{def} [%]	-	4.38	7.22	5.39	0	3.38

Table 4.3: Total charging cost and energy failed to deliver comparison.

It should be noted that the total energy charged with the ARM being higher than UNC is due to the simulation setup and the data resolution. For every time step (10 min in the simulation), the charging current of the ARM is constant and the minimum value is 6 A; thus, the minimum chargeable energy for a three-phase connection EV per step is 0.69 kWh. If the energy to be charged by referring to UNC is less than this value, the higher charged energy situation happens. In the meantime, there is an overcharge prevention mechanism to ensure that SoC never exceeds 1. From this table, it can be perceived that both the PSM and ARM reduce the charging cost and that PSM2 saves the most expenses. For the PSM, the value of the saved cost is correlated with the energy-deficient ratio, whereas the ARM does not compromise the energy being delivered. On the other hand, the VDM is the only method that costs more to charge but obtains less energy for EV users.

Every charging session has various energy demands and uses divergent price values. Hence, a comparative charging cost factor $(C_{k,norm}^{xM})$ is introduced for a fair comparison, with the charging sessions of UNC as the benchmark.

For every charging session, the relative charging cost of method xM (one of PSM, ARM and VDM) is first calculated by $C_k^{\rm xM}/C_k^{\rm UNC}$, where $C_k^{\rm xM}$ is the charging cost of session k with method xM and $C_k^{\rm UNC}$ is the charging cost of the same session but charged with UNC. Since not all of the energy demand is fulfilled in every charging session, especially with methods PSM and VDM, a charging fulfilment correction factor is introduced to correct the charging cost reduction due to the charging energy deficiency. The correction factor is calculated by $E_k^{\rm xM}/E_k^{\rm UNC}$, where $E_k^{\rm UNC}$ is the delivered energy with method UNC and $E_k^{\rm xM}$ is the charging energy delivered with method xM. The equation of the $C_{k, \rm norm}^{\rm xM}$ calculation

is shown in Eq. (4.5).

$$C_{k,\text{norm}}^{\text{xM}} = \frac{C_k^{\text{xM}}/C_k^{\text{UNC}}}{E_k^{\text{xM}}/E_k^{\text{UNC}}}$$
(4.5)

The comparative charging cost factor $C_{k,norm}^{xM}$ of every charging session with all charging schedule methods is visualised in the box plot in Fig. 4.14. From this figure, it can be concluded that both the ARM and PSM can reduce the charging price decently. Aside from the ARM in RR1, the PSM and ARM both have a mean $C_{k,norm}^{xM}$ value lower than 1 in all of the other grids. On average, 31.63% of PSM charging sessions have a $C_{k,norm}^{xM}$ value higher than 1 and they are solely caused by unfulfilled charging energy requests. With the ARM, this value is 30.83%. On the contrary, on average, 83.12% of VDM sessions have a significantly higher $C_{k,norm}^{xM}$ value because of both the high charging cost and unfinished charging requests. On the other hand, the VDM is excellent from a grid congestion perspective as seen in the previous section. The $C_{k,norm}^{xM}$ difference among PSM1, PSM2 and PSM3 is negligible. PSM2 has the lowest minimum $C_{k,norm}^{xM}$ value, as it has prolonged half and minimum charging limit time windows, where many EVs are charged more during the low price window.

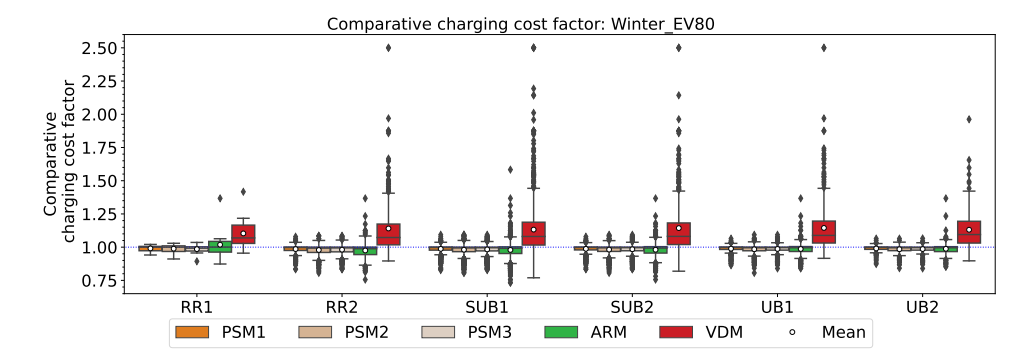


Figure 4.14: Comparative charging cost factor of EV 80% scenario in winter.

4.7. Conclusions

Heuristic charging techniques such as the PSM, ARM and VDM were compared with UNC in terms of the grid performance, charging demand fulfilment and economic benefits. These trends were quantified for different grid types with an increasing EV penetration for summer and winter, and the following are the main observations:

- The VDM is the most effective in improving the grid performance peak and median loading, as well as the node voltage drops relative to UNC, whereas the PSM can worsen the performance, particularly for suburban grids, where the percentage of home chargers is high.
- The ARM is most effective in simultaneously improving the grid performance and meeting the user energy demand. On the contrary, both the PSM and VDM lead to 10–20% unfinished charging sessions, with a total energy deficiency ratio of 4–8%.
- The PSM can reduce the total charging cost by 6-11% relative to UNC and the ARM

leading to cost savings of 2-4%. On the other hand, the VDM increases the charging cost by 0-2%.

Benchmark Index	Grid Performance	Charging Cost	Unfinished Charging	Fairness	Comm.	Forecasting
PSM	_	++	_	О	_	_
VDM	+	+	O	-		O
ARM	++	_	_		_	О

Table 4.4: Performance comparison.

From the study results, we can conclude that the PSM can be a preferred strategy for achieving a charging cost reduction where the grid performance is not a bottleneck for the given EV penetration. We also have confidence in the PSM concerning grid congestion alleviation if (1) the price signal can reflect the base load fluctuating and (2) the price segment division is updated so that the beginning moment of full power charging for overnight EVs can be shifted to 2–6 a.m. At the same time, the VDM should be preferred if user information on the parking time and energy demand is not consistently available. The ARM provides the best balance in the trade-offs associated with the mitigation of grid congestion and price reduction, as well as charging completion. However, user information related to the EV parking time and energy demand is necessary. The qualitative benefits and operational requirements of the explored charging schemes are summarised in Table 4.4.

For future work, several points can be covered further. Sensitivity analyses on more PSM price signal sources, as well as price segment division methods, can be beneficial. It could be appealing to investigate how the voltage droop response range impacts the VDM performance. In addition, it is worth inspecting how the node voltage fluctuates in between voltage droop command signal intervals. Last but not the least, the EV battery lifetime is a critical aspect that must be investigated in future work to compare the performance of these different charging methods.

^{&#}x27;O' Same,'-' Worse and '+' Better

Centralised EV charge management schemes aiming grid congestion assuagement

To tackle the potential grid overloading issue induced by excessive EV charging demand, a Low Voltage (LV) grid congestion management algorithm with three centralised EV charging management schemes is proposed in this study. The developed algorithm integrates grid information and – through linear programming (LP) or iterative calculations – aims at tackling the foreseen congestion issues by operating on the EV charging processes. While the first charging scheme aims at managing the congestion by only affecting the elements with the greatest influence on the congestion, the other two aim at maximising the social welfare and the overall energy transfer to the EVs, respectively. The simulated results are compared in terms of performance criteria such as grid impact, user satisfaction and fulfilment of charging energy demand. Overall, this study shows that the first scheme brings the best results from a grid perspective. On the other hand, the last scheme leads to competitive results from a grid point of view and the best overall results from a user perspective.

5.1. Introduction

The global constant growth in the number of EVs has led to the necessity of finding solutions to the technical issues that are expected to arise. One of these issues is the formation of overloads in the electrical grid due to the simultaneous charge of many EVs [103, 134]. To study this phenomenon and to alleviate grid congestion problems, a centralised EV charging control algorithm is proposed in this study. Within this algorithm, one out of three different developed Charging Management Schemes (CMS) – the logic according to which the charging stations where the charging power is adjusted are selected – can be integrated. These three schemes have been developed focusing on three different objectives. The first one aims at relieving the congestion by reducing the least total amount of power, the second one aims at distributing the power fairly among all charging stations, while the third option aims at optimising the success of the EV charging processes. These three CMSs are carried out via LP or iterative calculations. The algorithm is tested on two sub-urban LV distribution grid models with real grid data. In each grid, four different scenarios are simulated. In the first scenario, no CMS is applied. This is a reference case to

^oThis chapter is based on paper: D. Dreucci, Y. Yu, G. Ram Chandra Mouli, A. Shekhar, and P. Bauer, "Centralised distribution grid congestion management through ev charging control considering fairness and priority.", Submitted.

assess the effects of uncontrolled EV charging. In the remaining scenarios, the algorithm is implemented by integrating one of the CMSs for each scenario. The results of these simulations are studied and compared in terms of performance criteria such as grid impact, user satisfaction and fulfilment of charging energy demand.

5.1.1. Literature review

In literature, the methods to tackle grid congestion are generally categorised into two major groups: Distribution Network Reconfiguration (DNR) [135, 136] and Demand Response (DR) programs. Among DR, Direct Load Control (DLC) [137, 138], economic mechanisms [139], or the combination of both [140] are commonly applied. The economic mechanism based DR has a time scale from monthly, day-ahead to intra-day, while DLC aims at a very short term in the unit of minutes [141]. Moreover, DLC is more direct and accurate than the economic mechanism [142], making DLC a better candidate for the last-minute congestion management. To achieve the ideal congestion mitigation outcome, grid features often need to be incorporated in both the economic and the DLC approaches. For this reason, Distribution System Operators (DSO) usually play a key role in the process of grid congestion alleviation.

The economic mechanism-based grid congestion methods are always implemented first as they can plan ahead to prevent congestion and they have fewer hardware as well as regulation restraints in comparison with DLC. For precise, efficient, and thorough grid congestion alleviation, DSOs are usually heavily involved as the grid information is often requested.

In paper [143], a grid congestion mitigation method with a transactive control approach is proposed. In the proposed method, EV aggregators first submit the optimal charging schedule aiming at minimising the charging cost while ensuring the charging requests being fulfilled. On the other hand, DSO also uploads its optimise requests focusing on minimising the system loss while retaining the aggregator's charging schedule as much as possible. In the end, a third-party price coordinator was introduced, and it updates the congestion price to the aggregator and the DSO and coordinates both parties' schedules until the price converges. The proposed method reduces a maximum of 38.8% energy loss with EV 100% penetration and improved the minimal voltage by a maximum of 14% compared to the uncontrolled method. However, the more function it contains (e.g. considering transformer overloading and voltage drop), the more iteration thus the longer computational time is requested till the price value reaches equilibrium.

Economical based grid congestion management mechanism

To avoid excessively burdening the aggregator's computational power, new solutions to include grid congestion information in the electricity market mechanism are becoming more popular among economic-based DR mechanisms. Among these are Dynamic Tariff (DT) [140, 144], Dynamic Power Tariff (DPT) [139, 140] and Distribution Locational Marginal Price (DLMP) [145, 146]. DLMP is the marginal cost of energy, grid congestion and losses, DT is the energy tariff which synchronises with the load demand magnitude, and DPT is the power tariff with which the peak demand power of the customer is charged.

DLMP can be obtained at each node by solving a DC optimal power flow (DCOPF) problem in which the Power Transfer Distribution Factor (PTDF) concept is often used to establish the relation between the node injection power and the line power flow [145, 146]. With the help of PDTF, the location and scale of grid congestion can be easily obtained. The DCOPF solution can also be used to calculate the DT. In [140] the DT is calculated by the DSO for market-based congestion management. Through DT the energy tariff is synchronised with the load demand magnitude and so does the grid congestion trend reflected in the energy tariff. The congestion mitigation method proposed in [139] uses DPT, which is obtained by iterative transactions between the DSO and the aggregator, as a congestion signal. The OPF is executed at DSO side to check the network limitations in which the PTDF is calculated. In order to calculate the aforementioned congestion-coupled electricity price/tariff, the DSO needs to predict the spot market price as well as possess the whole knowledge of the load demand of the coming period [140, 144, 146].

Nevertheless, the results obtained in [139, 140, 144, 146] suggest that none of the congestion adapted market methods solely can guarantee a stable congestion alleviation outcome, due to the stochasticity from the spot market price, the load demand and the behaviour of aggregators. To stabilise and improve the performance, the market-based method is usually combined with a different market mechanism [140], a grid reconfiguration [144, 145] or another load response method to procure extra flexibility through the DSO intervention [144, 147]. For example, authors of [147] proposed a grid power flow denotation matrix in which binary values are used to mark whether current flow is detected in certain branches due to power injection happening at a specific bus. This matrix is then used to identify the congested regions in the grid, and then a decentralised sub-market (DSM) can be formed with responsible parties at the designated area. When occasional unsolved congestion appears, the DSO steps in to facilitate extra support via an optimisation program aims at relieve the grid capacity as much as possible while doing the power re-location as little and as locally as possible. A similar situation is found in [144] that a congestion mitigation method combining DT, DNR, as well as re-profiling, is proposed. The re-profiling part is the backup solution when the market method is not sufficient, and the DSO is in need of request extra capacity from the flexibility providers.

DLC-based congestion management

DLC methods could be a potential solution to the congestion issues. In [148] a decentralised Additive Increase and Multiplicative Decrease (AIMD) based EV charging method is proposed, in which EV charging currents are controlled locally by referring to the local voltage fluctuations. The results showed that the AIMD-based method maintained the grid operation within the allowed constraints. The case studies show that, even though none of the household's voltage value is lower than the critical threshold (0.9 p.u.) at 100% EV penetration level, there is still roughly 2 hours of power overload out of 8 hours of total simulation time. On the other hand, the results of the centralised baseline AIMD case show that none of the grid constraints was violated while the grid capacity usage was maximised for EV charging. A similar observation is concluded in [149], where the adaptive AIMD (A-AIMD) algorithm developed has excellent performance regarding transformer loading, charging fairness and user satisfaction. The centralised convex optimisation - whose objective is to maximise the EV charging power within the grid limits - outperforms the A-AIMD algorithm slightly, but it is computationally heavy due to the grid power flow in its optimisation procedure. Thereupon, a centralised grid congestion mitigation approach - where a central entity (e.g. DSO) oversees the grid operational condition and another entity like an EV aggregator executes the DLC command - is more favourable regarding effectiveness and computational power saving.

The multi-objective congestion management algorithm developed in [150] focuses on both cost saving and valley-filling. The DSO is in charge of relieving any grid congestion through an interactive approach with the aggregators. During the interactive operation, the DSO uses PTDF to update the grid congestion level dependent Pareto weight, then the aggregator uses this weight to solve the multi-objective function. This interactive process operates continuously until no more congestion is detected. The proposed algorithm showed a balance between the charging cost reduction and the peak load decrease. On the contrary, the Distributed Dynamic Tariff (DDT) method with which the algorithm was compared, led to grid congestion due to low price driven vast synchronised charging.

The algorithm proposed in [151] uses sparse grid measurement to extract grid information and estimate the grid congestion status. The DSO not only owns and operates the sparse measurement equipment, but also in charge with giving grid loading limits. Whenever congestion is detected, a signal is sent out from the DSO suggesting a pause or start of the charging process. The proposed method has a congestion detection accuracy between 73.07%-100%. The results also signify that the EV charging time could be prolonged up to 1.8 times in exchange for a congestion-free grid operation condition.

PTDF is a very efficient and effective way to identify the most congested branch as well as to recognise the power injection through which buses has the highest impact on the congestion [152, 153]. Besides, as stated in previous paragraphs, the DLC is a good candidate for accurate real-time grid congestion management. Therefore the PTDF involved DLC congestion management algorithm is an appealing option to oversees and alters the grid operation.

EV charging scheduling methods

EV user satisfaction is another key objective to consider while alleviating grid congestion through charging management. How to ensure the safety grid operation while balancing the capacity allocation efficiency, charging demand fulfilment and fairness is prominently challenging. EV expected connecting time and their requested departure SOC are usually used to calculate the charging urgency and by referring to this urgency, the charging order and power magnitude are sorted and allocated [154, 155]. However, only considering charging urgency could cause discrimination, especially for long-parking EVs with large battery capacity. How different priority criteria vary the fairness in EV smart charging are extensively discussed in [58, 64, 156]. Study [58] developed a fluid model to approximate the user behaviour under four charge queuing policies: Earliest Deadline First, Least Laxity First, Least Laxity Ratio (LLR) and Processor Sharing. The indices of attended versus requested service and the fairness show that the LLR method has the best performance. Paper [64] compares the power and time-coordinated charging methods in combination with three priority factors: SOC, slack time, and allotted time/energy. The charging accomplish results such as the probability of EVs not being charged, indicate that the combination of multiple priority criteria would achieve higher flexibility as well as fairness with different EV types. The fairness of EV smart charging is extended to the vehicle to grid (V2G) in research [156], where three EV management criteria are considered: the SOC level, the contribution to the V2G and the local load level. It is concluded that the contribution-based charging priority method can flatten the peak load while also shortening the EV charging time. The fairness of six EV charging queuing policies is compared with the quality of service/experience index in paper [157]. Besides, the performance of all six policies regarding node voltage drop and grid losses are compared.

Although the assessment of charging sequence policies are covered in multiple past works, there is not yet a study about charging capacity allocation-consolidated advanced grid congestion management being conducted coherently. The dominant motivation to deploy EV charging scheduling is limited resources like constrained grid capacity after all. It is hence our profound interest to explore how different priority criteria impact the efficacy of grid mitigation performance. Nevertheless, this chapter covers the research gap of developing the grid management algorithm with EV charging scheduling considering priority and fairness, thorough analysis w.r.b. to grid congestion mitigation, user satisfaction, load shifting over-compensation and so forth.

Following the above review and discussion, DLC appears to be a good candidate for accurate real-time grid congestion management, while PTDF is a great tool for identifying overloaded branches and their level of congestion. Instead of using PTDF to calculate the Available Transfer Capability (ATC) or to select the suitable branch for DR as most studies do, this chapter uses PTDF to obtain information regarding how to adjust the excessive EV charging demand to restore the overloaded elements back to their normal operational range. Besides, the above-reviewed EV-charging management research often concentrates on one main objective, which is to minimise EV user dissatisfaction or to improve the use of the grid. Conversely, this chapter developed a PTDF-involved DLC congestion management algorithm combining with three EV CMSs focusing on efficacy, fairness and priority, respectively. Therefore, the main contributions of this chapter can be summarised as follows:

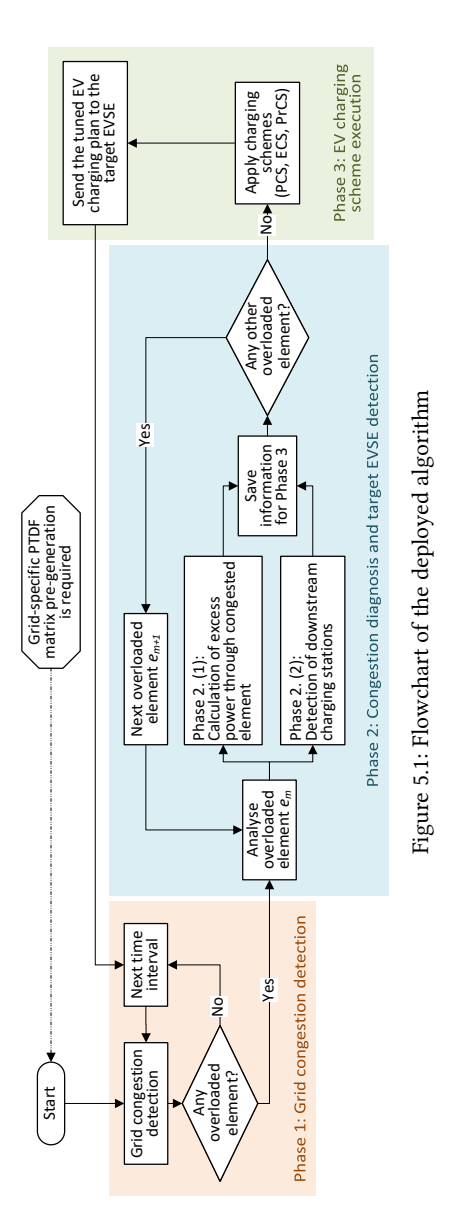
- Developed a high-efficacy, centralised grid congestion recognition and mitigation algorithm with DLC mechanism involving PTDF
- The congestion management algorithm is combined with three proposed EV CMSs where the congestion alleviation efficiency, EV user fairness and EV charging priority are selected as the primary target, respectively. Their performances have been compared
- Case studies were accomplished through grid simulation with two real grid models as well as real measurement-based EV charging data
- Simulation results were analysed from both DSO and user perspectives, including: branch overloading, voltage dip, EV charging demand satisfaction
- The over-compensation of grid congestion mitigation phenomenon was also discussed

The chapter is organised as follows: methodology in Section 5.2; grid modelling and input data explanation, as well as scenario description are in Section 5.3; simulation results and analyses are presented in Section 5.4; while conclusion and recommendations are in Section 5.5.

5.2. Methodology

The proposed centralised algorithm shown in Fig. 5.1 adjusts the charging power at Electric Vehicle Supply Equipment (EVSE) to mitigate the grid congestion considering three possible schemes that are described in subsequent subsections: (i) PTDF-based Char-

ging management Scheme (PCS) (ii) Egalitarian Charging management Scheme (ECS) (iii) Priority-based Charging management Scheme (PrCS).



In the proposed algorithm architecture, the DSO detects whether grid congestions are bound to happen as a result of EV charging requests and sends the signal to the aggregators. The aggregators and, in turn, the EV users would be compensated for their charging adjustments through agreements such as flexibility contracts. The PTDF matrix is built by activating all EVSEs one at a time and registering the effects on all the other elements of the grid to indicate the variation in real power that occurs on all lines [158].

This is necessary to determine all EVSEs whose charging processes have an influence on the overloaded grid elements. It should be noted that only the nodes where an EVSE is connected have been included in the construction of the PTDF matrix. A fixed PTDF is considered consistent throughout the simulation, based on the assumption that the grid condition is stable and the node voltages can be maintained within expected boundaries [159]. Once the grid-specific PTDF matrix is built, the charging control algorithm is ready to be launched.

5.2.1. Phase 1: Grid congestion detection

The algorithm evaluates whether the current grid status, in conjunction with the EV charging requests, leads to congestion issues at a fixed time step in the scale of minutes. In a real operational environment, this could be done by checking the smart meter readings, communicating with the EV aggregators in combination with the background system simulation or distribution system estimation run by the DSO [160].

All EVs' default charging requests at any given moment are set as uncontrolled, which is to charge immediately after plug-in at rated power. In this study, congestion detection is realised through load flow analyses.

5.2.2. Phase 2: Congestion diagnosis and target EVSE detection

The main characteristics of the overloading issue, corresponding to the problematic grid components such as the charging stations involved along with their location and the magnitude of the issue, are identified. This phase consists of two main mechanisms that are discussed in the following subsections.

Calculation of excess power through congested elements

For M overloaded grid elements – e_1 , e_2 , ..., e_m , ..., e_M – the excess power P_{e_m} of each overloaded element is estimated. The calculations shown here refer to the case of a congested line e_m , but the same logic applies in case the element is a transformer. The line loading percentage λ is given by Eq. (5.1).

$$\lambda = \frac{|I_{\text{line}}|}{I_{\text{r}}} \cdot 100 \tag{5.1}$$

where, I_{line} is the current registered at the line, while I_r is the rated current of the line. The apparent phase power S_p – at any phase p – corresponding to the active (P_p) and reactive (P_p) powers is given by Eq. (5.2).

$$S_{\rm p} = U_{\rm p} \cdot I_{\rm p^*} = P_{\rm p} + jQ_{\rm p}$$
 (5.2)

Where, the phase voltage U_p and the current I_p are written in terms of their complex representation in Eq. (5.3) and Eq. (5.4), respectively.

$$\underline{U_{\rm p}} = U_{\rm base}(u_{\rm p,real} + ju_{\rm p,imm}) \tag{5.3}$$

$$I_{p^*} = I_{\text{base}}(i_{\text{p,real}} - ji_{\text{p,imm}}) = I_{\text{p}}(\cos\phi_i - j\sin\phi_i)$$
 (5.4)

Here $U_{\rm base}$ (in V) and $I_{\rm base}$ (in A) are the base voltage and current, respectively, while the term $I_{\rm p}$ (in A) refers to the magnitude of the current and the term ϕ_i to the current angle. The terms u_p and i_p are expressed in p.u. . Combining Eq. (5.3) and (5.4) with Eq. (5.2) and considering only the real part, $P_{\rm p}$ can be written as shown in Eq. (5.5).

$$P_p = U_{base}(u_{p,real}cos\phi_i + u_{p,imm}sin\phi_i)I_p = K_{load}I_p$$
 (5.5)

 $P_{\rm p}$ can be rewritten in terms of λ in Eq. (5.6).

$$P_p = \frac{\lambda}{100} K_{load} I_r \tag{5.6}$$

For the maximum permitted power P_p' , the difference $\Delta P = P_p - P_p'$ should be reduced to resolve the overloading issue in phase p. Considering balanced operation, the three phase excess power is calculated as $P_{e_m} = 3 \cdot \Delta P$ for each overloaded element e_m .

Detection of downstream charging stations

The second part of the process consists in collecting data regarding N EVSEs potentially available to have their charging power managed (labelled as $s_1, s_2, ..., s_n, ..., s_N$) and their influence on the congested elements of the network in a matrix $\tilde{A}_{M,N}$ of size $M \times N$. The

indices $a_{m,n}$ of matrix $\tilde{A}_{M,N}$ are directly derived from the PTDF matrix, and they indicate the percentage of power asked by charger s_n that flows through element e_m . The index $a_{m,n}$ in the matrix $\tilde{A}_{M,N}$ corresponds to the absolute value of the element at the intersection between charger s_n and the element e_m in the PTDF matrix. This case applies only if all the following conditions apply.

- 1. The flow of power caused by the EV is in the same power direction as the overloads.
- 2. Charging processes with an impact greater than 5% on the congested element will be requested to have their charging power adjusted.
- 3. There is an EV connected currently asking for power at charging station s_n .

If any of the three options do not apply, the index $a_{m,n}$ will be set to zero.

5.2.3. Phase 3: EV charging scheme execution

The EV charging management scheme is activated and it determines, from a uncontrolled charging start point, which charging process to adjust at which EVSE to relieve the overloaded elements. Only one out of the three CMSs (PCS, ECS, PrCS) is used in this phase.

PTDF-based Charging management Scheme (PCS)

The PCS optimally distributes the power to be reduced from relevant charging processes considering a grid point of view only. In fact, the only parameter included in the analysis to discern among the charging points is their influence on the overloaded elements. This information is contained in matrix $\tilde{A}_{M,N}$. Therefore, this scheme aims at reducing the minimum total amount of power possible, by operating on the chargers that contribute the most to the overload. This is made by means of a LP algorithm with an objective to maximise the power provided to the charging stations, as in Eq. (5.7).

$$maximise \quad \sum_{n=0}^{N} P_{s_n}^{new} \tag{5.7}$$

The variables of the optimisation analysis are $P_{s_1}^{new}$, $P_{s_2}^{new}$, ..., $P_{s_N}^{new}$, that are the charging power at EVSEs s_1 , s_2 , ..., s_N , respectively, after the optimisation algorithm is applied. For these variables the following conditions apply:

$$P_{s_1}^{new}, P_{s_2}^{new}, ..., P_{s_N}^{new} \ge 0 {(5.8)}$$

$$P_{s_n}^{new} \le P_{s_n}^{ori} \tag{5.9}$$

Where $P_{s_n}^{ori}$ represents the original power request at EVSE s_n before the charging scheme is executed.

The constraints are built so that all congestion issues are solved once the optimisation analysis is carried out. These constraints can be expressed in matrix notation as in Eq. (5.10). In this, the vector \bar{p}_s (Eq. (5.11)) contains the difference – at all EVSEs – between the original charging value and the new value after the optimisation (i.e. the optimisation variables), namely the power to be reduced at each EV. On the other side of the inequality, \bar{p}_e (Eq. (5.11)) is a vector indicating the power that has to be reduced from the total power flowing through each congested element.

$$\tilde{A}_{M,N} \cdot \bar{p}_s \ge \bar{p}_e \tag{5.10}$$

where

$$\bar{p}_{s} = \begin{cases} P_{s_{1}}^{ori} - P_{s_{1}}^{new} \\ P_{s_{2}}^{ori} - P_{s_{2}}^{new} \\ \vdots \\ P_{s_{N}}^{ori} - P_{s_{N}}^{new} \end{cases} \qquad \bar{p}_{e} = \begin{cases} P_{e_{1}} \\ P_{e_{2}} \\ \vdots \\ P_{e_{M}} \end{cases}$$
 (5.11)

Egalitarian Charging management Scheme (ECS)

The ECS guarantees a fair absolute division of the burden among the chargers, disregarding any other aspect related with their influence on the congested elements or their need of power. The goal of the management scheme is to maximise the fairness of the reserve activation process, with a mechanism comparable to the one illustrated in [161]. As proved in that study, this charging management scheme also maximises social welfare and the Nash product of all EV users utilities.

In this case, the only variable is indicated as x ($x \ge 0$) and it can be described as the maximum charging power allowed at all EVSEs involved in the optimisation process. The objective is to maximise the variable x. The constraints are the same indicated in Eq. (5.10), but the vector \bar{p}_s of the variables is described in Eq. (5.12):

$$\bar{p}_{s} = \begin{cases} P_{s_{0}}^{ori} - min\{P_{s_{0}}^{ori}, x\} \\ P_{s_{1}}^{ori} - min\{P_{s_{1}}^{ori}, x\} \\ \vdots \\ P_{s_{N}}^{ori} - min\{P_{s_{N}}^{ori}, x\} \end{cases}$$
(5.12)

It should be noted that this optimisation analysis could be executed multiple times during the same time-step. This is done in order to avoid unnecessary power adjustments. In fact, if at the first iteration all the variables $P_{s_n}^{new}$ were set to the value x, all the overloading problems would be solved, but more power could have been reduced at the EVSEs than what was strictly necessary to solve the congestion.

To better explain this, it is important to consider that each constraint of the optimisation analysis represents a problem registered in the grid, namely an overloaded element. However, these problems are strongly interconnected. The same EV charging process(es) could be the common cause of multiple overloaded elements. Therefore, once the cause of an overloaded element has been addressed (through the reduction of power at one or multiple charging processes), other overloading issues could have been solved without the need of additional charging power reduction.

In practice, this is done by means of the concept of *Slack value* σ . This represents the difference between the right and the left side of an inequality constraint, when the variable assumes a determined value. In other words, it is the value that returns an equality when added to the inequality constraint.

Once the optimisation analysis is solved, the introduction of the *Slack value* σ allows to rewrite Eq. (5.10) in the form of an equality, as $\tilde{A}_{M,N} \cdot \bar{p}_s = \bar{p}_e + \bar{\sigma}_e$. In combination with

Eq. (5.12), these equalities can be written as in Eq. (5.13). Each line of this set of equations is indicated as C_e .

$$\begin{split} a_{1,1}\cdot (P_{s_{1}}^{ori} - min\{P_{s_{1}}^{ori}, x\}) + \dots \\ &+ a_{1,N}\cdot (P_{s_{N}}^{ori} - min\{P_{s_{N}}^{ori}, x\}) = P_{e_{1}} + \sigma_{e_{1}} \\ a_{2,1}\cdot (P_{s_{1}}^{ori} - min\{P_{s_{1}}^{ori}, x\}) + \dots \\ &+ a_{2,N}\cdot (P_{s_{N}}^{ori} - min\{P_{s_{N}}^{ori}, x\}) = P_{e_{2}} + \sigma_{e_{2}} \\ &\vdots \\ a_{M,1}\cdot (P_{s_{1}}^{ori} - min\{P_{s_{1}}^{ori}, x\}) + \dots \\ &+ a_{M,N}\cdot (P_{s_{N}}^{ori} - min\{P_{s_{N}}^{ori}, x\}) = P_{e_{M}} + \sigma_{e_{M}} \end{split}$$
 (5.13)

At each iteration, after the optimisation analysis is solved, the binding constraint C_b , i.e. the one with $Slack\ value$ equal to zero, is taken. The charging power of all EVSEs contained in this constraint is set to $min\{P_{s_n}^{ori},x\}$. This means that the overloading associated with constraint C_b is solved. Afterwards, it is checked whether also the other overloads, namely the remaining constraints, are solved. If so, the algorithm stops. Otherwise, it proceeds with the next iteration, where the previously binding constraint C_b is not considered anymore. The Pseudocode of the ECS scheme is listed in Algo. 1.

Algorithm 1 Egalitarian Charging management Scheme (ECS)

```
1: done = False
2: while not done:
     run optimisation and get x
4:
     if all Slack values are different than zero:
5:
        done = True
6:
     else:
7:
        get constraint C_b with Slack value equal to zero
        set power at all chargers s present in C_b at min\{P_{s_n}^{ori}, x\}
8:
9:
        remove constraint C_b
     if power is set at all chargers in all constraints
10:
        done = True
11:
```

Priority-based Charging management Scheme (PrCS)

One of the key points of this method is the definition of a priority parameter, so to translate the urgency of power request of a charging session into a number. This number can be compared with the ones of the other charging stations and, when necessary, charging power at EVSEs will be adjusted accordingly. In particular, a *priority factor* – similar to one of the priority parameters described by Kumar et al.[64] – can be defined for the charging session of the current connecting EV at charger s_n as

$$f_n = \frac{\Delta t_{min,n}}{\Delta t_n} \tag{5.14}$$

where Δt_n is calculated as the difference $T_{d,n}-t$, with t representing the time of calculation and $T_{d,n}$ the expected departure time of the vehicle connected. The term $\Delta t_{min,n}$ refers instead to the minimum time necessary to complete the charging process and it is calculated as

$$\Delta t_{min,n} = \frac{d_{ch,n}}{P_{r,n}} \tag{5.15}$$

where $d_{ch,n}$ is the remaining charging energy asked by the vehicle and $P_{r,n}$ is the rated charging power of the EV.

This priority factor f_n gives an indication of how urgent is the need of power at the studied element and the closer it gets to 1, the more urgent it needs power to charge its EV. In case $f_n > 1$, it will not be possible anymore to fully accomplish the original user charging demand. This parameter is used to decide which EVSE should be managed first to have their power reduced, in order to cause the least dissatisfaction possible. To do so, the EVSEs with a low f_n should have their charging power reduced first and the ones with a f_n close to 1 should not be reduced at all.

 f_{dict} is defined as the dictionary that associates all EVs involved in the charging management process with their priority factors organised in increasing order. This can be obtained once all the output data from Phase 2 is collected. The description of this scheme can be found in Algo. 2.

Algorithm 2 Priority-based Charging management (PrCS)

```
1: overloads = list of all overloaded elements
2: for s_n in f_{dict}:
     sub_overloads = sub-list of elements from overloads where corresponding value
of s_n
     in PTDF matrix is > 5%
     if sub_overloads not empty:
4:
        P_{s_n}^{new} = 0
5:
        create empty dictionary SOL<sub>dict</sub>
6:
7:
        for elem in sub overloads:
          SOL_{dict}[elem] = True if elem not overloaded anymore, checked via Eq. (5.10)
8:
9:
        if all elem in SOL_{dict} are True:
          maximise P_{s_n}^{new} such that all elem in SOL_{dict} are still True
10:
        for elem in sub_overloads:
11:
           if SOL_{dict}[elem] = True:
12:
             remove elem from overloads
13:
14:
     if overloads empty:
15:
        break
```

5.3. Modelling of elements and scenarios

5.3.1. Grid features

The congestion management algorithm has been coded in Python and tested via simulations on PowerFactory. The simulations have been run on two different LV grids. These

are real Dutch sub-urban distribution grids provided by the DSO Enexis. Their main characteristics can be found in Table 5.1.

All charging stations and regular loads included in the models are linked to nodes with a 3-phase connection. This simplification has been introduced in the model to increase the convergence ratio of the simulations, which otherwise resulted too complex to reach convergence at many time-steps. This assumption is in line with the intention of the authors not to include phase unbalance issues in the study, being it a distinct and extensive topic.

Grid	No.	Energy demand [MWh/yr]	PV installed [kWp]	Avg.line length [m]	Longest feeder length [m]	No. transformer
1	475	1394.1	180	7.3	566.0	1×400 kVA
2	266	800.8	100	8.1	546.6	1×400 kVA

Table 5.1: Summary of grids' characteristics

5.3.2. PV and load profiles

The baseload profile used for this study has been modelled on the base of the load characteristics included in the grid models, in combination with the Dutch normalised profiles [95]. These normalised profiles cover various connection types in different scales including household, business, agriculture and industrial usages. The load type as well as their yearly energy demand are provided in the original grid models.

To model the PV profile a previous study has been used as a base [100]. For both suburban grids used in this study a 15% PV penetration has been implemented, with a peak rated power of 2.5 kW assumed for each installation [97, 98].

5.3.3. EV data

The EV data concerns in particular two main aspects: the charging behaviour of the EV users and the composition of the EV fleet, i.e. the electric vehicle models currently in circulation. Such a list of the most common EV models currently in circulation has been implemented on the base of the Dutch market data [105].

The EV charging behaviour includes all the key habits that can be registered of a EV user, such as EV arrival and departure time, charging energy request, and the frequency of the charging processes. This data is derived from a previous study that analyses the data of a significant number of charging sessions [104, 109]. Based on the study, EV charging profiles are identified as home, semi-public and public charging featured sessions. In the case of a sub-urban grid, the percentage of home profile types represents 50% of the total sessions. The remaining half is equally divided between public and semi-public profiles. This is further described in [103]. The EV charging stations are modelled in PowerFactory as LV loads with a three phase AC connections and a maximum of 32 A per phase.

The EV penetration is defined for each grid as the percentage of electric vehicles with respect to the total amount of vehicles registered. Different EV penetrations can be simulated by increasing the amount of EV charging sessions and, in turn, increasing the number of charging stations.

The detailed description of the grid models, and how the simulation data were generated can be found in previous works [103, 134].

5.3.4. Simulation setups and scenarios

The simulations have been run by means of load flow analyses executed on intervals of 10 minutes. For each load flow the diagram in Fig. 5.1 applies and provides an overview of the algorithm logic, as explained more in details in Section 5.2.

All the simulations to test the different CMSs have been run on the previously described models. In particular, eight different scenarios have been simulated, as detailed in Table 5.3. All the scenarios simulate an entire week in Winter, as the PV generation is lower and the EV impact on the grid was expected to be more significant.

The percentages of EV penetrations simulated in the two grids have been selected with the objective to simulate a congested grid condition. To this end, grid 1 presented more severe loading conditions. In fact, it has been sufficient to increase the EV percentage to 50% in order to observe overloading phenomena up to 160% in the uncontrolled charging scenarios. On the other hand, for grid 2 it has been necessary to increase the EV penetration up to 100% in order to register significant activations of the charging schemes. In this case, though, the maximum loading percentages observed always stayed below 120%.

Parameter	Meaning
$\lambda_{\mathrm{trf}}^{\mathrm{max}}$ [%]	Maximum transformer loading per timestep
λ _{ln} ^{max} [%]	Maximum line loading per timestep
Λ _{trf} [%]	Peak transformer loading
Λ _{ln} ^{max} [%]	Peak line loading
J_{fail}	Number of unfinished charging sessions
$J_{ m tot}$	Total number of EV charging sessions
R _{fail} [%]	Percentage of unfinished charging sessions
Eobt [kWh]	Sum of delivered energy of all EV charging sessions
E _{req} [kWh]	Sum of requested energy of all EV charging sessions
R _{chr} [%]	Ratio of total delivered charging energy
E _{fail} [kWh]	Average failed to delivered energy per session
E ^{avg} [kWh]	Average requested charging energy per session
r _{chr} [%]	Ratio of average failed to deliver energy per session
$\delta_{ m max}$ [%]	Index of maximum grid overloading over-compensation

Table 5.2: Parameters appeared in result analysis

5.4. Simulations Results

In this section the simulation results are presented and analysed from three points of view: the grid congestion mitigation, the user satisfaction and the overcompensation of grid overloading. The overview of the overall performance of the three methods are listed in Table 5.3 while the meaning of results related parameters are summarised in Table. 5.2.

5.4.1. Grid congestion mitigation

The improvements to the grid performance brought by the three CMSs can be observed forthrightly with two main parameters: the maximum transformer loading ($\lambda_{\rm trf}^{\rm max}$) and the maximum line loading ($\lambda_{\rm ln}^{\rm max}$) registered at each time-step in the grid. The maximum of

 $E_{\rm fail}^{\rm avg}$ $\Lambda_{\rm trf}^{\rm max}$ Λ_{ln}^{max} $\delta_{
m max}$ R_{fail} $R_{\rm chr}$ $r_{
m chr}$ **CMS** [%] [%] [%] [%] [%] [kWh] [%] Grid 1: 50% EV penetration 1 OFF 146.03 160.42 / 100 0 0 2 PCS 99.99 99.99 13.79 92.27 69.58 10.97 10.68 3 **ECS** 100.04 99.93 8.38 94.34 12.65 6.76 44.04 **PrCS** 100.15 99.94 99.79 4.00 4 18.84 0.44 2.87 Grid 2: 100% EV penetration OFF 102.06 / 5 118.08 100 0 0 0 PCS 99.99 99.88 1.77 99.86 0.34 6.19 40.06 6 **ECS** 1.74 99.93 7 100.00 95.01 0.80 1.35 8.74 8 **PrCS** 100.00 99.56 2.54 99.99 0.02 0.13 0.11

Table 5.3: Simulation scenarios and main results

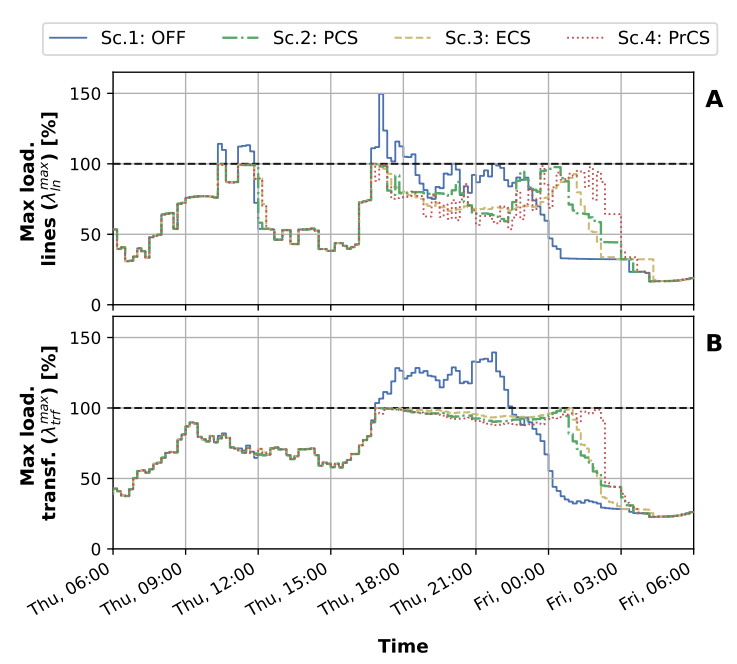


Figure 5.2: Scenarios 1-4: comparison of max loading percentage at (a) lines and (b) transformer

these values registered during the whole week of simulation are reported in Table 5.3 as Λ_{trf}^{max} and Λ_{ln}^{max} , respectively.

It can be seen from Table 5.3 that all three CMSs managed to keep the loading percentages of both transformer and lines within the desired value of 100% with a maximum positive deviation of 0.15% in the fourth scenario.

An overview of the results can also be observed in Fig. 5.2, which reports the effects on the maximum loading percentages registered at lines and at the transformer in grid 1. In

particular, Fig. 5.2 (b) highlights the presence of a "valley filling" effect. In fact, the high loading values registered in Scenario 1 – with peaks higher than 150% – are spread throughout the whole evening in the other 3 scenarios, with loading percentages constantly below 100%. This can be also observed in Fig. 5.4 (a), where the daily peak of EV power – greater than 200 KW – is moved to a later moment in the night.

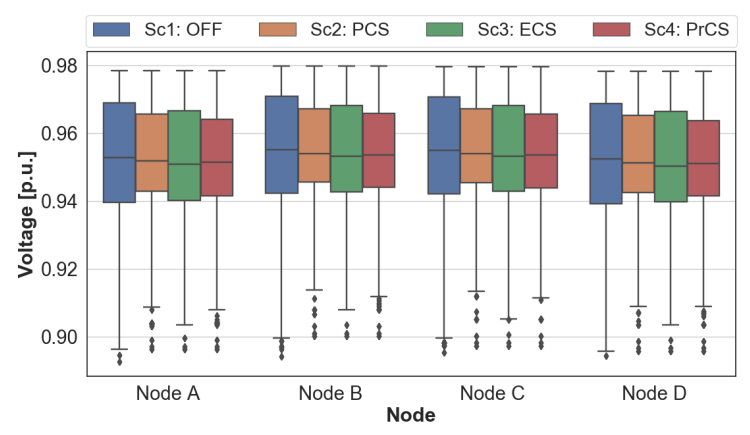


Figure 5.3: Scenarios 1-4: comparison of voltage distribution at the three most distant nodes from the transformer, with a connection to: Node A home charging station, B: public charging station, C: semi-public charging station. Node D is the node with the lowest average voltage registered during the simulation of the uncontrolled scenario (Scenario 1)

The distribution of the node voltage of Scenarios 1-4 are presented in the form of box plot in Fig. 5.3. In this graph four representative nodes are included.

From this graph it is possible to observe how the median value of the voltage decreases with the implementation of all CMSs. All three schemes kept the voltage less spread out, i.e. with lower inter-quartile ranges. In particular, the average value of this range for the four points considered is around 0.029 p.u. for the uncontrolled scenario, 0.026 p.u. for the ECS and around 0.022 p.u. for both PCS and PrCS. This can be explained as the integration of the algorithm of Fig. 5.1 – with any of the three CMSs – allows a better use of the available grid capacity. In contrast, in the uncontrolled scenarios very low voltages are registered during peak hours – which lead to lower whiskers below 0.9 p.u. – while at all other moments very stable voltage conditions are present in the network. On the other hand, no significant effects are registered on the upper whiskers.

As expected, from a voltage point of view, the PCS is the solution that performed the best of all three charging management schemes. In fact, next to leading to the lowest inter-quartile range (together with PrCS), the PCS also resulted in the lowest drop in the median value, with respect to the uncontrolled scenario. The average drop in the median value registered at the four points considered is approximately 0.0011 p.u. for the PCS, against the drop of 0.0019 p.u. and 0.0014 p.u. for the ECS and the PrCS, respectively.

The scheme that registered the worst voltage results is the ECS. Next to registering the highest drop of the median value, it also shows the worst results in terms of lower whisker. The average lower whisker improvement – of all four points with respect to Scenario 1 – is 0.0072 p.u. for ECS, against 0.0135 p.u. for PCS and 0.0123 p.u. for PCS.

5.4.2. User satisfaction

All three CMSs share the same fundamental mechanism, which is to reduce the excessive simultaneous charging request and delay the charging process as much as possible. By doing so the grid overloading is limited. However, the delayed charging process can also lead in some cases to a lower departure SOC for some EVs, with respect to the uncontrolled scenario. In fact, in the uncontrolled charging scenario the EVs get the maximum requested amount of energy technically obtainable during the parking time, disregarding all grid congestion issues that might occur.

In this study, the number of "failed charging process" ($J_{\rm fail}$) is defined as the absolute number of charging sessions performed by one of the three CMSs whose departure SOC is lower than the same session in the uncontrolled charging scenario. The charging energy received with uncontrolled charging strategy is considered as the ideal requested energy and is taken as a reference. In the following text, the term "requested energy" is used.

The percentage of failed charging process ($R_{\rm fail}$) is used to evaluate the user satisfaction and is reported for each scenario in Table 5.3. This percentage is calculated as the absolute number of failed charging process ($J_{\rm fail}$) divided by the total number of EV charging processes simulated ($J_{\rm tot}$)

$$R_{\text{fail}} = \frac{J_{\text{fail}}}{J_{\text{tot}}} \tag{5.16}$$

Another criteria employed for user satisfaction assessment is the total delivered charging energy ratio $R_{\rm chr}$. This is calculated as

$$R_{\rm chr} = \frac{E_{\rm obt}}{E_{\rm reg}} \tag{5.17}$$

where E_{req} refers to the sum of the requested energy of all EV charging processes simulated, while E_{obt} refers to the sum of the energy that was successfully provided during all charging processes. Therefore, it can be considered as a general indication of how the three CMSs performed in the simulated scenarios.

Looking at this last parameter from Scenarios 2 to 4, the best results are obtained, in order, by: the PrCS (99.79%), the ECS (94.34%) and the PCS (92.27%). The same pattern is observed when considering Scenarios 6 to 8, with percentages of total energy delivered of 99.99%, 99.93% and 99.86% for the PrCS, ECS and PCS, respectively.

However, when looking more in details into what happens to the single charging processes it is possible to observe the following aspect. Although the ECS scenarios (Scenarios 3 and 7) show a higher total EV energy delivered ($R_{\rm chr}$) than in the PCS case (Scenarios 2 and 6), the former has a $R_{\rm fail}$ higher than the latter by 1.68% (comparing Scenarios 2 and 3) and by 0.46% (comparing Scenarios 6 and 7). In other words, the ECS has led to a higher percentage of failed charging processes with respect to the PCS.

This can be easily explained by looking at the last two columns of the table. The first of them reports the average failed energy of each scenario. This is calculated as

$$E_{\text{fail}}^{\text{avg}} = \frac{E_{\text{req}} - E_{\text{obt}}}{I_{\text{fail}}} \tag{5.18}$$

In the table it can be observed that the average failed energy is significantly higher in the PCS scenario with respect to the ECS (e.g. 10.68 kWh against 6.76 kWh for Scenarios 2 and 3, respectively). The conclusion is that the ECS leads to a higher number of failed EV processes – which translates into a higher number of dissatisfied users – but with a lower dissatisfaction level for each user. This observation does not come unexpected, as the main purpose of the ECS is to distribute the burden of the charging power reduction as fairly as possible to the EVs. On the other hand, the PCS only looks at which charging stations allow to solve the overloading issue reducing the lowest amount of charging power possible. Therefore, the power adjustment burden is not shared fairly among charging stations and there is a higher chance that a smaller amount of EVs (with respect to the ECS) will see their charging process adjusted. The PrCS instead shows overall the best results, with a charging process failed percentage of 4.00% and an average failed energy of only 0.44 kWh for Scenario 4. Similar observations can be made for Scenarios 6 to 8.

The last column of Table 5.3 offers a clearer perspective on the relative energy that has been actually delivered during the failed charging processes. The parameter here reported is the average percentage of energy that has been failed to be provided to the EV, with respect to the energy requested ($r_{\rm chr}$). This is calculated dividing the average failed energy ($E_{\rm fail}^{\rm avg}$) of each scenario by the average requested energy of all charging processes that failed to be completed ($E_{\rm req}^{\rm avg}$), as in

$$r_{\rm chr} = \frac{E_{\rm fail}^{\rm avg}}{E_{\rm reg}^{\rm avg}} \tag{5.19}$$

The PCS scenarios show the most critical results, where this percentage reaches almost 70% in Scenario 2 and slightly over 40% in Scenario 6.

5.4.3. Overcompensation of grid overloading

The main reason behind the outstanding performance of the PrCS is the fact that the charging stations with a more urgent need of energy – translated into the value f_n of Eq. (5.14) – are never requested to reduce their charging power if not strictly necessary. On the other hand, the charging stations with lower f_n value are kept waiting so to give priority to the more urgent requests.

A direct consequence of this approach is the formation of longer "waiting lines", as it can be observed in Fig. 5.4. The increase in the average daily peak of waiting EVs – defined as the average of the daily maximum number of EVs simultaneously requesting charging power, calculated over the simulated week – with respect to Scenario 1 is 64.3%, 77.2% and 127.7% for Scenarios 2, 3 and 4, respectively. The same parameter increases for Scenarios 6, 7 and 8 – with respect to Scenario 5 – by 2.3%, 4.5% and 20.2%, respectively.

When considering the area below the curve of the number of active EVs, the increase of Scenarios 2, 3 and 4, with respect to Scenario 1 is 68.6%, 77.4% and 143.1%, respectively. A similar pattern, although less pronounced, is registered for Scenarios 6, 7 and 8, with respect to Scenario 5, with percentages of 1.7%, 1.9% and 7.5%, respectively.

This increase in number of waiting EVs affects directly the performance of the CMSs. It can be observed in Fig. 5.2 (b) that the transformer loading value during peak hours of Scenarios 2, 3 and 4 does not follow exactly the 100% line, but tends instead to create a valley shape. This is due to the fact that K_{load} (in Eq. (5.6)) is voltage dependent. The charging

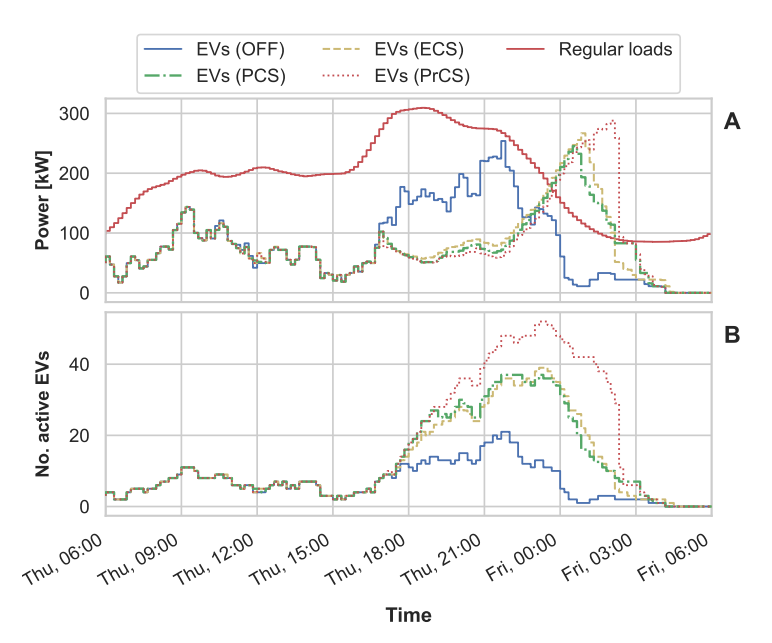


Figure 5.4: Comparison of (a) registered EV power and (b) number of EVs requesting power to charge for Scenarios 1-4

power to be reduced is calculated under voltage conditions that improve (increase) once the congestion issue in the network is actually solved. This improves in turn the loading condition of lines and transformer. This effect is more relevant when a significant amount of charging power is adjusted. This is visible in Table 5.3, where the value $\delta_{\rm max}$ is reported in Eq. (5.20).

$$\delta_{\max} = \max\{100 - \max\{\lambda_{\text{trf}}^{\max}, \lambda_{\text{ln}}^{\max}\}\}_{week}$$
 (5.20)

This represents the maximum over-compensation phenomenon registered during the whole week of each simulation. Table 5.3 shows that the over-compensation phenomena in the simulations of Grid 2 is significantly lower than in Grid 1.

Similarly, in both grids there is a higher over-compensation presence in the scenarios where higher waiting lines form. The reduction of this overcompensation phenomenon by means of a correction factor resulted in inconsistent results depending on the magnitude and the exact location of the overloading issues. Therefore, no correction factor has been included in the algorithm. Another way to tackle the phenomenon is to integrate in the algorithm a correction mechanism that considers the effect on the voltage of the charging power adjustments. However, this is expected to add great complexity to the algorithm, that could lead in turn to a longer computational time.

5.5. Conclusion and recommendations

Correctly managing the EV charging processes can be a key element to prevent the occurrence of congestion issues in the grid, while still delivering the required energy to the vehicles. In this study, three charging management schemes have been tested and compared to maintain the loading conditions of a congested grid within the desired limits. The activation of all three schemes was successful to solve overloading conditions at both the transformer and the lines, with a negligible error. Their integration also led to a better use of the available grid capacity, which affected in turn the voltage distribution in the network. However, the different objectives of the three management schemes resulted in different outcomes for what concerns the user satisfaction. When comparing the ECS with the PCS, the conclusion is that the former leads to higher number of dissatisfied users with respect to the latter, but with a lower dissatisfaction level for each user. On the other hand, the PCS is the scheme that resulted in the highest average charging energy that was failed to be delivered, both in absolute and relative terms. Overall, the PrCS is the scheme that performed the best, with the lowest percentages of failed charging processes and the greatest total delivered charging energy ratio. Finally, it was observed a significant growth in the volume of the EV "waiting lines" with respect to the uncontrolled scenarios. This increase was comparable for the PCS and ECS cases, while it was significantly higher for the PrCS. The direct consequence of the longer waiting lines is an increase in the overcompensation phenomena. Although this aspect did not impede to reach the main objective of the algorithm - i.e. to keep the loading percentages within the allowed limit - their presence suggest that the available grid capacity has not been exploited to the fullest. The reduction of this phenomenon will be the starting base for the future work. Furthermore, this algorithm evaluates the charging requests of the EVs at each time-step. In future work, a different mechanism could be implemented where EVs follow the assigned optimal charging profile until a new command is sent to further save computational power. This new signal could be sent when there is a relevant system status change. Finally, this algorithm aims at preventing the occurrence of congestion issues before they happen, but the same schemes could also be applied as a remedial action to solve congestion issues that have already been registered in the grid. This aspect could also be evaluated in future work.

Hierarchical EV smart charging algorithm development with HIL experimental evaluation

The rising demand for electric vehicles (EVs) in the face of limited grid capacity encourages the development and implementation of smart charging (SC) algorithms. Experimental validation plays a pivotal role in advancing this field. This chapter formulates a hierarchical mixed integer programming (MIP) EV SC algorithm designed for low voltage (LV) distribution grid applications. A flexible receding horizon scheme is introduced in response to system uncertainties. It also considers the practical constraints in protocols such as IEC/ISO 15118 and IEC 61851-1. The proposed algorithm is verified and assessed in a Power Hardware-Inthe-Loop (PHIL) testbed that incorporates models of real LV distribution grids. Furthermore, the algorithm's capabilities are examined through eight scenarios, out of which four focus on the uncertainties of the input data and two address the engagement of extra grid capacity restrictions. The results demonstrate that the SC algorithm adequately lowers the EV charging cost while fulfilling the charging demand, and substantially reduces the peak power as well as the overloading duration, even when faced with input data uncertainty. The additional grid restrictions in place are proven to improve peak demand reduction and overloading mitigation further. Finally, the limitations and potentials of the developed algorithm are scrutinised.

6.1. Introduction

Smart Electric Vehicle (EV) charging has gathered interest due to its potential in mitigating grid congestion [149, 162], enhancing renewable energy utilisation [163], and improving the profitability of different parties [164].

A plethora of EV smart charging algorithms have been developed in the past decade. The comprehensive reviews of these algorithms from the angle of for example, mathematical model/algorithm, control structures and application scenarios have been addressed in studies like [38, 165, 166]. The common EV smart charging algorithm can be categorised into rule-based or heuristic algorithms, conventional optimisation approaches like Linear, Quadratic, Mixed Integer and Nonlinear programming (LP, QP, MIP, NLP), and the Alenabled method. Centralised, decentralised and hierarchical control designs are widely

^oThis chapter is based on paper: Y. Yu, L. De Herdt, A. Shekhar, G. R. C. Mouli, and P. Bauer, Ev smart charging in distribution grids experimental evaluation using hardware in the loop setup. *IEEE Open Journal of the Industrial Electronics Society*, vol. 5, pp. 13 27, 2024.

adopted as control structures, while the optimisation objectives are often operational or economic.

The goals of EV smart charging algorithms designed for distribution grid applications regularly consist of three pillars: grid operation assurance, energy cost reduction, and the fulfilment of EV charging requests. Set minimising the energy cost as (part of) the objective function is very standard in smart charging algorithms development, such as in studies where MIP method are used [167-170], and in work [162] where a meta-heuristic method is suggested. With respect to considering grid operational requirements, researchers hold various preferences. For example, grid constraint is out of the scope in the study [169] while some other research embeds grid features like load flow into the algorithm's objective functions [167, 171]. In this case, heavy computations or a pre-linearisation process could be needed. On the other hand, meeting the user charging demand is not always covered in the existing research. Nevertheless, study [172] adapts the EV charging flexibility in the algorithm and research [167] include EV energy demand in the constraints. Although EV charging demand is not specifically mentioned in [170], the fairness in scheduling EV charging is addressed. In regard to control and communication structure design, centralised and decentralised control schemes are mixed-implemented in the above-reviewed work. The large-scale smart charging installation in a neighbourhoodlevel distribution grid introduced in [173] implies that the most flexible yet practical control scheme for grid constraint-involved EV smart charging in the Netherlands, given involved entities, is hierarchical control.

The practical-oriented hierarchical MIP EV Smart Charging algorithm proposed in our work, namely SC-Alg, aims to minimise the energy cost, maximise the local renewable energy generation self-consumption and meet the EV charging demand in the form of weighted combined objectives, while keeping the power exchange within the grid capacity which is reflected in the constraints.

An essential feature of the empirical EV smart charging algorithm is its capability to cope with the stochasticity of local renewable energy generation, load consumption, EV user behaviour, as well as grid status. The common approach for stochasticity in smart charging algorithm development includes but is not limited to stochastic optimisation [162] and robust optimisation [169] when at least part of the characteristics of the stochasticity can be adapted into the optimisation problem. Alternatively, the receding horizon method is often picked for its passive stochasticity resolving mechanism, which is to update uncertain parameters and re-optimise regularly [168, 174]. A fixed horizon length is applied in most cases, yet when a desired optimisation duration mismatches with the horizon length, a flexible horizon window size is superior [175]. The next challenge for the empirical smart charging algorithm is to adapt the implementation requirements. The current commonly employed AC charging standard IEC 61851 instructs that the minimum nonzero EV charging current setpoint is sent to the EV via Pulse Width Modulation (PWM) signals through Control Pilot (CP) pin in the charger is 6 A [45]. Besides, the EV charging current can only be adjusted with discrete steps, and the step size depends on the manufacturing design of the EVSE and the EV [72, 176]. Most of the existing works assume the EV charging current is continuously adjustable from zero whereas only a few research address these two constraints. The discrete charging current is emphasized in [177, 178] while the minimal 6 A non-zero setpoint value is not mentioned. Although authors of [72, 176] accommodate both the minimum 6 A limit as well as the discrete setpoint interval in their algorithms, the discrete setpoint in their research is achieved by rounding up/down to the nearest integer value after the optimisation.

To tackle the above-mentioned implementational challenges, SC-Alg integrates the current setpoint constraints and the passive stochasticity handling mechanism through the MIP approach with a flexible receding horizon technique.

To test the functionality of the proposed algorithm and its impact on the LV distribution grid, especially the passive stochasticity handling feature, a real-time virtual representation of the system is desired. Besides, flexibility in defining test scenarios is necessary to fulfil this goal. This can be realised by using Power Hardware-In-Loop (PHIL) containing a Digital Real-Time Simulator (DRTS) which runs the Real-Time Digital Twin (RTDT) of the target system. This real-time (RT) PHIL facility is especially beneficial for this type of research because the DRTS is capable of conducting simulations of wide-ranging power system models under numerous schemes in both transient and steady-state [78, 179, 180]. The RTDT makes the tests on large systems with diversified scenarios more flexible, scalable and achievable within a reasonable time span. Furthermore, the RTDT-embedded HIL is suited for demonstrating and verifying the innovation ideas with three or higher Technological Readiness Levels [181].

In the realm of EV and grid integration, the HIL facilities are often used to evaluate the performance of the target hardware and their impact on the grid; and test the system integrity including the intercommunication. A lab-scale flexible testbed for EV charging is developed in [182], with which the operation of the Electric Vehicle Supply Equipment (EVSE) and EV, the implementation of communication protocols are tested. In the study, a DC charging on/off event with 960V and 95A was successfully conducted. Research [183] explored the grid resilience during extreme EV fast charging through RT-PHIL grid simulations. The transient dynamics of the tested grid, including branch current, nodal voltage and frequency, are evaluated with the RT grid simulation.

EV charging algorithm-incorporated controllers are also commonly tested with HIL simulations to verify their functionalities. In study [184], an EV charging algorithm equipped controller for EV onboard bi-directional AC/DC converter is developed and verified with HIL simulation. The developed controller is integrated with an Additive Increase/Multiplicative Decrease EV charging algorithm for voltage drop mitigation in the distribution grid. The RT grid simulation indicates a 0.013 p.u. minimal voltage increase with the applied controller, proving the effectiveness of the algorithm. Study [185] tests the RT energy management controller for EV charging via a PHIL testbed that consists of one grid-connected micro-grid simulated by DRTS, and two EVs that are emulated by two HIL units. The linear convex optimisation equipped in the controller aims to minimise the cost of energy consumption at the workplace, and it is proven to be capable of reducing the weekly power consumption cost by 14%.

The application of HIL in investigating the innovative EV charging algorithm has become more popular as it bridges pure computer simulation and actual implementation. The HIL simulation offers a flexible platform for algorithm/hardware interface testing [186]. Placing the relevant hardware components in the HIL testbed introduces factors that can potentially alter the algorithm's performance. These factors include but are not limited to information flow, the refresh rate of parameter exchange, communication delay, response

lag and grid status [187, 188]. The authors of [189] proposed an EV adaptive Charging Characteristics Expectation algorithm with a primary objective of distributing the available capacity of the local electricity network evenly and efficiently among active EVs. The algorithm is validated through HIL simulations in which one Nissan leaf and one BMW i3 are connected to two sockets of one 22 kW charger separately. The HIL simulation results show that an 88-97% network capacity usage rate is achieved. Similarly, a decentralised demand response based EV charging algorithm for residential community applications is proposed and inspected with both software simulation and HIL simulation in research [186]. The results not only prove the efficacy of the algorithm but also signify that the high resolution contributed by HIL can reveal phenomena that can hardly be observed in pure software simulations, such as power consumption difference due to hardware losses, voltage bounce and dip caused by power variation and transient features of the grid [186].

Even while [190] emphasises the importance of the experimental study on the impact of EVs on the distribution grids, the offered results are predominantly simulations. In our work, we develop a laboratory test bed to showcase the highlighted aspects in real-time HIL environment. Paper [191] uses grid voltage regulation control for a 2 kVA laboratory EV charger to validate effectiveness up-to charging currents of 5 A. Our work demonstrates efficacy at much higher currents and voltages that include the practical limitations associated with 6 A standard and includes a smart charging algorithm for many other variables using the PHIL-RTDS environment.

Nevertheless, for such experimental algorithm validation with different and scalable distribution grids and the ability of flexible testing conditions at reasonable costs, an RTDT-based HIL setup is necessary. This chapter utilises such a setup to validate the proposed SC-Alg experimentally; explore its impact on the LV distribution grid; test the operation of relevant components and interfaces from both power and communication perspectives; and scrutinise its limitations and potential with eight scenarios from the perspectives of inaccurate PV/load prediction, EV information mismatch and grid limitation incorporation. The extensive guidance on how to upgrade SC-Alg as well as the testbed is subsequently encapsulated. The major contributions of this research can be summarised as follows:

- Suggesting a hierarchical MIP EV smart charging algorithm designed for LV distribution grid applications. A flexible receding horizon scheme is introduced as a passive mechanism to handle stochasticity within the algorithm.
- Integrating the implementational constraints arising from EVSE-EV communication protocols into the proposed algorithm.
- Performing a comprehensive assessment utilising an RTDT-based HIL setup encompassing eight scenarios. The scenarios explore the algorithm's performance considering input information stochasticity, user behaviour uncertainty and the integration of grid limitations.
- Offering detailed guidance for upgrading the proposed algorithm, drawing from the results obtained through HIL simulations.

The structure of the chapter is as follows: the architecture of the whole system, including the proposed SC algorithm, is outlined in Section 6.2. The PHIL testbed introduction and its interaction with the digital model and the SC algorithm are explained in Section 6.3. The detailed description of the simulation setup, including input data and test scenarios, can be found in Section 6.4. Section 6.5 presents a thorough analysis of the simulation

results, and finally, the conclusion and recommendations on future SC-Alg improvements are given in Section 6.6.

6.2. Architecture of system model and algorithm

6.2.1. System architecture

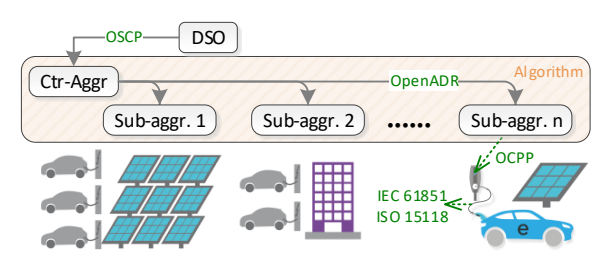


Figure 6.1: Schematic of the hierarchical algorithm structure

Our algorithm SC-Alg has a hierarchical structure with one centralised and one distribution level, as shown in Fig. 6.1. The Sub-aggregator (Sub-aggr) at the distribution level is responsible for the behind-the-meter optimisation at the grid node level. The primary goal of Sub-aggr is to obtain the optimal EV charging plan as well as the energy usage strategy for the local node by solving the mixed integer programming (MIP) problem. On top of that, a Central-aggregator (Ctr-aggr) is responsible for communicating the grid condition with the Distribution System Operator (DSO) and coordinates with the Sub-aggrs to ensure the grid capacity limitation is not violated. The Sub-aggr can be placed at a company campus, a household, or a public charging station connected to a node in the distribution grid.

The SC-Alg fits multiple control structures in different actual application scenarios. A possible control and communication structure used in this chapter is illustrated in Fig. 6.1. The grid status can be monitored by the grid estimations operated by the DSOs [160]. The obtained available grid capacity is then sent by the Capacity Provider – DSO, to the Flexibility Provider – Ctr-aggr, over the Open Smart Charging Protocol (OSCP) [42]. Then the Ctr-aggr, which serves as a Virtual Top Node, shares this grid status information with the Sub-aggr, which acts as a Virtual End Node, through Open Automated Demand Response (OpenADR) standard [43]. And finally at the distribution level, the optimal EV charging current, which is the maximum allowed phase current that the EV can draw from the charger namely setpoint, is calculated and sent from the Sub-aggr to the EVSE through the Open Charge Point Protocol (OCPP) [44]. Note that the OSCP and OpenADR can largely cover the same scenarios and are interchangeable in many EV smart charging contexts depending on which party presents as Capacity/Flexibility Provider and Virtual Top/End Node. Further discussion on the protocol implementation is out of scope for this chapter.

This study uses SC-Alg as an intermediary between the DSO and the EV charger. SC-Alg can be operated by two independent entities; for example, the Virtual Power Plant (VPP) aggregator is the Ctr-aggr, while an EV aggregator/Charge Point Operator (CPO) or a local Energy Management System (EMS) is the Sub-aggr. Alternatively, SC-Alg can be administrated solely by the CPO/EMS. In some cases, the DSO itself can take the role of a Ctr-aggr [192, 193].

6.2.2. Smart charging algorithm description

Objective Function

The primary goal of SC-Alg is to minimise the total node cost C_n^{tot} . The objective function Eq. (6.1) has two parts:

- 1) The compensation cost paid to the EV user from the Sub-aggr if the actual charged energy is less than the energy target. The energy target is what would be provided to the EV if an Uncontrolled Charging (UNC) policy was applied $(B_{n,j,T_i^d}^{\mathrm{UNC}})$;
- 2) The nodal net cost of buying/selling the electricity from/to the grid. The target argument to this optimisation problem is the EV charging current setpoint $i_{n,j,t}^{e+,Set}$ (in Eq. (6.2)).

Min.
$$C_n^{\text{tot}} = \sum_{j=1}^{J} \left(B_{n,j,T_j^d}^{\text{UNC}} - B_{n,j,T_j^d}^{\text{Set}} \right) C_{n,j}^{\text{comp}} + \Delta T \sum_{t=1}^{T} \left(p_{n,t}^{\text{g(imp)}} C_t^{\text{e(buy)}} - p_{n,t}^{\text{g(exp)}} C_t^{\text{e(sell)}} \right)$$
 (6.1)

The parameters of the objective function and constraints of SC-Alg are listed in Table 6.1 and 6.2 respectively.

Parameter	Meaning
$C_n^{\mathrm{tot}} [\epsilon]$	Total nodal costs at node n over the whole time T
B_{n,j,T_j^a} [kWh]	Energy in battery of EV j at node n upon arrival T_j^a
$B_{n,j,T_j^d}^{\text{Set}}$ [kWh]	Energy in battery of EV j at node n when departure T_j^d , calculate from setpoint
$B_{n,j,T_j^d}^{\mathrm{UNC}}$ [kWh]	Energy in battery of EV j at node n when departure if uncontrolled charging policy applied
$C_{n,j}^{\mathrm{comp}} \ [\epsilon/\mathrm{kWh}]$	Compensation for not meeting the energy demand of EV j at node n by departure
$p_{n,t}^{\mathrm{g(imp)}}$ [kW]	Grid import power of node <i>n</i> at time <i>t</i>
$i_{n,t}^{\text{g(exp)}}$ [kW] Grid export power of node n at time t	
$C_t^{\mathrm{e(buy)}}$ [ϵ/kWh]	Electricity purchase price at time t
$C_t^{\mathrm{e(sell)}} [\ell/\mathrm{kWh}]$	Electricity selling price at time t

Table 6.1: Parameters of smart charging objective function

Constraints

According to the current commonly employed AC charging standard IEC 61851 [45], the EV charging current setpoint is sent to the EV via Pulse Width Modulation (PWM) signals through the Control Pilot (CP) pin in the charger. The minimal non-zero charging current setpoint is 6 A, and the setpoint value can only be adjusted in discrete intervals. The charging current setpoint is set to be integer values in SC-Alg and is constrained in the equation listed below.

$$\left(i_{n,j,t}^{\text{e+,Set}} = 0\right) OR\left(i_{n,j,t}^{\text{e+,Set}} \ge 6\right) \tag{6.2}$$

The EV charging power is computed with the phase charging current setpoint, the number of phases and the node voltage.

$$p_{n,j,t}^{\text{e+,Set}} = i_{n,j,t}^{\text{e+,Set}} \times \phi_{n,j}^{\text{EV}} \times v_{n,t}$$
 (6.3)

The EV battery energy is calculated by integrating the charging power with time and multiplying the onboard charger efficiency. With the battery energy and capacity, the EV SoC is obtained.

$$B_{n,j,t}^{\text{Set}} = B_{n,j,T_j^a} + \Delta T \sum_{T_i^a}^{t} \left(p_{n,j,t}^{\text{e+,Set}} \times \eta_{n,j}^{\text{EV}} \right)$$
 (6.4)

$$S_{n,j,t}^{\text{Set}} = \frac{B_{n,j,t}^{\text{Set}}}{B_{n,j}^{\text{max}}}$$
 (6.5)

The power exchange between the grid and the local node is presented in the equation below.

$$p_{n,t}^{\text{exch}} = \sum_{j=1}^{J} \left(p_{n,j,t}^{\text{e+,Set}} / \eta_{n,j,t}^{\text{EVSE}} \right) + p_{n,t}^{\text{LL,Fcst}} - p_{n,t}^{\text{PV,Fcst}}$$
(6.6)

Where the import/export power from/into the grid is the positive/negative part of the node-grid exchange power respectively.

$$\begin{aligned} p_{n,t}^{\text{g(imp)}} &= \left\{ p_{n,t}^{\text{exch}} \middle| p_{n,t}^{\text{exch}} \ge 0 \right\} \\ p_{n,t}^{\text{g(exp)}} &= -1 * \left\{ p_{n,t}^{\text{exch}} \middle| p_{n,t}^{\text{exch}} < 0 \right\} \end{aligned}$$
(6.7)

The import/export node current/power $i(p)_{n,t}^{\mathrm{g(imp)/g(exp)}}$ is then limited by the current/power limit $i(p)_{n,t}^{\mathrm{G+/G-}}$. This value could be contracted between the local node and the DSO, or given by the Ctr-aggr when the central grid congestion management function is operating.

$$i(p)_{n,t}^{\text{g(imp)}} \le i(p)_{n,t}^{G+} i(p)_{n,t}^{\text{g(exp)}} \le i(p)_{n,t}^{G-}$$
(6.8)

EV charging model

The EV Battery Management System (BMS) can run its own charging strategy within the setpoint-defined maximum charging current. A study based on more than 10k detailed charging session data suggests that EVs' dominant AC charging strategy is the constant-current-constant-voltage (CC-CV) method [104]. Hence, this chapter assumes the EV BMS deploys a CC-CV strategy to set the EV's actual charging current $i_{n,j}^{e+,Act}$ referring to the setpoint sent through the EVSE. The BMS charging strategies are not incorporated in SC-Alg, and this model is only used to emulate the EV charging performance. The CC-CV method is simplified in this chapter in that the BMS sets EV's charging current at its rated value $I_{n,j}^{EV}$ until the SoC reaches the CC-CV switch point $S_{n,j}^{CV}$. After that, the charging current decreases linearly versus SoC till the car is fully charged, as exhibited in Eq. (6.9).

$$\begin{aligned} p_{n,j,t}^{\text{e+,Act}} &= i_{n,j,t}^{\text{e+,Act}} \times \phi_{n,j}^{\text{EV}} \times \nu_{n,t} \\ i_{n,j,t}^{\text{e+,Act}} &\leq \min \left(I_{n,j}^{\text{EV}} \times \frac{(1 - S_{n,j,t}^{\text{Act}})}{1 - S_{n,j}^{\text{EV}}}, I_{n,j}^{\text{EVSE}} \right) \end{aligned}$$
(6.9)

Table 6.2: Parameters of constraints

Parameter	Meaning
$i_{n,j,t}^{\text{e+,Set}}$ [A]	Charging current setpoint giving to EV j at time t and node n
$p_{n,j,t}^{\text{e+,Set}} [\text{kW}]$	Charging power calculated from current setpoint of EV j at node n at time t
$B_{n,j,t}^{\text{Set}}$ [kWh]	Energy in battery calculated from current setpoint of EV j at node n at time t
$S_{n,j,t}^{\mathrm{Set}}$	SoC calculated from setpoint of EV j at node n at time t
$i_{n,j,t}^{\mathrm{e+,Act}}$ [A]	Actual charging current of EV <i>j</i> , node <i>n</i> , time <i>t</i>
$p_{n,j,t}^{\text{e+,Act}} \text{ [kW]}$	Actual charging power of EV j , node n , time t
$B_{n,j,t}^{\text{Act}}$ [kWh]	Actual battery energy of EV j , node n , time t
$S_{n,j,t}^{\mathrm{Act}}$	Actual SoC of EV j , node n , time t
$B_{n,j}^{\max}$ [kWh]	Usable battery size of EV j at node n
$S_{n,j}^{\text{CV}}$	SoC switch point between CC and CV stage of EV <i>j</i> at node <i>n</i>
$\phi_{n,j}^{\text{EV}}$	Number of phases EV charge with
$\eta_{n,j}^{ ext{EV}}$	On-board charger efficiency of EV j at node n
$\eta_{n,j}^{ ext{EVSE}}$	Efficiency of charger j at node n
$I_{n,j}^{\mathrm{EV}}\left[\mathrm{A}\right]$	Rated current of the EV j at node n
$I_{n,j}^{\text{EVSE}}$ [A]	Rated current of the charger EV j plugged in at node n
$p_{n,t}^{\text{PV,Fcst}}$ [kW]	Forecast PV generation power at node n at time t
$p_{n,t}^{\text{LL,Fcst}}$ [kW]	Forecast local load power at node <i>n</i> at time <i>t</i>
$E_n^{\rm LL,r}$ [kWh/yr]	Yearly energy consumption of local load
$v_{n,t}$ [V]	Voltage of node <i>n</i> at time <i>t</i>
$i_{n,t}^{\mathrm{g(imp)}}$ [A]	Grid import current of node n at time t
$i_{n,t}^{\mathrm{g(exp)}}$ [A]	Grid export current of node <i>n</i> at time <i>t</i>
$i_{n,t}^{G+}$ [A]	Distribution network capacity for importing current from grid at node <i>n</i>
$i_{n,t}^{G-}[A]$	Distribution network capacity for exporting current to grid at node <i>n</i>

6.2.3. Algorithm execution and the Flexible receding horizon scheme

SC-Alg algorithm is written in Python, and a Linear Programming, Quadratic Programming and MIP specialised commercial solver Gurobi®is applied to solve the optimisation problem.

Considering the input data uncertainty, a passive stochasticity response mechanism - flexible receding horizon technique - is equipped in SC-Alg as introduced in Section 6.1. This scheme is basically to re-optimise the system regularly with updated information. The optimisation can be triggered in a fixed time interval or by events like new EV arrival, grid constraint adjustment and the estimated-real SoC disparity.

SC-Alg uses the flexible receding horizon method to set its optimisation horizon, and the length of the horizon is determined by the last future departure EV. How far to the future SC-Alg can optimise is limited by the prediction data availability and the computational power. To avoid an excessive optimisation horizon, long-term parking EVs can be exempt from the "future departure EV" list and will not be included until a certain period of time,

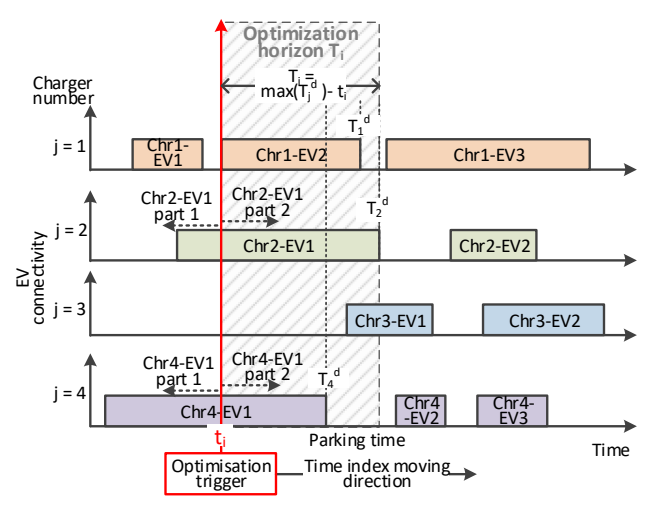


Figure 6.2: Schematic of the algorithm execution and the flexible receding horizon

like 24 hours, before their departures. Upon triggering re-optimisation, the optimisation horizon is automatically updated, and then the new optimisation results are sent to the chargers to replace the old setpoints. A schematic of SC-Alg execution and the explanation of the flexible receding horizon is presented in Fig. 6.2. In this figure, each coordinate represents one charger while each block symbolises one car, with its length indicating the parking duration. When a new car (Chr1-EV2) arrives at charger 1 and triggers the re-optimisation at t_i , the aggregator checks the in-use charger 1, 2 and 4, and compares the EV parking times of the three connected EVs. The latest departure time of all EVs $(T_{max}^d = \max\{T_i^d | j \in J\})$ is identified and the optimisation horizon T_i^J is determined as $T_i^J = T_{max}^d - t_i$. With this flexible receding horizon method, SC-Alg can run continuously and automatically adapt to the modification of the input parameters or the uncertainties in them. The Sub-aggr accesses the local PV generation and load demand profile through smart meters and obtains the dynamic energy price information published in the market by the central price settlement entity. The EV-related information like the EV type, arrival SoC, and expected departure time is provided by the user upon arrival through, for example, a smartphone App.

6.3. Hardware-Software configuration

6.3.1. HIL setup

The schematic of the HIL setup used in this chapter and its lab photo are shown in Fig. 6.3 and 6.4 respectively [194]. The whole setup consists of four parts. The solid lines in the plot depict the power flow while the information flows are illustrated in dotted lines.

The controller in block 1 is the brain of the whole setup; it has one target machine – a DRTS OPAL-RT® 5700 and one host computer for the user interface. The testing model, containing a distribution grid with loads, PVs and EVs, is built with MATLAB®/Simulink® in the host computer and converted to C code, then uploaded to the simulator through the OPAL-RT interface software RT-LAB. When the model runs in DRTS, the host computer

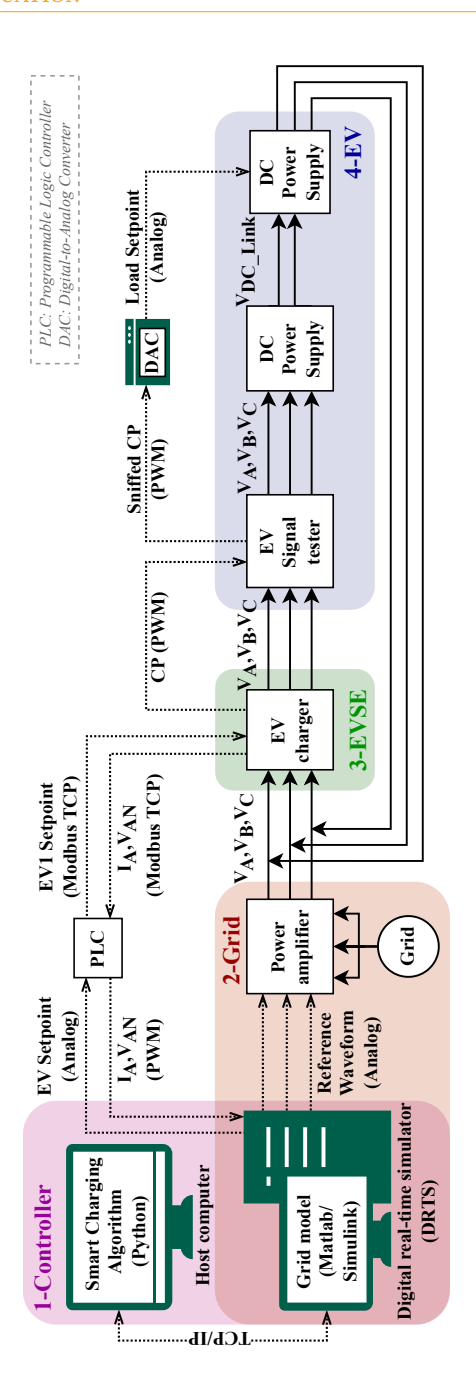


Figure 6.3: Overview of the HIL testbed setup

monitors its performance and communicates the input/output data through TCP/IP protocols. The DRTS manages the physical I/O signals and controls/communicates with the hardware devices in the power loop part. SC-Alg written in Python script also runs on the host computer. SC-Alg computes the optimal charging strategy and interacts with

the model in DRTS. In block 2 sits the grid model inside the DRTS and a grid emulator comprising three 1.5 kVA rated power California Instruments®AST1501 power amplifiers. One node of the grid is picked and each phase is emulated by a power amplifier.

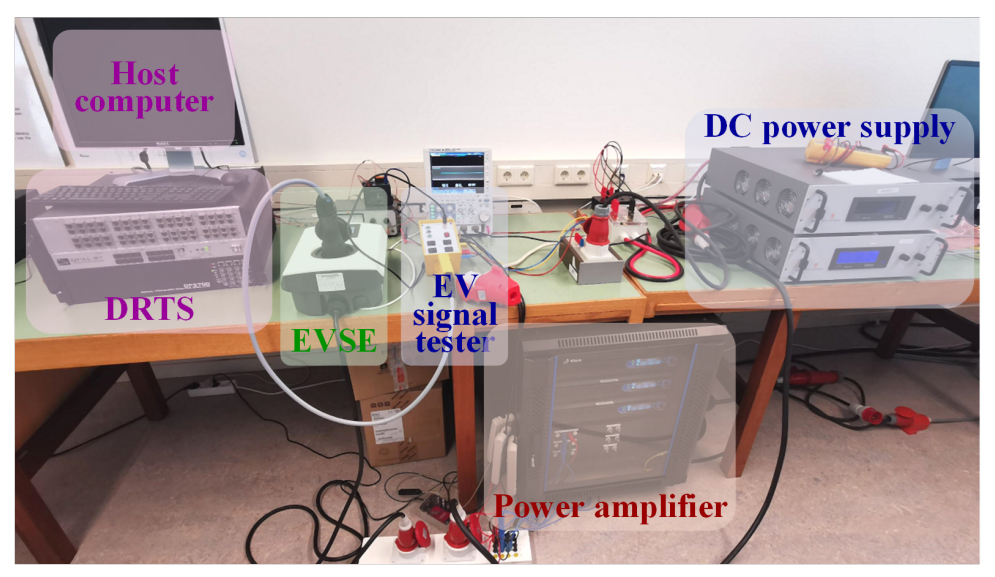
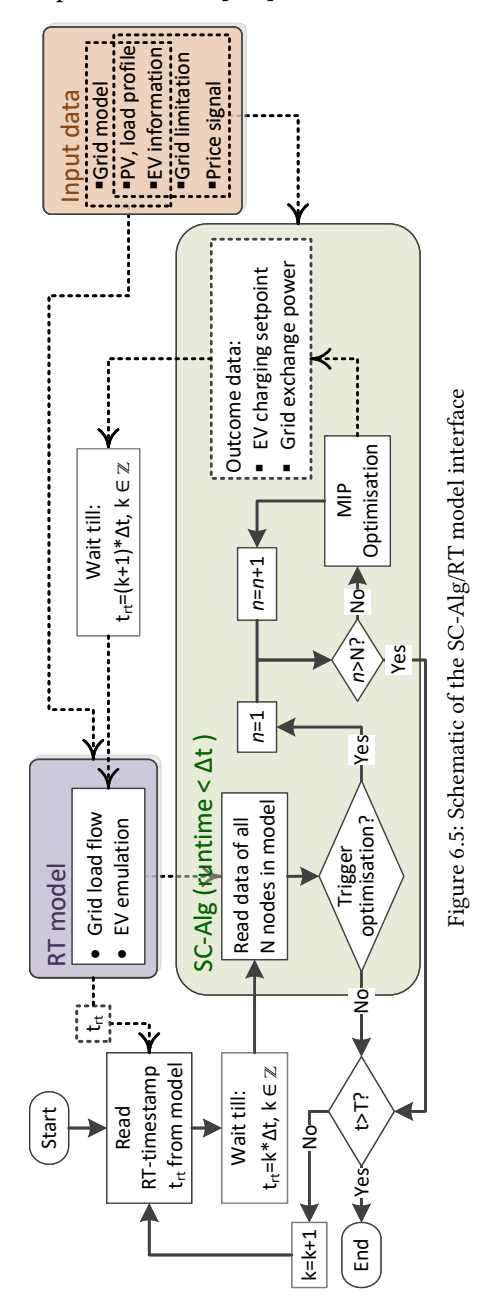


Figure 6.4: Photo of the HIL setup in the lab

The next component is the EVSE in block 3, an Alfen®EVE Single Pro-Line AC charger that can provide power in both single and three-phase with a maximum 32 A phase current. When the smart charging is not initiated, the charger simply provides the power requested by the EV emulator as long as it is not higher than the maximum allowed phase current. However, when SC-Alg takes effect, the computed optimal current setpoint is sent to the EVSE from the DRTS via Modbus TCP/IP. Conversely, the EVSE measures the voltage and current drawn by the car and communicates them back to the DRTS.

The last part of the testbed, which is placed in block 4, is the EV emulator composed of one signal tester and one power circulation unit. The Walther-Werke®EV signal tester can communicate the EV connection/ready-to-charge status to the EVSE through the Control Pilot (CP) pin. Even though the EV signal tester has the option to send up to 63 A rated current signal to the EVSE, a maximum of 16 A current is allowed to pass through due to its hardware limitation. The power circulation unit in block 4 processes the power with two Delta Elektronika®SM15K bidirectional AC/DC power supplies that are connected back-to-back, forming a conventional regenerative AC load (AC-DC-AC) and then returns this power to the connection between the power amplifier and the EVSE. The quantity of the circulating power is controlled by manoeuvring the second power supply's current while keeping the DC link voltage constant. Each power supply can process up to 15 kW power at a maximum of 500 V or 90 A.

The power circulation feature of the setup allows a much higher charging power with built-in bi-directionality as compared to the AC power amplifier, which is unidirectional and only supplies the losses of the system. More technical details about the experimental setup can be found in our previous work [194].



6.3.2. Testbed/Algorithm interface

To ensure a steady data transmission between the SC-Alg in the host computer and the model in the target machine during real-time simulation, some adaptions as well as an extra interface are requested (Fig. 6.5). The Python API in DRTS's software RT-lab is employed to allow the variables to be read and written from/to the target machine while the RT model is operating. A one-minute re-optimisation trigger resolution ensures sufficient timing for parameter exchange and optimisation computation. Besides, frequent re-optimisation can improve the stochasticity handling ability.

SC-Alg can serve in several nodes in a distribution grid simultaneously over multiple days. Schematic Fig. 6.5 shows how SC-Alg interacts with the model and how the simulation times are synchronised.

- Once all the variables are initialised, the grid model launches in DRTS, and its simulation timestamp (t_{rt}) is read by SC-Alg
- whenever the simulation timestamp reaches the multiple of one timestep ($t_{rt} = k \times \Delta t, k \in \mathbb{Z}$), the SC-Alg checks if a new round of optimisation needs to be triggered
- If optimisation is requested, the SC-Alg would go through every relevant node and calculate each node's best EV charging profiles separately. This whole calculation process is finished within one timestep
- The SC-Alg waits till the DRTS's simulation time reaches the next timestep ($t_{\rm rt} = (k+1) \times \Delta t, k \in \mathbb{Z}$), then sends the calculated optimal charging profile to the target node in the grid model
- Repeats the whole process until the RT simulation ends

6.4. Assumptions and test scenarios

6.4.1. Grid model and input data

The grid model used in this study is adapted from data of a Dutch rural LV distribution grid as a representative example [195]. Therefore, only the results pertaining to SC-Alg's performance relative to the defined base case are relevant and the conclusion cannot be inferred to reflect actual congestion issues in actual Dutch grids. This grid has in total 19 nodes, with loads connected at nodes 5, 15 and 19, EV chargers connected at Node 5, 15 and one PV system installed at Node 5, as illustrated in Fig. 6.6. Node 5 & 15 are equipped with one Sub-aggr each for local optimisation while the Ctr-aggr oversees the whole grid conditions.

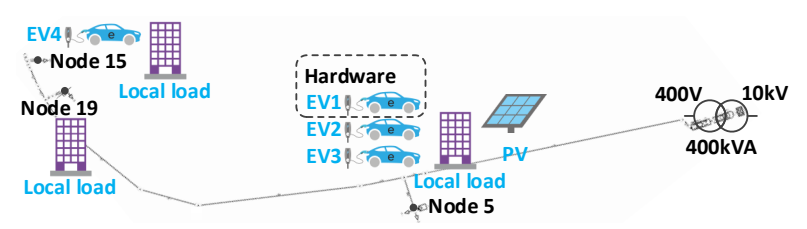


Figure 6.6: Schematic of the simulated Dutch rural grid

Each node is assumed to have a $3\times50\,\mathrm{A}$ connection capacity. Further, Node $5\,\&$ 15 are two small businesses where employees park and charge their EVs during weekday working hours. It is also assumed that the grid is three-phase balanced, and all EVs are charged with three phases. Considering the power limitation of individual testbed components, the emulated EV's maximum charging current is set as $16\,\mathrm{A}$ per phase. This is a reason-

able assumption as most onboard chargers are rated for 3×16 A. In the simulation, each charger serves a maximum of one EV per day. Among all four simulated EVs, only EV1 is represented in the PHIL system while the others are virtual. The parameters of two types of EVs (Tesla Model 3 Standard Range & Model S P100D [196, 197]) are used in the model. All four EVs share the same arrival SoC of 40% and the expected departure SoC at 100%.

One arbitrary summer working day 9:00 - 17:00 is selected for the PHIL simulation. The load consumption power profile is derived from Dutch standard load profiles [95] with the yearly energy consumption value $E^{\rm LL,r}$ provided in the grid model. The PV profile is generated based on the Dutch historical solar irradiation data [198]. A 25 kWp PV installation in Node 5 is assumed.

It is found that dynamic electricity price which encloses grid loading information could guide the consumer's behaviour and significantly mitigate grid congestion [140, 144]. The adoption of a variable energy tariff, combined with an EV SC algorithm is therefore preferred, in the absence of a mature congestion market incorporating grid loading information in the Netherlands [133]. Historical Dutch Day-Ahead market (DAM) price data is utilised as the benchmark for determining electricity purchasing prices as the DAM price trend frequently aligns with the electricity consumption patterns during peak and off-peak periods. A constant value of $C_t^{e(sell)} = 20 \in MWh$ electricity selling price, which is always lower than the selected buying price, is set. Compensation from the Sub-aggr to the EV user for the inadequate EV charged energy compared to the UNC scheme is set to be $C_{n,j}^{\text{comp}}$ = 0.1 €/kWh. This value instead, is always higher than the selected electricity buying price. Note here that DAM is much lower than the retail electricity price (capped at $0.4\,\mathrm{\&f/kWh}$ in 2023 [199]) as a wholesale market price, and thus the $C_t^{\text{e(sell)}}$ and $C_{n,j}^{\text{comp}}$ are also low. However, the absolute value of the electricity price is not the imperative factor of the algorithm's performance; it is the ratio between $C_t^{\text{e(buy)}}$, $C_t^{\text{e(sell)}}$ and $C_{n,j}^{\text{comp}}$ that matters. Other costs such as PV installation and maintenance costs are not considered.

The forecast PV and load profiles $p_{n,t}^{\text{PV,Fcst}}$, $p_{n,t}^{\text{LL,Fcst}}$ of Node 5, and the energy price are presented in Fig. 6.7.

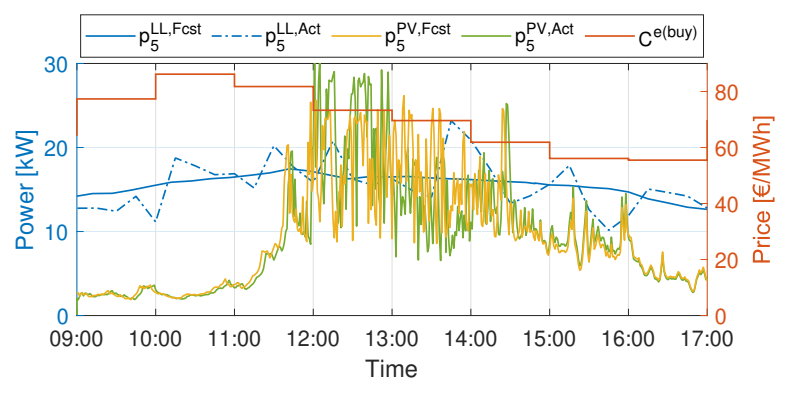


Figure 6.7: Input PV, load and price profile

6.4.2. Simulation scenarios

The testbed has subsequently been used to study the effect of uncontrolled and controlled charging on the simulated distribution grid for a total of eight different scenarios. Apart from two scenarios that serve as a benchmark: the uncontrolled charging (Case 0) and the proposed SC-Alg running without extra intervention (Case 1), the system was tested with six other scenarios with different impact factors. These scenarios are categorised into three groups: inaccurate PV/load prediction, EV information mismatch and grid limitation incorporation. The first two groups focus on testing SC-Alg's performance with the impact of stochasticity, while the last group explores the grid congestion mitigation potential of the SC-Alg. Each scenario only has one parameter changed with respect to Case 1 to avoid cross-correlation issues. The input parameters for all simulation scenarios are summarised in Table 6.3.

Parameters		Node 5		Node 15
p ^{PV,r} [kW]		25		0
E ^{LL,r} [kWh]		88779		3556
	EV1	EV2	EV3	EV4
T_j^a	9:00	9:00	9:30	9:00
T_j^d	16:30	16:30	17:00	16:30
$B_{n,j}^{\max}$ [kWh]	50	50	100	50
$I_{n,j}^{ ext{EV}}$	3x16 A	3x16 A	3x24 A	3x16 A

Table 6.3: Parameters for all simulation scenarios

Inaccuracy in PV and Load Prediction

Case 2 and 3 evaluate SC-Alg's outcome when the input PV and load predict profiles are inaccurate, respectively.

Case 2: Inaccuracy in PV Forecast

To emulate the actual PV generation profile $p_{n,t}^{\text{PV,Act}}$, the forecast PV profile $p_{n,t}^{\text{PV,Fcst}}$ is multiplied by a random multiplier generated by a normal distribution with its mean $\mu=1$. It is reported that even though the weather forecast technique has developed significantly nowadays, intra-hour forecast errors of solar irradiance could still be up to 30% [200]. Therefore, the standard deviation σ of the normal distribution is set to be 0.15. On top of that, a correction factor C is added to ensure the total PV generated energy stays the same compared to the other cases, as stated in Eq. (6.10).

$$p_t^{\text{PV,Act.}} = p_t^{\text{PV,Fcst}} \times N_t (\mu, \sigma^2) \times C$$
Where:
$$C = \frac{\int p_t^{\text{PV,Fcst}} dt}{\int (p_t^{\text{PV,Fcst}} \times N_t (\mu, \sigma^2)) dt}$$
(6.10)

Case 3: Inaccuracy in Load Forecast

A similar process is applied to the load profile. The same random multiplier as Case 2 and a correction factor is adapted.

Both predicted and actual PV and load profiles are shown in Fig. 6.7. Note that the SC-Alg still uses the provided forecast profiles ($p_t^{\text{PV,Fcst}}$, $p_t^{\text{LL,Fcst}}$) for the optimisation.

EV information mismatch

Case 4: Mismatch in EV Charging Current Information

As mentioned in Section 6.2.2, the charging current setpoint is transmitted from EVSE to EV. However, the onboard BMS decides the actual current to be drawn, ensuring it remains below the setpoint. Even when the BMS is configured to adhere to the specified setpoint, the actual current drawn can be up to 10% lower than the provided setpoint [201]. If the BMS is set to run an internal charging program which only uses the provided setpoint as the upper limit, the maximum bias between the actual current drawn and the setpoint per phase can be anywhere between 0-100%. For example, a maximum 53% of difference between the setpoint and real charging current in "low mode" is reported in [80]. This charging control mechanism poses a challenge to smart charging when an unknown gap between the given setpoint and the actual EV charging current exists. Case 4 is then designed to test how much the inequivalent EV charging currents can affect the SC-Alg's behaviour. In this case, all EVs' BMS follow the setpoint, but the actual-drawn currents are always 10% lower.

Case 5: Disparity in EV Battery Capacity Information

Another EV information mismatch which could hinder SC-Alg's performance is the disparity in EV battery capacity. Protocol IEC 61851-1 does not communicate the EV SoC to the EVSE. Regardless, it is assumed that users can provide their EV arrival SoC to the Sub-aggr through a mobile phone app for the SC-Alg to calculate EV SoC with a non-guaranteed accuracy, especially when the EV battery is degraded. This potentially deviated SoC estimation will obstruct SC-Alg's behaviour. Case 5 is thence proposed to test the 30% battery capacity fading scenario. For a fair comparison, the actual EV charged energy needs to be kept the same across all cases. In order to do that, the battery capacity stated in Table 6.3 is set as the "actual capacity of aged battery", and the EV battery capacity that is read by the SC-Alg is $\frac{50}{0.7}$ = 71 kWh for EV1, 2, 4 and $\frac{100}{0.7}$ = 143 kWh for EV3 respectively.

Incorporation of grid restriction

When EV charging demands from multiple users appear at the same time, the grid faces the risk of overloading. In the last two scenarios, extra constraints from the grid side, namely Grid Restriction Incorporation (GRI), are in place to prevent potential grid congestion.

Case 6: Centralised Grid Capacity Allocation (GCA)

The design idea of GCA is that the Ctr-aggr allocates the grid capacity among multiple Sub-aggrs based on the nodal sum of the remaining EV charging energy demand. Assume the tested grid has a total of 50 A grid import current capacity for EV charging, and the Ctraggr assigns this capacity among Node 5 & 15 based on the energy still needed to fulfil each node's EV charging target. However, if one node has too small a remaining energy target value compared to others, the allocated capacity for this node could be lower than the minimal EV charging current setpoint 6 A. To prevent this, a minimal grid import current limit is reserved to ensure at least one EV can still charge with the minimum current. Besides, the grid should always be able to supply the local load demand. The grid capacity determination equation is listed in Eq. (6.11).

$$i_{n,t}^{G+} = \max\left(6 + \frac{p_{n,t}^{\text{LL,Fcst}}}{v_{n,t}}, 50 \times \frac{\sum_{j=1}^{J} (B_{n,j,T_j^d}^{\text{UNC}} - B_{n,j,t}^{\text{Act}})}{\sum_{n=1}^{N} \sum_{j=1}^{J} (B_{n,j,T_j^d}^{\text{UNC}} - B_{n,j,t}^{\text{Act}})}\right)$$
(6.11)

Case 7: Decentralised Voltage Droop method (VDM)

The decentralised GRI method - local VDM, is activated in Case 7. The charging current of each EV is tuned between 6 A and $I_{n,j}^{\rm EV}$ proportionally to the local node voltage [202], when the voltage falls between 0.92 and 0.95 p.u.. The illustration of how the EV charging setpoint is determined is in Fig. 6.8.

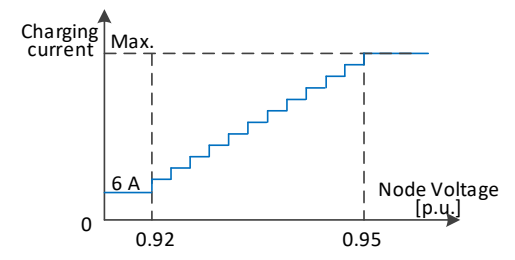


Figure 6.8: Charging current adjustment as a function of bus voltage - Case 7

6.5. Results and analysis

6.5.1. Base case

The performance of Case 0 and Case 1 regarding grid behaviour impacted by UNC and SC is reflected in Fig. 6.9, and the EV charging behaviour comparison is presented in Fig. 6.10.

EV charging demand fulfilment

Overall performance

First of all, it can be observed in Fig. 6.9 (a) that SC-Alg significantly flattened the grid import power at Node 5 and it shifts the EV charging demand $\sum_{1}^{J} p_{5,j}^{\text{Act}}$ from morning to the afternoon when the PV generation is high and the energy price is cheaper, as shown in Fig. 6.7. SC-Alg also improves the voltage drop provoked by simultaneous EV charging, especially in Node 5.

However, Fig. 6.10 depicts that the calculated EV charging current setpoint $i_{n,j}^{\text{e+},\text{Set}}$ oscillates. This can potentially stress the hardware in the charger, especially when the setpoint shifts between zero and non-zero too regularly which requests a too frequent open/close of the relay in the charger, and in turn decreases the charger's lifetime in the long run. A function to reduce the zero/non-zero charging current alteration frequency is thus helpful.

Another thing that can be perceived in Fig. 6.10 is that none of the EVs can be charged to 100% upon departure, and two factors cause this. The first factor is related to the nature of the EVSE-EV communication practice. As explained in Section 6.4.2, the actual EV charging current with the same given setpoint deviates from EV to EV, differences in charging efficiency, embedded charging strategy, CV switch point and the nature of current dropping in CV region. This setpoint-real charging current value discrepancy deviates the actual charging progress away from the optimal plan. Even though the periodic SoC update

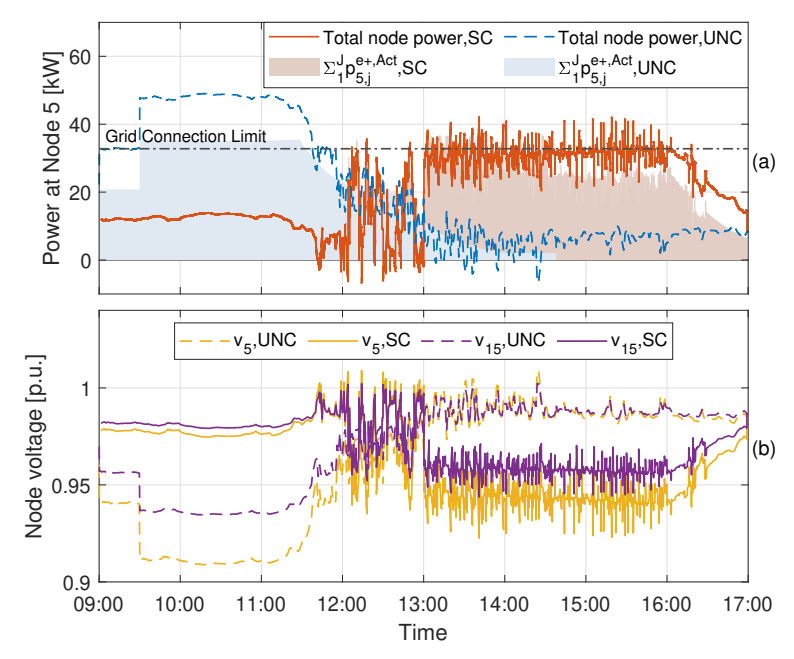


Figure 6.9: Comparison of grid impact of UNC and SC. (a) Total node power and the sum of EV charging power in Node 5, (b) Voltage fluctuation in Node 5 & 15

between EV and the Sub-aggr is supported by the SC-Alg, it is still impractical for the SC-Alg to correct the energy deficiency in time due to the lack of actual charging power and SoC relation. The second factor is that the optimal charging profile calculation is based on the voltage value at the optimisation trigger moment. However, the node voltage inevitably drops when the charging process starts with sudden EV power drawn. This voltage drop in turn, leads to a lower actual EV charging power than what is calculated by the SC-Alg. Both factors produce the same outcome: the actual charging power is lower than what is calculated by the SC-Alg, and as a result, the EVs are not fully charged.

A potential solution for the first factor is to add a feedback loop to detect and correct the setpoint-real charging current value discrepancy. Another simpler and more effective solution is to accommodate this potential error in the SC-Alg, which is to set a slightly higher charging energy goal or a sooner charging completion time limit.

Grid import power ripples

In Fig. 6.9 (a), especially between 13:00 and 16:00, the grid import power fluctuates intensively around the grid input power limit.

It can be observed in Fig. 6.11 that the grid import limit is breached for approximately 5 s due to the actual hardware (EV1) delay in response and ramp down its power following the given setpoint. This behaviour will be missed in a pure software simulation and highlights the importance of HIL experimental demonstration. The high-resolution RT-PHIL simulation manifests another factor leading to the grid import power oscillations, that is discrete optimisation combined with continuously evolving environmental parameters such as PV generation, as shown in Fig. 6.12. In real applications, communication delay has a wide

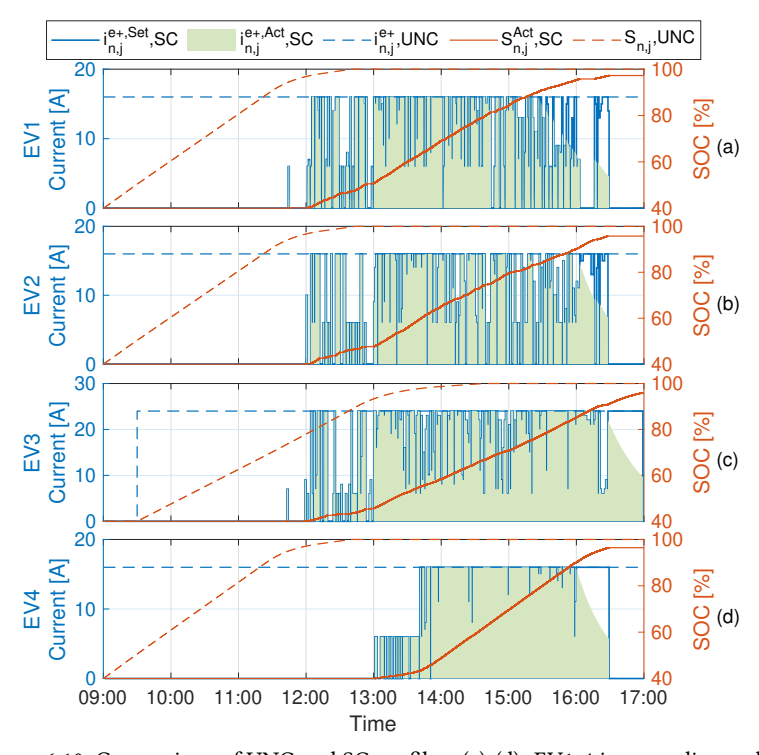


Figure 6.10: Comparison of UNC and SC profiles. (a)-(d): EV1-4 in ascending order

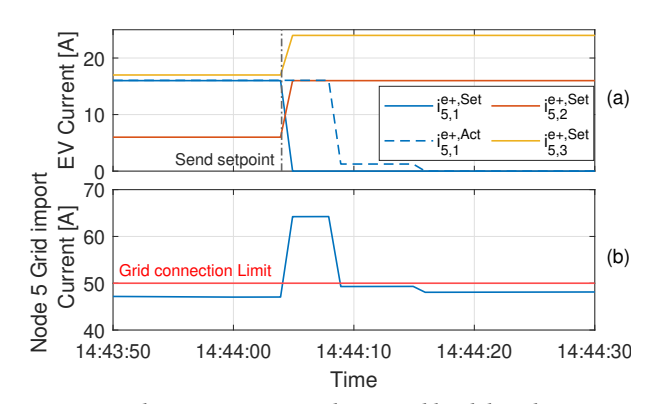


Figure 6.11: Grid import current spike caused by delayed EV response

range from less than 5 s to 60 s depending on the characteristics of the transceiver, the network and the protocols [45, 47, 79]. Preventing the grid power ripples caused by various communication delays is effortful due to its unpredictability. It is thus worth exploring the grid impact induced by discordant communication latency and how to moderate it in the future.

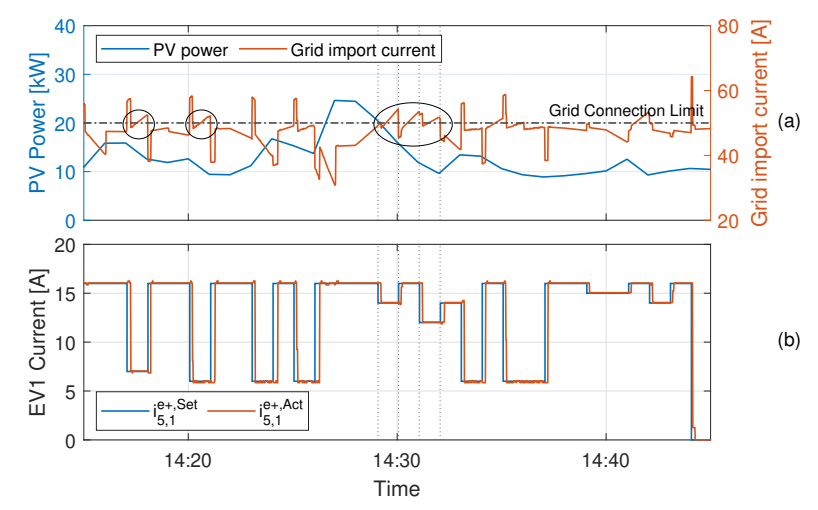


Figure 6.12: Node 5 Grid import current spike in between optimisation intervals

6.5.2. Impact of stochasticity

This section analyses the results of the SC-Alg operating with inaccurate PV/load demand prediction (Case 2 & 3) and mismatched EV information (Case 4 & 5).

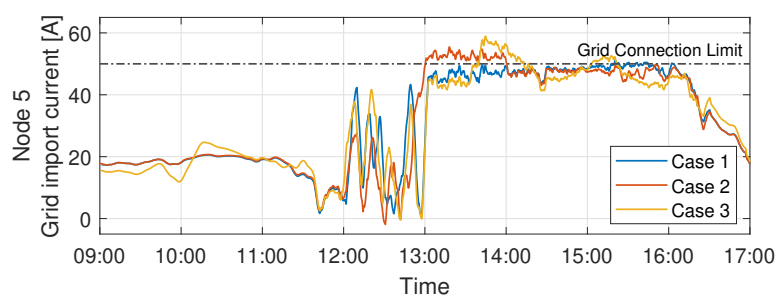


Figure 6.13: Impact of inaccurate PV/load demand prediction: Grid import current comparison (5 min moving average)

Fig. 6.13 presents the 5-min moving average grid import current of Node 5 under the influence of inaccurate forecasts. The dissonance of the actual and predicted PV/load profile (in Fig. 6.7), is reflected in the grid import current results, even though the difference is moderate. On the other hand, if the predicted–actual profile error of both PV and load happens at the same time, they may cancel each other out or in reverse, add up and worsen the situation. It is thus appealing to view the multi-variable inaccuracy as a whole and investigate the impact of joint stochasticity in the future. This investigation can be demonstrated with the experimental testbed implementing actual PV and load conditions with minor adaptions.

The EV charging current and their corresponding SoC values of Case 4 & 5 are illustrated in Fig. 6.14 (a), (b). The comparison of 5 min moving average grid loading of Case 1, 4 and 5 are shown in Fig. 6.14 (c). It can be noticed from Fig. 6.14 (a), (c) that the 10% lower actual

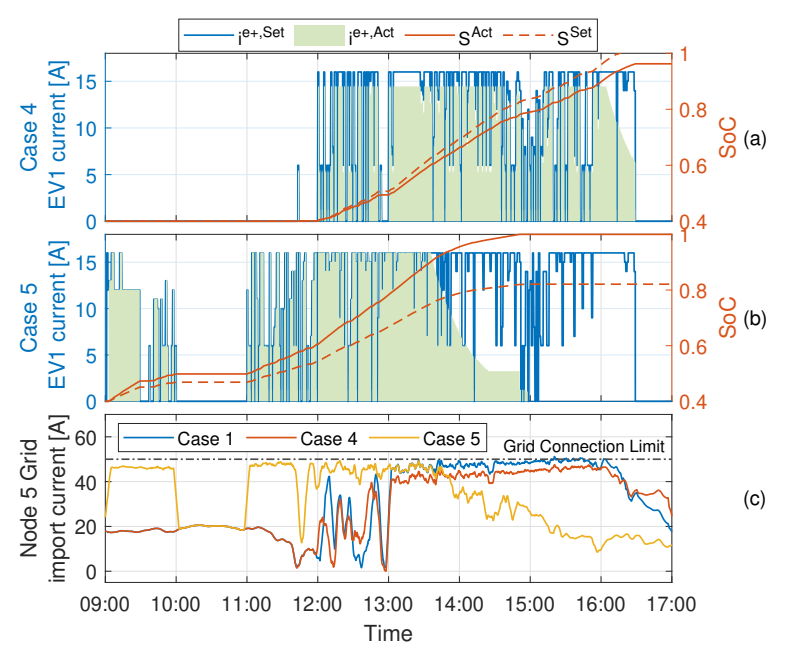


Figure 6.14: EV charging performance and grid loading results with mismatched EV information (a) charging performance of EV1, Case 4, (b) charging performance of EV1, Case 5, (c) EV information mismatch impact on the grid import current.

charging current $i^{\text{e+,Act}}$ than the setpoint $i^{\text{e+,Set}}$ of Case 4 leads to a reduced grid loading at the cost of a lower departure SoC than Case 1. In Case 5, the battery degradation provoked imprecise SoC estimation and leads to an unnecessarily rushed charging when the electricity price is not the lowest relative to Case 1, as presented in Fig. 6.14 (b), (c). In other words, battery-aged EVs require less energy to be fully charged, and the SC-Alg can use this information to yield a better solution. Yet, this inaccurate usable battery size information leads to a pleasant by-product that the battery is fully charged, even earlier than expected.

Case 4 & 5 advocate that the self-correction function mentioned in Section 6.5.1 is essential for the SC-Alg's passive stochasticity handling capability. For example, a feedback loop regularly reads the measured $i^{e+,Act}$ could help the SC-Alg to count the $i^{e+,Set}/i^{e+,Act}$ offset value in the setpoint computation. Although it is difficult to obtain the actual battery size information for an aged EV, regularly updated SoC information together with measured charging power could help rectify the SC-Alg's internal SoC tracking system. Unfortunately in practice, neither the IEC 61851-1 protocol nor the High-Level Communication Control protocol ISO 15118 supports the dynamic SoC information exchange during AC charging [45, 47]. However, there is a possibility to work around it if both EV manufacturer and CPO support the direct bilateral communication between the EV and the CPO. In summary, a closed-loop self-correction function is crucial and beneficial to add to the future version of the SC-Alg.

6.5.3. Efficacy of incorporating grid limitation

Finally, the results of two GRI scenarios are analysed and compared. The sum of EV setpoint, the 5 min moving average grid import power and the node voltage of Node 5 & 15 are illustrated in Fig. 6.15.

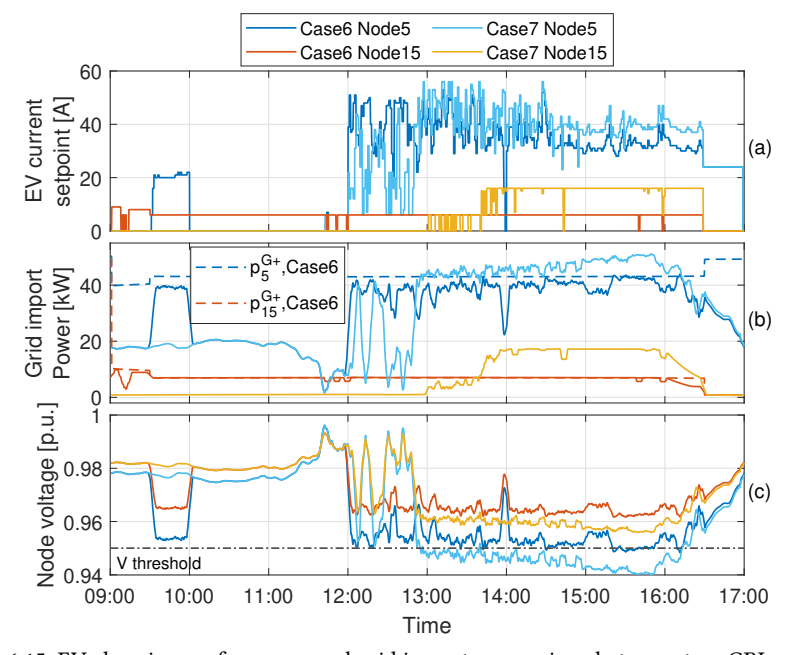


Figure 6.15: EV charging performance and grid impact comparison between two GRI methods

Fig. 6.15 (b), (c) show that GCA decreases the grid peak power and improves the voltage drop better than the VDM. In contrast to Case 1's "charge as late as possible" outcome due to the price and PV generation trend, the EV charging processes are already initiated in the morning in Case 6 as can be seen in Fig. 6.15 (a). That is because limited grid capacity cannot fulfil all EV charging requests at the lowest price even when the PV generation reaches its peak due to the employment of extra grid constraints. This spread-out charging phenomenon is especially distinct for Node 15.

As for the VDM's grid congestion mitigation performance, the voltage drop improvement is not as good as expected. One possible explanation is the voltage droop response range is relatively low. To achieve a better voltage increase effect, the voltage adjustment range can be expanded to, for example 0.95-1.05 p.u.. However it also means the users would experience a higher unfinished charging demand [202].

The centralised GCA could create an unfair situation where nodes with less total requested energy get less power and in turn, have less flexibility to shift the charging windows of its connected EVs. For example, Node 15 has a much lower grid capacity than Node 5, causing EV4 to only charge with minimal power. This limited charging power subsequently forces EV4 to charge almost the whole of its parking duration, which covers the high price moment, and the user has to bear this cost. This unfairness can be alleviated by adjusting the centralised capacity distribution principle. For example, equally share the power

among all active EVs instead [203].

The averaged departure SoC of Case 6 is 97.63%, less than the 96.68% for Case 7. With GCA, the Sub-aggr is informed about the future grid limitation through Ctr-aggr upon EV connection. With this information, the Sub-aggr tends to expedite the charging process to ensure a full departure SoC. However, the grid constraint information is not in place with VDM until the high power demand - like EV charging - induced node voltage dip appears. This gives the SC-Alg a tight schedule to plan the charging to fulfil the energy demand in time.

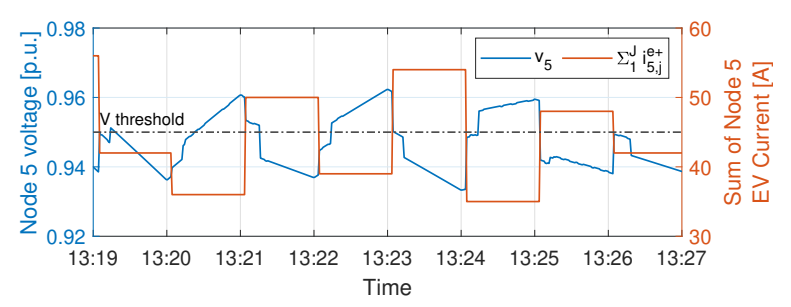


Figure 6.16: Decentralised VDM provoked low-frequency voltage oscillation

A feature of VDM worth mentioning is that it can provoke low-frequency voltage oscillation if the parameters of the VDM are not carefully set. Fig. 6.16 exhibits the circle of node voltage oscillation. Three potential solutions can ease this phenomenon; the first one is to use historical moving average voltage value as the VDM reference voltage; the second one is to add a time threshold that activates the VDM only if the voltage dips longer than a certain amount of time; and the third method is to adapt hysteresis control in the VDM.

6.5.4. Comparison

The key performance indexes of two EV-connected nodes with all eight simulated cases are listed in Table. 6.4. It includes departure SoC of each EV, the per unit charging cost of all EVs $C_{\rm sum}^{\rm EVch}$, the minimal node voltage value $V_{\rm node}^{\rm min}$, the peak overloading percentage $Pl_{\rm node}^{\rm peak}$ and the overloaded import energy $E_{\rm node}^{\rm ol}$ of Node 5 & 15. $E_{\rm node}^{\rm ol}$ is the energy obtained by the node from the part of the imported current which exceeds the limit. The illustrative explanation of $E_{\rm node}^{\rm ol}$ can be found in Fig.13 (i) in [134]. On top of that, the relative value of each scenario compared to the UNC scenario (Case 0) is listed in the right part of this table. Test cases with the best peak values are highlighted in green, and the worst ones are indicated in red in the table.

This comparison shows that the proposed SC-Alg can significantly reduce the charging cost and alleviate grid congestion compared to UNC. Even though inaccurate input data lead to less optimal outcomes, the SC-Alg still outperforms the UNC in Case 2–5. Case 3 could reduce the least grid peak values, and Case 2 shares a very close outcome. This is because PV and load profile are purely input parameters and are the ones most likely to cause power ripples among all parameters in this study, especially when there are high uncertainties. Regarding the charging cost reduction, Case 4 has the lowest charging cost, although the difference among Case 1–4, 7 are negligible. The EV capacity fading issue in Case 5 leads to a noticeable charging cost rise, and this is because the SC-Alg missed the

			Table	6.4: Cc	Table 6.4: Comparison of simulation results for different cases	imulatic	n result	s for diffe	rent case	S		
) Dě	Departure SoC [%]	e SoC [[%]		Peak values	nes		Relativ	re value v	Relative value w.r.t. Case 0 [%]	[%] 0
Case	EV1	EV2	EV2 EV3	EV4	CEVch/ Sum [cent/kWh]	Vmin node [p.u.]	$Pl_{ m node}^{ m peak}$ [%]	Enode [kWh]	$rC_{ m sum}^{ m EVch}$	$rV_{ m node}$	$rPl_{ m node}^{ m peak}$	$rE_{ m node}^{ m ol}$
0	100	100	100	100	8.05	0.909	56.3	54.1	ı	,		
1	97.3	95.8	0.96	96.4	6.25	0.923	32.4	2.1	-22.4	1.50	-42.5	-96.1
2	98.3	96.4	96.1	96.5	6.26	0.918	39.8	4.2	-22.3	1.03	-29.3	-92.2
3	96.5	2.96	95.7	96.4	6.24	0.915	46.6	4.4	-22.4	69.0	-17.2	-91.9
4	96.2	95.3	9.06	94.7	6.23	0.929	22.0	0.5	-22.6	2.17	6.09-	-99.1
5	100	100	100	100	7.08	0.924	30.0	1.5	-12.0	1.64	-46.7	-97.2
9	0.66	97.0	92.8	98.7	6.65	0.931	18.2	0.3	-17.3	2.39	-67.6	-99.4
7	7.76	8.96	95.5	96.5	6.26	0.925	27.2	1.5	-22.2	1.82	-51.5	-97.2

optimal charging window with outdated EV capacity data. Note that the charging cost variation impacted by the charging time shift away from the ideal time window strongly relates to the electricity price trend. A rushed or delayed charging which falls into an equally good or even cheaper price window would not necessarily be inferior to the optimal results. Therefore, a sensitivity analysis on applied input data, like electricity price is worth exploring in future work.

Results of Case 6 and 7 suggest that incorporating grid constraints on top of the SC-Alg further improves the grid congestion mitigation performance. Results of Case 6 suggest GCA-incorporated SC-Alg has the best grid congestion prevention as this case gives the highest V_{node}^{\min} and the lowest $Pl_{\text{node}}^{\text{peak}}, E_{\text{node}}^{\text{ol}}$ among all cases.

6.6. Conclusions and recommendations

This chapter introduces a hierarchical mixed integer programming (MIP) EV smart charging algorithm designed for low voltage (LV) distribution grid applications. The proposed SC-Alg incorporates the implementational constraints and is equipped with a flexible receding horizon scheme to manage the stochasticity passively. Afterwards, the SC-Alg is verified and thoroughly assessed in an RTDT-based PHIL testbed that uses models of real LV distribution grids. Lastly, recommendations to further upgrade the SC-Alg's are given.

The SC-Alg presents promising and steady outcomes with or without external stress factors. The results show that the SC-Alg reduces the per-unit charging cost by over 22% in 5 out of 7 scenarios. Even with a 30% EV capacity input error, the charging cost is still 12% less than the UNC scenario. The SC-Alg also proves its substantial capability in alleviating grid congestion with an average of 39.35% peak power reduction, a 1.41% average minimal voltage increase, and a 95.32% reduction in overloaded energy for Case 2–5. Additionally, the GRI implemented in Case 6–7 enhances the peak power reduction by 33.5% and curtails the overloaded energy by 65.9% further than Case 2–5.

This research has identified several intriguing factors that impact the SC-Alg's performance. These findings provide valuable insights for future studies. It is highly recommended to conduct sensitivity analyses on how input data influences the SC-Alg's behaviour. The suggested input data are the joint uncertainty of multiple input parameters and the timing/geographical/seasonal variability of input profiles, especially the price volatility. Due to the multi-protocol nature of the EV charging ecosystem, communication latency is very common in diverse applications. Investigating how much the communication latency interferes with the SC-Alg's performance is meaningful.

Several recommendations on how the proposed SC-Alg can be upgraded in the future are also defined in this study. Implementing the SC-Alg should not impose undue strain on the hardware, ensuring the frequency of switching between zero/non-zero setpoint values is within a reasonable range. A self-correction function is needed to overcome EV information mismatch issues and to track the actual charging progress with higher accuracy. We recommend using the actual EV charging current and the regularly updated actual EV SoC to decipher the $i^{e+,Set} - i^{e+,Act} - S^{Act}$ correlation and revise the internal SoC tracking system dynamically. Besides, a slightly higher charging energy or an earlier charging completion target can always be set to suffice the EV users' requests.

Concerning the GRI methods, the SC-Alg's sensitivity to the grid constraint can be lowered to reduce the grid power oscillations. One example is to selectively disclose grid capacity information and trigger re-optimisation only when constraints experience substantial and sustained magnitude variations over a specific duration. Additionally, using a moving-average historical record as the GRI reference and the hysteresis control can also be added. The further development of Ctr-aggr level advanced GRI methods is worth exploring as a separate topic in the future.

Finally, this study can be extended to encompass different grid types, using real EVs, incorporating different chargers and adapting the latest communication protocols such as IEC/ISO 15118 and OCPP.

Smart charging algorithm advancement addressing experiment results and visioning implementations

This study significantly enhances the previously developed (in Ch. 6) smart charging (SC) algorithm SC-Alg in terms of both efficacy and viability. The enhancements to effectiveness include charging current command levelling for a steadier charging process, upgrading grid balancing services, and approaching optimality. The operative practices that are compressed into the new SC version including future charging event inclusion, ad-hoc admittance system for erratic charging events and self-correction of charging parameters. This work aims to prepare the SC algorithm for handling practical applications and real installations by improving its ability to process unpredictable events. This updated SC algorithm, namely SC-AlgS, is tested through simulations and assessed by comparing it to uncontrolled charging as well as a heuristic charging method — averaged charging method (ARM). The algorithm's capabilities, including charging cost reduction and contribution to grid balancing services, have been quantified. Its passive stochasticity management features have been validated through crosschecking among a large quantity of optimisation iterations. Additionally, the algorithm's proximity towards optimality and how to further increase it are discussed. The study results authenticate the advocated enhancements of the new SC version and demonstrate its improved performance and reliability.

7.1. Introduction

It is universally acknowledged that engaging EV smart charging is advantageous for accommodating massive EV connections to LV grids from multiple perspectives. However, transitioning from proof of concept to pilot demonstration is a long process, and it is vital to take into account implementational constraints at the early design stage.

Multiple pilot projects have successfully demonstrated the feasibility and functionalities of simple EV charging scheduling methods [68–70]. Expanding this initiative is crucial for the practical development and validation of smart EV charging algorithms. The algorithms need to accommodate diverse EV charging behaviours across various distribution grid topologies with contrasting innate characteristics. Additionally, they need to connect to different levels of baseload as well as renewable energy resources, such as wind and solar, while also being capable of handling energy price variability. [26, 134].

The realisation of a developed SC algorithm in the practical environment not only requires the adaptation of the effectuating constraints but also demands robustness towards the unpredictability in an operational environment. From the perspective of smart charging algorithm installation and exertion, there are two major factors which directly link to the EV charging process that alter the outcome of the algorithm.

The first one is if the charging event information shared with the SC algorithm matches the real situation. The information often covers EV specifications and charging event time frames. No matter how well-designed the SC algorithm is, its output is determined by the input. It is therefore essential to implement mechanisms that focus on filtering and correcting the input data. The possible approaches for SC algorithm are often either improving the algorithm's ability to forecast or enhancing the algorithm's uncertainty-coping functionality. For instance, measuring the elasticity in parking duration [204] and predicting the probability of a charging event's time and energy [205] can help to obtain refined input data. Or a stochastic model involved robust optimisation [206] to achieve a higher uncertainty resilience.

The second one is if the charging command is sent, received, and executed by the target EV on time with high precision; and then the EV's response and subsequent behaviour, which in turn affects the accuracy of the algorithm's outcome, falls within the algorithm's calculation. The command-conduct discrepancy could be rooted in the EV pre-installed charging strategies [80, 201] and the capacity shrinks and efficiency drops due to battery ageing [207]. It is discovered that EV fleet's literal response concerning alternative controls can inversely affect the system behaviour [208].

Furthermore, the compatibility of the developed algorithm with standards and protocols facilitating communication between the different parties influences the algorithm deployment potency. The three most relevant protocols for realising EV charging algorithms are the Open Charge Point Protocol (OCPP) for communication between the Charge Point Operator (CPO) and Electric Vehicle Supply Equipment (EVSE), and IEC/ISO 15118 and IEC 61851-1 for communication between EVSE and EV [209-211]. Using communication delay as an example. In real applications, chargers installed at different geographical locations or connected to different back-end offices may experience varying communication delays depending on the network and the engaged protocols. The message delivery timing requirements are not specified in OCPP since the communication timing strongly depends on the implemented network. The CPO is responsible for setting the timeout limit, and the guidance given by OCPP is 30 s [79]. When OCPP is employed in combination with ISO 15118, the time limit of charging profile delivery from CPO to EVSE is 60 s, and this is constrained by the EVSE to EV reply timeout indicated in ISO 15118 [79]. According to IEC 61851-1, EVSE has 10 s to adjust its PWM signal responding to an AC line current adjustment requirement posted by the grid, with manual settings or automatic calculations [45]. Regarding EVSE to EV communication delay, it is stated in both IEC 61851-1 and ISO 15118 that the EV has 5 s to respond to the given setpoint [45, 47]. The communication latency is eventually reflected in the charging outcome in the form of a mismatch between the charging setpoint and the actual charging current.

All the above-listed SC algorithm application difficulties, together with the identified deficiencies of the previous SC version SC-Alg, have motivated the upgrades of the algorithm to the new version – SC-AlgS, in this work. The primary upgrades can be briefly summar-

ised into three major parts and they are: A stochasticity processing system where unsure circumstances such as upcoming charging events, the mutable parking time span and charging energy requests, and the unplanned insertion/cancellation of charging sessions are treated dexterously. An error-correction service with which the disparity between the anticipated algorithm output and the EV response is rectified, thence the actual EV operation condition and the algorithm tracking system are synchronised. And lastly, an exercise aims to boost the algorithm's overall convergence to optimality. This article is organised as follows; Section 7.2 specifies the algorithm structure and the mathematical formulations, while Section 7.3 describes the operative qualities. The simulation setup and assumptions are provided in Section 7.4, and the results analyses as well as discussions are placed in Section 7.5. Finally, the conclusions and recommendations can be found in Section 7.6.

7.2. Algorithm mathematical build explained

The SC algorithm proposed in this study is a successor of an older version algorithm called SC-Alg from our previous work [212]. Several insufficiencies were observed in the antecedent version and thus the upgrades are solicited from this new version of the algorithm, namely SC-AlgS. Three major inadequacies are summarised below.

<u>Current setpoint and actual value disparity</u>: The most conspicuous phenomenon is the discrepancy between the current setpoint sent to the EV and the actual EV charging current. The current setpoint sent to the EV is merely the maximum allowed current draw from the EVSE while the actual charging current could be significantly lower than that. The origins of this charging current value difference are twofold: one is tied to the communication protocol attributes such as the minimal nonzero setpoint value, and the other one is how well the EV can or chooses to follow the setpoint.

<u>Current oscillation:</u> The second deficiency that appears in the charging current setpoint is high-frequency oscillation, especially crossing between zero and nonzero values. Not only does this oscillation impose strains on the physical relay in the charger, but it also breaks the continuity of the current setpoint, which prolongs the unnecessary response time and ramp-up/ramp-down periods on the EV side, leading to non-ideal performance.

<u>SoC and energy tracking inaccuracy:</u> The third leading potential upgrade is the SoC tracking function in the optimisation. Since the communication protocols between EVSE and EV do not support dynamic SoC value updates, the SoC estimation is internalised as a function in the algorithm. EV-related uncertainties like the unknown charging efficiency and battery state of health (SoH), plus the mismatch between setpoint and actual charging current, leading a high possibility of instigating inaccurate SoC tracking, which may fail the EV charging energy demand.

Moreover, the algorithm's competence in enduring the charging event unpredictability is indispensable. That is because no matter how superb the solution computed by the algorithm is, the adjustment of the EV charging session itself hazards the feasibility of the algorithm's outcome fundamentally. With the algorithm enhancement aspirations being precisely defined, the specifications of the SC-AlgS are explained in the following sections.

7.2.1. System structure

SC-AlgS inherits the hierarchical structure of the SC-Alg (in Section 6.2), which consists of one central and one distributed level as shown in Fig. 7.1. The central aggregator (Ctr-aggr) at the central level receives the grid condition information from the Distribu-

tion System Operator (DSO) and shares the limited grid capacity among the relevant subaggregators (Sub-aggrs). The Sub-aggr optimises the nodal energy usage and the EV charging strategy while taking the grid limitations sent by Ctr-aggr as constraints. The detailed system architecture and implemented protocols can be found in [212].

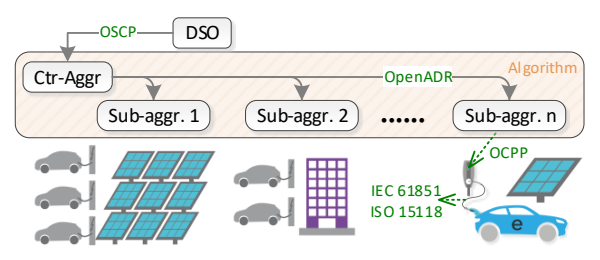


Figure 7.1: System structure

Ideally, the developed centralised congestion management algorithm, which is introduced in Chapter 5, can be incorporated in Ctr-aggr. Whereas this chapter focuses on the distributed level, a simple grid capacity division principle – which is to divide grid available capacity based on active connecting EVs – is used.

7.2.2. Smart charging algorithm

Objective function

Table 7.1: Parameters of objective functions

Parameter	Meaning
$C_n^{\mathrm{tot}} [\in]$	Total nodal costs at node <i>n</i>
B_{n,j,T_j^a} [kWh]	Energy in battery of EV j at node n upon arrival T_j^a
$B_{n,j,T_j^d}^{\mathrm{intl}}$ [kWh]	Energy in battery of EV j at node n when departure T_j^d , calculated from setpoint
$B_{n,j,T_j^d}^{\mathrm{UNC}}$ [kWh]	Energy in battery of EV j at node n when departure if uncontrolled charging policy applied
$C_{n,j}^{\mathrm{comp}} \left[\mathbb{\epsilon}/\mathrm{kWh} \right]$	Compensation for not meeting the energy demand of EV j at node n by departure
$p_{n,t}^{\mathrm{g(imp)}}, p_{n,t}^{\mathrm{g(exp)}}$ [kW]	Grid import/export power of node n at time t
$C_t^{\text{e(buy)}}, C_t^{\text{e(sell)}} [\text{€/kWh}]$	Electricity purchase/sell price at time t
$p_{n,t}^{\text{FCR,ava}} \text{ [kW]}$	Available power of node n at time t for providing FCR service
$C_t^{\text{FCR}}[\mathbf{\epsilon}/\text{kW}]$	FCR price at time t, up/down symmetrical, updates every 4 hours
$i_{n,j,t}^{\text{ramp}}$ [A]	Charging current ramp of EV j at node n between time $t-1$ and t

SC-AlgS has two objectives, one aims at minimising the total node cost C_n^{tot} while the second objective targets improving the continuity of the charging current setpoint and hence reducing its fluctuations. Two objectives can be found in Eq. (7.1) and (7.2) while the meanings of relevant parameters are listed in Table 7.1. Similar to the previous chapter, the target argument to this optimisation problem is the derived EV charging current $i_{n,i,t}^{\text{e+,intl}}$

(see detailed explanation in Section. 7.2.2).

The node cost listed in Eq. (7.1) consists of three parts:

- 1) the compensation cost that the Sub-aggr pays the EV user if the charging energy target is not met. The energy target is set to be the energy that would be provided to the EV if the uncontrolled charging (UNC) policy was applied $(B_{n,j,T_i^d}^{\mathrm{UNC}})$.
- 2) The net cost of the node buying/selling the electricity from/to the grid.
- 3) The extra income of the node providing ancillary service to the grid. Balancing servicing, especially Frequency Containment Reserve (FCR) service, is considered in this case.

In our previous research [212], the charging current setpoints are observed to oscillate significantly with high-frequency zero-nonzero switching, which burdens the mechanical relay in the charger. A supplementary condition is thence enclosed in SC-AlgS to moderate the current zero-nonzero fluctuation, such so the second objective is introduced. The second objective is simply to minimise the sum of every step's absolute charging current ramp value as shown in Eq. (7.2), and the current ramp value is defined in Eq. (7.5). This can help reduce the sudden change of the current, and therefore improve its continuity.

Obj.1: Min.
$$C_n^{\text{tot}} = \sum_{j=1}^{J} \left(B_{n,j,T_j^d}^{\text{UNC}} - B_{n,j,T_d^d}^{\text{intl}} \right) C_{n,j}^{\text{comp}} + \Delta T \sum_{t=1}^{T} \left(p_{n,t}^{\text{g(imp)}} C_t^{\text{e(buy)}} - p_{n,t}^{\text{g(exp)}} C_t^{\text{e(sell)}} \right) - \sum_{t=1}^{T} p_{n,t}^{\text{FCR},\text{ava}} C_t^{\text{FCR}}$$

$$(7.1)$$

Obj.2: Min.
$$\sum_{t=1}^{T} \sum_{j=1}^{J} \left| i_{n,j,t}^{\text{ramp}} \right|$$
 (7.2)

Constraints

The constraints-related parameters are summarised in Table 7.2.

Equations per EV

The two most commonly employed communication protocols between EVSE and EV that are considered in this study are IEC 61851 [45] and ISO 15118[46]. As elaborated in the previous chapter (Chapter 6), IEC 61851 specifies the minimal non-zero charging current setpoint that can be transmitted by Pulse Width Modulation (PWM) signals is 6 A. Although ISO 15118 supports high-level communication, it has the same basic signalling request as established in IEC 61851. Therefore, the charging current setpoint, which is the command value calculated by the algorithm, shall cap the 6 A as its minimal non-zero value, see the equation below.

$$\left(i_{n,j,t}^{\text{e+,cmd}} = 0\right) OR\left(i_{n,j,t}^{\text{e+,cmd}} \ge 6\right) \tag{7.3}$$

It is established in the former chapter that the current setpoint sent to the EV merely is the maximum allowed current draw from the EVSE while the actual EV charging current could be significantly lower than that. When a value difference is observed between the current setpoint and the measured charging current, this mismatch shall be counted in the optimisation to effectuate an anticipated outcome.

Therefore a dual charging ruling system — module command (cmd) and module internal (intl) — is introduced. Using charging current as an example, in this dual system, the command module is solely responsible for adjusting the current setpoint $(i_{n,j,t}^{e+,cmd})$ that is sent

Table 7.2: Parameters of constraints

Parameter	Meaning
$i_{n,j,t}^{\text{e+,cmd}}$ [A]	Charging current setpoint giving to EV j at time t and node n
$i_{n,j,t}^{\text{e+,intl}}$ [A]	Derived EV charging current <i>j</i> at time <i>t</i> and node <i>n</i>
$p_{n,j,t}^{\text{e+,intl}} [\text{kW}]$	Derived EV charging power of EV j at node n at time t
$B_{n,j,t}^{\text{intl}}$ [kWh]	Energy in battery of EV j at node n at time t
$S_{n,j,t}^{\text{intl}}$	SoC calculated from derived EV status j at node n at time t
$i_{n,j,t}^{\mathrm{e+,Act}}$ [A]	Actual charging current of EV <i>j</i> , node <i>n</i> , time <i>t</i>
$p_{n,j,t}^{\text{e+,Act}} \text{ [kW]}$	Actual charging power of EV j , node n , time t
$B_{n,j,t}^{\text{Act}}$ [kWh]	Actual battery energy of EV j , node n , time t
$S_{n,j,t}^{\mathrm{Act}}$	Actual SoC of EV <i>j</i> , node <i>n</i> , time <i>t</i>
$I_{n,j}^{\mathrm{EV}}\left[\mathrm{A}\right]$	Rated current of the EV <i>j</i> at node <i>n</i>
$\phi_{n,j}^{\mathrm{EV}}$	Number of EV charging phases
$B_{n,j}^{\max}$ [kWh]	Usable battery size of EV j at node n
$S_{n,j}^{\mathrm{CV}}$	SoC switch point between CC and CV stage of EV j at node n
$\eta_{n,j}^{ ext{EV}}$	On-board charger efficiency of EV <i>j</i> at node <i>n</i>
$\eta_{n,j}^{ ext{EVSE}}$	Efficiency of charger j at node n
$I_{n,j}^{\text{EVSE}}$ [A]	Rated current of the charger EV j plugged in at node n
$p_{n,t}^{\text{PV,Fcst}}$ [kW]	Forecast PV generation power at node <i>n</i> at time <i>t</i>
$p_{n,t}^{\text{LL,Fcst}}$ [kW]	Forecast local load power at node <i>n</i> at time <i>t</i>
$E_n^{\rm LL,r}$ [kWh/yr]	Yearly energy consumption of local load
$v_{n,t}$ [V]	Voltage of node <i>n</i> at time <i>t</i>
$p_{n,t}^{\text{FCR(up)}}, p_{n,t}^{\text{FCR(dn)}}$	Available up/down FCR service power of node n at time t ;
[kW]	Also uniformly denoted as $p_{n,t}^{\text{FCR,ava}}$ thanks to symmetry
$p_{n,t}^{G+}, p_{n,t}^{G-}$ [kW]	Distribution network capacity for importing/exporting power from grid at node <i>n</i>
p ^{Glim} [kW]	Overall grid capacity
$J_{n,t}^{\mathrm{cnt}}$	Number of connecting EVs of node <i>n</i> at time <i>t</i>

to the EV, adding the offset value $(i_{n,j,t}^{\rm offset})$ calculated from the historical and measured disparities. The internal module, on the other hand, reads the measured EV's actual charging information $(i_{n,j,t}^{\rm e+,Act})$ and derives the EV's actual charging status $(i_{n,j,t}^{\rm e+,intl})$ in the optimisation. Besides, it is found that the constant-current-constant-voltage (CC-CV) charging strategy is commonly implemented in AC charging [104], the CC-CV charging method is thus adapted in the internal module. The derived EV actual charging current in the internal module $i_{n,j,t}^{\rm e+,intl}$ is constrained by both the current setpoint command $i_{n,j,t}^{\rm e+,cmd}$ considering the offset value $(i_{n,j,t}^{\rm offset})$, as well as the natural CV-stage current descending, as stated in the equation below.

$$i_{n,j,t}^{\text{e+,intl}} = \begin{cases} i_{n,j,t}^{\text{e+,cmd}} - i_{n,j,t}^{\text{offset}}, & \text{SoC} < S_{n,j}^{\text{CV}} \\ I_{n,j}^{\text{EV}} \times \frac{(1 - S_{n,j,t}^{\text{intl}})}{1 - S_{n,j}^{\text{CV}}}, & \text{SoC} \ge S_{n,j}^{\text{CV}} \end{cases}$$
(7.4)

The current ramp is calculated from the derived EV status in the optimisation, by the internal module, as shown in Eq. (7.5).

$$i_{n,j,t}^{\text{ramp}} = i_{n,j,t}^{\text{e+, intl}} - i_{n,j,t-1}^{\text{e+, intl}}$$
 (7.5)

The EV charging power, EV battery energy and its dynamic SoC calculations are listed below.

$$p_{n,j,t}^{\text{e+,intl}} = v_{n,t} \times \phi_{n,j}^{\text{EV}} \times i_{n,j,t}^{\text{e+,intl}}$$
 (7.6)

$$B_{n,j,t}^{\mathrm{intl}} = B_{n,j,T_j^a} + \Delta T \sum_{T_i^a}^t \left(p_{n,j,t}^{\mathrm{e+,intl}} \times \eta_{n,j}^{\mathrm{EV}} \right)$$
 (7.7)

$$S_{n,j,t}^{\text{intl}} = \frac{B_{n,j,t}^{\text{intl}}}{B_{n,i}^{\max}}$$
(7.8)

Node level equations

Same as in SC-Alg, the node power exchange with the grid, including both the import and export parts, is defined in the equations below.

$$p_{n,t}^{\text{exch}} = \sum_{j=1}^{J} \left(p_{n,j,t}^{\text{e+,intl}} / \eta_{n,j,t}^{\text{EVSE}} \right) + p_{n,t}^{\text{LL,Fcst}} - p_{n,t}^{\text{PV,Fcst}}$$
(7.9)

$$p_{n,t}^{\text{g(imp)}} = \left\{ p_{n,t}^{\text{exch}} \middle| p_{n,t}^{\text{exch}} \ge 0 \right\}$$

$$p_{n,t}^{\text{g(exp)}} = -1 * \left\{ p_{n,t}^{\text{exch}} \middle| p_{n,t}^{\text{exch}} < 0 \right\}$$
(7.10)

Providing FCR service through EV charging is explored in SC-AlgS, and thence are the new constraints added.

It is requested that the offered FCR power up and down be symmetrical, that means the offered source has to be able to regulate the same amount of power in both directions or able to increase and decrease the same power level during the contracted periods [213].

In this research, the sum of available storage devices in each node — all active EVs in this case — is viewed as one combined unit of flexible power source for the FCR service. The available FCR capacity of an individual EVSE and its connected EV is constrained by the active charging power and the power upper limit of both the EVSE and EV as illustrated in Fig. 7.2. On top of that, the maximum node available FCR power is delimited by the sum of each EVSE & EV combination's FCR capacity, as formulated in Eq. (7.12).

$$p_{n,t}^{\text{FCR}(\text{dn})} = p_{n,t}^{\text{FCR}(\text{up})} \ge 0 \tag{7.11}$$

$$\begin{aligned} p_{n,t}^{\text{FCR}(\text{dn})} &\leq \sum_{j=1}^{J} \left(\text{Min.}(p_{n,j,t}^{\text{e+,max}}, p_{n,j}^{\text{EVSE,max}}) - p_{n,j,t}^{\text{e+,intl}} \right) / \eta_{n,j}^{\text{EVSE}} \\ p_{n,t}^{\text{FCR}(\text{up})} &\leq \sum_{j=1}^{J} p_{n,j,t}^{\text{e+,intl}} / \eta_{n,j}^{\text{EVSE}} \end{aligned} \tag{7.12}$$

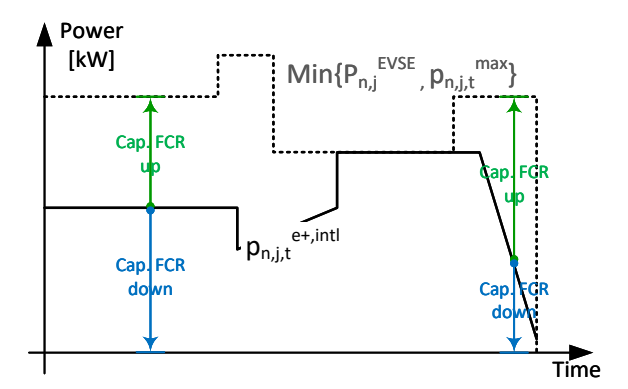


Figure 7.2: Maximum FCR capacity of individual EVSE and its connected EV

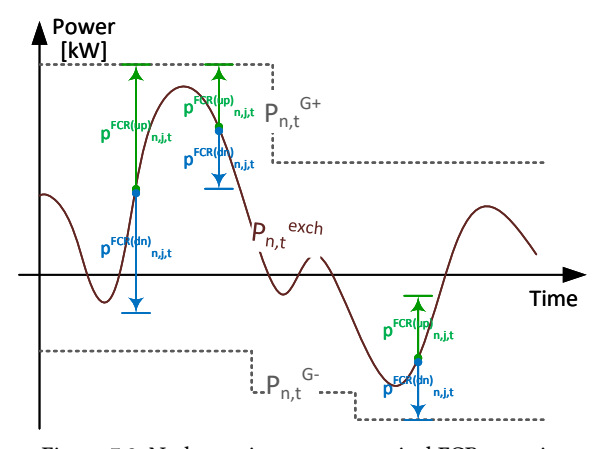


Figure 7.3: Node maximum symmetrical FCR capacity

The available FCR power of each node shall remain within the grid connection power limit, as well as have to be symmetrical. Hence the available capacity is bounded by the tighter limit between the import and export power limit, as shown in Fig. 7.3 and explicated in Eq. (7.13). This available node FCR power value is uniformly denoted as $p_{n,t}^{\rm FCR,ava}$ for simplification, as used in Eq. (7.1).

$$\begin{array}{l} p_{n,t}^{\rm g(imp)} + p_{n,t}^{\rm FCR(dn)} \leq p_{n,t}^{\rm G+} \\ p_{n,t}^{\rm g(exp)} - p_{n,t}^{\rm FCR(up)} \leq p_{n,t}^{\rm G-} \end{array} \tag{7.13}$$

Lastly, the overall grid capacity p^{Glim} is dispensed to each node for EV charging using the ratio of connecting EV numbers per node $J_{n,t}^{\text{cnt}}$.

$$p_{n,t}^{G+} = \frac{J_{n,t}^{\text{cnt}}}{\sum_{n=1}^{N} J_{n,t}^{\text{cnt}}} \times p^{\text{Glim}}$$
 (7.14)

7.3. Algorithm implementational practice

7.3.1. Future EV inclusion

In SC-Alg, the flexible receding horizon (FRH) scheme was introduced, with which the optimisation horizon is set and is restricted by the latest departure EV among all connecting EVs. Whenever the (re-)optimisation is triggered, the optimisation horizon is updated automatically. In SC-Alg, the potential future arrival EVs are not considered, which may cause essential information missing. The Sub-aggr is responsible for acquiring the energy in the most economical and efficient way, and then splitting the finite resources like energy and power strategically and fairly to the local loads, as well as among all active EVs. Any upcoming EV means future energy and power demand; therefore, as early as possible pre-announcement of future arrival provides valuable information and grants extra time for the Sub-aggr to adjust the charging agenda. Pre-registration is also beneficial for EV users, since it can help secure a charger instead of risking queuing for an available charger when the user comes to the site spontaneously.

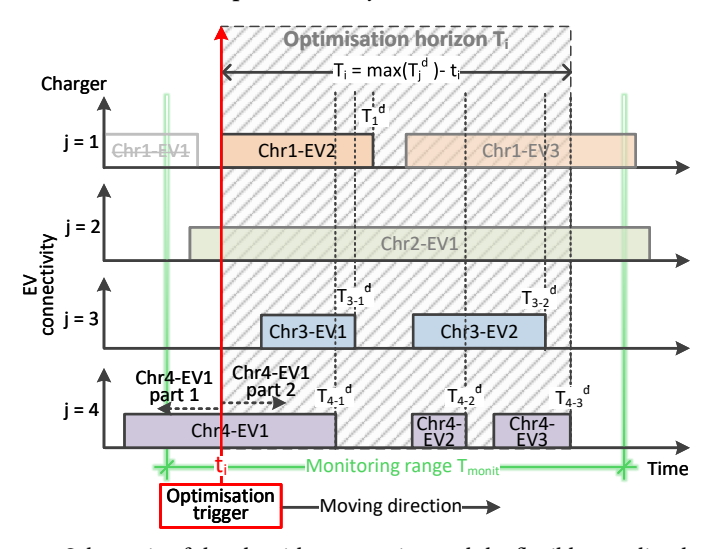


Figure 7.4: Schematic of the algorithm execution and the flexible receding horizon

Expanding on SC-Alg, a near-future involved flexible receding horizon (f-FRH) scheme is introduced and its illustration is shown in Fig. 7.4. To let the upcoming EVs notify their arrival to the Sub-aggr, the EV charging pre-registration function is enabled. The planned EVs are requested to inform the Sub-aggr of the EV model information, including the EV battery size and rated charging power, and the estimated time of arrival/departure. Pre-registration is not mandatory, non-registered EVs can initiate their charging session as usual and their charging session information is uploaded to the system upon arrival.

In Fig. 7.4, four chargers are represented by four coordinates respectively, the blocks on them symbolise the EVs connected to the corresponding chargers, and the length of each block specifies the parking duration of each EV. The f-FRH is basically the same as the FRH of the SC-Alg in which the optimisation horizon is regularly updated with the latest departure EV settles the horizon window. The difference is that future arrival EVs are

included in f-FRH. However, not all EVs that are in the system — consisting of connected EVs and pre-registered future arrival EVs — are considered admissible for optimisation. That is mainly because the long-term parking EVs, especially the future arrival ones, tend to have a distant-future departure time, which may result in an extensively prolonged optimisation horizon. As a result, a monitoring range for f-FRH ($T_{\rm monit}$) is set to confine the involved EVs, so that any EV departs later than the monitoring range is not considered in the pending optimisation. For example, the glow green frame in Fig. 7.4 outlines the monitoring range and all coloured blocks depict the EVs registered in the system. Among all the registered EVs, the planned departure time of Chr-EV3 and Chr2-EV1 are out of the monitoring range, and so they are exempted from being included in the optimisation triggered at time t_i . The horizon window is then set to end by the planned departure of Ch4-EV3.

7.3.2. Passive stochasticity coping mechanism

The f-FRH is particularly reliable in handling stochasticity dynamically. The re-optimisation triggering events that are comprised in SC-AlgS are: EV fleet reformation & charging session alterations like EV insert/removal, EV arrival/parking time modification, SC participation revisit etc.; charging power and SoC synchronisation; and grid power constraints shift. The uncertainties that are initiated by the charging events and present throughout the charging processes are explicated in detail in this section.

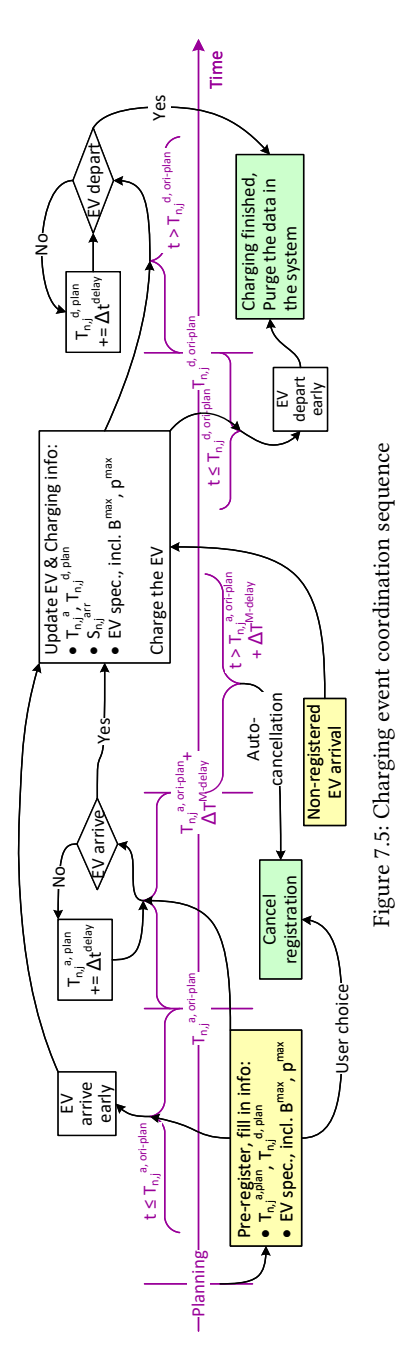
Erratic charging events coordination

Although EV pre-registration function grants the early acquisition of future EV charging demand information, it inevitably draws more uncertainties in the meantime, especially those related to EV charging behaviours, like EV arrival/departure time, EV arrival SoC and EV specifications. Constructively, the charging session information is updated to the Sub-aggr in the same manner when the EV actually arrives, whether an arrival EV is pre-registered or not. After the charging session is successfully authenticated upon plug-in, the precise EV specifications are assumed to be identified by the back-end office together with their EV ID in the Session Setup stage of the Communication Setup Sequence; whilst the charging process parameters, such as the power range, nominal voltage, energy demand, departure time and so on, are transmitted during the Charge Parameter Discovery stage of the Target Setting and Charge Scheduling sequence [47].

A charging event coordinator is equipped and responsible for sorting arbitrary charging events and accommodating the charging request as much as possible. It is assumed that the charger availability information is synchronised and visible to the users in the registration system, and there is extra buffer time added upon registration for slight early or late arrival/departure between two consecutive charging slots.

The charging event coordinator working sequence is displayed in Fig. 7.5. As high-lighted in yellow boxes, EV users can choose to pre-register or come to the charging station straight away. On the other hand, the charging session could conclude in either cancellation or charging completion.

1. When the user pre-registers its EV charging session in the system, the EV model, planned arrival $(T_{n,j}^{a, \text{ ori-plan}})$ and departure time $(T_{n,j}^{d, \text{ ori-plan}})$ are requested. The SC-AlgS uses the information in the optimisation to alter the currently active sessions, as well as pre-plan the upcoming charging sessions.



2. EV user can cancel its pre-registered charging session at any time prior $T_{n,j}^{a, \text{ ori-plan}}$, this charging session data will be erased from the system.

^{3.} When the EV arrives, the actual arrival time, arrival EV SoC, accurate EV model data and other information the user wishes to change or add, like planned departure time,

energy demand etc, are updated in the system. Then the charging session starts.

- 4. If the EV has not arrived passed the $T_{n,j}^{\rm a,\, ori-plan}$, the system will add a small amount of delay time ($\Delta t^{\rm delay}$) to the originally planned arrival time ($T_{n,j}^{\rm a,\, ori-plan}$). However, the system would only hold the planned charging session for a fixed amount of time $\Delta T^{\rm hold}$, if the planned EV still has not come when the holding time passed, this planned session will be automatically aborted.
- 5. For the unplanned EV charging event, the same procedure happens as stated in step 3 above.
- 6. When EV departs, its actual departure time updates in the system and one round of optimisation is triggered if needed. The rest information regarding this charging session is moved to the archive.
- 7. If the EV is still connected after $T_{n,j}^{\rm d,\, ori-plan}$, the system will add the delay time $\Delta t^{\rm delay}$ in a fixed frequency continuously until the EV eventually leave. There is no maximum overtime post the originally planned departure moment because the charging session termination is initiated by the EV, and physical removal of the plug is necessary for the charger to be available again.

Self-correction in charging processes

As briefly described at the beginning of Section 7.2, two deficiencies of SC-Alg hinder its performance: the current setpoint - actual value discrepancy and the SoC tracking inaccuracy. A self-correction function is embedded in SC-AlgS taking the form of feedback loops. Two values are monitored and regularly rectified, the charging current $(i_{n,j,t}^{e+, \text{ intl}})$ and the EV charging efficiency $(\eta_{n,j,t}^{EV, \text{ intl}})$, matching the two above-mentioned deficiencies respectively. The SC-AlgS's dual charging ruling system which is explained in Section 7.2.2 is the pillar of the self-correction function. How is the self-correction carried out through this system is illustrated in Fig. 7.6.

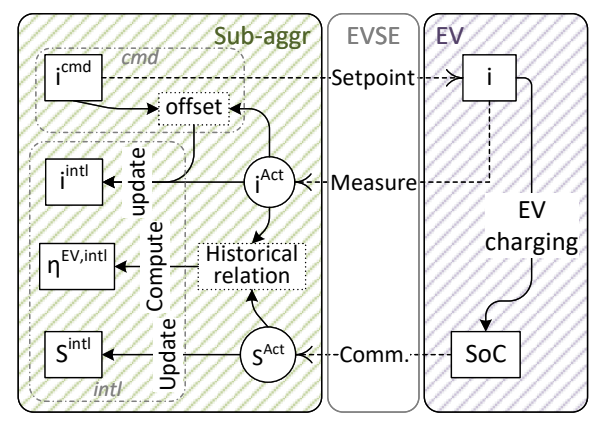


Figure 7.6: The self-correction carried out by the command and internal module of the dual charging ruling system in the optimisation

During active charging sessions, the actual charging current $(i_{n,j,t}^{e+, Act})$ and power $(p_{n,j,t}^{e+, Act})$ are measured and sent to the Sub-aggr by the charger. Since the dynamic SoC value ex-

change during AC charge is not supported by protocol ISO 15118, the actual battery SoC $(S_{n,j,t}^{\mathrm{EV},\,\mathrm{Act}})$ is assumed to be communicated from EV to the Sub-aggr directly instead. This function requests the EV OEM's collaboration. When the value difference between the actual charging status and the derived EV status in the internal module is higher than a pre-set threshold, the value discrepancies during a fixed historical period ($\Delta T^{\mathrm{trace}}$) are calculated and compensated.

For the charging current, the offset value is simply the mean value of the charging command minus the actual charging current, as listed in Eq. (7.15).

$$i_{n,j,t}^{\text{EV, offset}} = \frac{\sum_{t}^{t+\Delta T^{\text{trace}}} (i_{n,j,t}^{\text{e+, cmd}} - i_{n,j,t}^{\text{e+, Act}})}{\Delta T^{\text{trace}}/\Delta t}$$
(7.15)

The EV charging efficiency is computed from the charged energy (through the SoC value given by the EV) and the measured charging power, as shown in Eq. (7.16).

$$\eta_{n,j,t}^{\text{EV, intl}} = \frac{\left(S_{n,j,t+\Delta T^{\text{trace}}}^{\text{EV, Act}} - S_{n,j,t}^{\text{EV, Act}}\right) \times B_{n,j}^{\text{EV}}}{\Delta T^{\text{trace}}} \\
\div \frac{\sum_{t}^{t+\Delta T^{\text{trace}}} p_{n,j,t}^{\text{e+,Act}}}{\Delta T^{\text{trace}}/\Delta t} \tag{7.16}$$

7.4. Simulation setup, input data and assumptions

The verification and evaluation of the SC-AlgS are actualised through computer simulations on an LV microgrid consisting of three nodes. Each node in this microgrid has one local entity (Sub-aggr) that implements the SC-AlgS, and on top of that, a Ctr-aggr is responsible for coordinating the grid capacity distribution among these three nodes.

Besides the upgraded SC algorithm SC-AlgS, two other benchmark charging strategies that are used to set EV maximum charging current are simulated: uncontrolled charging (UNC), which is to commence the charging as early as possible with the highest available power; and the average-rate charging scheme (ARM), where the charging session eventuates with the lowest possible power aiming at spread the charging process throughout the whole parking duration as much as possible. The detailed description of ARM can be found in our previous work [202]. CC-CV charging strategies are applied in all three methods for a fair comparison base.

Although the algorithm's passive stochasticity coping mechanism can process uncertainties originated from charging events, the reliability of the system and its components is not deliberated in this thesis. It is assumed that the tested power system, its components, as well as the measurements and communication devices interfacing among system components function properly throughout the simulation period.

Charging events data and assumptions

The EV charging events data is generated with the upgraded method originally introduced in our previous work [134, 202], and based on the Dutch market data [214] combined with large-scale actual EV charging database [215]. To explore if and how the effectiveness of SC-AlgS varies with different charging behaviours, each node has one dedicated charging event type taking place, namely Home, Semi-public and Public respectively. Several

random events like cancelling charging reservations, delayed arrival/departure, no-shows, and arrive without reservation are arbitrarily scattered and placed in the EV charging sessions. Besides, not all charging sessions are marked as SC participants, and this is to mimic real applications when the users choose not to join SC. In this simulation, EV charging sessions with short parking duration and low arrival SoC are automatically marked as not joining SC. The major configuration of input uncertain charging events for SC-AlgS testings are summarised in Table 7.3. The values in this table are selected solely for the purpose of functionality validation and thus do not represent any real-world applications nor carry any specific meaning.

% Sessions on time	Erratic charging events distribution	User SC preferences		Max. reserving time for late Arr. sessions
80%	7.5% Cancellation 7.5% ad-hoc admittance 5% no-show	25% sessions no SC	24 [h]	60 [min]

Table 7.3: Charging events stochasticity settings

Referring to studies which investigate charging session efficiencies [216, 217], for instance, the charging event energy/power loss, charger and EV components efficiency under different conditions like charging power, environmental temperature, AC/DC charging, if bi-directional charging is involved etc. It is assumed in this study that both EVSE and EV onboard charger' efficiencies are randomly dispersed between the range 90-99% in normal distribution.

Input profiles

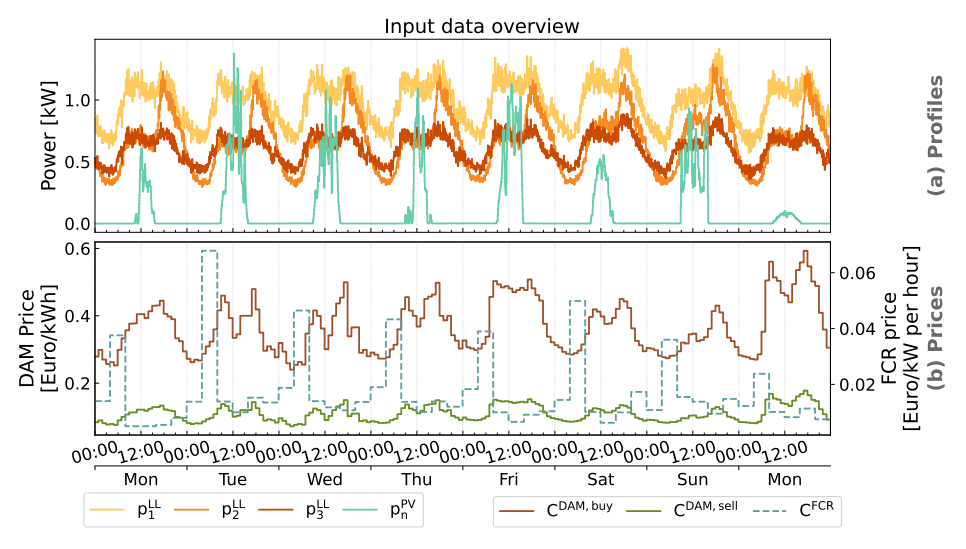


Figure 7.7: Simulation input data

The PV profiles are derived from the measurement of a Dutch PV site's generation [218]

while the load profiles are modified from the Dutch standard load profile [219]. The Dutch Day-Ahead Market electricity price is employed as the electricity buying price and the selling price is set to be 30 % of the buying price. Both the DAM price and the FCR price are available via the open pan-European electricity market platform ENTSO-E [220]. Grid impact and performance analysis are not the focus of this study, hence no grid load flow analysis is involved. From the previous chapter (Chapter 6), we demonstrate that the uncertainty of PV and load profiles have relatively the least impact on the SC outcomes in comparison to other stochasticities. Besides, this work focuses on EV charging rather than the local energy system optimisation, plus the local loads are assumed to be non-flexible, the PV and Load profiles are hence treated as simple input base data. Thereby, a small magnitude of PV and load profiles are added for demonstration purposes. The input data summary is listed in Table 7.4 and the nodal input profiles together with the global price information are presented in Fig. 7.7.

From this figure, it can be easily seen that every day from 21:00 till the next day 8:00 is often a good time to charge the EV due to low electricity price, low load demand and high FCR price. The second suitable moment for charging the EV is between 11:00 and 13:00 daily, thanks to the peak PV generation and a slight dip in the electricity price as well as the local load.

Table 7.4: Simulation settings

Node	Num. EVSE	Charging event type	PV Inst. [kWp]	Load Consum. [kWh/yr]	
none1	3	Home	10	8000	
node2	5	Semi-public	12.5	5000	
node3	3	Public	12.5	8000	

Grid connection limitation

Impor	Two times $3 \times 60A$ connections	
Export	Two times $3 \times 16A$ connections	

Simulation time setting

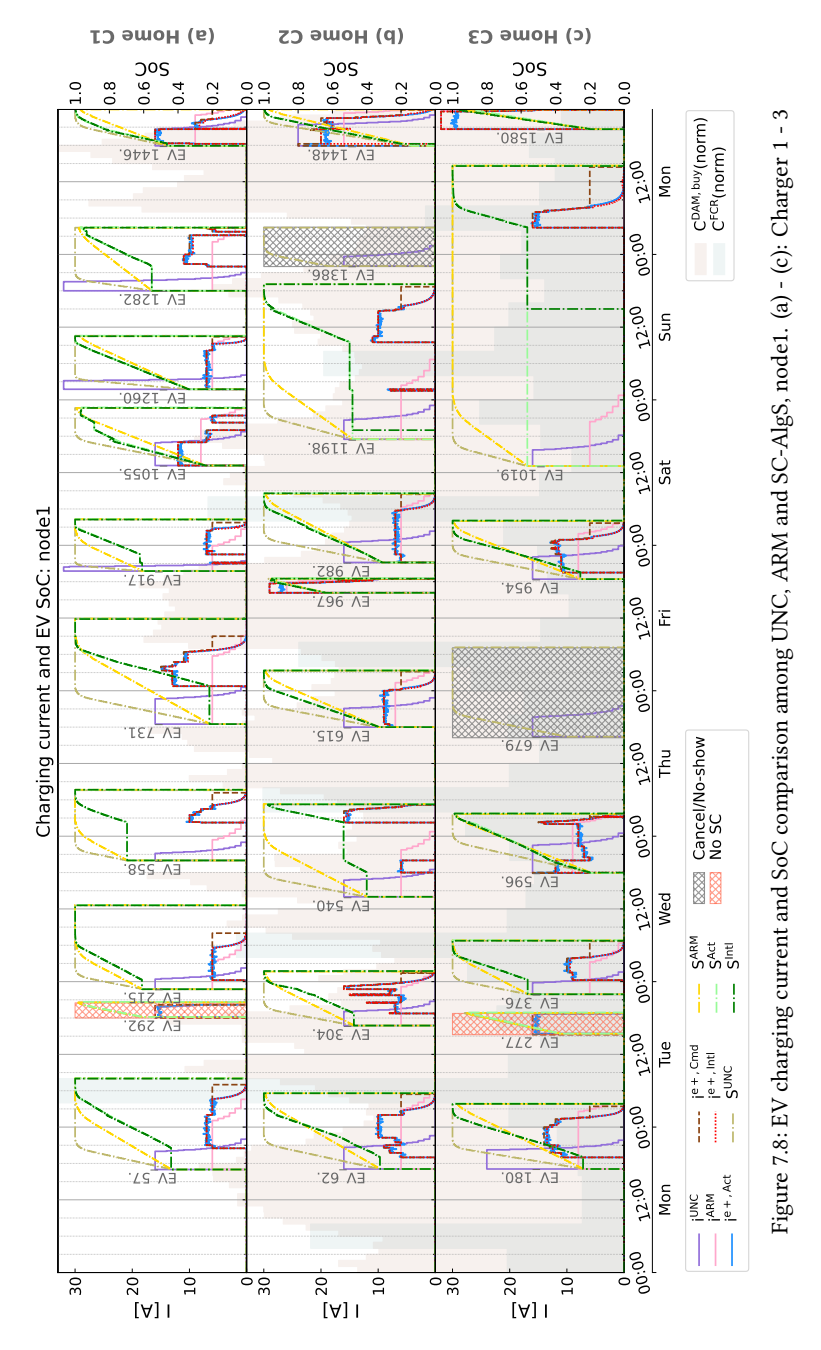
Season	Winter
Duration	Eight days (Mon — Mon)

7.5. Results

7.5.1. Smart charging performance evaluation

Overall performance

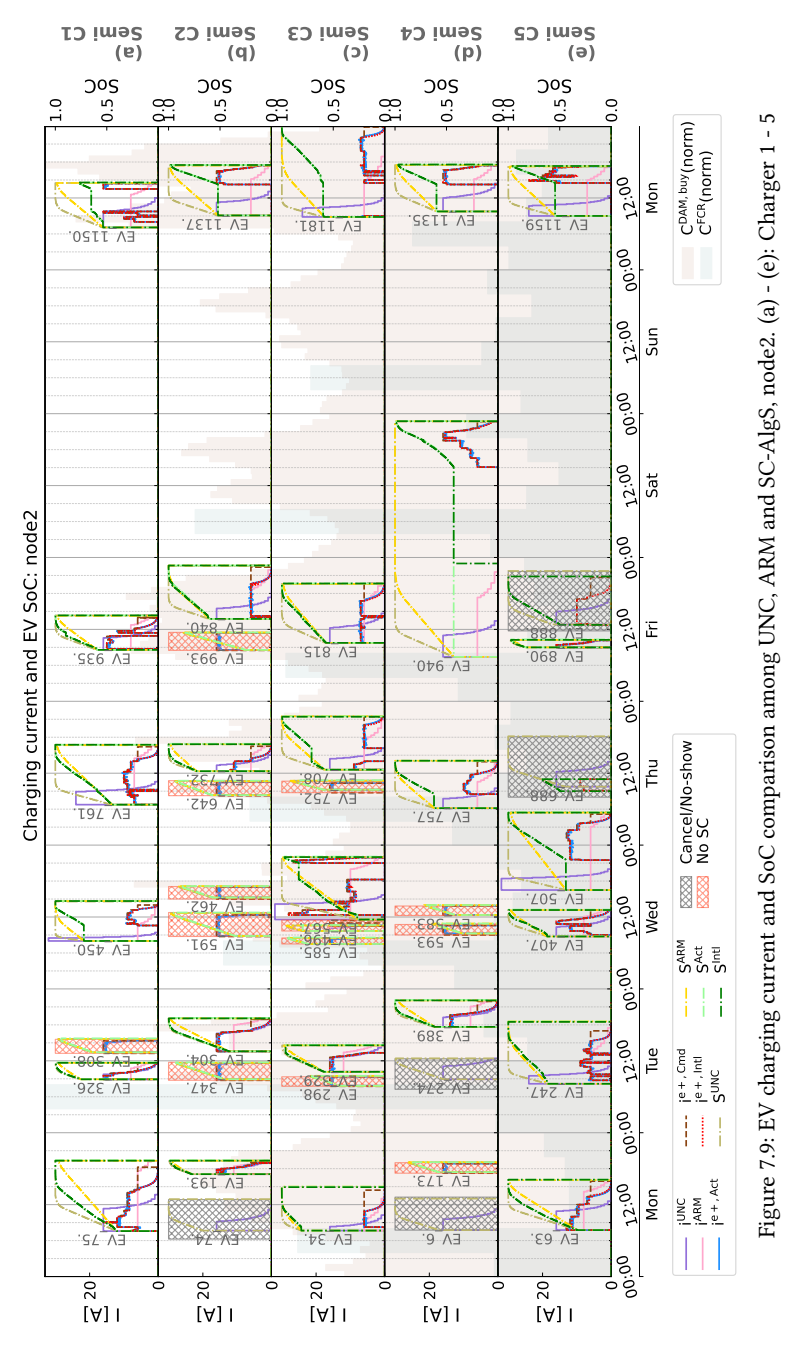
The charging current and corresponding EV SoC values of the EV charging events that occur in node1, using three charging methods respectively, are illustrated in Fig. 7.8. Note that three charging current and SoC simulation results obtained from three sub-systems (Command - cmd; Internal - intl, and the emulated actual EV behaviours - Act, as explained in Section 7.3) are all plotted in this figure, and the actual EV charging profiles are used for the following evaluation. The normalised electricity price C^{DAM} , buy and FCR price C^{FCR} are placed in the background for reference. Cancelled or no-show charging events



are crossed out with grey meshed blocks, and the charging events in which the smart charging is not applied (UNC policy instead) are marked with red meshed blocks.

SC-AlgS computed charging profiles

It is clearly shown in this plot that SC-AlgS shifts the charging moment towards when



 $C^{\mathrm{DAM,\,buy}}$ is low and the C^{FCR} is high within the EV connection window, in most of the charging events with some exceptions present. Besides, the charging current setpoint of the majority of charging sessions is observed to maintain a notably lower value than their rated current value. This phenomenon is by reason of two key factors, and the first one

is related to FCR service providing. The offered FCR product is requested to be symmetrical, meaning the FCR service engaged EV ought to retain its charging current within the power range of zero to rated power, allowing both power increase (regulate down) and decrease (regulate up). The closer the charging current is to half of the rated power, the higher FCR capacity the EV can offer. Further elaboration on the FCR service pertained results is provided in the subsequent context. Secondly, the optimisation encompasses two objectives as detailed in Section 7.2.2, one of which focuses on minimising the charging current ramp value to ensure a stable charging process (Eq. (7.2)). Given the CC-CV charging strategy, where the charging current gradually descends to 0 as SoC approaches 1 is implemented, a smaller charging current value is preferable for the purpose of minimising current ramp value.

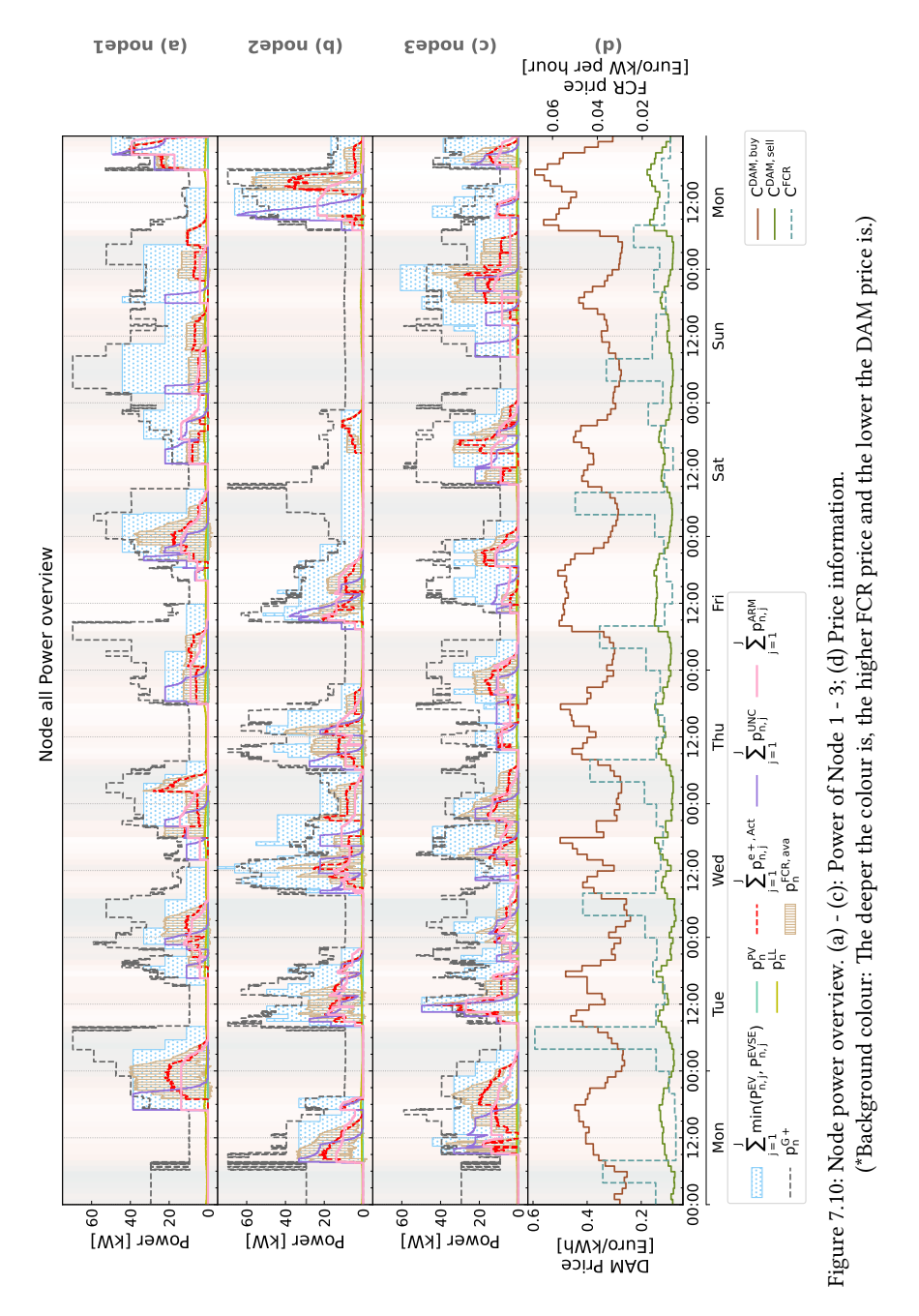
Examine sub-optimal outcomes

The MIP optimisation performance determines how well the charging schedule is computed. Take the charging event of EV 940 occurs around Fri 12:00 to Sat 23:00 at charger Semi C4 as an example (Fig. 7.9 (d)). Since no other charging events are present at the node during this time window, it is reasonable to conclude that the best charging moment for this event would be 0:00-8:00 instead of the current appointed time window of 15:00-21:00. Upon the inclusion of EV 940 to the smart charging monitoring range, which is 24 hours prior to its departure as introduced in Section 7.3, the optimisation triggers for the first time. However, this round of MIP calculation fails to identify the optimal option through branch and bound searching before reaching the time limit, resulting in a 22.08% MIP gap. Furthermore, the re-optimisation trigger conditions, including EV fleet change, charging current/power/SoC correction, and grid limit updates, are not activated during this charging event, resulting in the suboptimal outcome for this charging session.

Even when multiple opportunities for re-optimisation do arise during charging sessions, there still remain possibilities that these opportunities emerge too late or the obtainment of the optimal results is too late, such as after the most appealing price window has passed, thereby limiting the MIP procedure's ability to enhance the outcome. Charging events that take place at node2 on the 2nd Monday set a befitting example (Fig. 7.9). EVs that are connected to charger Semi C1&2, 4&5 share similar parking duration, roughly between 9:00 and 18:00, with the most economical charging time for these four EVs being around 11:00 - 14:00. Nonetheless, it is not until the 2nd Mon 15:00 does the MIP optimisation converges within the time limit. By then, the EV connected to Semi C1 has departed while the preferable charging moment for EVs that connected to Semi C2, C4 &C5 has already passed. Hence, securing the optimal result at the outset is of utmost importance, considering the timeliness nature of approximating optimality in this case.

Benchmark SC-AlgS with UNC and ARM

The overview of all power in each node is placed in Fig. 7.10 to illustrate the overall performance of three tested charging methods from the node level. Note here that the sum of EV charging power does not include the events where the user chooses not to be included in SC. In this figure, the EV charging power of three methods alongside the offered FCR power computed by SC-AlgS are presented. On top of that, the sum of rated power across the EV's parking duration $\sum_{j=1}^{J} \min(p_{n,j}^{\rm EV}, p_{n,j}^{\rm EVSE})$ as well as the grid import power limit $p_n^{\rm G+}$ are displayed denoting the power constraints from both the EV connection time and the grid point of view. This plot highlights that ARM substantially flattened and



smoothed the charging curve while the SC-AlgS shifts the charging time and peak power towards the price-favourable period (indicated by the colour shade) in comparison to the UNC method. Besides, charging sessions with UNC sometimes exceed the grid power limit while those sessions that are managed by ARM or SC-AlgS never breach this constraint.

Yet, the power curves of ARM and SC-AlgS do not exhibit significant differences, especially in node2 and node3, due to the characteristics of their charging event types. Charging events in node2 (Semi-public) and node3 (Public) typically span across the daytime or have very short parking continuations, leaving limited room for the algorithm to adjust the power allocations.

User experience

After the general performance of SC-AlgS is assessed, its capability to gratify the interest of potential users is numerically analysed in detail here. The first thing to be addressed is the charging related costs, as node cost reduction comprises a significant element of the objective function.

$$C_{k,\text{norm}}^{X} = \frac{C_{k}^{X}/C_{k}^{\text{UNC}}}{E_{k}^{X}/E_{k}^{\text{UNC}}}, \text{ where } X = \text{ARM or SC}$$
 (7.17)

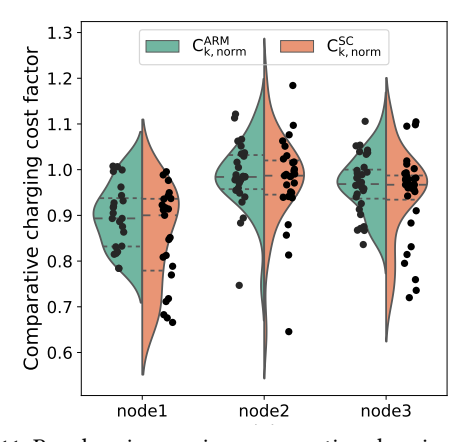


Figure 7.11: Per charging session comparative charging cost factor

It is established that the upper limit of the charging current is given by the three charging methods while the EV charging follows the CC-CV charging strategy, resulting in disparities in actual delivered energies thanks to the divergent CV stages. Hence, the comparative charging cost factor ($C_{k,norm}^{X}$) is employed to eliminate the discrepancy in delivered energy for a fair evaluation as introduced in our previous research [202]. Each charging session's comparative charging cost factor of ARM and SC-AlgS, which is denoted by the fraction of the charging cost ratio and the actual charged energy ratio relative to UNC, as formulated in Eq. (7.17), is computed and depicted in Fig. 7.11.

This plot displays that aside from sessions where SC shows superior performs like the ones in node1 and partially in node3, the rest of them share similar factor values between ARM and SC. The underlying reason for this phenomenon mentioned in the previous section is that Semi-public and Public charging sessions take place in these two nodes, and these types of events usually have short parking duration, or the parking time coincides when the electricity reaches its peak of the day. These features confine the operable range of the SC for improving the charging cost reduction.

Node	$\begin{bmatrix} \overline{C}_{k, \text{ p.u.}}^{\text{UN}} \\ [\ell/kWh] \end{bmatrix}$	$\frac{\overline{C}_{k,\mathrm{p.u.}}^{\mathrm{ARM}}}{[\epsilon/\mathrm{kWh}]}$	$\frac{\overline{C}_{k, p.u.}^{SC}}{[\epsilon/kWh]}$	$r\overline{C}_{ m k, p.u.}^{ m ARM}$	$r\overline{C}_{ m k, p.u.}^{ m SC}$	$C_{\mathrm{n}}^{\mathrm{tot,UN}}$ $[\mathfrak{E}]$	$C_{\mathrm{n}}^{\mathrm{tot,ARM}}$ $[\mathbf{\epsilon}]$	$C_{\mathrm{n}}^{\mathrm{tot,SC}}$ $[\mathbf{\epsilon}]$	$rC_{ m n}^{ m tot,ARM}$	$rC_n^{\text{tot, SC}}$
node1	0.425	0.380	0.361	10.65%	14.98%	462.42	420.81	406.40	9.00%	12.12%
node2	0.468	0.459	0.455	1.82%	2.73%	499.33	488.31	467.35	2.21%	6.41%
node3	0.430	0.414	0.404	3.74%	6.08%	591.70	573.12	549.14	3.14%	7.19%

Table 7.5: Charging and node cost comparison

The average per unit charging cost as well as the sum of node cost of the whole simulation period are summarised in Table 7.5. The total node cost consists of EV charging cost and grid power exchange net cost; the FCR service offer calculation and evaluation are discussed in the following section. The delivered energy by SC-AlgS is, on average, 8.61% less than the energy delivered by UNC, and this value is 8.98% for ARM. Charging scheduling achieves the most effectiveness in node1, at which the home charging events transpire. Not only do the per unit charging costs decrease the most (10.65% by ARM, 14.98% by SC) at node1, but also the delivered energy has the smallest gap relative to UNC, which is 3.18% and 4.38% for ARM, SC-AlgS respectively. Although the total node cost is reduced by employing ARM and SC-AlgS, a small part of it is actually from the delivered energy gap in comparison to UNC.

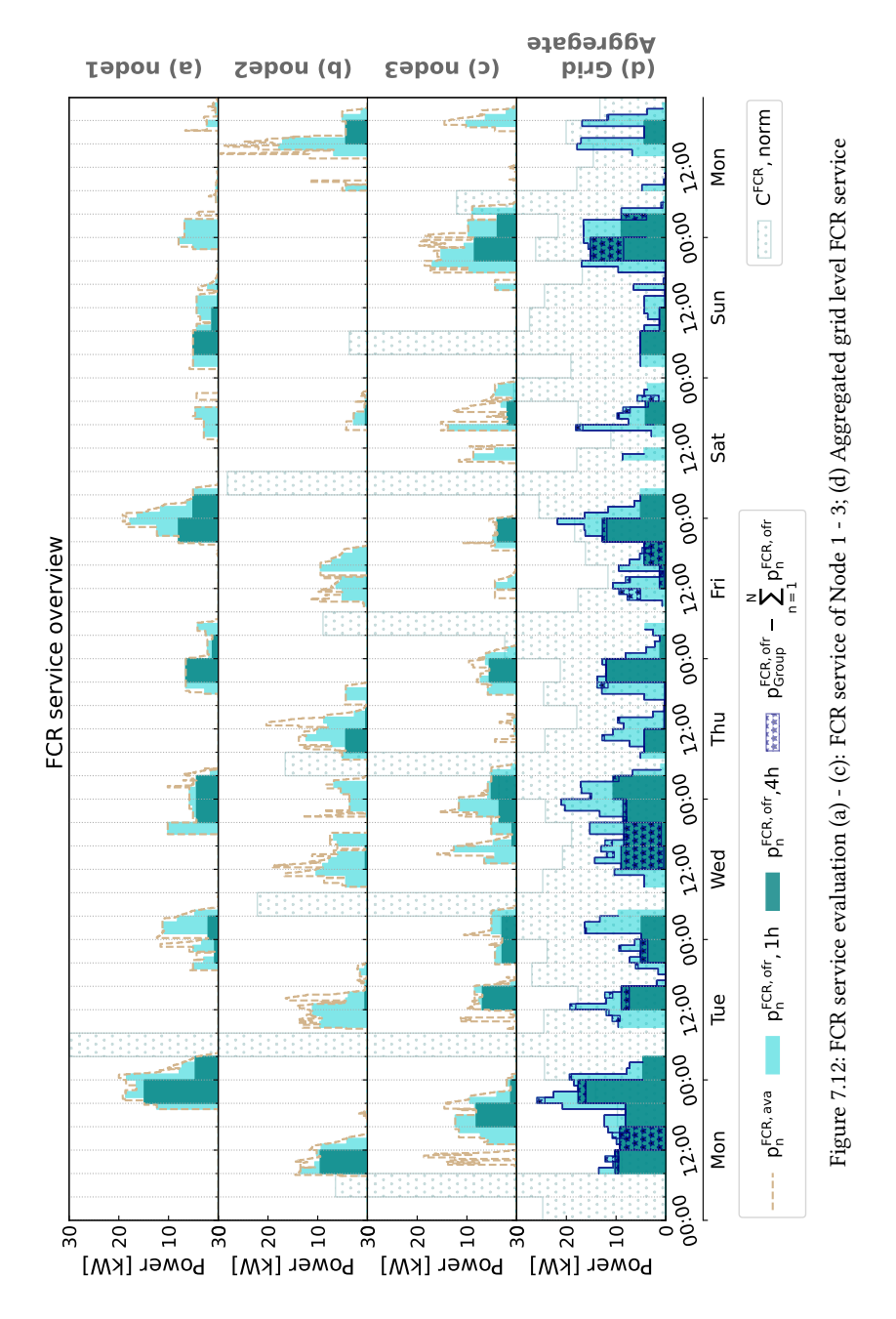
Nonetheless, the results indicate that SC-AlgS indeed improves the overall node profit and shows better performance than ARM. Yet, to what extent the SC-AlgS can enhance the benefits is fundamentally determined by the potential of the optimisation horizon where the target charging events sit, i.e., whether the parking duration is sufficiently long and if a profitable price moment is enclosed. Charging events like Semi-public and Public are thus less favourable than the Home charging events in that regard.

FCR provision

Even though the SC-AlgS incorporates the functionality for providing FCR service, the provision of FCR service in the actual application must adhere to several conditions. A market participant must first be qualified as a Balancing Service Party (BSP) before engaging in FCR trading activities in the electricity market and then providing balancing services. In the Dutch electricity market, the basic FCR bidding requirements stipulate tha bids must be up and down symmetrical and fall within the range of 1 to 25 MW, with step intervals of 0.1 MW. Auctions occur over 4-hour periods, leading to six fixed bidding blocks spanning consecutive time intervals e.g. 0:00-4:00, 4:00-8:00, and so forth, daily. Additionally, once the BRP wins the FCR bid and contracts the offered capacity with the TSO, the Reserve Providing Units/Group (RPU/RPG, which are the power sources that actualise the balancing service) are expected to preserve the contracted capacity throughout the entire 4-hour course [213, 221].

Fulfill the FCR bidding requirements

The requirements on FCR supply post at least two major obstacles for the EVs to serve as RPU/RPG. One is to guarantee a 4-hour reserve considering the high mobility and uncertainty associated with EVs, and the other one is the 1 MW bidding threshold, which necessitates the availability of tens of thousands of EVs simultaneously. The FCR entry capacity can be attained by aggregating EVs with other assets as also supported and promoted by the TSO [213]. The 4-hour bidding duration can also be circumvented by aggregating into



a large assets pool that is overseen by a BRP. On one hand, aggregated assets can substitute each other's asynchronous power thereby enhancing the likelihood of forming 4-hour bidding windows in which power is continuously available, On the other hand, the bidding duration limitation of each asset is ruled by the BRP, making a shorter window possible.

From each node or even per EV level, the 4-hour bidding duration can be factored in when scheduling the EV charging. However, incorporating the 4-hour block reserved-capacity into optimisation constraints would exponentially increase the MIP complexity, posing challenges to the computation process as well as the overall capability of pursuing optimality due to the non-linearity. Consequently, the node level FCR offer $p_n^{\rm FCR, off}$ is calculated post-optimisation by extracting the minimal power value from the selected 4-hour blocks, whose available FCR capacity $p_n^{\rm FCR, ava}$ remains non-zero across the whole 4-hour window.

Benefits of aggregation on top of smart charging in FCR provision

The offerable FCR capacity is investigated for two cases, which are: 1) when each node provides the service independently — namely Unit mode; 2) when all the assets in the microgrid are aggregated and treated as one unitary RPG — namely Group mode. In addition, the same analysis is replicated under a different scenario in which the EVs are aggregated by a third-party BRP and a shortened 1-hour bidding length is applied. The offerable FCR power of all nodes' sum $\sum_{n=1}^{N} p_n^{\text{FCR}}$, of and from aggregation across the grid $p_{\text{Group}}^{\text{FCR}}$, of is depicted in Fig. 7.12, with the normalised FCR price plotted in the background for reference. The 4-hour and 1-hour bidding constraint differed scenarios are named "4h" and "1h" respectively. Specially, the extra offerable FCR capacity in Group mode than in Unit mode is marked with a navy-coloured shade.

Key paramet & Scenario	ers	Unit mode	Group mode	Rel. value Group w.r.t. Unit mode
TFCR,ofr [h]	4h	108	124	14.81%
1 [11]	1h	157	157	0
Rel. value (1h	w.r.t. 4h)	45.37%	26.61%	-
$\overline{p}^{FCR, ofr}$ [kW]	4h	4.94	6.01	21.67%
p [kW]	1h	8.79	9.10	3.56%
Rel. value (1h	w.r.t. 4h)	77.76%	51.31%	-
CFCR,ofr [€]	4h	6.72	8.93	32.88%
	1h	17.70	18.24	3.05%
Rel. value (1h	w.r.t. 4h)	163.48%	104.32%	-

Table 7.6: Summary of FCR service in various modes and scenarios

The Group mode substantially upturns the FCR offerable capacity in the 4-hour scenario pertaining to both bidding hour length and average power, and a shortened 1-hour bidding window amplifies this effect even further. Among the overall 192 simulation hours, three nodes collectively provide 108 hours of FCR service in Unit mode, but the Group mode extends 14.81% of this duration and turns it into a total of 124 biddable hours. On top of that, the 1h scenario contrives to prolong another 26.61% of the bidding-possible time window, reaching 157 hours in total after all. The mean offerable power during these bidding hours also sees a considerable rise, from 4h + Unit mode's 4.94 kW, to 4h + Group mode's 6.01 kW and eventually achieves 9.10 kW with 1h + Group mode, the incremental steps are 21.67% and 51.31% respectively.

The enhanced availability of assets' capacity ultimately serves to increase BRP's profit

by enabling more FCR service supply. The overall supplementary capacity of 1h + Group mode with respect to 4h + Unit mode is 894.99 kW×hour, and it gains $11.02\,$ € more income than the original $6.72\,$ € value. That is to say, the combination of the minimum bidding duration condition relaxation and the capacity-complimentary assets aggregation, contribute a 167.62% additional tradeable capacity and eventually grants a 175.51% growth in potential profit.

The summary of FCR offerable service comparison can be found in Table 7.6. It shall be noted that grid transient and dynamic analysis are beyond the scope of this thesis, thus the FCR service provision focuses solely on the power capacity span the bidding window. Nonetheless, further investigation into how EVs provide FCR services and how smart charging influences FCR provision from a transient perspective, particularly in response to grid frequency fluctuations at the seconds level, is essential.

7.5.2. Stochasticity management validation

Section 7.3 explicates the passive stochasticity coping mechanism of SC-AlgS that consists of a charging event coordinator and a charging process self-correction function. One leading process of this mechanism is the regular parameter correction and update, as well as frequent re-optimisations. The validation of the stochasticity coping mechanism is placed in this section.

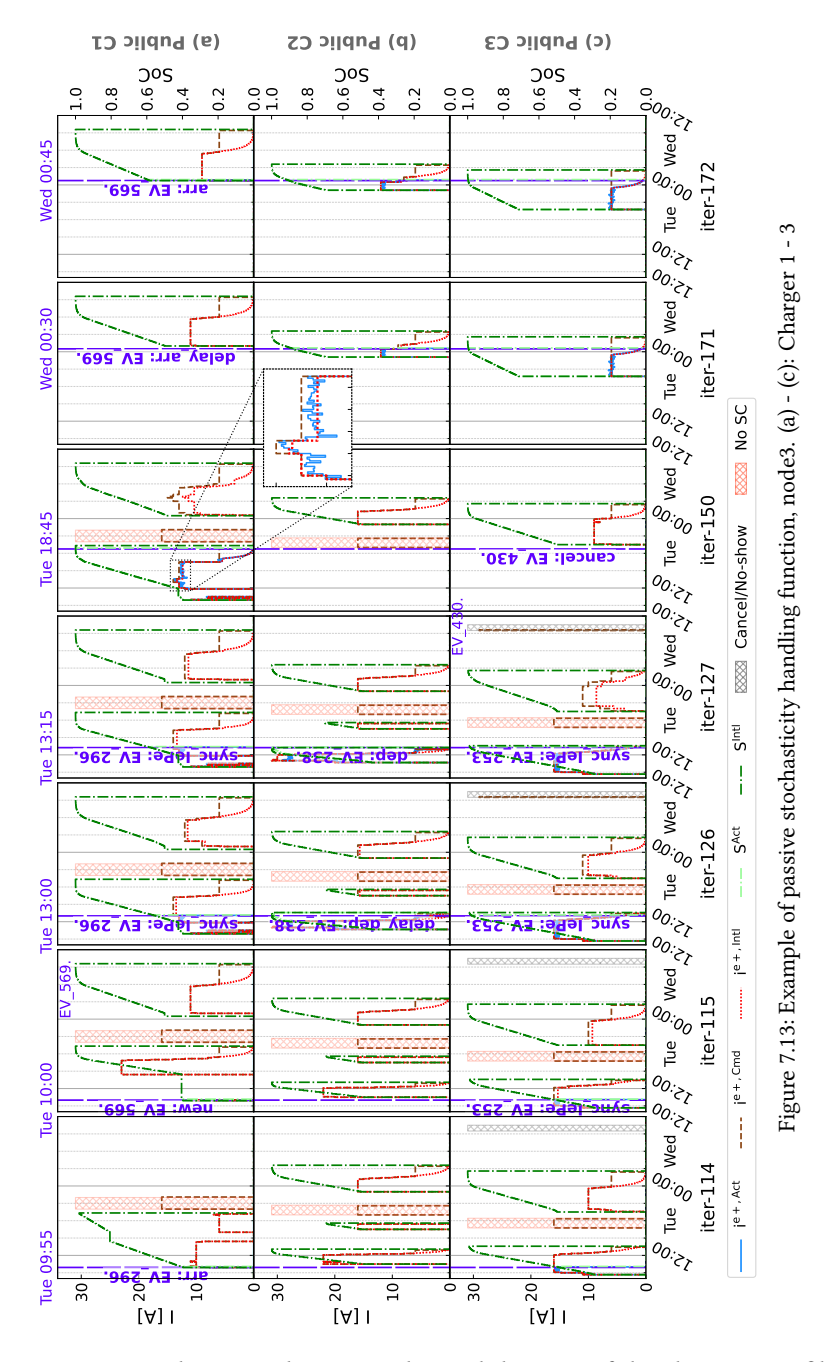
The results of SC-AlgS that are scrutinised in the previous section are the upshot of continual adjustments and calibrations through hundreds of MIP recursions. Several reoptimisation cycles triggered by representative events that take place between Tue 8:00 - Wed 12:00 are exhibited in Fig. 7.13. In this figure, the charging profiles of each charger are displayed in separate rows and each column depicts the snapshot of the selected optimisation iteration. The iteration number is listed at the bottom of each column. The time of each optimisation iteration is pointed by a purple time-index line with the corresponding time annotated at the top, and the optimisation triggering factor is written next to the time-index line.

Future EV inclusion

The evolution of the charging profiles over the course of re-optimisations is reflected in the columns progressing from left to right. The event of a new EV (EV_569) entering the SC monitoring range and thus joining the SC pool is illustrated in the sub-figure of iteration 115 at charger C1 (denote as \langle iter-115, C1 \rangle , same format applied to the following text). The sub-plots \langle iter-114,115,126; C1 \rangle , demonstrate how the charging profile of the attime-connected EV_296 is influenced by the joining of the new EV and eventually reaching the stable state. The processing of EV charging cancellation is straightforward and the EV discard from the SC pool is much simpler than take-in. The cancellation initiated by the user successfully provokes the removal of EV_430's data from the system, as demonstrated in sub-plots \langle iter-127, 150; C3 \rangle .

Uncertain event coordination

It is quite common that the actual arrival and departure of an EV deviate from the original planned schedule. By adjusting the planned and actual EV connection timetable, the charging event coordinator of SC-AlgS can adapt to the charging event modification with high flexibility, as introduced in Section 7.3. One example of the delayed arrival of EV_569 is exhibited in sub-figures (iter-171, 172; C1). EV_569 does not show up as planned at Wed 00:30, and thus SC-AlgS suspends the arrival record for 30 min in the system database,



leaving a narrow gap between the time-index and the start of the charging profile as depicted in the sub-figure (iter-171; C1). The arrival SoC is unknown to the SC-AlgS prior to the actual connection of the EV, and the default value of 50% is used as a temporary solution before the update of EV specifications and the user settings upon EV-EVSE hand-

shake when plugged in. The alignment of the arrival SoC value in the SC-AlgS system is visible from the SoC start point shifting in sub-plots (iter-171 \rightarrow 172; C1), as well as clearly spotted from sub-plots (iter-150 \rightarrow 171; C2), (iter-150 \rightarrow 171; C3) and so forth.

Charging process self-correction

The self-correction during charging processes is actuated when the disparity between the measured current/power/Soc value and SC-AlgS internal tracking value is higher than the pre-set threshold. Multiple instances are eventuated during the demonstration time window in Fig. 7.13. One example showing the effect of charging process self-correction is pinpointed and zoomed-in in sub-figure \langle iter-150; C1 \rangle . The zoomed-in curves evince the calibration of $i^{e+,intl}$ to match the measured actual EV charging current $i^{e+,Act}$ via the employment of the computed offset value. A minor inconvenience that the charging current offset value stretches to the upcoming EVs can be noticed in sub-plots \langle iter-115, 126, 127; C3 \rangle and \langle iter-126, 127, 150; C3 \rangle . This phenomenon appears due to the self-correction function applying the charging command offset value to the rest of the optimisation horizon. This incidence can be easily ironed out by limiting the offset effective duration to only the current connecting EVs.

Conclusively, the stochasticity coping mechanism in SC-AlgS proves to perform as expected. Both the coordination of changeable charging events as well as the charging process self-correction operate properly.

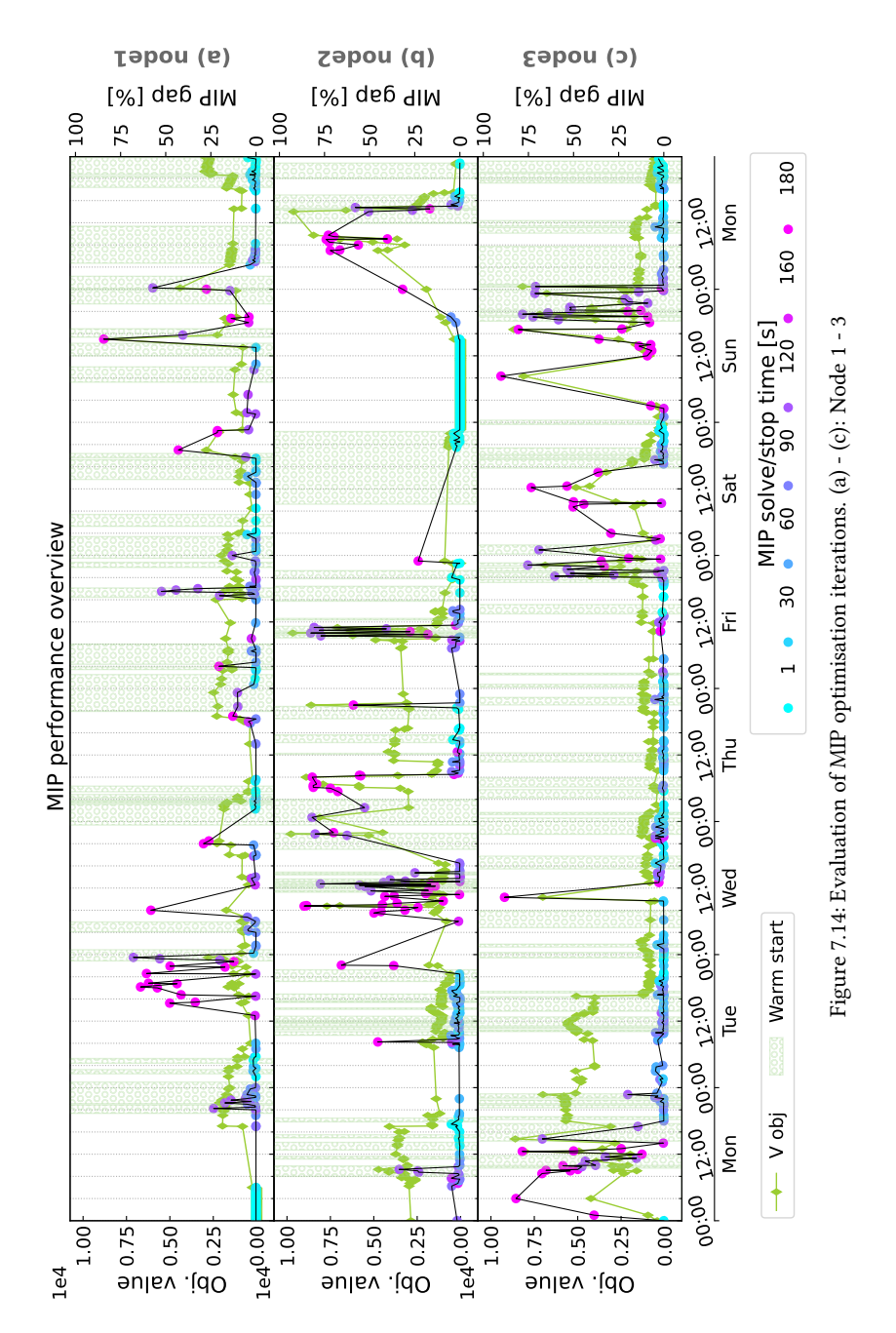
7.5.3. Pursuing optimality

Optimisation-embedded algorithms frequently encounter the challenge of achieving and demonstrating optimality. It is often nearly implausible to mathematically prove the optimality of an engineering solution, particularly in implementation-oriented optimisation problems. Moreover, due to real-world errors and stochasticity, the gains in solution effectiveness through approaching optimality tend to be marginal. As a result, approximate optimality is commonly defined to indicate a practically satisfactory result. In this thesis, "optimality" refers to proximate optimality (proxi-optimality) with a MIP gap of less than 5%. This section then investigates the propinquity to optimality of SC-AlgS and explores the possibility of improving it.

Appraisal of proximity to optimality

As explained in the previous content, there are numerous instances of MIP optimisation sourced from the passive stochasticity handling mechanism. The optimisation triggering factors include: a) EV fleet reformation like EV (delayed) arrival/departure, cancelled/no-show reservation and arrival without reservation; b) EV charging process inconsistencies such as charging current/power/SoC value dissonant between the measurements and SC internal system estimations; and c) The grid capacity limitation adjustment. Based on the optimisation triggers, the MIP iterations are categorised into two groups: prime and light. The prime group contains events related to EV fleet change including new EVs being added to the SC monitoring range, EV arrival/departure, cancel/no-show registration and arrival without reservation. Basically, the prime events are those additions and removals of EVs from the SC fleet pool, as well as the physical connection and disconnection of EVs. The rest of the events are classified as light group.

The prime group MIP iterations have major parameter renewal, while the light group coincides with most of the parameters with the prior MIP occurrence. When re-optimisation



is initiated for the purpose of updating one parameter while a full-functional charging plan is obtained from earlier optimisation in commission, it would be time inefficient and computational resource depletion to conduct a full re-run of the MIP process without recycling the serviceable profiles. Therefore, all MIP iterations in light group inherit the preceding

round's MIP results as the MIP warm start of the subsequent term. Additionally, an extra filter mechanism is engaged after each MIP iteration in the light group to serve the paramount purpose of EV charging – fulfil the charging request. This filter checks the result and dismisses the ones that deliver less energy to the EV than their predecessors. The simulation time interval is 5 min, and the optimisation duration has to be shorter than that to avoid overrun. Thus, a 3 min time limit for the prime group and 2 min for the light group is set beside the 5% MIP gap stopping criteria.

To assess the convergence to optimality of all optimisation iterations, the objective value, MIP gap and the MIP solve/stop time are visualised in Fig. 7.14. The MIP instances that utilise warm start are marked with green shade. This plot manifests that the majority of MIP sessions reach their optimality and the warm start does improve the optimisation performance, seeing the MIP gap's gradual decrease during, for example, node1 $1^{\rm st}$ -Mon 20:00 - Tue 5:00, node2 $2^{\rm nd}$ -Mon 12:00 - 16:00, node3 Sat 16:00-20:00, and so on. Overall, there are 79.41% of iterations reached optimality, and 70.5% of the warm start sessions obtained either a better objective value or a smaller MIP gap than its prior iteration. However, it shall be noticed that even when the MIP gap suggests certain iterations of MIP obtained optimality, it does not mean the SC-AlgS acquires the optimal charging solution. That is because the MIP optimality could be obtained when the favourable moment already passed, as showcased in Section 7.5.1.

Enhance convergence towards optimality

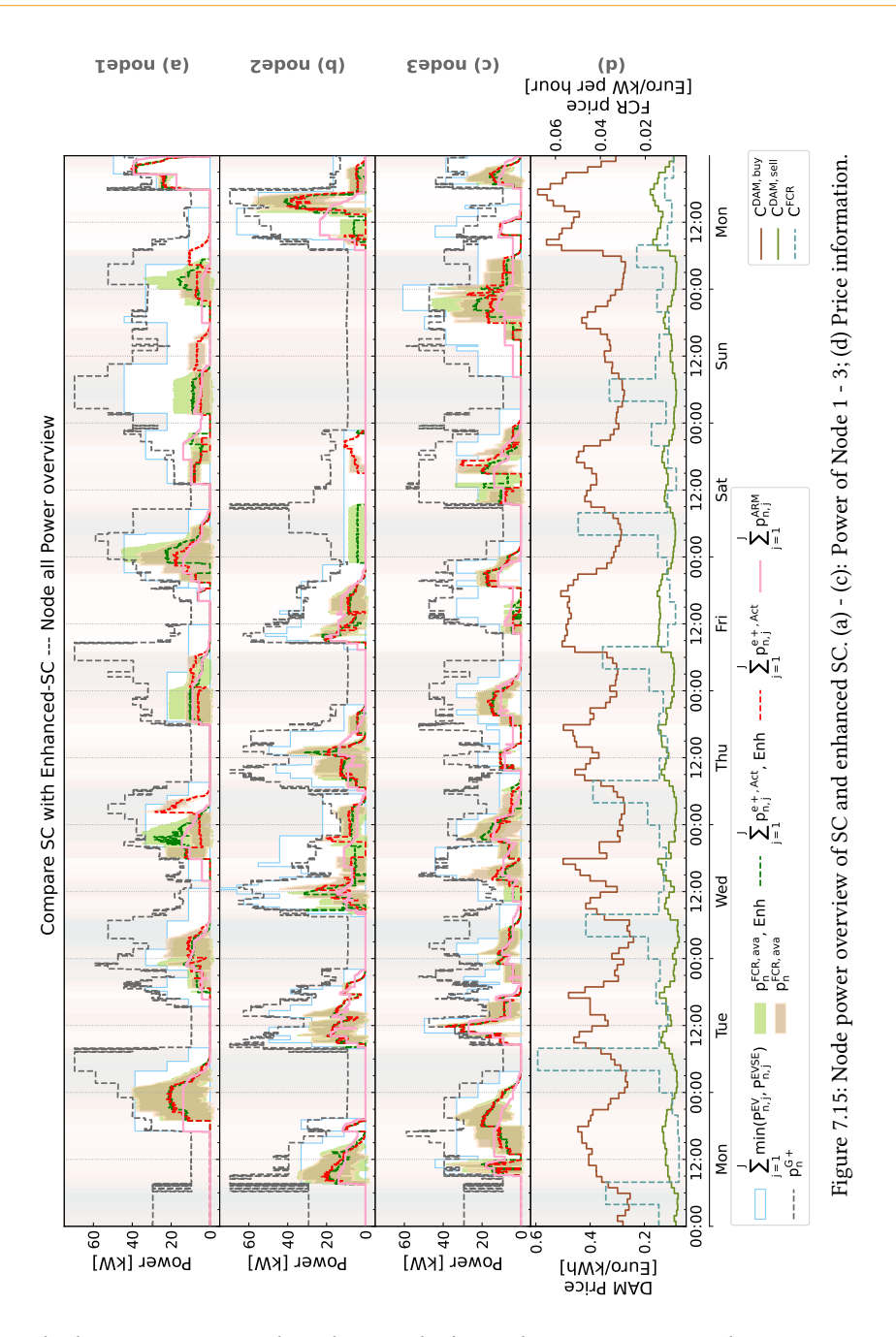
Results presented in Section 7.5.1 reveal that ARM possesses competitive capability in reducing the charging cost and the total node cost. This insight inspires a theory that further enhancement of the SC-AlgS's propinquity to optimality can be achieved through the help of ARM. One extra round of simulation is conducted to substantiate this hypothesis. In this round of simulation, the ARM profiles are used as the MIP warm start for the prime group sessions, and the MIP sessions in the light group still use its former cycle's output as the warm start. This ARM profile-inspired version of SC-AlgS is named SC-AlgS $_{\rm E}$ and is symbolised with "Enh" in the plots.

SC-AlgS_E shows improved results in cost-saving, energy delivery as well as FCR service

		node1	node2	node3	Overall
p.u. Charging cost [€/kWh]					0.409 0.407
Rel. cost red	0.74%	0.65%	0.34%	0.55%	

Table 7.7: Charging cost comparison between two versions of SCs

The power overview of all nodes between SC-AlgS and SC-AlgS $_{\rm E}$ can be found in Fig. 7.15. The charging profiles of the two versions of algorithms largely overlap with each other in node2 and node3 due to the charging event types' (Semi-public and Public) features – relatively short parking duration and routinely occur in the daytime. Whether SC-AlgS $_{\rm E}$ is consistently more effective in lowering the node's cost is inconclusive solely from reading Fig. 7.15. For example in node1, there are moments when SC-AlgS $_{\rm E}$ migrates the charging power towards the advantageous price range like the curves drawn between Sun 0:00 and 6:00 $_{\rm E}$ Mon. There are also occasions where the SC-AlgS $_{\rm E}$'s profiles appear further away



from the lower price range than the SC-AlgS's results. As numeric analysis may provide more insight, the per unit charging cost comparison between two SC versions can be found in Table 7.7, through which a marginal advantage of SC-AlgS $_{\rm E}$ in cost saving is suggested. On the other hand, SC-AlgS $_{\rm E}$ exhibits surprisingly solid competency in enabling FCR

		Node sum			Aggregated			
		SC-AlgS	SC-AlgS _E	Rel.	SC-AlgS	SC-AlgS _E	Rel.	
T ^{FCR,ofr} [h]	4h	108	88	-18.52%	124	112	-9.68%	
1 [11]	1h	157	147	-6.37%	157	150	-4.46%	
FCR,ofr [kW]	4h	4.94	7.62	54.20%	6.01	7.59	26.14%	
$\overline{p}^{ren,on}$ [kW]	1h	8.79	10.07	14.55%	9.10	10.18	11.88%	
C ^{FCR,ofr} [€]	4h	6.72	9.02	34.27%	8.93	10.91	22.22%	
[€]	1h	17 70	19.51	10.25%	18 24	20.06	9 98%	

Table 7.8: Compare FCR service between two versions of SCs

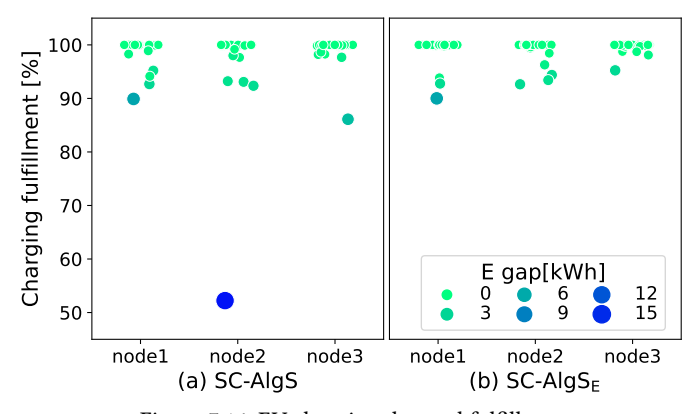


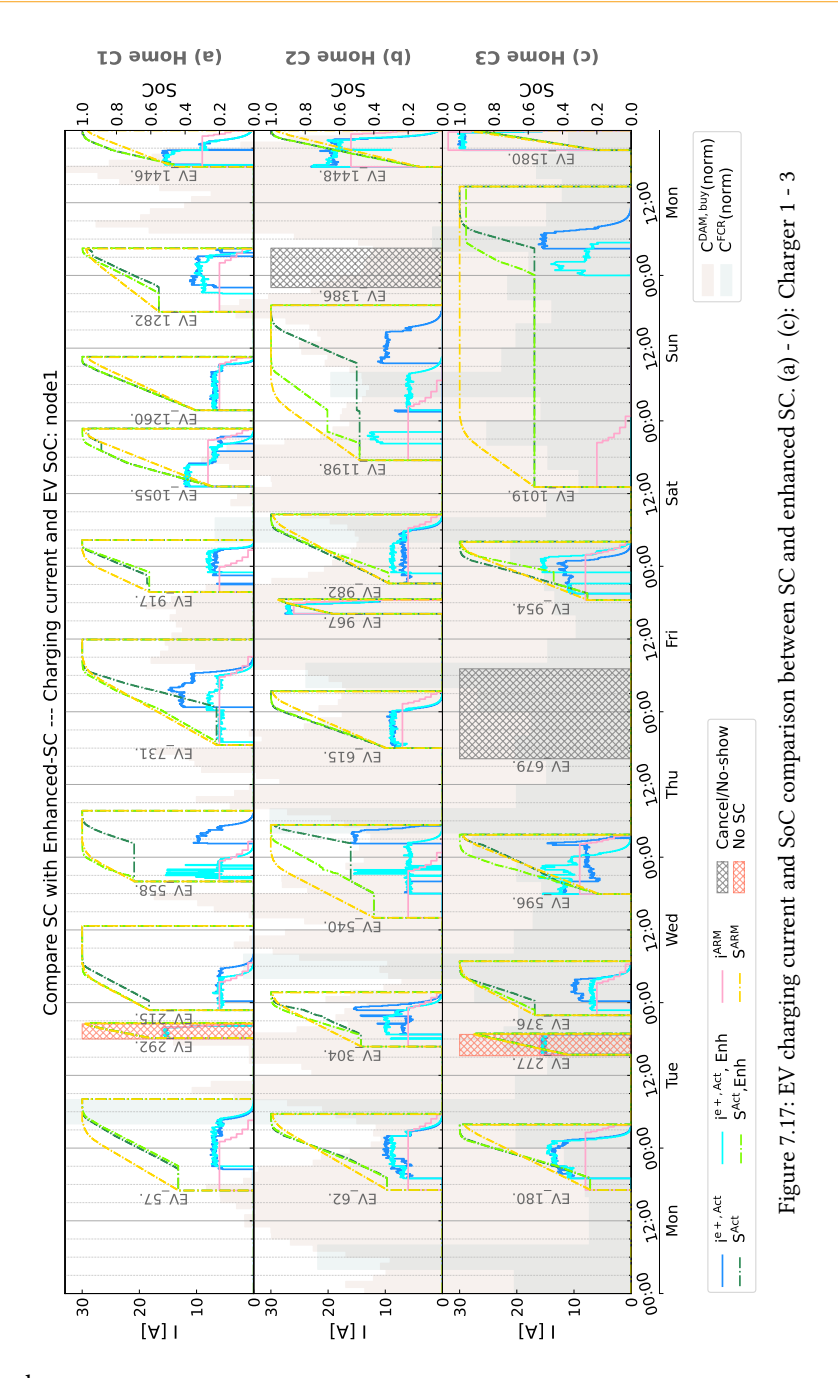
Figure 7.16: EV charging demand fulfillment

service provision that contributes to significant growth in income for offering FCR service. This outcome is largely thanks to the ARM profile's lower rate and long-lasting feature that naturally facilitates a higher FCR service availability. The numeric comparison of FCR service capability between SC-AlgS and SC-AlgS_E is summarised in Table 7.8. It can be observed from the table that, SC-AlgS_E is slightly short in offering FCR available hours but compensates by providing a considerably higher FCR serviceable power level relative to SC-AlgS. The imperfection in rendering FCR hours of SC-AlgS_E is connected to the declined continuity of the computed EV charging power. It is further discussed in the following context.

In addition, SC-AlgS $_{\rm E}$ can slightly enhance the charging energy delivery rate, which is the fraction of energy delivered by the algorithm divided by the energy delivered by UNC. The scattered plot of every charging event's energy delivery rate is presented in Fig. 7.16. This figure affirms the amelioration of SC-AlgS $_{\rm E}$'s energy delivery rate. Moreover, the SC-AlgS $_{\rm E}$ in total delivers 2.27% more energy than SC-AlgS.

The effectiveness of proximity to optimality enhancement is application scenario sensitive

Last but not least, the optimality acquisition of individual MIP sessions is also examined in the contrast between SC-AlgS and SC-AlgS_E. The overall MIP performance indicators, including averaged MIP gap (\overline{g}^{MIP}) , numerical mean of MIP stop/solve time $(\overline{\tau}_{fin}^{MIP})$, as well as the percentage of total iterations that acquire optimum (γ_{iter}^{opt}) , are listed in Table 7.9. For each item per node compared between SC-AlgS and SC-AlgS_E, the better results are



coloured green.

The numbers in Table 7.9 disclose that SC-AlgS $_{\rm E}$ is effective in pursuing optimality for Semi-public and Public charging events, but less so for home charging events where long parking duration often span a few opportune charging windows. A fully spread-out char-

	node1		node2		node3		Overall	
	SC-AlgS	SC-AlgS _E						
<u>g</u> ^{MIP} [%]	6.44	11.19	12.88	11.80	10.43	9.29	10.33	10.75
$\overline{\tau}_{\rm fin}^{\rm MIP}$ [s]	66.48	67.59	64.94	64.98	81.49	80.58	71.30	71.20
γ _{iter} [%]	82.53	78.45	77.98	78.48	78.68	79.55	79.41	78.85

Table 7.9: Compare MIP performance between SC and enhanced SC

ging method, like ARM, may miss the best opportunity, making it less desirable in these scenarios. Therefore, the ARM-inspired warm start applied in Home charging events may mislead the branch & bound process, potentially causing a counterproductive effect.

Although SC-AlgS_E proves to be more effective in cost-saving, energy delivery as well as FCR service than SC-AlgS, node profit is merely one aspect of the objectives. The other important objective is to minimise the charging current ramp for the purpose of obtaining a continuous and smooth charging current, as clarified in Section 7.2.2. The charging current of two SC versions at node1 is portrayed in Fig. 7.17. The curves of SC-AlgS are visibly less oscillating and smoother than SC-AlgS_E, especially between 12:00 Wed and 12:00 Thu. These current vacillations are not only undesirable for steady and effective charging processes, but also risky in undermining the FCR service supply. Any zero-nonzero value swap could likely interrupt a potential continuous FCR bidding time window. This explains why the FCR offerable time window of SC-AlgS_E is shorter than SC-AlgS. The current fluctuation of SC-AlgS_E perchance contributes to the minor descent in optimality convergence.

Despite that the ARM warm start boosts the overall SC effectiveness to a certain degree, the optimisation problem on its own is a difficult task to accomplish, seeing the unsatisfactory value of $\overline{g}^{\text{MIP}}$, $\overline{\tau}^{\text{MIP}}_{\text{fin}}$ and $\gamma^{\text{opt}}_{\text{iter}}$ in Table 7.9. This signifies that the MIP procedure can be refined. For example, provide further strengthened MIP start, dynamically guide and speed up the MIP using customised heuristics and steer the branch and bound while the MIP procedure is ongoing. Altering the MIP output utilisation can also help; for instance, instead of terminating the MIP process when passing the time limit, extracting the best feasible solutions at the time being as temporary solutions while keeping the MIP running in the background and updating the results when it eventually succeeds optimum. Lastly, accessing higher computational power is always an easy resort.

After all, the ARM warm start backed $SC-AlgS_E$ presents an adequate outcome with major potency being superior to SC-AlgS.

7.6. Conclusion

This research presents an upgraded EV smart charging algorithm, SC-AlgS, built on our previous work in Chapter 6.

The primary advancements concentrate on: stabilising and smoothing the charging profile, upgrading grid balancing service provision, uplifting the propinquity to optimality of MIP iterations, broadening the applicability of EV smart charging for future scenarios through an updated flexible moving horizon mechanism, adapting to prompt change of charging events with high pliability, and dynamically calibrating and correcting the charging parameters.

The SC-AlgS's functionalities are validated through simulations, affirming the effectiveness of its passive stochasticity coping mechanism and the self-correction during charging as expected.

In terms of profit-related outcomes, the comparison between SC-AlgS, UNC and ARM, suggests that SC-AlgS transcends both UNC and ARM across most metrics, with ARM emerging as a strong contender. Regardless of the reduction in charging cost due to scheduled charging, neither SC-AlgS nor ARM accomplishes the same level of charged energy as UNC.

Despite the activation of the 4-hour bidding window limitation, sizable capacities remain available for providing FCR services from EV charging. Considering the minimal bidding entry size, participation in FCR service is unattainable without aggregation. Furthermore, aggregation remarkably maximises the capacity reservoirs, enabling the conversion of available capacity into usable FCR offers, far surpassing the simple summation of individual assets. Beyond that, aggregation offers the possibility to congregate assets of short availabilities as a grouped unit to suffice the bidding window (4-hour) requirement. By doing so, providing FCR service is accessible to the short-term assets who participate in FCR service supply as a single unit is otherwise inapplicable.

The investigation into optimality across all MIP iterations concludes that SC-AlgS reaches adequate optimality with given settings. An additional test is carried out to examine whether using ARM profile as MIP warm start can further enrich the SC-AlgS's functionality. The results substantiate that SC-AlgS_E indeed outperforms SC-AlgS in cost saving, energy delivery and FCR contribution. However, a minor decline in convergence to optimality inspected in Home charging events signifies that how well heuristics can improve optimality attainment is dependent on the application scenarios.

It is consequently logical to assert that a rightfully designed heuristic holds promise for improving optimisation productivity. Aside from providing updated warm starts, heuristic-guided MIP search and branch and bound represent another encouraging approach.

Key insights

This thesis aims to construct a systematic framework for integrating Electric Vehicles (EVs) into Low Voltage (LV) distribution grids. The ultimate goal is to develop a multifunctional, flexible and reliable smart charging algorithm enabling EV mass deployment in distribution grids. The framework for achieving the main research objective is segmented into several key parts:

- 1. Conducting a thorough study on the mass deployment of EVs in distribution grids.
- 2. Performing a comparative investigation of representative heuristic EV charging tactics to establish a foundation for a smart charging algorithm.
- 3. Developing a grid congestion prevention mechanism from the DSO perspective in anticipation of widespread EV connections.
- 4. Designing, validating, upgrading & refining and eventually assessing a flexible, efficient and reliable EV smart charging algorithm.

With the presented framework, this thesis offers systematic solutions to various key stakeholders in the EV-grid integrated ecosystem. The PTDF-based centralised grid congestion prevention and mitigation algorithm serves as a potential tool for DSOs to manage congestion. The hierarchical EV smart charging algorithm can be incorporated in the backend of aggregators while the BRP can include EVs as their flexible asset by adopting the FCR function included smart charging algorithm. Local energy users can benefit from employing the smart charging algorithm through increasing the utilisation of their local renewable energy generations and reducing electricity costs.

The key observations and takeaways gathered through each preceding chapter are consolidated and presented in this chapter. The following reflections are correspondent to the objectives that are presented in Section 1.2. The final part of this chapter, following the reflections on the objectives, presents the recommendations on the future work.

Reflection on O1: The thorough study of EV mass deployment in the distribution grid

Grid congestion related to uncontrolled EV charging is highly conditional

From the uncontrolled EV charging-induced grid congestion study, it is observed that all grid components, including transformers, lines and nodes, generally follow a similar trend. When the transformers experience high loading, the maximum line loading also has the tendency to increase while the minimal node voltage is more likely to have deep dips. However, there are occasional instances of local line overloading and regional voltage drops, particularly in rural grids of remote areas.

The inherent grid features such as its designed capacity, component specifications, inhabited connections and their load demand, are the fundamental factors contributing to

congestion risks. Grids of higher designed density, with a greater number of connections, notably households (which correlate with EV penetration level), tend to experience more grid congestion issues. Suburban grids, which fit this characterisation, experience more frequent and higher severity of EV charging-related congestion than other grid types. Interestingly, while the trend in line loading does not exhibit a strong correlation with the average line ratings, a noticeable association is observed between decreased minimal node voltage and the combination of average line length and the longest feeder length. This suggests that voltage issues may arise well before line overloading becomes apparent.

LV grids are more susceptible to voltage drop than other overloading issues

The simulation results show that there are more grids that have under-voltage problems than grids with transformer and line overloading issues. During winter, two out of seven high under-voltage risk grids suffer from voltage drop even without the presence of EVs, the situation is exacerbated by excessive EV demand. In an 80% EV penetration scenario, at least one-fifth of the grid experiences under-voltage problems for nearly half of the simulation time. Conversely, a maximum of <3% of overloaded line length among all the simulated grids reveals the scale of line overloading is relatively limited. This problem mainly occurs at specific lines, such as the main buses near the transformer or local lines connected to exceptionally high consumption loads.

Most grids that are not at risk of inherent overloading, can sustain a fair level of EV penetration

It can be concluded that the majority of the grids do not face major congestion when accommodating 50% EVs. Most of the problematic grids have a small scale and short duration of grid limit breaching. Where the grids do experience severe congestion, it opens the opportunity to look into alternative methods beyond upgrading grid facilities. For example, smart charging scheduling can be considered in addition to traditional grid facility upgrades.

Reflection on O2: Comparative investigation of representative heuristic EV charging tactics

Three representative heuristic EV charging strategies are selected and tested for their potential and limitations in promoting EV and grid integration. They are: voltage droop method (VDM), price-signal-based method (PSM) and average rate method (ARM). Each method focuses on one specific aspect: PSM on charging cost reduction, VDM on grid impact mitigation and ARM on user-centric considerations.

Heuristic EV charging scheduling outshines uncontrolled charging (UNC) under majority situations

The effectiveness of the three tested charging methods is assessed through the perspectives of cost savings, grid impact and user experience. The results conclude that VDM is most successful in improving grid performance concerning peak branch loading reduction (reduces 7.74%), and the node voltage drops alleviation (under-voltage issue decreases from 23.53% to 0%) relative to UNC. ARM proves to be the most reliable in simultaneously improving the grid performance and meeting users' charging energy demand. Both ARM and VDM effectively flatten the loading curve while lowering the peak load. While ARM is viable for reducing total node costs, PSM can achieve charging cost savings that are two

to three times greater.

The restrictions of heuristic EV charging methods originate from their limited access to system information and delegated purposes

Even though the heuristic EV charging methods evince acceptable outcomes, their imperfections lie in the limited system information and restricted specialities can result in unbalanced or even biased results. For instance, unfair charging power curtailment can occur in VDM, and simultaneous charging at moments of lower prices can provoke peak load issues in PSM. Therefore, the design logic and reference parameters for heuristic methods must be carefully evaluated.

Reflection on O3: Constructing a centralised grid congestion prevention mechanism

This thesis proposes a Low Voltage (LV) grid congestion management algorithm incorporating three centralised EV charging management schemes: PTDF-based Charging Management Scheme (PCS), Egalitarian Charging Management Scheme (ECS) and Priority-based Charging Management Scheme (PrCS). Each scheme addresses congestion management from a different perspective:

- 1) The PCS focuses on the elements that have the greatest influence on congestion;
- 2) The ECS aims to share the congestion pressure in the fairest way;
- 3) The PrCS seeks to maximise the overall energy transfer to EVs.

Proposed schemes show encouraging outcomes in congestion mitigation, and favouring their destined optimisation priorities

The activation of all three schemes successfully resolves the overloading conditions of both the transformer and the lines with high precision. Their integration also leads to better utilisation of the available grid capacity, which in turn promotes balanced voltage levels throughout the network. Quantitatively, all three schemes ensure that grid branch loading does not exceed 100.15% in all cases, while simultaneously meeting an average of 97.7% of the charging demand. Overall, this part of the work demonstrates that PCS provides the best results from a grid management perspective. Correspondingly, the PrCS delivers competitive results in terms of grid performance and achieves the best overall outcomes from a user standpoint.

Centralised congestion management principally assigns confined grid capacity and postpones further requests, while smart charging can fundamentally dissolve the source of congestion

This congestion management-oriented charging control scheme fundamentally processes the sustained charging request and allocates the available grid capacity in divergent orders until the EV is fully charged or departs. This mechanism has a potential drawback. A significant growth in the volume of the EV "waiting lines" with respect to uncontrolled charging is observed. This increase is comparable for the PCS and ECS cases, which reach the maximum of 64.3% and 77.2% respectively, while it is significantly higher – 127.7% – for the PrCS. The direct consequence of the longer waiting lines is an increase in overcompensation phenomena. Although this aspect does not impede the achievement of the main objective of the algorithm i.e. to keep the loading percentages within the allowed limit—their presence suggests that the available grid capacity has not been exploited to

the fullest.

Alternatively, instead of suspending and postponing the charging request, planning the charging events in advance with a smart charging algorithm may intrinsically prevent grid congestion from happening.

Reflection on O4 & O5: Design and validation of the EV smart charging algorithm

This thesis provides a systematic EV smart charging solution in three stages.

- 1. First, a primary hierarchical mixed integer programming EV smart charging algorithm (namely SC-Alg) is formulated with the aim of maximising local system profit while maintaining unbreached grid capacity.
- 2. Subsequently, this first version of the algorithm SC-Alg is verified and assessed in a power hardware-in-the-loop (HIL) testbed that incorporates models of real LV distribution grids.
- 3. Finally, the algorithm is upgraded based on the HIL evaluation results and the advanced implementation requirements. The final stage is discussed in the next subsection.

Promising results are attained through smart charging

The SC-Alg presents promising and steady outcomes with or without external stress factors, including uncertainties and grid restrictions, in contrast to uncontrolled charging. The results show that the SC-Alg reduces the per-unit charging cost by over 22% in five out of seven scenarios. Even with a 30% EV capacity input error, the charging cost is still 12% less than uncontrolled charging. The SC-Alg also proves its substantial capability in alleviating grid congestion with an average of 39.35% peak power reduction, a 1.41% average minimal voltage increase, and a 95.32% reduction in overloaded energy when no extra grid restraints are present. Additionally, the incorporation of grid constraints enhances the peak power reduction by 33.5% and curtails the overloaded energy 65.9% more than cases without added grid limitations.

Inappropriately adjusted charging schedule could potentially harm the physical components

However, the oscillation of the EV charging current setpoint caused by unregulated MIP calculation can potentially stress the hardware in the charger, especially when the setpoint frequently shifts between zero and nonzero. This behaviour causes the relay in the charger to constantly open and close, resulting in a shortened charger lifespan over time. Therefore, a function to reduce the frequent zero to nonzero charging current alterations is valuable.

Randomness in EV charging behaviour and specifications are the predominant uncertainty source that hinders the charging process

While input parameter-related uncertainties affect the cost-saving of the charging session and the grid's operational range, the unpredictable EV charging behaviour and specifications can pivot the reliability and validity of the planned charging session in regard to charging completion. A simple example is that a 30 min delayed arrival of a 30 min charging session basically invalidates the entire session. The stochasticity in charging parameters is crucial for the algorithm's efficacy. Such as in the HIL simulation, the 30% of hidden battery degradation deviates 20% of the SOC estimation.

As a result, augmenting SC-AlgS's stochasticity management is highly recommended.

Reflection on O4 & O5: Upgrading and evaluating the EV smart charging algorithm

The last content chapter of this thesis elaborates on the upgraded smart charging algorithm, named SC-AlgS. The upgraded features are as follows:

- 1) an advanced EV stochastic charging events processing system;
- 2) a charging process uncertainly handling mechanism through a feedback-loop-incorporated flexible-receding-horizon method;
- 3) functionality-enhanced, warm-start assisted and parameter fine-tuned MIP optimisation procedure.

The functionalities and performance of SC-AlgS are evaluated through simulations and compared to uncontrolled charging (UNC), as well as a benchmark heuristic charging method ARM.

The algorithm enhancement achieves its intended goals

The results indicate that the passive stochasticity coping mechanism and the self-correction capabilities of SC-AlgS in the charging process are confirmed to be effective as anticipated. The comparison in profit-related results, as opposed to UNC and ARM, suggests that SC-AlgS surpasses both UNC and ARM in most perspectives, but ARM appears to be a competitive runner-up. The optimality investigation of all MIP iterations concludes that SC-AlgS reaches adequate proximity to optimality with the given settings.

Technology actualisation for real application is a long ladder to climb

The practical applicational obstacles include but are not limited to: power electronic component constraints, interoperability and technical requirements of communication protocols, and compatibility among different system parts. The communication delay and computational requirements are the other essential factors strongly tied to the feasibility and efficacy of the charging plan execution.

Asset aggregation as well as optimisation improvement are remarkably beneficial in FCR service provision

The FCR service provision under various adjusted entry conditions is scrutinised in the study. It is proved that the greater in size the EV fleet is, the higher FCR available service can be contributed through system-level aggregation than the simple accumulation of the same assets. The aggregation of assets can add a maximum of 32.88% more FCR service income. Furthermore, if the minimal bidding duration (4-hour) constraint can be circumvented and decreased to 1-hour through aggregation, the FCR service income could potentially be 163.48% higher.

It is discovered that an increment in overall convergence to optimality can expand the FCR serviceable reservoir. This growth is even more attractive – achieving a highest of 34.27% more FCR service income – than the offerable capacity boosts through aggregation.

Heuristic charging method has great potential in bringing the algorithm closer to optimality

It is discovered that the heuristic charging method can be efficaciously used to raise the propinquity towards optimality in suitable scenarios. The ARM-inspired MIP warm start enhancement in optimisation results in a marginal decrease in p.u. EV charging cost and

it expands the charging energy delivery by 2.27%. The most significant improvement is reflected in the FCR service provision, which is mentioned in the above subsection. Aside from strengthening the MIP with the heuristic-inspired warm start, another auspicious approach is adapting the heuristic in MIP search as well as branch and bound.

Last but not lease, the recommendations for future possible work are summarised below.

It is recommended to extend the EV uncontrolled and heuristic charging impact study to the MV grid level, in which multiple interconnected LV grids are encompassed. This research expansion allows for the a more all-round understanding of the grid performance with a broader range of LV grid samples, while also incorporating EV traffic patterns and behaviours that are characteristic of interconnected grids in larger areas.

System or component reliability are beyond the scope of the thesis. However, when developing algorithms for complex systems like EV integrated LV distribution grids, it is vital to account for the potential failures in the power grid, the charger, the EV, as well as the defects in measurements and communication devices.

For a solution intended for real-world implementation, it is crucial to further elevate the Technology Readiness Level (TRL) of the testing phase. Such as assessing and adapting the developed grid congestion prevention and mitigation algorithm in collaboration with its potential end user — the DSO. The same principle applies to the hierarchical EV smart charging algorithm. Its true capability cannot be demonstrated without testing in the actual back-end systems of a CPO. On top of that, factors related to human behaviours on both the user and service provider sides could be incorporated.

Bibliography

- [1] EUROPEAN COMMISSION, "The european green deal striving to be the first climate-neutral continent," 2024, accessed: 2024-03-08. [Online]. Available: https://commission.europa.eu/strategy-and-policy_en
- [2] "Sustainable and Smart Mobility Strategy putting European transport on track for the future," EUROPEAN COMMISSION, Brussels, Belgium, EUROPEAN COMMISSION COMMUNICATION COM(2020) 789 final, 12 2020, accessed: 2024-03-08. [Online]. Available: https://eur-lex.europa.eu/homepage.html
- [3] "Grids, the missing link An EU Action Plan for Grids," EUROPEAN COMMISSION, Brussels, Belgium, EUROPEAN COMMISSION COMMUNICATION COM(2023) 757 final, 11 2023, accessed: 2024-03-07. [Online]. Available: https://eur-lex.europa.eu/homepage.html
- [4] Partners in Energie, "Regional congestion reports," 2024, accessed: 2024-03-07. [Online]. Available: https://mijn.partnersinenergie.nl/nl-NL/congestionreports/
- [5] Distribution Systems Working Group, "Ceer paper on alternative connection agreements," Council of European Energy Regulators (CEER), Brussels, Belgium, White paper C23-DS-83-06, 5 2023, accessed: 2024-03-07. [Online]. Available: https://www.ceer.eu/eer_publications/ceer_papers
- [6] "Promotion of e-mobility through buildings policy," EUROPEAN COMMISSION, Brussels, Belgium, EUROPEAN COMMISSION REPORT COM(2023) 76 final, 2 2023, accessed: 2024-03-08. [Online]. Available: https://eur-lex.europa.eu/homepage.html
- [7] S. Shafiee, M. Fotuhi-Firuzabad, and M. Rastegar, "Investigating the impacts of plug-in hybrid electric vehicles on distribution congestion," 2013.
- [8] E. Sortomme, M. M. Hindi, S. J. MacPherson, and S. Venkata, "Coordinated charging of plugin hybrid electric vehicles to minimize distribution system losses," *IEEE transactions on smart* grid, vol. 2, no. 1, pp. 198–205, 2010.
- [9] Q. Gong, S. Midlam-Mohler, V. Marano, and G. Rizzoni, "Study of pev charging on residential distribution transformer life," *IEEE Transactions on Smart Grid*, vol. 3, no. 1, pp. 404–412, 2011.
- [10] J. Taylor, A. Maitra, M. Alexander, D. Brooks, and M. Duvall, "Evaluation of the impact of plug-in electric vehicle loading on distribution system operations," in 2009 IEEE Power Energy Society General Meeting, 2009, pp. 1–6.
- [11] L. P. Fernandez, T. G. San Román, R. Cossent, C. M. Domingo, and P. Frias, "Assessment of the impact of plug-in electric vehicles on distribution networks," *IEEE transactions on power systems*, vol. 26, no. 1, pp. 206–213, 2010.
- [12] K. Clement-Nyns, E. Haesen, and J. Driesen, "The impact of charging plug-in hybrid electric vehicles on a residential distribution grid," *IEEE Transactions on power systems*, vol. 25, no. 1, pp. 371–380, 2009.
- [13] G. Putrus, P. Suwanapingkarl, D. Johnston, E. Bentley, and M. Narayana, "Impact of electric vehicles on power distribution networks," in 2009 IEEE Vehicle Power and Propulsion Conference. IEEE, 2009, pp. 827–831.
- [14] S. Shafiee, M. Fotuhi-Firuzabad, and M. Rastegar, "Investigating the impacts of plug-in hybrid electric vehicles on power distribution systems," *IEEE Transactions on Smart Grid*, vol. 4, no. 3, pp. 1351–1360, 2013.
- [15] K. Qian, C. Zhou, M. Allan, and Y. Yuan, "Modeling of load demand due to ev battery charging in distribution systems," *IEEE Transactions on Power Systems*, vol. 26, no. 2, pp. 802–810, 2011.

- [16] A. S. B. Humayd and K. Bhattacharya, "A novel framework for evaluating maximum pev penetration into distribution systems," *IEEE Transactions on Smart Grid*, vol. 9, no. 4, pp. 2741–2751, 2018.
- [17] J. Coignard, P. MacDougall, F. Stadtmueller, and E. Vrettos, "Will electric vehicles drive distribution grid upgrades?: The case of california," *IEEE Electrification Magazine*, vol. 7, no. 2, pp. 46–56, 2019.
- [18] R. A. Verzijlbergh, M. O. W. Grond, Z. Lukszo, J. G. Slootweg, and M. D. Ilic, "Network impacts and cost savings of controlled ev charging," *IEEE Transactions on Smart Grid*, vol. 3, no. 3, pp. 1203–1212, 2012.
- [19] A. T. Procopiou, J. Quirós-Tortós, and L. F. Ochoa, "Hpc-based probabilistic analysis of lv networks with evs: Impacts and control," *IEEE Transactions on Smart Grid*, vol. 8, no. 3, pp. 1479–1487, 2017.
- [20] M. S. ElNozahy and M. M. A. Salama, "A comprehensive study of the impacts of phevs on residential distribution networks," *IEEE Transactions on Sustainable Energy*, vol. 5, no. 1, pp. 332–342, 2014.
- [21] E. Mancini, M. Longo, W. Yaici, and D. Zaninelli, "Assessment of the impact of electric vehicles on the design and effectiveness of electric distribution grid with distributed generation," *Applied Sciences*, vol. 10, no. 15, p. 5125, 2020.
- [22] J. Quirós-Tortós, L. F. Ochoa, S. W. Alnaser, and T. Butler, "Control of ev charging points for thermal and voltage management of lv networks," *IEEE Transactions on Power Systems*, vol. 31, no. 4, pp. 3028–3039, 2016.
- [23] M. Lillebo, S. Zaferanlouei, A. Zecchino, and H. Farahmand, "Impact of large-scale ev integration and fast chargers in a norwegian ly grid," *The Journal of Engineering*, vol. 2019, no. 18, pp. 5104–5108, 2019.
- [24] L. Calearo, A. Thingvad, K. Suzuki, and M. Marinelli, "Grid loading due to ev charging profiles based on pseudo-real driving pattern and user behavior," *IEEE Transactions on Transportation Electrification*, vol. 5, no. 3, pp. 683–694, 2019.
- [25] K. J. Dyke, N. Schofield, and M. Barnes, "The impact of transport electrification on electrical networks," *IEEE Transactions on Industrial Electronics*, vol. 57, no. 12, pp. 3917–3926, 2010.
- [26] S. Wagh, Y. Yu, A. Shekhar, G. R. C. Mouli, and P. Bauer, "Aggregated impact of ev charger type and ev penetration level in improving pv integration in distribution grids," in 2021 IEEE Transportation Electrification Conference Expo (ITEC), 2021, pp. 595–600.
- [27] N. Brinkel, W. Schram, T. AlSkaif, I. Lampropoulos, and W. van Sark, "Should we reinforce the grid? cost and emission optimization of electric vehicle charging under different transformer limits," *Applied Energy*, vol. 276, p. 115285, 2020.
- [28] S. Deb, A. K. Goswami, P. Harsh, J. P. Sahoo, R. L. Chetri, R. Roy, and A. S. Shekhawat, "Charging coordination of plug-in electric vehicle for congestion management in distribution system integrated with renewable energy sources," *IEEE Transactions on Industry Applications*, vol. 56, no. 5, pp. 5452–5462, 2020.
- [29] M. Secchi, G. Barchi, D. Macii, and D. Petri, "Smart electric vehicles charging with centralised vehicle-to-grid capability for net-load variance minimisation under increasing ev and pv penetration levels," Sustainable Energy, Grids and Networks, vol. 35, p. 101120, 2023.
- [30] H. Shareef, M. M. Islam, and A. Mohamed, "A review of the stage-of-the-art charging technologies, placement methodologies, and impacts of electric vehicles," *Renewable and Sustainable Energy Reviews*, vol. 64, pp. 403–420, 2016.
- [31] M. Amjad, A. Ahmad, M. H. Rehmani, and T. Umer, "A review of evs charging: From the perspective of energy optimization, optimization approaches, and charging techniques," *Transportation Research Part D: Transport and Environment*, vol. 62, pp. 386–417, 2018.

- [32] Z. Yang, K. Li, and A. Foley, "Computational scheduling methods for integrating plug-in electric vehicles with power systems: A review," *Renewable and Sustainable Energy Reviews*, vol. 51, pp. 396–416, 2015.
- [33] Q. Wang, X. Liu, J. Du, and F. Kong, "Smart charging for electric vehicles: A survey from the algorithmic perspective," *IEEE Communications Surveys Tutorials*, vol. 18, no. 2, pp. 1500–1517, 2016
- [34] S. Salhi and J. Thompson, "An overview of heuristics and metaheuristics," in *The Palgrave Handbook of Operations Research*, S. Salhi and J. Boylan, Eds. Palgrave Macmillan, Cham, 2022, pp. 353–403.
- [35] I. Rahman, P. M. Vasant, B. S. M. Singh, M. Abdullah-Al-Wadud, and N. Adnan, "Review of recent trends in optimization techniques for plug-in hybrid, and electric vehicle charging infrastructures," *Renewable and Sustainable Energy Reviews*, vol. 58, pp. 1039–1047, 2016.
- [36] P. Zhang, F. Yan, and C. Du, "A comprehensive analysis of energy management strategies for hybrid electric vehicles based on bibliometrics," *Renewable and Sustainable Energy Reviews*, vol. 48, pp. 88–104, 2015.
- [37] K. E. Adetunji, I. W. Hofsajer, A. M. Abu-Mahfouz, and L. Cheng, "A review of metaheuristic techniques for optimal integration of electrical units in distribution networks," *IEEE Access*, vol. 9, pp. 5046–5068, 2021.
- [38] N. I. Nimalsiri, C. P. Mediwaththe, E. L. Ratnam, M. Shaw, D. B. Smith, and S. K. Halgamuge, "A survey of algorithms for distributed charging control of electric vehicles in smart grid," *IEEE Transactions on Intelligent Transportation Systems*, vol. 21, no. 11, pp. 4497–4515, 2020.
- [39] J. García-Villalobos, I. Zamora, J. San Martín, F. Asensio, and V. Aperribay, "Plug-in electric vehicles in electric distribution networks: A review of smart charging approaches," *Renewable* and Sustainable Energy Reviews, vol. 38, pp. 717–731, 2014.
- [40] J. C. Mukherjee and A. Gupta, "A review of charge scheduling of electric vehicles in smart grid," *IEEE Systems Journal*, vol. 9, no. 4, pp. 1541–1553, 2015.
- [41] J. Hu, H. Morais, T. Sousa, and M. Lind, "Electric vehicle fleet management in smart grids: A review of services, optimization and control aspects," *Renewable and Sustainable Energy Reviews*, vol. 56, pp. 1207–1226, 2016.
- [42] Open Charge Alliance, "OSCP 2.0 Specification," Open Charge Alliance, Standard, 10 2020. [Online]. Available: https://www.openchargealliance.org/protocols/oscp-20/
- [43] U. Herberg, J. Zuber, D. Mashima, and R. Bienert, "OpenADR 2.0 Profile Specification B Profile," The OpenADR Alliance, Standard, 11 2015. [Online]. Available: https://www.openadr.org/specification
- [44] Open Charge Alliance, "OCPP 2.0.1: Part 1 Architecture Topology," Open Charge Alliance, Arnhem, Standard, 3 2020. [Online]. Available: https://www.openchargealliance.org/protocols/ocpp-201/
- [45] "IEC 61851-1:2017 Electric vehicle conductive charging system Part 1: General requirements," The International Electrotechnical Commission (IEC), Geneva, Switzerland, Standard, 2 2017. [Online]. Available: https://webstore.iec.ch/en/publication/33644
- [46] "INTERNATIONAL STANDARD ISO 15118-1, Road vehicles Vehicle-to-Grid Communication Interface Part 1: General information and use-case definition," International Organization for Standardization, Standard, 2013. [Online]. Available: https://www.iso.org/home.html
- [47] "INTERNATIONAL STANDARD ISO 15118-2, Road vehicles Vehicle-to-Grid Communication Interface Part 2: Network and application protocol requirements," International Organization for Standardization, Standard, 2014. [Online]. Available: https://www.iso.org/home.html
- [48] "INTERNATIONAL STANDARD ISO 15118-3, Road vehicles Vehicle-to-Grid Communication

- Interface Part 3: Physical and data link layer requirements," International Organization for Standardization, Standard, 2015. [Online]. Available: https://www.iso.org/home.html
- [49] A. Dubey and S. Santoso, "Electric vehicle charging on residential distribution systems: Impacts and mitigations," *IEEE Access*, vol. 3, pp. 1871–1893, 2015.
- [50] D. Steen, L. A. Tuan, O. Carlson, and L. Bertling, "Assessment of electric vehicle charging scenarios based on demographical data," *IEEE Transactions on Smart Grid*, vol. 3, no. 3, pp. 1457–1468, 2012.
- [51] J. E. Cardona, J. C. López, and M. J. Rider, "Decentralized electric vehicles charging coordination using only local voltage magnitude measurements," *Electric Power Systems Research*, vol. 161, pp. 139–151, 2018.
- [52] F. Lehfuss and M. Nöhrer, "Evaluation of different control algorithm with low-level communication requirements to increase the maximum electric vehicle penetration," vol. 2017, no. 1, 2017, pp. 1750–1754.
- [53] E. Ucer, M. C. Kisacikoglu, M. Yuksel, and A. C. Gurbuz, "An internet-inspired proportional fair ev charging control method," *IEEE Systems Journal*, vol. 13, no. 4, pp. 4292–4302, 2019.
- [54] J.-M. Clairand, J. Rodríguez-García, and C. Álvarez Bel, "Smart charging for electric vehicle aggregators considering users' preferences," *IEEE Access*, vol. 6, pp. 54624–54635, 2018.
- [55] M. Kefayati and R. Baldick, "Harnessing demand flexibility to match renewable production using localized policies," in 2012 50th Annual Allerton Conference on Communication, Control, and Computing (Allerton). IEEE, 2012, pp. 1105–1109.
- [56] Y.-T. Liao and C.-N. Lu, "Dispatch of ev charging station energy resources for sustainable mobility," *IEEE Transactions on Transportation Electrification*, vol. 1, no. 1, pp. 86–93, 2015.
- [57] B. Vaidya and H. T. Mouftah, "Smart electric vehicle charging management for smart cities," IET Smart Cities, vol. 2, no. 1, pp. 4–13, 2020.
- [58] M. Zeballos, A. Ferragut, and F. Paganini, "Proportional fairness for ev charging in overload," IEEE Transactions on Smart Grid, vol. 10, no. 6, pp. 6792–6801, 2019.
- [59] z. liu, Q. Wu, M. Shahidehpour, C. Li, S. Huang, and W. Wei, "Transactive real-time electric vehicle charging management for commercial buildings with pv on-site generation," *IEEE Transactions on Smart Grid*, vol. 10, no. 5, pp. 4939–4950, 2019.
- [60] Q. Yan, B. Zhang, and M. Kezunovic, "Optimized operational cost reduction for an ev charging station integrated with battery energy storage and pv generation," *IEEE Transactions on Smart Grid*, vol. 10, no. 2, pp. 2096–2106, 2019.
- [61] G. R. Chandra Mouli, M. Kefayati, R. Baldick, and P. Bauer, "Integrated pv charging of ev fleet based on energy prices, v2g, and offer of reserves," *IEEE Transactions on Smart Grid*, vol. 10, no. 2, pp. 1313–1325, 2019.
- [62] O. Frendo, N. Gaertner, and H. Stuckenschmidt, "Real-time smart charging based on precomputed schedules," *IEEE Transactions on Smart Grid*, vol. 10, no. 6, pp. 6921–6932, 2019.
- [63] K. Zhou and L. Cai, "Randomized phev charging under distribution grid constraints," IEEE Transactions on Smart Grid, vol. 5, no. 2, pp. 879–887, 2014.
- [64] K. N. Kumar, B. Sivaneasan, and P. L. So, "Impact of priority criteria on electric vehicle charge scheduling," *IEEE Transactions on Transportation Electrification*, vol. 1, no. 3, pp. 200–210, 2015.
- [65] S. Yang, S. Zhang, and J. Ye, "A novel online scheduling algorithm and hierarchical protocol for large-scale ev charging coordination," *IEEE Access*, vol. 7, pp. 101 376–101 387, 2019.
- [66] S. I. Vagropoulos, D. K. Kyriazidis, and A. G. Bakirtzis, "Real-time charging management framework for electric vehicle aggregators in a market environment," *IEEE Transactions on Smart Grid*, vol. 7, no. 2, pp. 948–957, 2016.

- [67] D. Wu, H. Zeng, C. Lu, and B. Boulet, "Two-stage energy management for office buildings with workplace ev charging and renewable energy," *IEEE Transactions on Transportation Elec*trification, vol. 3, no. 1, pp. 225–237, 2017.
- [68] P. Bons, A. Buatois, G. Ligthart, R. van den Hoed, and J. Warmerdam, "Final report amsterdam flexpower operational pilot: A detailed analysis of the effects of applying a static smart charging profile for public charging infrastructure." Interreg, North Sea Region, Amsterdam University of Applied Science, Nuon, Liander and ElaadNL, Tech. Rep., 7 2020, accessed: 2023-02-28. [Online]. Available: https://research.hva.nl/en/publications/
- [69] The InterFlex consortium, "Interflex: Local use of flexibilities for an increasing share of renewable on the distribution grid," 2020, accessed: 2023-02-28. [Online]. Available: https://interflex-h2020.com/
- [70] INVADE, "Smart system of renewable energy storage based on integrated evs and batteries to empower mobile, distributed and centralised energy storage in the distribution grid," 2020, accessed: 2023-02-28. [Online]. Available: https://h2020invade.eu/
- [71] P. C. Bons, A. Buatois, G. Ligthart, F. Geerts, N. Piersma, and R. van den Hoed, "Impact of smart charging for consumers in a real world pilot," World Electric Vehicle Journal, vol. 11, no. 1, 2020.
- [72] Z. J. Lee, G. Lee, T. Lee, C. Jin, R. Lee, Z. Low, D. Chang, C. Ortega, and S. H. Low, "Adaptive charging networks: A framework for smart electric vehicle charging," *IEEE Transactions on Smart Grid*, vol. 12, no. 5, pp. 4339–4350, 2021.
- [73] G. Rajendran, C. A. Vaithilingam, N. Misron, K. Naidu, and M. R. Ahmed, "A comprehensive review on system architecture and international standards for electric vehicle charging stations," *Journal of Energy Storage*, vol. 42, p. 103099, 2021.
- [74] H. Das, M. Rahman, S. Li, and C. Tan, "Electric vehicles standards, charging infrastructure, and impact on grid integration: A technological review," *Renewable and Sustainable Energy Reviews*, vol. 120, p. 109618, 2020.
- [75] L. Schriewer and J. Farkas, "Importance of interoperability for a seamless ev charging experience," in 36th International Electric Vehicle Symposium and Exhibition (EVS36), 2023, pp. 766-772.
- [76] E. ElGhanam, M. Hassan, A. Osman, and I. Ahmed, "Review of communication technologies for electric vehicle charging management and coordination," World Electric Vehicle Journal, vol. 12, no. 3, 2021.
- [77] B. Kirpes, P. Danner, R. Basmadjian, H. d. Meer, and C. Becker, "E-mobility systems architecture: a model-based framework for managing complexity and interoperability," *Energy Informatics*, vol. 2, pp. 1–31, 2019.
- [78] E. García-Martínez, J. F. Sanz, J. Muñoz-Cruzado, and J. M. Perié, "A review of phil testing for smart grids - selection guide, classification and online database analysis," *Electronics*, vol. 9, no. 3, 2020.
- [79] Open Charge Alliance, "OCPP 2.0.1: Part 2 Specifications," Open Charge Alliance, Arnhem, Standard, 12 2022. [Online]. Available: https://www.openchargealliance.org/protocols/ocpp-201/
- [80] K. Rauma, T. Simolin, A. Rautiainen, P. Järventausta, and C. Rehtanz, "Overcoming non-idealities in electric vehicle charging management," *IET Electrical Systems in Transportation*, vol. 11, no. 4, pp. 310–321, 2021.
- [81] K. J. Dyke, N. Schofield, and M. Barnes, "The impact of transport electrification on electrical networks," *IEEE Transactions on Industrial Electronics*, vol. 57, no. 12, pp. 3917–3926, 2010.
- [82] K. Clement-Nyns, E. Haesen, and J. Driesen, "The impact of charging plug-in hybrid electric vehicles on a residential distribution grid," *IEEE Transactions on Power Systems*, vol. 25, no. 1,

- pp. 371-380, 2010.
- [83] J. Xiong, K. Zhang, Y. Guo, and W. Su, "Investigate the impacts of pev charging facilities on integrated electric distribution system and electrified transportation system," *IEEE Transactions on Transportation Electrification*, vol. 1, no. 2, pp. 178–187, 2015.
- [84] M. A. Awadallah, B. N. Singh, and B. Venkatesh, "Impact of ev charger load on distribution network capacity: A case study in toronto," Canadian Journal of Electrical and Computer Engineering, vol. 39, no. 4, pp. 268–273, 2016.
- [85] H. Turker, S. Bacha, and A. Hably, "Rule-based charging of plug-in electric vehicles (pevs): Impacts on the aging rate of low-voltage transformers," *IEEE Transactions on Power Delivery*, vol. 29, no. 3, pp. 1012–1019, 2014.
- [86] M. K. Gray and W. G. Morsi, "Power quality assessment in distribution systems embedded with plug-in hybrid and battery electric vehicles," *IEEE Transactions on Power Systems*, vol. 30, no. 2, pp. 663–671, 2015.
- [87] M. F. Shaaban, Y. M. Atwa, and E. F. El-Saadany, "Pevs modeling and impacts mitigation in distribution networks," *IEEE Transactions on Power Systems*, vol. 28, no. 2, pp. 1122–1131, 2013.
- [88] C. Jiang, R. Torquato, D. Salles, and W. Xu, "Method to assess the power-quality impact of plugin electric vehicles," *IEEE Transactions on Power Delivery*, vol. 29, no. 2, pp. 958–965, 2014.
- [89] R.-C. Leou, C.-L. Su, and C.-N. Lu, "Stochastic analyses of electric vehicle charging impacts on distribution network," *IEEE Transactions on Power Systems*, vol. 29, no. 3, pp. 1055–1063, 2014.
- [90] L. Pieltain Fernández, T. Gomez San Roman, R. Cossent, C. Mateo Domingo, and P. Frías, "Assessment of the impact of plug-in electric vehicles on distribution networks," *IEEE Transactions on Power Systems*, vol. 26, no. 1, pp. 206–213, 2011.
- [91] D. Steen, L. A. Tuan, O. Carlson, and L. Bertling, "Assessment of electric vehicle charging scenarios based on demographical data," *IEEE Transactions on Smart Grid*, vol. 3, no. 3, pp. 1457–1468, 2012.
- [92] C. Crozier, T. Morstyn, and M. McCulloch, "The opportunity for smart charging to mitigate the impact of electric vehicles on transmission and distribution systems," *Applied Energy*, vol. 268, p. 114973, 2020.
- [93] "Synthetic load profiles," Power Clearing Settlement Austria (APCS), accessed: 2021-04-20. [Online]. Available: https://www.apcs.at/
- [94] "Standardlastprofile strom," Bundesverband der Energie-und Wasserwirtschaft (BDEW), accessed: 2021-07-13. [Online]. Available: https://www.bdew.de/
- [95] "verbruiksprofielen-profielen 2018," De Vereniging Nederlandse EnergieDataUitwisseling (NEDU), Accessed: 2022-12-06; Old site: https://www.nedu.nl; switch to new site from 2021. [Online]. Available: www.mffbas.nl
- [96] "PVwatts calculator," NREL, accessed: 2021-04-20. [Online]. Available: https://pvwatts.nrel.
- [97] "Zonnestroom; vermogen bedrijven en woningen, regio(indeling 2018),2012-2018," Centraal Bureau voor de Statistiek, accessed: 2021-04-20. [Online]. Available: https://opendata.cbs.nl
- [98] "Factsheets zon," Rijksdienst voor Ondernemend Nederland (RVO), accessed: 2021-04-20.
 [Online]. Available: https://www.rvo.nl
- [99] "Regionale kerncijfers nederland," Centraal Bureau voor de Statistiek, accessed: 2021-04-20. [Online]. Available: https://opendata.cbs.nl
- [100] G. C. Mouli, P. Bauer, and M. Zeman, "System design for a solar powered electric vehicle charging station for workplaces," *Applied Energy*, vol. 168, pp. 434–443, 2016.

- [101] "Energie umwelt innovation mobilitaet kraftfahrzeuge-neuzulassungen," Statistik Austria, accessed: 2021-04-20. [Online]. Available: https://www.statistik.at/
- [102] "Autobezit naar regio en persoonskenmerken, 2018," Centraal Bureau voor de Statistiek (CBS), accessed: 2021-04-20. [Online]. Available: https://www.cbs.nl
- [103] Y. Yu, A. Shekhar, G. C. R. Mouli, P. Bauer, N. Refa, and R. Bernards, "Impact of uncontrolled charging with mass deployment of electric vehicles on low voltage distribution networks," in 2020 IEEE Transportation Electrification Conference Expo (ITEC), 2020, pp. 766–772.
- [104] N. Refa and N. Hubbers, "Impact of smart charging on evs charging behaviour assessed from real charging events." Lyon, France: 32th International Electric Vehicle Symposium, 2019, pp. 1–10.
- [105] "Statistics electric vehicles and charging in the netherlands up to and including november 2018," Rijksdienst voor Ondernemend Nederland (RVO), accessed: 2021-04-20. [Online]. Available: https://www.rvo.nl
- [106] "Neuzulassungen nach umwelt-merkmalen (fz 14) (New registrations according to environmental characteristics)," Kraftfahrt-Bundesamt (KBA), accessed: 2021-04-20. [Online]. Available: https://www.kba.de
- [107] S. K. R. F. G. J. G. K. S. Tomschy.R., Herry.M., "Österreich unterwegs 2013/2014 (Results report for the Austria-wide Mobility survey "Austria on the move 2013/2014")," Bundesministerium für Verkehr, Innovation und Technologie, et al., Wien, Tech. Rep., 2016.
- [108] T. Schlößer, E. Tröster, and L. Hülsmann, "Probabilistic modeling of charging profiles in low voltage networks." Stockholm, Sweden: 2nd E-Mobility Power System Integration Symposium, 2018.
- [109] "Elaad open data platform, 2018," Elaad, accessed: 2021-05-11. [Online]. Available: https://platform.elaad.io/
- [110] "EN-50160 voltage characteristics of electricity supplied by public electricity networks," European Committee for Electrotechnical Standardization, Standard, 2010.
- [111] A. Dubey and S. Santoso, "Electric vehicle charging on residential distribution systems: Impacts and mitigations," *IEEE Access*, vol. 3, pp. 1871–1893, 2015.
- [112] J. Stiasny, T. Zufferey, G. Pareschi, D. Toffanin, G. Hug, and K. Boulouchos, "Sensitivity analysis of electric vehicle impact on low-voltage distribution grids," *Electric Power Systems Research*, vol. 191, p. 106696, 2021.
- [113] N. I. Nimalsiri, C. P. Mediwaththe, E. L. Ratnam, M. Shaw, D. B. Smith, and S. K. Halgamuge, "A survey of algorithms for distributed charging control of electric vehicles in smart grid," *IEEE Transactions on Intelligent Transportation Systems*, vol. 21, no. 11, pp. 4497–4515, 2020.
- [114] M. T. Hussain, D. N. B. Sulaiman, M. S. Hussain, and M. Jabir, "Optimal management strategies to solve issues of grid having electric vehicles (ev): A review," *Journal of Energy Storage*, vol. 33, p. 102114, 2021.
- [115] M. H. Mobarak and J. Bauman, "Vehicle-directed smart charging strategies to mitigate the effect of long-range ev charging on distribution transformer aging," *IEEE Transactions on Transportation Electrification*, vol. 5, no. 4, pp. 1097–1111, 2019.
- [116] P. Dimitroulis and M. Alamaniotis, "A fuzzy logic energy management system of on-grid electrical system for residential prosumers," *Electric Power Systems Research*, vol. 202, p. 107621, 2022.
- [117] P. Hogeveen, M. Steinbuch, G. Verbong, and A. Wargers, "Revisiting static charge schedules for electric vehicles as temporary solution to low-voltage grid congestion with recent charging and grid data," Sustainable Energy, Grids and Networks, vol. 31, p. 100701, 2022.

- [118] Y. Cao, S. Tang, C. Li, P. Zhang, Y. Tan, Z. Zhang, and J. Li, "An optimized ev charging model considering tou price and soc curve," *IEEE Transactions on Smart Grid*, vol. 3, no. 1, pp. 388–393, 2012.
- [119] P. Olivella-Rosell, R. Villafafila-Robles, A. Sumper, and J. Bergas-Jané, "Probabilistic agent-based model of electric vehicle charging demand to analyse the impact on distribution networks," *Energies*, vol. 8, no. 5, p. 4160–4187, May 2015.
- [120] E. Veldman and R. A. Verzijlbergh, "Distribution grid impacts of smart electric vehicle charging from different perspectives," *IEEE Transactions on Smart Grid*, vol. 6, no. 1, pp. 333–342, 2015.
- [121] A. S. B. Humayd and K. Bhattacharya, "A novel framework for evaluating maximum pev penetration into distribution systems," *IEEE Transactions on Smart Grid*, vol. 9, no. 4, pp. 2741–2751, 2018.
- [122] S. Zaferanlouei, V. Lakshmanan, S. Bjarghov, H. Farahmand, and M. Korpås, "Battpower application: Large-scale integration of evs in an active distribution grid–a norwegian case study," *Electric Power Systems Research*, vol. 209, p. 107967, 2022.
- [123] S. Fahmy, R. Gupta, and M. Paolone, "Grid-aware distributed control of electric vehicle charging stations in active distribution grids," *Electric Power Systems Research*, vol. 189, p. 106697, 2020.
- [124] N. Leemput, F. Geth, J. Van Roy, A. Delnooz, J. Büscher, and J. Driesen, "Impact of electric vehicle on-board single-phase charging strategies on a flemish residential grid," *IEEE Transac*tions on Smart Grid, vol. 5, no. 4, pp. 1815–1822, 2014.
- [125] "Phase-wise enhanced voltage support from electric vehicles in a danish low-voltage distribution grid," *Electric Power Systems Research*, vol. 140, pp. 274–283, 2016.
- [126] A. T. Al-Awami, E. Sortomme, G. M. Asim Akhtar, and S. Faddel, "A voltage-based controller for an electric-vehicle charger," *IEEE Transactions on Vehicular Technology*, vol. 65, no. 6, pp. 4185–4196, 2016.
- [127] S. Faddel, A. A. Mohamed, and O. A. Mohammed, "Fuzzy logic-based autonomous controller for electric vehicles charging under different conditions in residential distribution systems," *Electric Power Systems Research*, vol. 148, pp. 48–58, 2017.
- [128] J. Van Roy, N. Leemput, F. Geth, R. Salenbien, J. Büscher, and J. Driesen, "Apartment building electricity system impact of operational electric vehicle charging strategies," *IEEE Transactions* on Sustainable Energy, vol. 5, no. 1, pp. 264–272, 2014.
- [129] W. Tushar, C. Yuen, S. Huang, D. B. Smith, and H. V. Poor, "Cost minimization of charging stations with photovoltaics: An approach with ev classification," *IEEE Transactions on Intelligent Transportation Systems*, vol. 17, no. 1, pp. 156–169, 2016.
- [130] G. R. C. Mouli, J. Kaptein, P. Bauer, and M. Zeman, "Implementation of dynamic charging and v2g using chademo and ccs/combo dc charging standard," in 2016 IEEE Transportation Electrification Conference and Expo (ITEC), 2016, pp. 1–6.
- [131] J. Hu, R. Harmsen, W. Crijns-Graus, E. Worrell, and M. van den Broek, "Identifying barriers to large-scale integration of variable renewable electricity into the electricity market: A literature review of market design," *Renewable and Sustainable Energy Reviews*, vol. 81, pp. 2181–2195, 2018.
- [132] "Day-ahead prices," ENTSO-E Transparency Platform, accessed: 2021-08-19. [Online]. Available: https://transparency.entsoe.eu/
- [133] "Congestion management research zeeland," TenneT TSO B.V., C1 Public Information, 02 2021, Reference: PU-AMN. [Online]. Available: https://netztransparenz.tennet.eu/
- [134] Y. Yu, D. Reihs, S. Wagh, A. Shekhar, D. Stahleder, G. R. C. Mouli, F. Lehfuss, and P. Bauer, "Data-driven study of low voltage distribution grid behaviour with increasing electric vehicle penetration," *IEEE Access*, vol. 10, pp. 6053–6070, 2022.

- [135] X. Zhang, Y. Liu, H. Gao, L. Wang, and J. Liu, "A bi-level corrective line switching model for urban power grid congestion mitigation," *IEEE Transactions on Power Systems*, vol. 35, no. 4, pp. 2959–2970, 2020.
- [136] A. S. Bouhouras, G. C. Christoforidis, C. Parisses, and D. P. Labridis, "Reducing network congestion in distribution networks with high dg penetration via network reconfiguration," in 11th International Conference on the European Energy Market (EEM14), 2014, pp. 1–5.
- [137] S. C. Shabshab, P. A. Lindahl, J. K. Nowocin, J. Donnal, D. Blum, L. Norford, and S. B. Leeb, "Demand smoothing in military microgrids through coordinated direct load control," *IEEE Transactions on Smart Grid*, vol. 11, no. 3, pp. 1917–1927, 2020.
- [138] L. Zhang, Y. Tang, T. Zhou, C. Tang, H. Liang, and J. Zhang, "Research on flexible smart home appliance load participating in demand side response based on power direct control technology," *Energy Reports*, vol. 8, pp. 424–434, 2022.
- [139] S. Huang, Q. Wu, M. Shahidehpour, and Z. liu, "Dynamic power tariff for congestion management in distribution networks," *IEEE Transactions on Smart Grid*, vol. 10, no. 2, pp. 2148–2157, 2019.
- [140] M. A. Fotouhi Ghazvini, G. Lipari, M. Pau, F. Ponci, A. Monti, J. Soares, R. Castro, and Z. Vale, "Congestion management in active distribution networks through demand response implementation," Sustainable Energy, Grids and Networks, vol. 17, p. 100185, 2019.
- [141] G. G. Dranka and P. Ferreira, "Review and assessment of the different categories of demand response potentials," *Energy*, vol. 179, pp. 280–294, 2019.
- [142] X. Gong, E. Castillo-Guerra, J. L. Cardenas-Barrera, B. Cao, S. A. Saleh, and L. Chang, "Robust hierarchical control mechanism for aggregated thermostatically controlled loads," *IEEE Transactions on Smart Grid*, vol. 12, no. 1, pp. 453–467, 2021.
- [143] J. Hu, G. Yang, H. W. Bindner, and Y. Xue, "Application of network-constrained transactive control to electric vehicle charging for secure grid operation," *IEEE Transactions on Sustainable Energy*, vol. 8, no. 2, pp. 505–515, 2017.
- [144] F. Shen, S. Huang, Q. Wu, S. Repo, Y. Xu, and J. Østergaard, "Comprehensive congestion management for distribution networks based on dynamic tariff, reconfiguration, and re-profiling product," *IEEE Transactions on Smart Grid*, vol. 10, no. 5, pp. 4795–4805, 2019.
- [145] J. Zhao, Y. Wang, G. Song, P. Li, C. Wang, and J. Wu, "Congestion management method of low-voltage active distribution networks based on distribution locational marginal price," *IEEE Access*, vol. 7, pp. 32 240–32 255, 2019.
- [146] Z. Liu, Q. Wu, S. S. Oren, S. Huang, R. Li, and L. Cheng, "Distribution locational marginal pricing for optimal electric vehicle charging through chance constrained mixed-integer programming," *IEEE Transactions on Smart Grid*, vol. 9, no. 2, pp. 644–654, 2018.
- [147] A. Asrari, M. Ansari, J. Khazaei, and P. Fajri, "A market framework for decentralized congestion management in smart distribution grids considering collaboration among electric vehicle aggregators," *IEEE Transactions on Smart Grid*, vol. 11, no. 2, pp. 1147–1158, 2020.
- [148] E. Ucer, M. C. Kisacikoglu, and M. Yuksel, "Decentralized additive increase and multiplicative decrease-based electric vehicle charging," *IEEE Systems Journal*, vol. 15, no. 3, pp. 4272–4280, 2021.
- [149] A. A. Zishan, M. M. Haji, and O. Ardakanian, "Adaptive congestion control for electric vehicle charging in the smart grid," *IEEE Transactions on Smart Grid*, vol. 12, no. 3, pp. 2439–2449, 2021.
- [150] O. G. M. Khan, A. Youssef, M. Salama, and E. El-Saadany, "Robust multi-objective congestion management in distribution network," *IEEE Transactions on Power Systems*, pp. 1–11, 2022.
- [151] C. García Veloso, K. Rauma, J. Fernández, and C. Rehtanz, "Real-time control of plug-in electric vehicles for congestion management of radial lv networks: A comparison of implementations,"

- Energies, vol. 13, no. 16, 2020.
- [152] E. Dehnavi, S. Afsharnia, A. A. S. Akmal, and M. Moeini-Aghtaie, "A novel congestion management method through power system partitioning," *Electric Power Systems Research*, vol. 213, p. 108672, 2022.
- [153] A. Baczyńska and W. Niewiadomski, "Power flow tracing for active congestion management in modern power systems," *Energies*, vol. 13, no. 18, 2020.
- [154] K. Prakash, M. Ali, M. Siddique, A. Karmaker, C. Macana, D. Dong, and H. Pota, "Bi-level planning and scheduling of electric vehicle charging stations for peak shaving and congestion management in low voltage distribution networks," *Computers and Electrical Engineering*, vol. 102, p. 108235, 2022.
- [155] L. Liu and K. Zhou, "Electric vehicle charging scheduling considering urgent demand under different charging modes," *Energy*, vol. 249, p. 123714, 2022.
- [156] S. Xie, W. Zhong, K. Xie, R. Yu, and Y. Zhang, "Fair energy scheduling for vehicle-to-grid networks using adaptive dynamic programming," *IEEE Transactions on Neural Networks and Learning Systems*, vol. 27, no. 8, pp. 1697–1707, 2016.
- [157] D. Danner and H. de Meer, "Quality of service and fairness for electric vehicle charging as a service," *Energy Informatics*, vol. 4, no. 3, pp. 1–20, 2021.
- [158] X. Cheng and T. Overbye, "PTDF-based power system equivalents," *IEEE Transactions on Power Systems*, vol. 20, no. 4, pp. 1868–1876, 2005.
- [159] R. Baldick, "Variation of distribution factors with loading," *IEEE Transactions on Power Systems*, vol. 18, no. 4, pp. 1316–1323, 2003.
- [160] F. Ahmad, A. Rasool, E. Ozsoy, R. Sekar, A. Sabanovic, and M. Elitaş, "Distribution system state estimation-a step towards smart grid," *Renewable and Sustainable Energy Reviews*, vol. 81, pp. 2659–2671, 2018.
- [161] B. Hekkelman and H. la Poutré, "Fairness in smart grid congestion management," in 2019 IEEE PES Innovative Smart Grid Technologies Europe (ISGT-Europe), 2019, pp. 1–5.
- [162] A. H. Einaddin and A. S. Yazdankhah, "A novel approach for multi-objective optimal scheduling of large-scale ev fleets in a smart distribution grid considering realistic and stochastic modeling framework," *International Journal of Electrical Power Energy Systems*, vol. 117, p. 105617, 2020.
- [163] Q. Huang, Q.-S. Jia, and X. Guan, "Robust scheduling of ev charging load with uncertain wind power integration," *IEEE Transactions on Smart Grid*, vol. 9, no. 2, pp. 1043–1054, 2018.
- [164] F. Ahmad, M. S. Alam, S. M. Shariff, and M. Krishnamurthy, "A cost-efficient approach to ev charging station integrated community microgrid: A case study of indian power market," *IEEE Transactions on Transportation Electrification*, vol. 5, no. 1, pp. 200–214, 2019.
- [165] R. Fachrizal, M. Shepero, D. van der Meer, J. Munkhammar, and J. Widén, "Smart charging of electric vehicles considering photovoltaic power production and electricity consumption: A review," eTransportation, vol. 4, p. 100056, 2020.
- [166] Y. Wu, Z. Wang, Y. Huangfu, A. Ravey, D. Chrenko, and F. Gao, "Hierarchical operation of electric vehicle charging station in smart grid integration applications —an overview," *International Journal of Electrical Power Energy Systems*, vol. 139, p. 108005, 2022.
- [167] S. Pirouzi, M. A. Latify, and G. R. Yousefi, "Conjugate active and reactive power management in a smart distribution network through electric vehicles: A mixed integer-linear programming model," Sustainable Energy, Grids and Networks, vol. 22, p. 100344, 2020.
- [168] J. Su, T. Lie, and R. Zamora, "A rolling horizon scheduling of aggregated electric vehicles charging under the electricity exchange market," *Applied Energy*, vol. 275, p. 115406, 2020.

- [169] Y. Cao, L. Huang, Y. Li, K. Jermsittiparsert, H. Ahmadi-Nezamabad, and S. Nojavan, "Optimal scheduling of electric vehicles aggregator under market price uncertainty using robust optimization technique," *International Journal of Electrical Power Energy Systems*, vol. 117, p. 105628, 2020.
- [170] O. Frendo, N. Gaertner, and H. Stuckenschmidt, "Real-time smart charging based on precomputed schedules," *IEEE Transactions on Smart Grid*, vol. 10, no. 6, pp. 6921–6932, 2019.
- [171] I. Şengör, A. K. Erenoğlu, O. Erdinç, A. Taşcıkaraoğlu, and J. P. Catalão, "Day-ahead charging operation of electric vehicles with on-site renewable energy resources in a mixed integer linear programming framework," *IET Smart Grid*, vol. 3, no. 3, pp. 367–375, 2020.
- [172] G. Zhang, S. T. Tan, and G. G. Wang, "Real-time smart charging of electric vehicles for demand charge reduction at non-residential sites," *IEEE Transactions on Smart Grid*, vol. 9, no. 5, pp. 4027–4037, 2018.
- [173] M. Zweistra, S. Janssen, and F. Geerts, "Large scale smart charging of electric vehicles in practice," *Energies*, vol. 13, no. 2, 2020.
- [174] G. C. Wang, E. Ratnam, H. V. Haghi, and J. Kleissl, "Corrective receding horizon ev charge scheduling using short-term solar forecasting," *Renewable Energy*, vol. 130, pp. 1146–1158, 2019.
- [175] P. Sharifi, A. Banerjee, and M. J. Feizollahi, "Leveraging owners' flexibility in smart charge/discharge scheduling of electric vehicles to support renewable energy integration," *Computers Industrial Engineering*, vol. 149, p. 106762, 2020.
- [176] A. Zecchino, S. D'Arco, A. G. Endegnanew, M. Korpås, and M. Marinelli, "Enhanced primary frequency control from evs: a fleet management strategy to mitigate effects of response discreteness," *IET Smart Grid*, vol. 2, no. 3, pp. 436–444, 2019.
- [177] M. Saeedirad, E. Rokrok, and M. Joorabian, "A smart discrete charging method for optimum electric vehicles integration in the distribution system in presence of demand response program," *Journal of Energy Storage*, vol. 47, p. 103577, 2022.
- [178] M. H. Schoot Uiterkamp, M. E. Gerards, and J. L. Hurink, "Online electric vehicle charging with discrete charging rates," Sustainable Energy, Grids and Networks, vol. 25, p. 100423, 2021.
- [179] M. D. Omar Faruque, T. Strasser, G. Lauss, V. Jalili-Marandi, P. Forsyth, C. Dufour, V. Dinavahi, A. Monti, P. Kotsampopoulos, J. A. Martinez, K. Strunz, M. Saeedifard, X. Wang, D. Shearer, and M. Paolone, "Real-time simulation technologies for power systems design, testing, and analysis," *IEEE Power and Energy Technology Systems Journal*, vol. 2, no. 2, pp. 63–73, 2015.
- [180] G. F. Lauss, M. O. Faruque, K. Schoder, C. Dufour, A. Viehweider, and J. Langston, "Characteristics and design of power hardware-in-the-loop simulations for electrical power systems," *IEEE Transactions on Industrial Electronics*, vol. 63, no. 1, pp. 406–417, 2016.
- [181] A. Shekhar, G. Rituraj, R. Van Der Sande, M. Ahmadi, R. Deshmukh, P. Bauer, V. Nougain, A. Lekić, and P. Palensky, "Development of reliable power electronic systems using real time digital twin based power hardware-in-the-loop testbed," in 2023 IEEE Belgrade PowerTech, 2023, pp. 1–6.
- [182] S. Ledinger, D. Reihs, D. Stahleder, and F. Lehfuss, "Test device for electric vehicle grid integration," in 2018 IEEE International Conference on Environment and Electrical Engineering and 2018 IEEE Industrial and Commercial Power Systems Europe (EEEIC / ICPS Europe), 2018, pp. 1–5.
- [183] M. Hosseinzadehtaher, D. Tiwari, N. Kouchakipour, A. Momeni, M. Lelic, and Z. Wu, "Grid resilience assessment during extreme fast charging of electric vehicles via developed power hardware-in-the-loop," in 2022 IEEE Transportation Electrification Conference Expo (ITEC), 2022, pp. 929–934.
- [184] C. Flack, E. Ucer, C. P. Smith, and M. Kisacikoglu, "Controller hardware-in-the-loop (c-hil) testing of decentralized ev-grid integration," in 2022 IEEE Power Energy Society General Meeting

- (PESGM), 2022, pp. 01-05.
- [185] V. Lakshminarayanan, V. G. S. Chemudupati, S. K. Pramanick, and K. Rajashekara, "Real-time optimal energy management controller for electric vehicle integration in workplace microgrid," *IEEE Transactions on Transportation Electrification*, vol. 5, no. 1, pp. 174–185, 2019.
- [186] A. Marinescu, A. Taylor, S. Clarke, I. Serban, and C. Marinescu, "Optimising residential electric vehicle charging under renewable energy: Multi-agent learning in software simulation and hardware-in-the-loop evaluation," *International Journal of Energy Research*, vol. 43, no. 8, pp. 3853–3868, 2019.
- [187] F. Arraño-Vargas and G. Konstantinou, "Modular design and real-time simulators toward power system digital twins implementation," *IEEE Transactions on Industrial Informatics*, vol. 19, no. 1, pp. 52–61, 2023.
- [188] M. Zhou, J. Yan, and D. Feng, "Digital twin framework and its application to power grid online analysis," *CSEE Journal of Power and Energy Systems*, vol. 5, no. 3, pp. 391–398, 2019.
- [189] T. Simolin, K. Rauma, A. Rautiainen, P. Järventausta, and C. Rehtanz, "Foundation for adaptive charging solutions: Optimised use of electric vehicle charging capacity," *IET Smart Grid*, vol. 4, no. 6, pp. 599–611, 2021.
- [190] Y. Zou, J. Zhao, X. Gao, Y. Chen, and A. Tohidi, "Experimental results of electric vehicles effects on low voltage grids," *Journal of Cleaner Production*, vol. 255, p. 120270, 2020.
- [191] J. Y. Yong, V. K. Ramachandaramurthy, K. M. Tan, and J. Selvaraj, "Experimental validation of a three-phase off-board electric vehicle charger with new power grid voltage control," *IEEE Transactions on Smart Grid*, vol. 9, no. 4, pp. 2703–2713, 2018.
- [192] J. I. Guerrero Alonso, E. Personal, S. García, A. Parejo, M. Rossi, A. García, F. Delfino, R. Pérez, and C. León, "Flexibility services based on openadr protocol for dso level," Sensors, vol. 20, no. 21, 2020.
- [193] A. Hoekstra, R. Bienert, A. Wargers, H. S. (Greenlots), and P. Voskuilen, "Using openadr with ocpp: Combining these two open protocols can turn electric vehicles from threats to the electricity grid into demand-response assets," The OpenADR Alliance, Tech. Rep., 2016. [Online]. Available: https://www.openadr.org/case-studies
- [194] L. De Herdt, A. Shekhar, Y. Yu, G. R. C. Mouli, J. Dong, and P. Bauer, "Power hardware-in-the-loop demonstrator for electric vehicle charging in distribution grids," in 2021 IEEE Transportation Electrification Conference Expo (ITEC), 2021, pp. 679–683.
- [195] L. De Herdt, "Hardware-in-the-Loop Simulation of Controlled and Uncontrolled EV Charging in a Distribution Grid," Master's thesis, Delft University of Technology, the Netherlands, 2020, accessed: 2022-07-05.
- [196] EV Database, "Tesla Model 3 Standard Range Plus Specifications," 2022, accessed: 2023-07-05. [Online]. Available: https://ev-database.nl/
- [197] E. Database, "Tesla Model S Long Range Specifications," 2022, accessed: 2023-07-05. [Online]. Available: https://ev-database.nl/
- [198] Koninklijk Nederlands Meteorologisch Instituut (KNMI), "CESAR Database," 2018, accessed: 2022-12-06. [Online]. Available: https://ruisdael-observatory.nl/cesar/
- [199] "Price cap for gas, electricity and district heating," Government of The Netherlands, Accessed: 2023-5-19. [Online]. Available: https://www.government.nl/
- [200] R. Blaga, A. Sabadus, N. Stefu, C. Dughir, M. Paulescu, and V. Badescu, "A current perspective on the accuracy of incoming solar energy forecasting," *Progress in Energy and Combustion Science*, vol. 70, pp. 119–144, 1 2019.
- [201] D. Stahleder, M. Nöhrer, F. Lehfuss, and H. Müller, "Implementation of a real time capable, flexible and accurate Electric Vehicle model to holistically evaluate Charging Services and

- Methods," in 7th Transport Research Arena, Vienna, 4 2018, pp. 1-9.
- [202] Y. Yu, A. Shekhar, G. R. Chandra Mouli, and P. Bauer, "Comparative impact of three practical electric vehicle charging scheduling schemes on low voltage distribution grids," *Energies*, vol. 15, no. 22, 2022.
- [203] D. Dreucci, Y. Yu, G. Ram Chandra Mouli, A. Shekhar, and P. Bauer, "Centralised distribution grid congestion management through ev charging control considering fairness and priority," Submitted.
- [204] K. Phipps, K. Schwenk, B. Briegel, R. Mikut, and V. Hagenmeyer, "Customized uncertainty quantification of parking duration predictions for ev smart charging," *IEEE Internet of Things Journal*, vol. 10, no. 23, pp. 20649–20661, 2023.
- [205] J. Huber, D. Dann, and C. Weinhardt, "Probabilistic forecasts of time and energy flexibility in battery electric vehicle charging," *Applied Energy*, vol. 262, p. 114525, 2020.
- [206] W. Sun, F. Neumann, and G. P. Harrison, "Robust scheduling of electric vehicle charging in lv distribution networks under uncertainty," *IEEE Transactions on Industry Applications*, vol. 56, no. 5, pp. 5785–5795, 2020.
- [207] E. Braco, I. S. Martín, A. Berrueta, P. Sanchis, and A. Ursúa, "Experimental assessment of firstand second-life electric vehicle batteries: Performance, capacity dispersion, and aging," *IEEE Transactions on Industry Applications*, vol. 57, no. 4, pp. 4107–4117, 2021.
- [208] M. Ledro, L. Calearo, J. M. Zepter, T. Gabderakhmanova, and M. Marinelli, "Influence of realistic ev fleet response with power and energy controllers in an ev-wind virtual power plant," Sustainable Energy, Grids and Networks, vol. 31, p. 100704, 2022.
- [209] Elaad NL, "EV Related Protocol Study," Elaad NL, Arnhem, Tech. Rep., 2016. [Online]. Available: https://www.elaad.nl/research/ev-related-protocol-study/
- [210] Open Charge Alliance, "OCPP 2.0.1: Part 0 Introduction," Open Charge Alliance, Arnhem, Standard, 3 2020. [Online]. Available: https://www.openchargealliance.org/protocols/ocpp-201/
- [211] M. Multin, "ISO 15118 as the Enabler of Vehicle-to-Grid Applications," in 2018 International Conference of Electrical and Electronic Technologies for Automotive, AUTOMOTIVE 2018. Institute of Electrical and Electronics Engineers Inc., 10 2018.
- [212] Y. Yu, L. De Herdt, A. Shekhar, G. R. C. Mouli, and P. Bauer, "Ev smart charging in distribution grids experimental evaluation using hardware in the loop setup," *IEEE Open Journal of the Industrial Electronics Society*, vol. 5, pp. 13–27, 2024.
- [213] TenneT, "FCR Manual for BSP's Requirements and procedures for supply of FCR," TenneT, C1 Public Information, 2 2024. [Online]. Available: https://www.tennet.eu/markets/ancillary-services/fcr-documents
- [214] "Electric vehicles statistics in the netherlands up to and including june 2022," Rijksdienst voor Ondernemend Nederland (RVO), accessed: 2022-12-06. [Online]. Available: https://www.rvo.nl
- [215] "Charging session data analysis," Elaad, accessed: 2024-05-03. [Online]. Available: https://platform.elaad.io/analyses/sessie-data.html
- [216] E. Apostolaki-Iosifidou, P. Codani, and W. Kempton, "Measurement of power loss during electric vehicle charging and discharging," *Energy*, vol. 127, pp. 730–742, 2017.
- [217] J. Sears, D. Roberts, and K. Glitman, "A comparison of electric vehicle level 1 and level 2 charging efficiency," in 2014 IEEE Conference on Technologies for Sustainability (SusTech), 2014, pp. 255–258.
- [218] Het Nederlandse PV Portaal, "Open-source pv power databases," TUD-PVMD, KNMI, accessed: 2024-5-03. [Online]. Available: https://pvportal-4.ewi.tudelft.nl

- [219] "Verbruiksprofielen 2022," Het Marktfaciliteringsforum (MFF), Accessed: 2024-5-03. [Online]. Available: www.mffbas.nl
- [220] "Entso-e transparency platform," European Network of Transmission System Operators for Electricity (ENTSO-E), Accessed: 2024-5-03. [Online]. Available: https://transparency.entsoe.eu/
- [221] "Frequency Containment Reserves (FCR)," European Network of Transmission System Operators for Electricity (ENTSO-E), accessed: 2024-05-06. [Online]. Available: https://www.entsoe.eu/network_codes/eb/fcr/

Acknowledgements

YOU KNOW HOW IT IS: you pick up a freshly printed thesis and rifle through to the acknowledgements only to find that the author has acknowledged a lot more people than you would have thought.

Not this time.

While I typically steer clear of cliches, I'll happily make a slight exception here: every tale has its start and finish. This dissertation has been a journey filled with valleys, plateaus, again valleys, more sleepless nights than should be legally or morally allowed, and ultimately, a whole lot of perseverance.

Although it is my name that shows on the cover, I would not have been able to complete it without the support of nearly everyone around me.

To you, who have supported me throughout these years, and you know who you are, I want to convey a heartfelt *Thank you* for your encouragement, patience and understanding.

Author profile

Biography

Yunhe Yu was born in 1992 in Nanjing, China. She earned her B.Sc. degree in Environmental Sciences from Nanjing Agricultural University. Driven by a desire to explore the world and delve into the field of energy transition, she moved to the Netherlands, where she obtained her M.Sc. in Sustainable Energy Technology from Delft University of Technology in 2017. From 2017 to 2018, Yunhe worked as a teaching assistant for the edX DelftX Electric Cars series courses. Since 2018, she has been pursuing her Ph.D. in eMobility. Her research interests and expertise include EV-grid integration, smart charging, energy system optimisation, power system flexibility, and electricity market participation.

List of publications (PhD related)

- J Y. Yu, D. Reihs, S. Wagh, A. Shekhar, D. Stahleder, G. R. C. Mouli, F. Lehfuss, and P. Bauer, Data-driven study of low voltage distribution grid behaviour with increasing electric vehicle penetration. *IEEE Access*, vol. 10, pp. 6053–6070, 2022
- J Y. Yu, A. Shekhar, G. R. Chandra Mouli, and P. Bauer, Comparative impact of three practical electric vehicle charging scheduling schemes on low voltage distribution grids. *Energies*, vol. 15, no. 22, 2022.
- J Y. Yu, L. De Herdt, A. Shekhar, G. R. C. Mouli, and P. Bauer, Ev smart charging in distribution grids experimental evaluation using hardware in the loop setup. *IEEE Open Journal of the Industrial Electronics Society*, vol. 5, pp. 13 27, 2024.
- J D. Dreucci, Y. Yu, G. Ram Chandra Mouli, A. Shekhar, and P. Bauer, Centralised distribution grid congestion management through ev charging control considering fairness and priority. Submitted.
- C Y. Yu, A. Shekhar, G. C. R. Mouli, P. Bauer, N. Refa and R. Bernards, Impact of Uncontrolled Charging with Mass Deployment of Electric Vehicles on Low Voltage Distribution Networks. 2020 IEEE Transportation Electrification Conference & Expo (ITEC), Chicago, IL, USA, 2020, pp. 766-772.
- C S. Wagh, Y. Yu, A. Shekhar, G. R. C. Mouli and P. Bauer, Aggregated Impact of EV Charger Type and EV Penetration level in Improving PV Integration in Distribution Grids. *2021 IEEE Transportation Electrification Conference & Expo (ITEC)*, Chicago, IL, USA, 2021, pp. 595-600.
- C L. De Herdt, A. Shekhar, Y. Yu, G. R. C. Mouli, J. Dong and P. Bauer, "Power Hardware-in-the-Loop Demonstrator for Electric Vehicle Charging in Distribution Grids," 2021 IEEE Transportation Electrification Conference & Expo (ITEC), Chicago, IL, USA, 2021, pp. 679-683.
- C N. Damianakis, Y. Yu, G. C. R. Mouli and P. Bauer, Frequency Regulation Reserves Provision in EV Smart-Charging. 2023 IEEE Transportation Electrification Conference & Expo (ITEC), Detroit, MI, USA, 2023, pp. 1-6.

Propositions

accompanying the dissertation

ORCHESTRATING MASS DEPLOYMENT OF ELECTRIC VEHICLES IN DISTRIBUTION GRIDS

A Systematic Framework for Advancing EV Smart Charging

by

Yunhe Yu

- 1. [This thesis] The balance between complexity and computational effort in algorithm design involves a trade-off between the generosity of functionalities and the precision in performance.
- 2. [This thesis] The most crucial component in a smart charging algorithm is not the mathematical formula itself, but the surrounding factors that ensure the formula's accurate actualisation.
- 3. Optimality should not only encompass the maximum utilisation of resources, but also their equitable distribution; otherwise limited supply can lead to autonomous allocation by the populace with prejudice guaranteed.
- 4. The biggest obstacle in popularising sustainability is its priceyness, simply because negative externalities are not embraced in its true price it is time to concede that destroying the environment is not free.
- 5. Being a rigorous engineer involves not only precision in numerical accuracy but also acceptance of the existence of nonsensical elements.
- 6. Global disparity in cognition, where one part of the world may lack the luxury of sympathy and compassion while the other underestimates the necessity of harsh measures for survival, reflects how far resource scarcity can drive human values apart.
- 7. Ironically, censorship may promote creativity more vigorously than freedom of speech. When the birth of an expression must navigate through sensitive tags and dodge keywords, the process of encoding becomes an art in itself. The preservation of essence in its subtle and abstract form in high-context culture exemplifies the creativity in human intelligence.
- 8. We are just anthrobots being piloted by the nervous system.

These propositions are regarded as opposable and defendable, and have been approved as such by the promotor Prof. dr. P. Bauer, copromotor Dr. ir. G.R. Chandra Mouli.